2022 Design, Build, Fly Competition Summary

The 2021-22 AIAA/Textron Aviation/Raytheon Technologies Design, Build, Fly Competition Flyoff was held at the Textron Aviation Employees' Flying Club in Wichita, KS on the weekend of April 21-24, 2022. This was the 26th year for the competition. Of the 127 proposals submitted and judged, 110 teams were invited to submit a formal report for the next phase of the competition. 97 teams submitted design reports to be judged, and 64 teams attended the flyoff (10 international), including one team who had not entered this year's competition but wanted to experience DBF in person in preparation for next year. About 750 students, faculty, and guests were present. Of the 64 teams in attendance, 58 successfully completed tech inspection. The weather was very windy on Friday and Saturday but just about perfect on Sunday, which allowed for non-stop flying and achieving what may be a record number of flight attempts in one day. Of the 152 official flight attempts, 87 resulted in a successful score with 40 teams achieving at least one successful flight score and 15 teams successfully completing all four missions (one ground and three flight). Even with a two year break for the fly-off due to COVID, the quality of the teams, their readiness to compete, and the execution of the flights was exceptional.

The contest theme this year was Humanitarian Mission. Each aircraft was limited to an 8 foot maximum dimension in any direction. The aircraft were required to complete three flight missions, each taking off within 25 feet. The first mission was a Deployment Flight with no payload for three laps within five minutes. The second mission was a Staging Flight to deliver vaccination components (30 ml syringes) with the score based on the number of syringes carried and flight time to complete three laps. The final mission was a Vaccine Delivery Flight which included deployment of environmentally sensitive vaccine vial packages. During this mission, ten minutes were provided to land and deploy a single package in a drop zone per lap with the score based on number of successful deployments without tripping a shock sensor on the package. Teams were also required to complete a timed ground mission demonstrating capability to carry all payloads and deploy packages one at a time. As usual, the total score is the product of the total mission score and design report score. More details on the mission requirements can be found at the competition website: http://www.aiaadbf.org.

First Place went to the Georgia Institute of Technology, Second Place went to Embry-Riddle Aeronautical University – Daytona Beach and Third Place went to the FH JOANNEUM University of Applied Sciences. A full listing of the results is included below. The Best Paper Award, sponsored by the Design Engineering TC for the highest report score, went to the FH JOANNEUM University of Applied Sciences with a score of 93.33.

We owe our thanks for the success of the DBF competition to the efforts of many volunteers from Textron Aviation, Raytheon Technologies, and the AIAA sponsoring technical committees: Applied Aerodynamics, Aircraft Design, Flight Test, and Design Engineering. These volunteers collectively set the rules, judge the proposals and reports, and execute the flyoff. Thanks also to the Premier Sponsors: Textron Aviation and Raytheon Technologies, and to the AIAA Foundation for their financial support as well as our Gold sponsors this year – AeroVironment, General Atomics Aeronautical, Mathworks, and Spirit AeroSystems. Special thanks go to Textron Aviation for hosting the flyoff this year.

Finally, this event would not be nearly as successful without the hard work and enthusiasm from all the students and advisors. If it weren't for you, we wouldn't keep doing it!!

Brian Richardet
For the DBF Organizing Committee

2022 Design, Build, Fly Competition Summary

2022 Design/Build/Fly Competition Final Results

Rank	Team		Mission Scores					Report	2022 DBF
	Queue #	Name	GM	M1	M2	M3	Total		SCORE
1	9	Georgia Institute of Technology	0.52	1.00	1.54	2.89	5.95	88.48	526.59
2	17	Embry-Riddle Aeronautical University - Daytona Beach, FL	0.12	1.00	1.93	3.00	6.05	86.77	525.19
3	1	FH JOANNEUM University of Applied Sciences	0.32	1.00	1.55	2.56	5.43	93.33	506.32
4	21	University of Southern California	0.35	1.00	2.00	2.33	5.69	84.75	481.82
5	5	Virginia Tech	0.46	1.00	1.25	2.44	5.15	89.77	462.40
6	29	University of Kansas	0.47	1.00	1.22	2.56	5.25	81.97	430.01
7	7	Arizona State University	0.11	1.00	1.36	2.22	4.69	89.15	417.94
8	16	Embry-Riddle Aeronautical University: Prescott Campus	0.13	1.00	1.22	2.33	4.68	86.77	406.06
9	35	University of Washington, Seattle	0.12	1.00	1.29	2.67	5.07	79.70	404.14
10	27	The University of Akron	0.16	1.00	1.33	2.33	4.82	82.60	398.18
11	3	Washington University in St. Louis	0.11	1.00	1.09	2.22	4.42	90.00	398.12
12	31	University of California, Irvine	0.15	1.00	1.50	2.22	4.87	81.52	396.89
13	38	University of Texas at Austin	0.10	1.00	1.36	2.56	5.01	78.67	394.29
14	56	University of Oklahoma	0.37	1.00	1.42	2.33	5.12	72.23	369.94
15	41	Franklin W. Olin College of Engineering	0.08	1.00	1.18	2.11	4.38	78.17	342.11
16	6	University of California, Los Angeles	0.18	1.00	1.33	0.00	2.51	89.55	225.12
17	24	Universidad Pontificia Bolivariana	0.00	1.00	1.55	0.00	2.55	83.90	214.17
18	20	Western Michigan University	0.00	1.00	1.49	0.00	2.49	84.90	211.01
19	15	VEERMATA JIJABAI TECHNOLOGICAL INSTITUTE	0.00	1.00	1.33	0.00	2.33	86.95	202.74
20	48	San Jose State University	0.07	1.00	1.19	0.00	2.26	76.27	172.63
21	36	University of Central Florida	0.00	1.00	1.19	0.00	2.19	78.83	172.39
22	42	The Pennsylvania State University	0.09	1.00	1.10	0.00	2.19	77.95	170.83
23	70	The University of South Alabama	0.00	1.00	1.49	0.00	2.49	63.33	157.73
24	68	New Mexico State University	0.17	1.00	1.07	0.00	2.24	63.53	142.49
25	66	Purdue University	1.00	1.00	0.00	0.00	2.00	64.67	129.34
26	34	The University of Tennessee - Knoxville	0.34	1.00	0.00	0.00	1.34	80.37	107.98
27	25	University of Florida	0.26	1.00	0.00	0.00	1.26	83.75	105.35
28	4	California Polytechnic State University, San Luis Obispo	0.13	1.00	0.00	0.00	1.13	89.97	101.45
29	53	Rutgers, The State University of New Jersey – New Brunswick	0.36	1.00	0.00	0.00	1.36	73.88	100.66
30	46	University of Alaska Fairbanks	0.19	1.00	0.00	0.00	1.19	76.93	91.73
31	39	Ghulam Ishaq Khan Institute of Engineering Sciences and Technology	0.17	1.00	0.00	0.00	1.17	78.57	91.57
32	2	Massachusetts Institute of Technology	0.00	1.00	0.00	0.00	1.00	91.33	91.33
33	26	Missouri University of Science and Technology	0.05	1.00	0.00	0.00	1.05	83.58	88.12
34	43	Cornell University	0.00	1.00	0.00	0.00	1.00	77.80	77.80
35	47	San Diego State University	0.00	1.00	0.00	0.00	1.00	76.35	76.35
36	83	Utah State University	0.30	1.00	0.00	0.00	1.30	54.37	70.70
37	63	Gebze Technical University	0.00	1.00	0.00	0.00	1.00	66.77	66.77
38	69	Trine University	0.00	1.00	0.00	0.00	1.00	63.37	63.37
39	77	University of Ljubljana	0.00	1.00	0.00	0.00	1.00	58.53	58.53
40	11	University of Notre Dame	0.53	0.00	0.00	0.00	0.53	87.93	46.50
41	12	Rensselaer Polytechnic Institute	0.46	0.00	0.00	0.00	0.46	87.53	40.35
42	92	John Brown University	0.00	1.00	0.00	0.00	1.00	40.33	40.33
43	10	University of Petroleum and Energy Studies	0.45	0.00	0.00	0.00	0.45	88.47	40.21
44	8	The Ohio State University	0.37	0.00	0.00	0.00	0.37	89.08	32.54
45	37	University of Maryland, College Park	0.40	0.00	0.00	0.00	0.40	78.75	31.70
46	51	North Dakota State University	0.41	0.00	0.00	0.00	0.41	74.00	30.38
47	49	Worcester Polytechnic Institute	0.15	0.00	0.00	0.00	0.15	75.77	11.02
48	64	Lehigh University	0.13	0.00	0.00	0.00	0.13	65.95	8.38
49	61	Rose-Hulman Institute of Technology	0.11	0.00	0.00	0.00	0.11	68.57	7.62
50	18	West Virginia University	0.08	0.00	0.00	0.00	0.08	86.42	7.13

2022 Design, Build, Fly Competition Summary

2022 Design/Build Fly Competition Final Results (cont)

Rank	Team		Mission Scores					Report	2022 DBF
	Queue #	Name	GM	M1	M2	M3	Total		SCORE
51	97	University at Buffalo	0.07	0.00	0.00	0.00	0.07	0.00	0.00
52	13	North Carolina State University	0.00	0.00	0.00	0.00	0.00	87.33	0.00
53	14	National University of Singapore	0.00	0.00	0.00	0.00	0.00	87.23	0.00
54	19	Dayananda Sagar College of Engineering	0.00	0.00	0.00	0.00	0.00	86.25	0.00
55	22	University of Michigan -- Ann Arbor	0.00	0.00	0.00	0.00	0.00	84.50	0.00
56	23	Cairo University	0.00	0.00	0.00	0.00	0.00	84.22	0.00
57	28	George Washington University	0.00	0.00	0.00	0.00	0.00	82.15	0.00
58	30	The University of Hong Kong	0.00	0.00	0.00	0.00	0.00	81.83	0.00
59	32	YILDIZ TECHNICAL UNIVERSITY	0.00	0.00	0.00	0.00	0.00	81.22	0.00
60	33	University of California, San Diego	0.00	0.00	0.00	0.00	0.00	80.77	0.00
61	40	Case Western Reserve University	0.00	0.00	0.00	0.00	0.00	78.37	0.00
62	44	Military Technical College	0.00	0.00	0.00	0.00	0.00	77.50	0.00
63	45	Wentworth Institute of Technology	0.00	0.00	0.00	0.00	0.00	77.42	0.00
64	50	State University of New York at Binghamton	0.00	0.00	0.00	0.00	0.00	75.17	0.00
65	52	Military Institute of Science and Technology	0.00	0.00	0.00	0.00	0.00	73.92	0.00
66	54	Clarkson University	0.00	0.00	0.00	0.00	0.00	72.87	0.00
67	55	University of California, Merced	0.00	0.00	0.00	0.00	0.00	72.35	0.00
68	57	Brigham Young University Provo	0.00	0.00	0.00	0.00	0.00	72.03	0.00
69	58	University of Colorado Boulder	0.00	0.00	0.00	0.00	0.00	71.43	0.00
70	59	The Hong Kong University of Science and Technology	0.00	0.00	0.00	0.00	0.00	70.90	0.00
71	60	Tribhuvan University, Institute of Engineering, Pulchowk Campus	0.00	0.00	0.00	0.00	0.00	69.92	0.00
72	62	University of Illinois Urbana-Champaign	0.00	0.00	0.00	0.00	0.00	68.53	0.00
73	65	The University of Alabama	0.00	0.00	0.00	0.00	0.00	65.40	0.00
74	67	University of New South Wales	0.00	0.00	0.00	0.00	0.00	64.25	0.00
75	71	Columbia University in the City of New York	0.00	0.00	0.00	0.00	0.00	61.47	0.00
76	72	University of Maryland, Baltimore County	0.00	0.00	0.00	0.00	0.00	61.07	0.00
77	73	Florida Institute of Technology	0.00	0.00	0.00	0.00	0.00	61.00	0.00
78	74	University of Massachusetts Amherst	0.00	0.00	0.00	0.00	0.00	58.83	0.00
79	75	Texas Tech University	0.00	0.00	0.00	0.00	0.00	58.83	0.00
80	76	University of Massachusetts Lowell	0.00	0.00	0.00	0.00	0.00	58.60	0.00
81	78	Oregon State University	0.00	0.00	0.00	0.00	0.00	56.10	0.00
82	79	Syracuse University	0.00	0.00	0.00	0.00	0.00	55.83	0.00
83	80	Johns Hopkins University	0.00	0.00	0.00	0.00	0.00	55.48	0.00
84	81	Manhattan College	0.00	0.00	0.00	0.00	0.00	55.15	0.00
85	82	Kent State University	0.00	0.00	0.00	0.00	0.00	54.67	0.00
86	84	Rowan University	0.00	0.00	0.00	0.00	0.00	51.48	0.00
87	85	Youngstown State University	0.00	0.00	0.00	0.00	0.00	50.13	0.00
88	86	Ankara Yıldırım Beyazıt University	0.00	0.00	0.00	0.00	0.00	49.37	0.00
89	87	Birla Institute of Technology and Science, Pilani K.K. Birla Goa Campus	0.00	0.00	0.00	0.00	0.00	48.85	0.00
90	88	University of Tennessee at Chattanooga	0.00	0.00	0.00	0.00	0.00	47.75	0.00
91	89	Texas A&M University	0.00	0.00	0.00	0.00	0.00	44.07	0.00
92	90	University of Missouri-Columbia	0.00	0.00	0.00	0.00	0.00	42.00	0.00
93	91	Alfred University	0.00	0.00	0.00	0.00	0.00	41.33	0.00
94	93	University of Arkansas - Fayetteville	0.00	0.00	0.00	0.00	0.00	38.45	0.00
95	94	The City College of New York (CCNY) of the City University of New York	0.00	0.00	0.00	0.00	0.00	35.77	0.00
96	95	Villanova University	0.00	0.00	0.00	0.00	0.00	27.97	0.00
97	96	New York University Tandon School of Engineering	0.00	0.00	0.00	0.00	0.00	25.67	0.00

joanneum

AERONAUTICS

2021 - 2022

Aircraft Design Report

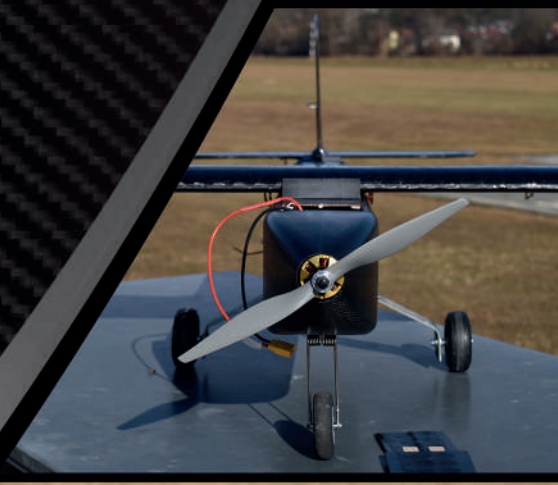

FH JOANNEUM

Graz, Austria

FH | JOANNEUM
University of Applied Sciences

AIAA DESIGN/BUILD/FLY COMPETITION

Contents

List of Abbreviations

AoA	Angle of attack
AWG	American wire gauge
A	Wing area
CAD	Computer aided design
CFD	Computional fluid dynamics
CG	Center of gravity
CNC	Computer numerical control
C	Compliant
DBF	Design Build Fly
EPS	Expanded polystyrol
ESC	Electronic speed control
FoM	Figures of merit
GFRP	Glass fiber reinforced polymer
GM	Ground mission
jA	joanneum Aeronautics
LiPo	Lithium-Polymer
LW-PLA	Light weight polymerized lactic acid
M1	Mission 1
M2	Mission 2
M3	Mission 3
MAC	Mean aerodynamic chord length
MCU	Microcontrol unit
MTOW	Maximum takeoff weight
NiCd	Nickel-Cadmium
NiMH	Nickel-Metal Hybrid
PCB	Printed circuit board
PLA-Carbon	Polymerized lactic acid carbon reinforced
PWM	Pulse with modulation value
RC	Radio controlled
RPM	Revolutions per minute
Rx	Receiver
R	Review
T	Test
XPS	Extruded polystyrol

Nomenclature

α	Angle of attack
η	Airfoil efficiency
ρ	Air density
τ_{max}	Maximum required torque
a	Aaa
AR	Aspect Ration
b	Wingspan
b_c	Span of control surface
c	Chord length
C_D	Drag coefficient
C_L	Lift coefficient
C_M	Moment coefficient
$C_{f,turb}$	turbulent skin friction coefficient
F_D	Drag force
F_N	Normal force
F_T	Tangential force
F_L	Lift force
g	Gravitational force
I	Current
k	Induced drag factor
L	Characteristic length
P	Power
P_{max}	Total stored energy
q	Dynamic pressure
Re	Reynolds Number
$S_{c,max}$	Maximal control surface deflection
S_{ref}	Reference area
$S_{s,max}$	Maximal servo deflection
s_{TO}	Maximal takeoff distance
U	Voltage
v	Airspeed
V_{stall}	Stall speed
WCL	Maximum wing cube loading

1 Executive Summary

This report describes the design, manufacturing, and testing of the FH JOANNEUM's radio-controlled (RC) model aircraft *Hornet* designated to compete in the 2021-22 American Institute of Aeronautics and Astronautics (AIAA) Design, Build, and Fly (DBF) competition. The *Hornet* has been developed by the joanneum Aeronautics (jA) DBF team of the FH JOANNEUM University of Applied Sciences Graz, Austria, according to this year's objective including all design and mission requirements stated by the AIAA. In all flight missions, the aircraft must complete laps along a pre-defined flight course. While Mission 1 (M1) purely serves the flight demonstration, the team must perform time-effectively for Mission 2 (M2), Mission 3 (M3), and the Ground Mission (GM). Both M2 and M3 require the aircraft to carry payload. During M2, three laps must be flown rapidly within a given time limit while carrying a maximum number of vaccination syringes. In M3, a 10-minute time window is given to remotely deploy one environmentally-sensitive vaccine vial package with each landing, without actuating the integrated 25G shock sensors. The GM requires fast loading and unloading of the M2 and M3 payload. In addition, the aircraft must meet the required takeoff distance of 25 ft and fit inside an 8 ft x 8 ft box in its assembled flight configuration.

The *Hornet*'s high-wing configuration and conventional empennage contribute to excellent flight characteristics and offer sufficient space for the mission payload. With a wingspan of 7.37 ft and a total length of 5.28 ft, the design of the *Hornet* exploits the 8 ft maximal dimension requirement to provide sufficient space for a total number of 80 syringes and 5 vaccine vial packages. The radio controlled (RC) aircraft is driven by a single tractor motor and has maximum takeoff weight (MTOW) of 15.17 lb. A thrust-to-weight ratio of 0.96 enables the aircraft to take off in the required 25 ft and cruise at a speed of 60 mph, satisfying the speed requirements for both M2 and M3. The tricycle landing gear with a steerable nosewheel and implemented brake system guarantees safe and gentle landings. In M3, a successful deployment of the vial packages is ensured by a purpose-built and remote-controlled conveyor belt system carrying the packages with the integrated shock sensors. In each lap, one package can be deployed by a ramp through an open hatch door at the bottom rear end of the fuselage without exceeding the 25G load limitation.

The *Hornet* was developed, designed, manufactured, and tested by a team of 16 undergraduate students and 21 master's students. Each of the three sub-teams *Engineering & Design*, *Management & Marketing* and *Technical Documentation* was led by a team leader. A sensitivity study was conducted in order to ensure compliance with design requirements. Based on the outcome, it was decided to design the *Hornet* mainly around M3 requirements. During the preliminary design phase, two prototypes were developed and continuously improved in an iterative process. The final competition aircraft was completed during the detail design phase. Manufacturing included CNC-cutting, 3D-printing as well as composite molding, laminating, and vacuum bagging. The majority of the *Hornet's* fuselage consists of a carbon fiber structure reinforced by foam cores and plywood, ensuring a lightweight design and maximum structural strength. Ground and flight tests were crucial to iteratively improve the design. During flight testing, the final design of the *Hornet* proved to have outstanding stability characteristics.

With its competition aircraft *Hornet*, the jA DBF team aims to achieve a maximum mission score with an estimated GM time of 144 seconds, a total number of 80 syringes carried during an overall M2 time of 80 seconds and 5 successfully deployed vaccine vial packages in M3.

2 Management Summary

The joanneum Aeronautics (jA) DBF team from the FH JOANNEUM, University of Applied Sciences, consists of 16 undergraduate students from the bachelor's and 21 postgraduate students from the master's program. All participants collaborated in designated teams with specific areas of responsibility. A milestone chart that was established in an early project phase was kept under review throughout the process.

2.1 Team Organization

The hierarchical composition of the team depicted in Figure 1 provided the framework for a clear organizational structure and a comprehensible allocation of tasks within the joanneum Aeronautics (jA) DBF team. During the design phase, each of the main divisions *Engineering & Design*, *Management & Marketing*, and *Technical Documentation* was separately managed by one student team leader. These responsible persons distributed the workload among the participants in their sub-team. Because of a high number of varying tasks, the main division *Management & Marketing* was further split up into the sub-teams *Organization*, *Fundraising* and *Public Relations*. The main division *Engineering & Design* was divided into the sub-teams *Avionics & Propulsion*, *Aerodynamics* and *Fuselage & Deployment mechanism*, each which focused on the sub-systems of the aircraft. On the part of the university support was given by two faculty advisors in linguistic and engineering matters.

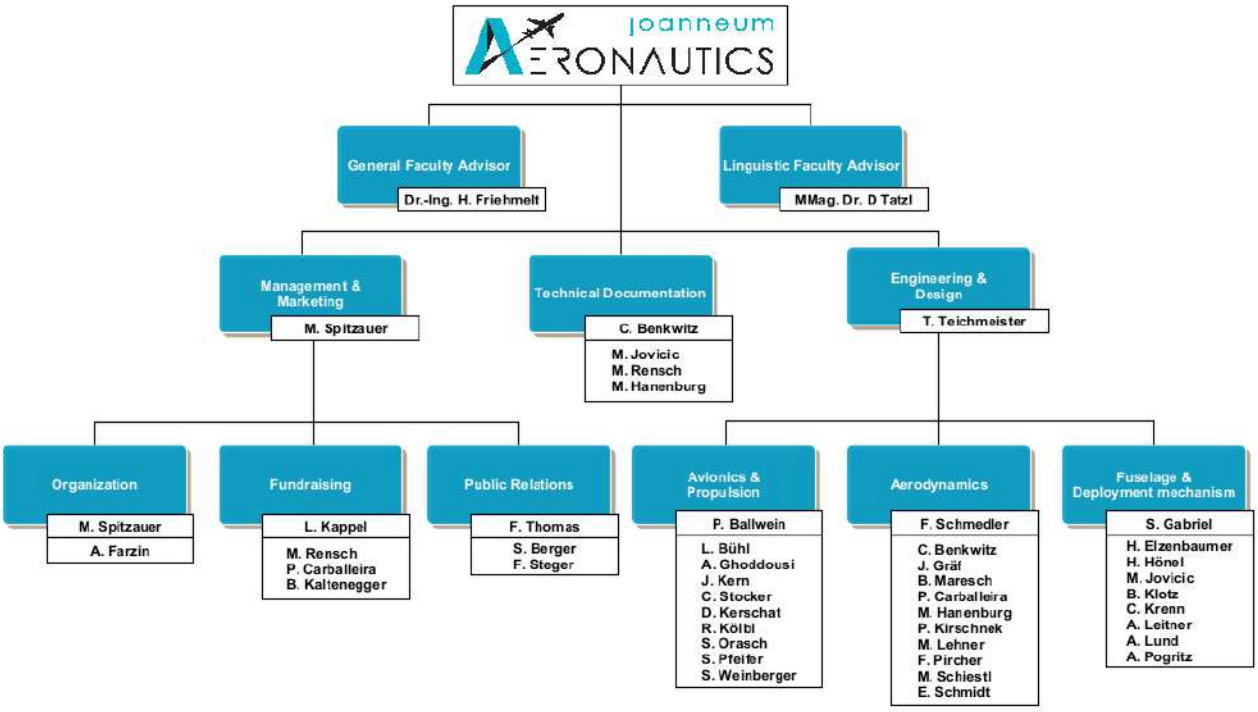

Figure 1: Organizational structure of the jA DBF team

During the design of the competition aircraft, each sub-team had its own assignment areas. While the management team focused on the overall project organization, obtained funding, and took care of the contest's social media appearance, the engineering team designed, built, and tested both prototypes and the final competition aircraft.

Meanwhile, the third sub-team accompanied the other teams in documenting all important steps in the design process. A more specific listing of the different responsibilities can be found in Table 1.

Table 1: Sub-team responsibilities

Group	Responsibilities
Organization	Project-, budget and travel-planning
Fundraising	Sponsorship acquisition
Public Relations	Social media communication
Technical Documentation	Writing and editing of proposal and design report
Avionis & Propulsion	Avionic harness design and determination of electrical propulsion components
Aerodynamics	Comparison of suitable airfoils and calculation of aerodynamic design parameters
Fuselage & Deployment mechanism	Design of the fuselage and deployment mechanism concerning a fixed CG position

2.2 Milestone chart

At the beginning of the design process, the competition team committed itself to a time schedule that contained important milestones and deadlines along the way until the flyoff. The team leaders monitored the project's progress and compared the planned and actual timing on a regular basis. The outcome of these regular process revisions is shown in the milestone chart in Figure 2.

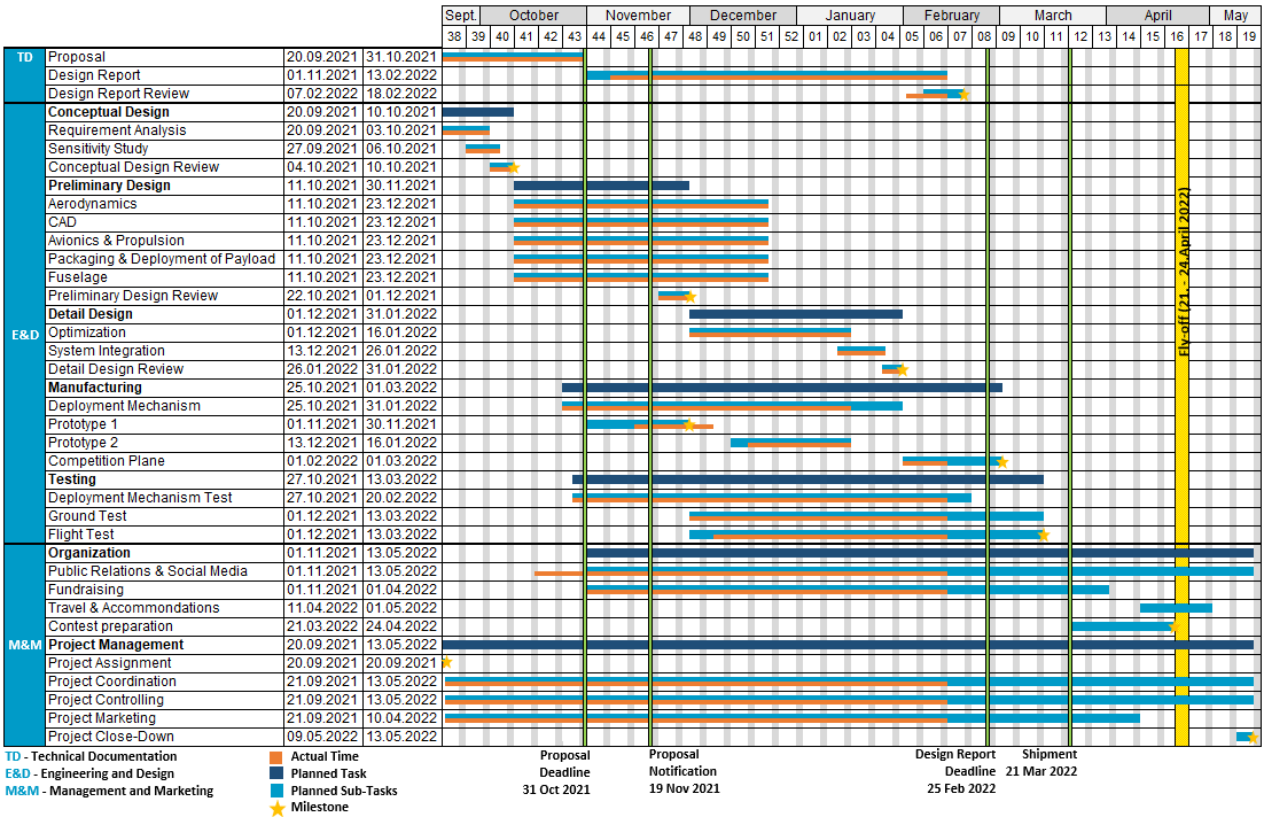

Figure 2: Milestone chart outlining the contest schedule

3 Conceptual Design

The conceptual design phase was primarily used to analyze the mission requirements, translate them into design parameters, and outline a feasible configuration that has the greatest potential to maximize the final score. Additionally, a quantitative scoring analysis was performed in order to identify the scoring drivers. The scoring analysis and mission requirements were translated into figures of merit (FoM), a metric to weigh different solutions against each other to find the most promising aircraft configuration. The FoM resulted in a conventional airplane configuration with a tricycle landing gear, high-wing design, and a single engine. The conceptual solution for the deployment mechanism was to deploy the payload at the rear of the aircraft.

3.1 Mission Requirements

The mission requirements resulted from the "Problem Statement" and the "Mission and Score Summary".

3.1.1 Problem Statement

This year's contest objective is a humanitarian mission in which vaccination components must be delivered safely. This mission includes the deployment of the aircraft, the staging of vaccination syringes, and the delivery of environmentally-sensitive vaccine vial packages without actuating the integrated 25G shock sensors. Each team must accomplish four missions. One ground mission and three flight missions. This year's challenge is to find a compromise between the missions to optimize the total mission score.

3.1.2 Mission and Score Summary

The overall score is computed from the design report score and total mission score as shown in Equation 3.1.

$$SCORE = Written\ Report\ Score * Total\ Mission\ Score \tag{3.1}$$

The individual flight mission and ground mission scores add up to the total mission score, Equation 3.2.

$$Total\ Mission\ Score = M1 + M2 + M3 + GM \tag{3.2}$$

Whereas the flight missions have to be flown in order, the GM can be attempted at any time. The GM score is dependent on the loading time. For a short loading time, the aircraft must have an easily accessible payload compartement for loading and unloading the payload of M2 and M3. The loading time is measured for two runs. First, the payload for M2 needs to be loaded, and, then, in the second run, the payload for M2 will be removed, and the payload for M3 will be loaded. The sum of these two runs is the loading time. The final GM score is the ratio between the fastest time among all teams and the loading time of each team, as shown in Equation 3.3.

$$GM = \frac{Fastest\ Time}{Time} \tag{3.3}$$

All three flight missions are flown along the same flight course pattern, shown in Figure 3. The standard mission profile consists of two 1000 ft straights and one 360-degree turn. A successful lap is defined as beginning and ending at the start/finish line, while the aircraft is still airborne. The required number of laps is dependent on the mission. The maximum takeoff distance is limited to 25 ft of the start/finish line. To successfully finish each mission, a landing on the paved runway without significant damages is required.

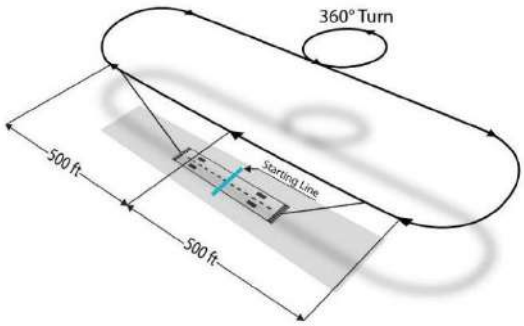

Figure 3: AIAA competition flight course [1, p.4]

Mission 1 - No payload: For M1, no payload is required. The aircraft must complete three laps (Figure 3) within a flight window of 5 minutes. A successful completion of this mission is rewarded with 1.0 points (Equation 3.4).

$$M1 = 1.0 \text{ for successful mission} \tag{3.4}$$

Mission 2 - Syringes: The required payload for M2 is a minimum of 10 syringes (Figure 4). The approximated dimensions of the syringes are stated in Table 2. The aircraft must complete 3 laps within five minutes. The score for this mission is a function of the number of syringes flown in relation to the flight time needed for 3 laps. As Equation 3.5 states, the score is computed as the ratio of the individual team score to the highest score reached out of all teams plus 1.

$$M2 = 1 + \frac{N\_\left(\frac{\#Syringes}{Time}\right)}{Max\_\left(\frac{\#Syringes}{Time}\right)} \tag{3.5}$$

Table 2: Payload composition for Mission 2

Sizing of syringe		
Outside diameter	**Total length**	**Weight**
0.95 in	5.22 in	0.65 oz

Figure 4: Syringe as payload for M2 [1, p.7]

Mission 3 - Vaccine Vial Packages: The required payload for M3 consists of a minimum of 1 vaccine vial package (Figure 5). The approximated dimensions of the vaccine vial packages are stated in Table 3. On the down wind leg of the pattern, a single vaccine vial package must be remotely deployed in the designated vaccine vial package drop area after the landing of the aircraft. The vaccine vial package must then be retrieved by a ground crew member and brought to the scoring table. One point is given for each successful deployment. A successful deployment only counts, if none of the three attached 25G shock sensors is activated. If at least one of the 25G shock sensors triggered, the deployment does not count as successful. There will be a ten-minute time window for this mission. Equation 3.6 shows that the resulting score for this mission is the ratio of the individual team score to the highest score reached out of all teams plus 2.

$$M3 = 2 + \frac{N\_(\#Successful\ Deployments)}{Max\_(\#Successful\ Deployments)} \tag{3.6}$$

Table 3: Payload composition for Mission 3 [1, p.4]

Sizing of vaccine vial package			
Lenght	**Width**	**Heigth**	**Weight**
3.50 $\pm$ 0.13 in	2.50 $\pm$ 0.13 in	3.00 $\pm$ 0.13	8.00 $\pm$ 0.10 oz

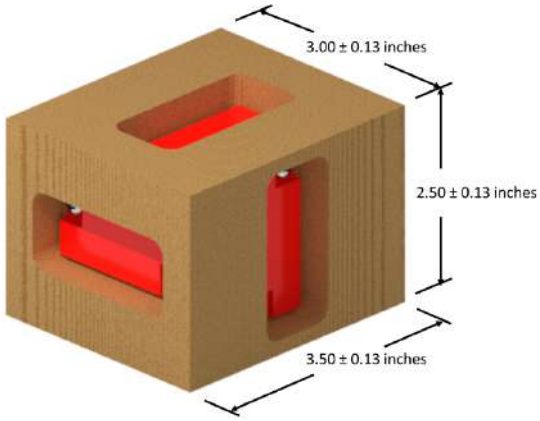

Figure 5: Vaccine vial package as payload for M3 [1, p.8]

3.2 General Requirements and Restrictions

The general requirements and restrictions for the aircraft as stated in the official rules [1], were summarized in a compliance matrix depicted in Table 4. The matrix is structured according to the three main divisions *Avionics & Propulsion*, *Aerodynamics*, and *Fuselage & Deployment mechanism* which correspond to the *Engineering & Design* sub-teams and the division *Takeoff*. To be able to check whether the final design fulfills all requirements, an adequate means of compliance (MoC) was defined in the right column, where T stands for test and R for review of design. As the team focused exclusively on compliant requirements, the state of compliance (SoC) is compliant (C) for all listed requirements.

Table 4: System compliance matrix

Division	Requirement	MoC	SoC
General	• Must be unmanned.	R	C
	• Must be flown in the same configuration for all missions.	R	C
	• All structures/components must stay with the aircraft at all times during flight.	R	C
	• Aircraft TOGW (takeoff gross weight with payload) must be less than 55 lb.	R	C
	• Must be flown by a human pilot. Autopilots are not allowed.	R	C
	• Cannot be flown FPV for competition.	R	C
Sizing	• Assembled aircraft in flight configuration must fit inside an 8 ft x 8 ft box.	R	C
Avionics & Propulsion	**Avionics**		
	• Aircraft must be radio controlled.	R	C
	• Aircraft must have an externally accessible switch to turn on the radio control system.	R	C
	• Aircraft must have an externally accessible mechanical motor arming system.	R	C
	• The arming system must be hard mounted on the outside of the aircraft.	R	C
	• Must use either NiCd/NiMH or Lithium-Polymer (LiPo) batteries.	R	C
	Propulsion		
	• Aircraft must be propeller driven and electrically powered.	R	C
	• Propulsion battery must be a separate one from the receiver/flight controls battery.	R	C
	• Must use either NiCd/NiMH or Lithium Polymer (LiPo) batteries.	R	C
	• One battery type must be used for propulsion.	R	C
	• Propulsion power total stored energy must be below 100 watt-hours.	R	C
	• Motor must be an unmodified over-the-counter model electric motor.	R	C
	• Aircraft propulsion must be disarmed during Ground Mission.	R	C
Aerodynamics	• Must use commercially produced propellers/blades.	R	C
	• Must pass wing tip load test in the flight configuration.	T	C
Fuselage & Deployment Mechanism	• All payloads must be carried internally to the aircraft.	R	C
	• The minimum number of syringes that must be flown in Mission 2 is ten (10).	R	C
	• Aircraft must remotely release/deploy one (1) vaccine vial package for Mission 3.	T	C
	• Max. number of M3 payload is defined by M2 payload and Tech Inspection statement.	R	C
	• Separate fixtures, jigs, racks etc. must stay on the aircraft during all mission phases.	R	C
	• Safety critical items (external doors, access panels, etc.) must be free of magnets.	R	C
	• Method of carrying the syringes must maintain a constant CG of the airplane.	T	C
Takeoff	• Must use ground rolling takeoff and landing.	R	C
	• Must takeoff within 25 feet of the start/finish line.	T	C
	• All energy for takeoff must come from the onboard propulsion battery pack(s).	R	C
	• All ground contact points of the aircraft must be forward of the start/finish line.	R	C

In addition to the general requirements and restrictions, the scope for the freedom of design was identified by specifying all allowances explicitly mentioned in the official rules [1] in Table 5. The allowance matrix summarizes all components, configurations, and modifications which are allowed in the competition.

Table 5: Allowance matrix

Division	Allowance
General	• May be of any configuration except rotary wing or lighter-than-air.
Sizing	• Aircraft size may vary between hangar storage and flight configuration.
Avionics & Propulsion	**Avionics** • Battery type may differ from propulsion battery type. • Battery configurations may vary between missions. • The mechanical motor arming system may be a "blade"-style fuse or an arming plug. • Commercially procured (COTS) flight stabilization systems and gyros are allowed. • A secondary transmitter/radio is allowed. **Propulsion** • Motors may be any commercial brush or brushless electric motor. • Motors may be direct drive or with gear or belt reduction. • May use multiple motors. • Systems to assist in un/loading the payloads can be activated during Ground Mission.
Aerodynamics	• May use multiple propellers. • Propeller can have folding blades. • Propeller diameter may be modified by clipping the tip. • Propellers may be balanced by painting the blades. • Commercially ducted fan units are allowed. • Propeller diameter/pitch may be changed for each flight attempt.
Fuselage & Deployment mechanism	• The payload compartment may be open as long as the payload is within the fuselage. • Devices for loading payloads are allowed. • Devices for securing the payload (fixtures, jigs, protective materials, etc.) are allowed. • Ballast can be configured differently for each mission to maintain stable flight. • Mission specific components can be restrained or secured during other missions. • There is no upper limit on the number of syringes that can be flown in Mission 2. • There are no specific requirements to restrain the syringes. • There is no requirement to drop all carried vaccine vial packages.
Takeoff	• Landing gear brakes can restrain aircraft during power up.

3.3 Translation of Mission Requirements into Design Requirements

In addition to the general requirements and restrictions, the aircraft's sub-systems had to meet the following design requirements derived from the mission requirements Table 6.

Table 6: Translation of the mission requirements into design requirements

Mission	Score	Flight Description	Subsystem Requirement
GM	$GM = \frac{Fastest\ Time}{Time}$	Loading of M2 payload. Unloading of M2 and loading of M3 payload. Deployment of vaccine vial packages one at a time.	Fast payload loading capability. Fast payload unloading capability. Functional and fast deployment mechanism. Easy access to payload.
M1	$M1 = 1.0 \quad for\ successful\ mission$	No payload. Takeoff within 25 ft. Complete 3 laps within the 5-minute time window. Land safely.	Short takeoff capability. Stable flight capability. Reliable and strong landing gear.
M2	$M2 = 1 + \frac{N\_\left(\frac{\#Syringes}{Time}\right)}{Max\_\left(\frac{\#Syringes}{Time}\right)}$	Payload is a minimum of 10 syringes. Takeoff within 25 ft. Complete 3 laps with payload as fast as possible. Be faster than the 10-minute flight window. Land safely.	Sufficient payload compartment. Short takeoff capability. Stable flight capability. Fast speed capability. Reliable and strong landing gear.
M3	$M3 = 2 + \frac{N\_(\#Successful\ Deployments)}{Max\_(\#Successful\ Deployments)}$	Payload is a minimum of 1 vaccine vial package. Takeoff within 25 ft. 10-min flight window to safely deliver as many vaccine vial packages as targeted. Each lap consists of takeoff, flying the standard mission profile, landing, and deploying one vaccine vial package in the drop area. A new lap starts with a full stop at the start/finish line. Land safely.	Sufficient payload compartment. Short takeoff capability. Safe unloading of vaccine vial packages. Payload must not be exposed to forces greater than 25G. Stable flight capability. Functional and fast deployment mechanism. Reliable and strong landing gear.

3.4 Flight and Ground Score Sensitivity Analyses

To further asses the design range of the model aircraft and determine the most beneficial approach for maximizing the total score, flight and ground score sensitivity analyses were conducted with the help of an analytic model in the numerical computing software MATLAB® [2]. First, the payload for M3 was chosen as the main limiting factor for all missions. As the maximum number of deployed vaccine vial packages is mainly restricted by the 10-minute time window for M3, the maximum number possible was defined by considering the aircraft's speed and thus estimating the maximum number of possible flight laps. To estimate a reasonable number of flight laps, the average lap time and average cruise speed of previous jA DBF aircraft depicted in Table 7 were referred to for comparison.

Table 7: Average speed and lap times of previous jA DBF aircraft

			
jA DBF aircraft	**Bobby DBF19**	**Mosquito DBF20**	**Stingray DBF21**
Average speed in ft/s	66	65	127
Average lap time in s	37	42	36

Taking into account the average lap time of 38 seconds and a safety factor of around 50%, 1 minute per lap results as realistic flight time excluding takeoff, landing, and ground handling. Based on previous competition years and experiences, the required time for the remaining lap phases can be assumed with 10 seconds each. When dividing the M3 time limitation (t_{M3}) by the required total lap time, Equation 3.7 shows that the number of packages to be delivered in 10 minutes will not exceed the maximum of 6.

$$QTY_{packages,max} = \frac{t_{M3}}{t_{takeoff} + t_{lap} + t_{landing} + t_{deployment}} = \frac{600\ seconds}{(10 + 60 + 10 + 10)\ seconds} = 6 \tag{3.7}$$

In addition, the *Engineering & Design* team decided to prioritize a safe deployment of the packages over the possible quantity of deployments. Therefore, the conceptual design aims to carry and safely deploy 5 packages. Design parameters such as payload quantity, aircraft sizing, drag, and cruise speed were considered in the sensitivity flight score analysis. The scoring analysis revealed that the overall flight score is driven primarily by the M3 score, so that the team decided to design the aircraft around M3 requirements. Figure 6 shows the absolute change in the individual score of M2 and M3 in dependence of the number of syringes and vaccine vial packages deployed. As this assumed flight time limits the maximum number of vaccine vial packages which can be deployed successfully, the team estimated a maximal payload of 80 syringes and 5 vaccine vial packages.

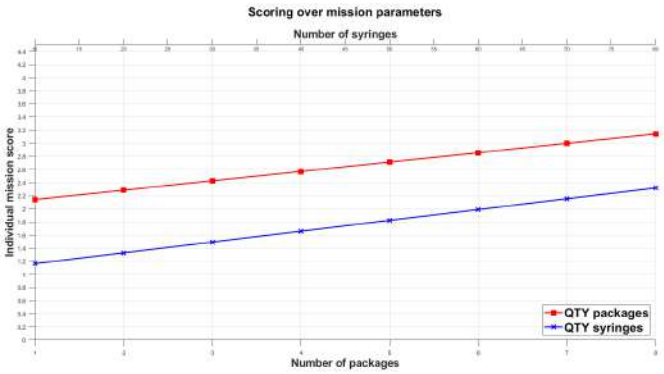

Figure 6: Mission equilibrium

3.5 Configurations Considered, Concept Weighting, and Selection Process

In the following, the configurations considered for aircraft design, tail design, wing placement, payload placement, propulsion placement, and the landing gear design are outlined. In order to evaluate each concept and to identify the optimal configuration, a FoM analysis was conducted. Prior to the analysis, following quantities listed in Table 8 were defined as figures of merit characterizing the performance and effectiveness of each configuration relative to their alternatives.

Table 8: Figures of merit

FoM Criteria	Score Factor	Reasoning
Ease of fabrication	5	Producibility, time efficiency, economics
Payload capacity	5	Payload optimum outweighs payload maximum
Payload safety	5	Driving factor for M2 and M3
Weight	5	Aircraft stability, strength, cargo capacity
Maneuverability	3	Pilot training and skills compensate for sensitivity
Payload accessibility	3	Driving factor for GM
Shock limitation	3	Driving factor for M3
Simplicity of design	3	Feasibility, GM and FM handling, economics
Velocity	3	Driving factor for M2
Efficiency	2	Focus on the required energy
Stability of flight	2	Pilot training and skills compensate for sensitivity

3.5.1 Conceptual Fuselage and Deployment Mechanism Design

For the conceptual design of the fuselage three different configurations each were considered for the type of aircraft, the payload placement, and the deployment mechanism.

3.5.1.1 Aircraft Configuration

Three aircraft configurations were weighted in the FoM analysis shown in Table 9: a blended wing-body, a biplane, and a conventional monoplane design. Although, the blended wing-body configuration is the fastest with the least drag, the high design complexity makes it difficult to fabricate. The biplane and conventional aircraft configurations offer similar properties. However, because of a second wing, the drag of a biplane is slightly bigger, with a decreased payload capacity. Therefore, the conventional monoplane configuration was selected. Out of all configurations considered, it is the easiest to be manufactured, offers the highest payload capacity, and has excellent velocity, and drag characteristics. Additionally, the structural arrangement of the monoplane configuration can be designed and adapted rapidly, ensuring flexibility during the development, manufacturing, and testing processes.

Table 9: FoM for the aircraft configuration

Blended wing-body		Biplane	Conventional
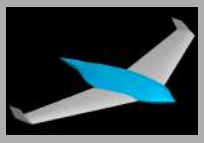		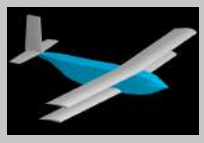	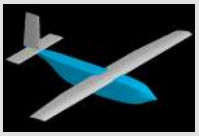
FoM criteria	Factor	Weighted value	
Ease of fabrication	5	1	2	3
Payload capacity	5	1	2	3
Velocity	3	3	1	2
Result		19	23	**36**

3.5.1.2 Payload Placement and Configuration

For the payload configuration inside the fuselage, all possible spatial directions were considered for M2 and M3 payloads. The vertical storage configuration accords with the yaw axis, the lateral storage configuration with the pitch axis, and the longitudinal storage configuration with the roll axis of the aircraft. However, it is detrimental if the frontal area of the fuselage is defined by the length of the syringes. In the third case, the payload capacity is limited by the ration between the length of the fuselage and the length of the syringes. Nevertheless, the number of syringes was considered sufficient which lead positioning the syringes in the longitudinal direction. For the positioning of the vaccine packages, the change of the center of gravity (CG) when a package gets dropped was the main factor. This shift was reduced by aligning the packages laterally which also resulted in the shortest and lightest deploy mechanism. Those results are congruent with the calculations in Table 10 and Table 11.

Table 10: FoM for the M2 payload configuration

Vertical storage		Lateral storage		Longitudinal storage
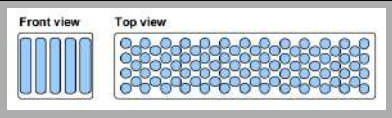		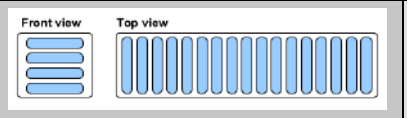		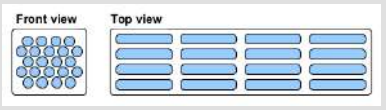
FoM criteria	Factor	Weighted Value		
Simplicity of design	3	1	1	3
Efficiency	2	1	1	3
Payload capacity	5	3	3	2
Result		20	20	**25**

Table 11: FoM for the M3 payload configuration

Vertical storage		Lateral storage		Longitudinal storage
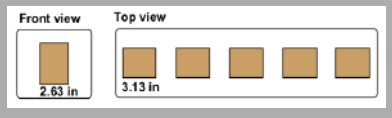		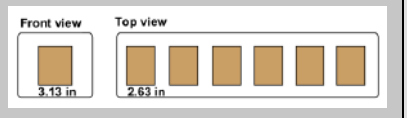		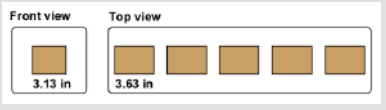
FoM criteria	Factor	Weighted value		
Simplicity of design	3	2	3	2
Weight	5	2	3	2
Stability of flight	2	1	3	1
Result		18	**30**	18

3.5.1.3 Deployment Mechanism Configuration

For the remote deployment system of the vaccine vial packages, three concepts were drafted for testing. All concepts are fully automatic and have been designed to deploy the vaccine vial packages in a controlled way. The initial system thought to be most promising (rail wagon system) did not agree with the M3 requirements published in the first DBF Q&A [3]. Therefore, the team decided to implement the conveyor belt system Table 12 as the second-most promising concept. The mechanism is beneficial as it assures a safe deployment of the M3 payload without exceeding the shock limitation and additionally improves the aircraft's stability by an easily adjustable center of gravity.

Table 12: FoM for the deployment mechanism configuration

Hatch door system			Rail wagon system	Conveyor belt system
FoM criteria	Factor	Weighted value		
Simplicity of design	3	1	3	2
Shock limitation	3	0	3	2
Stability of flight	2	1	1	2
Result		5	20	16

3.5.2 Conceptual Aerodynamics Design

For the conceptual aerodynamics design the wing placement, empennage configuration, and landing gear type were determined in a corresponding FoM analysis.

3.5.2.1 Wing Placement

A low-, mid-, and high-wing configuration were considered for the main wing position Table 13. Although the low-wing configuration offers the best payload accessibility, it lacks in payload capacity and stability. The main disadvantage of the mid-wing is that the wing root passes through the fuselage and interferes with the available space for the payload compartment. A high-wing configuration features mediocre payload accessibility but good payload capacity. However, out of all configurations considered, a high wing offers the best roll characteristics and thus the highest stability of flight and maneuverability.

Table 13: FoM for the wing configuration

Low-wing			Mid-wing	High-wing
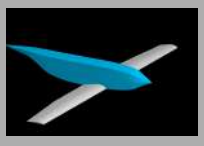				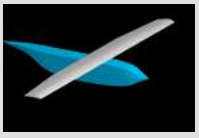
FoM criteria	Factor	Weighted value		
Payload accessibility	3	3	1	2
Payload capacity	5	2	1	3
Stability of flight	2	1	2	2
Result		21	12	**25**

3.5.2.2 Empennage Configuration

Three possible empennage configurations were compared: a conventional tail, a T-tail, and a V-tail in the corresponding FoM (see Table 14). The team decided on the conventional tail, as this type is not only easy to design and fabricate but also offers good stability and control at the required flight speed. Although the V-tail contributes to the least drag, it is the most difficult type to design and control with only two control surfaces used for pitching and yawing. A T-tail features similar drag coefficients as a conventional tail, with the advantage of being free from wing wake and vortices. However, T-tails are susceptible to deep stalling and are more difficult to manufacture to the same quality as a T-tail.

Table 14: FoM for the tail configuration

V-Tail		T-Tail		Conventional tail
				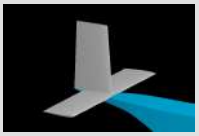
FoM criteria	Factor	Weighted value		
Simplicity of design	3	1	2	3
Velocity	3	3	2	2
Stability of flight	2	1	2	2
Result		14	16	**19**

3.5.2.3 Landing Gear Configuration

Three landing gear configurations were considered for the FoM in Table 15: a tail-wheel gear, a multiple-wheel gear, and a tricycle gear. As the weight and the difficulty of design increase with the number of wheels, more than three wheels were ineligible. A tricycle gear allows excellent stability with the main wheels being located behind the aircraft's CG. Furthermore, a tricycle configuration does not interfere with the deployment mechanism utilized in M3 and supports the aircraft to maintain stability during the remote deployment of the payload.

Table 15: FoM for the landing gear configuration

Tail-wheel gear		Multiple-wheel gear		Tricycle gear
FoM criteria	Factor	Weighted value		
Simplicity of design	3	2	1	3
Weight	5	4	1	3
Maneuverability	3	1	4	3
Result		29	20	**33**

3.5.3 Conceptual Avionics and Propulsion Design

To choose a conceptional design for the avionics and propulsion system following three possible configurations were considered in a FoM analysis: a pusher motor, a twin wing mounted configuration, and a tractor motor.

3.5.3.1 Propulsion Placement and Configuration

For the placement of the propulsion system, a tractor motor emerges as a result of the FoM analysis depicted in Table 16. The advantages of a tractor motor clearly outweigh the other configurations. Compared to a pusher and a twin wing-mounted configuration, a tractor mechanism is lightweight, easier to mount, and aerodynamically stable with a stabilized (fixed) CG. Furthermore, a pusher configuration can interfere with deployed packages which represents a red flag for this concept and makes it unuseable.

Table 16: FoM for the propulsion configuration

Pusher			Twin wing mounted	Tractor
FoM criteria	Factor	Weighted value		
Simplicity of design	5	2	1	4
Velocity	3	2	3	2
Efficiency	2	3	1	3
Result		22	16	**32**

3.6 Final Conceptual Design Configuration

The final configuration is a high-wing aircraft with a conventional empennage. It offers minimum loading time while allowing a high mission speed and high payload count. The aircraft has a tricycle landing gear and a tractor propulsion system. The final conceptual configuration is designed to carry 80 syringes and 5 vaccine vial packages. Using the assumed best capabilities of the other aircraft in the competition, this aircraft would be capable of achieving the mission scores summarized in Table 17. The calculation of the mission scores and final score were made according to the formulae contained in the competition rules [1]. Due to the fact that the calculation of the flight mission score also includes the mission performance parameters of the best-performing team of each mission, these values were assumed accordingly.

Table 17: Predicted mission scores

Aircraft	GM	M1	M2		M3
	Time in seconds		#Syringes	Time in seconds	#Successful Deployments
The *Hornet*	200	1	80	160	5
Assumed best	30	1	120	120	7
Personal mission score	0.15	1	1.5		2.71
Total personal mission score	**5.36**				

4 Preliminary Design

The preliminary design builds the concept chosen in the preceding chapter and focuses on meeting the general requirements as well as the design requirements. Based on the estimations made during the conceptual phase, an iterative design process led to the preliminary design. Frequent flight testing enabled the improvement of the design by comparing and adapting values gained through theoretical estimations and calculations with data points of real-world performance. The preliminary design provided a foundation for the detailed design as well as the final manufacturing plan.

4.1 Design and Analysis Methodology

The design and analysis methodology applied, is based on experiences of previous jA DBF competition teams, and well established methods. First a sensitivity study was carried out considering the technical constraints and rules. Several configurations and structures were taken into account to evaluate and set first design parameters. Empirical and numerical calculations were performed with the help of the software MATLAB® [2], the propulsion application eCalc [4], the airfoil analysis tool XFLR5 [5], and the computational fluid dynamics (CFD) software Ansys CFX [6].

First geometries were created in the computer aided design (CAD) software CATIA V5-6R2012 [7]. Based on the results obtained, the first design, and material data the maximum takeoff weight and wing area were estimated. The team has tested and verified various propulsion systems in combination with propeller diameters, to find out, which will meet the mission requirements best. Mission models were developed to simulate mission requirements and help improving design parameters for the preliminary analysis. Establishing compliance with the mission performance requirements allowed the team to tailor the aircraft's design trades to an optimum in the detailed design phase. Designing, manufacturing and flight testing the components and subsystems evaluated the performance. As seen in Figure 7 the process is highly iterative, improving every component and subsystem with every iteration, if the requirements are not met or lack to deliver satisfying performance.

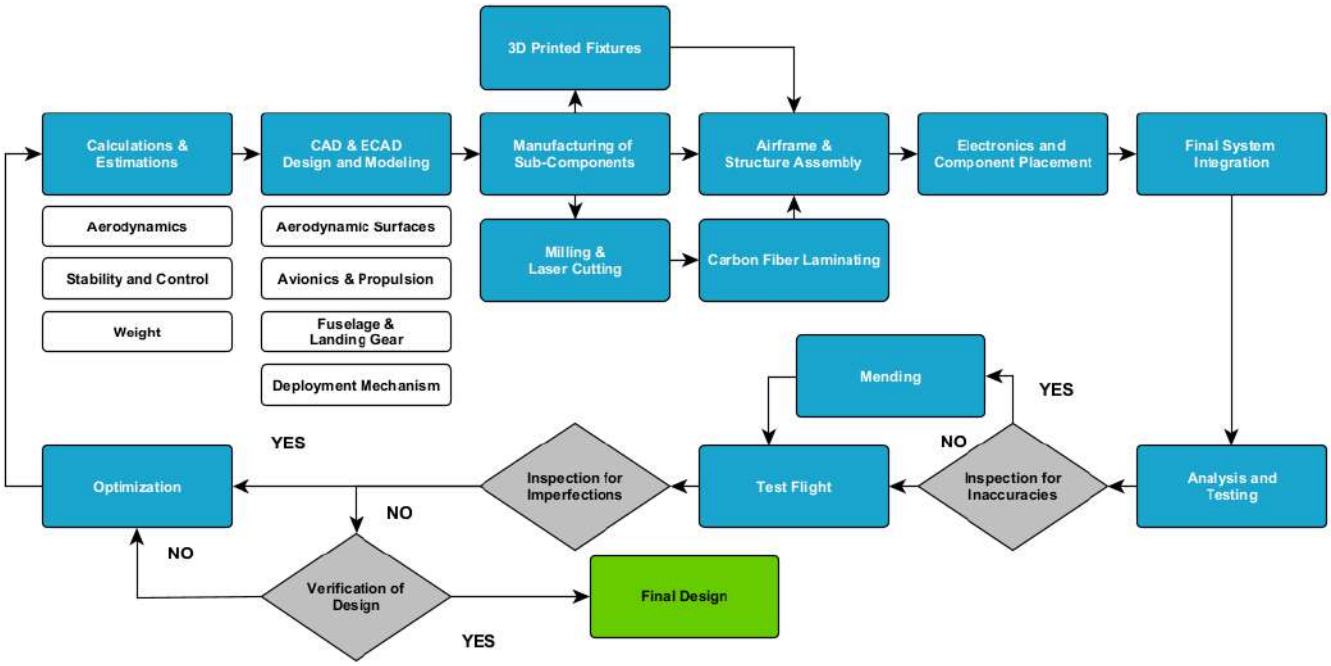

Figure 7: Design and analysis methodology

4.2 Design and Sizing Trades

During every iteration of the design process, design and sizing trades were performed. On the one hand, the goal was to reach a high scoring number while meeting the previously defined requirements and on the other hand to build a well-designed and well-performing aircraft. Initial trades were based on the final conceptual design configuration and preliminary estimations. The design was then adapted according to experiences and findings gained during the iterative design process. To reduce the risk of a structural failure of the aircraft during the contest, the robustness of the airframe was favored over its weight.

4.2.1 Preliminary Fuselage and Deployment Mechanism Design and Sizing

The preliminary fuselage and deployment mechanism was designed and sized considering the mission requirements for M2 and M3. The fuselage sizing was restricted to the maximal allowable dimensions of 8 ft, while the 25G drop sensors of the vaccine vial packages represented the biggest limitation for the design of the deployment mechanism.

4.2.1.1 Preliminary Fuselage Design and Sizing

The goal for the fuselage design and sizing was to find the optimum length and cross-sectional area at minimum weight and minimum drag characteristics. Furthermore, structural strength was deemed important, as the fuselage carries the payload and connects all components of the aircraft. The sizing mainly depended on the payload carried including all required avionics, the M2 and M3 payloads and the deployment mechanism. Therefore, the sizing was roughly estimated based on the M3 payload number and placement defined in the conceptual design. The total length of the fuselage was assumed to be 5 ft, with the estimated sizing of the sub-parts (cowling, avionics compartment, payload compartment, and tail section) depicted in Figure 8. The bottom rear end of the fuselage includes an adjustable hatch door for the deployment of the M3 payload.

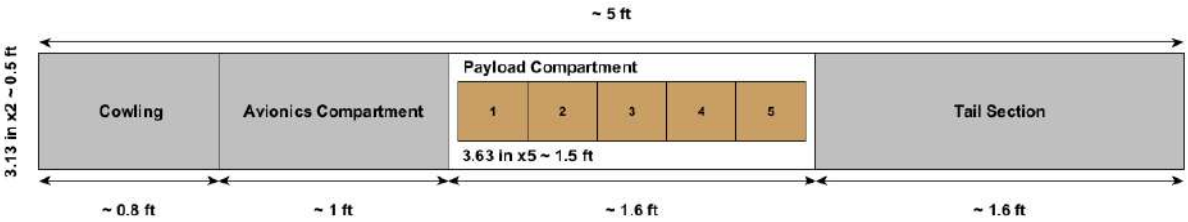

Figure 8: Top view of the preliminary fuselage sizing

For ensuring lightweight design and maximum structural strength, a carbon fiber reinforced sandwich structure was used. Based on experiences from previous competition years, the empty fuselage was estimated to weigh maximally 1.75 lb and to have a maximum takeoff weight (MTOW) of 16.50 lb. The preliminary design and sizing parameters for the fuselage are summarized in Table 18.

Table 18: Preliminary fuselage design and sizing parameters

Total length	Maximum width	Maximum height	Maximum empty weight	Maximum takeoff weight
5 ft	0.5 ft	0.5 ft	1.75 lb (28 oz)	16.50 lb (264 oz)

4.2.1.2 Deployment Mechanism Design and Sizing

For the remote deployment of the vaccine vial packages in M3, a conveyor belt system was agreed on in the conceptual design phase. The driving design factors for the deployment mechanism were sufficient space for the estimated number of packages, a locking mechanism for securing the payload during flight as well as the assurance of a fast and especially a safe deployment without exceeding the shock limitation of 25G. The conveyor belt system was planned to be positioned in the payload compartment of the fuselage reaching into the tail section of the aircraft. Its preliminary design was based on two parallel drive belts operated by a stepper motor-gear configuration. The packages are carried on the drive belts and can be deployed over a ramp through the open hatch door at the bottom rear end of the fuselage. For securing the M3 payload in all axes, the following precautions were taken: two U-shaped shells at each side of the drive belts provide lateral guidance and fixture, nobs on the drive belt hinder longitudinal movements, and a rod mounted above the packages restrains them from moving vertically. To minimize additional weight, most of the sub-components are 3D-printed. The preliminary design and sizing parameters for the deployment mechanism are summarized in Table 19.

Table 19: Preliminary deployment mechanism design and sizing parameters

Total length	Maximum width	Maximum height	Maximum empty weight	Maximum weight with M3 payload
1.6 ft	0.4 ft	0.3 ft	2.5 lb (40 oz)	5 lb (80 oz)

4.2.2 Preliminary Aerodynamic Surface Design and Sizing

The aerodynamic configuration was based on the main design criteria for lifting and control surfaces, first assumptions, and ongoing improvements. First empirical estimations of the sizing and aerodynamic performance were conducted in MATLAB® [2], which later also served the analysis and comparison of several airfoils. The airfoil analysis tool XFLR5 [5] was applied to analyze the performance of several airfoils and high-lift devices as well as to compute the static and dynamic stability derivatives.

4.2.2.1 Preliminary Wing Design and Sizing

Generally spoken, the most critical phase during a flight is the takeoff phase. The goal for the design of the wing shape was to generate sufficient lift for lifting the aircraft with its estimated MTOW of 16.50 lb. As shown in Equation 4.1, the lift coefficient (C_L) and the wing area (S_{ref}) need to be as high as possible for a high lift force (F_L).

$$F_L = \frac{1}{2} \cdot \rho \cdot C_L \cdot v^2 \cdot S_{ref} \quad \longrightarrow \quad C_L = \frac{2 \cdot F_L}{\rho \cdot v^2 \cdot S_{ref}} \tag{4.1}$$

To achieve the highest possible wing reference area and for reasons such as a low wing loading, lower stall velocity, design simplicity, and ease of manufacturing, it was decided that the initial wing would be rectangular rather than tapered. Based on the estimated MTOW of 264 oz, the wing area was estimated by considering the maximum wing cube loading (WCL). The WCL is generally used to group aircraft by similar flight characteristics. Assuming the aircraft with a typical WCL for advanced scaled model airplanes equal to 12 [8], and by rearranging the formula for the WCL (Equation 4.2), a planform area of approximately 990 in^2 can be derived.

$$WCL = MTOW \cdot \left(\frac{S_{ref}}{144}\right)^{-\frac{3}{2}} \quad \longrightarrow \quad S_{ref} = 144 \cdot \left(\frac{MTOW}{WCL}\right)^{\frac{3}{2}} \tag{4.2}$$

The next consideration was the wingspan, which was chosen based on the goal of improving the lift characteristics of the wing. Good lift characteristics are indicated by a high C_L/C_D ratio. As shown in Equations 4.3 and 4.4, the lift-induced drag $C_{D,I}$ can be reduced by minimizing the so-called k factor, also known as the induced drag factor, which behaves inversely proportional to the aspect ratio (AR). Therefore, it is reasonable to maximize the AR.

$$C_{D,I} = (C_L)^2 \cdot k \tag{4.3}$$

$$k = \frac{1}{\pi \cdot e \cdot AR} \tag{4.4}$$

When considering a rectangular wing, the AR can be increased by maximizing the wingspan-to-chord length ratio as depicted in Equation 4.5.

$$AR = \frac{b^2}{S_{ref}} = \frac{b^2}{b \cdot c} = \frac{b}{c} \tag{4.5}$$

This was achieved by exploiting the allowable maximum outer linear dimensions of 8 ft. To remain within the allowable wingspan maximum during manufacturing, a safety factor of approximately 6% was subtracted from the allowable wingspan maximum, which resulted in a wingspan of 7.5 ft. Finally, a chord length of 11 inches was calculated based on the higher end of the range recommended for RC aircraft, which reaches from 5 to 8 [9]. The preliminary design and sizing parameters for the wing are summarized in Table 20.

Table 20: Preliminary wing design and sizing parameters

WCL	Area	Span	Chord length	AR	Sweep angle	Taper ratio	Incidence angle	Weight
12	990 sqr. in	7.5 ft (90 in)	11 in	8	0	1	2°	2.5 lb (40 oz)

4.2.2.2 Airfoil Selection

Apart from defining the wing size, selecting an optimal airfoil is an important step in determining flight characteristics and maximizing mission scores. To select the optimal airfoil, various airfoils of previous jA team reports and winning competition reports were analyzed, compared, and filtered according to their characteristics and the design criteria. Regarding the design criteria, the difficulty lays in designing a wing which suits the different flight envelopes of all three flight missions. As specified in the conceptual design phase, the main design criteria for the airfoil selection were the required 25 ft takeoff distance and the estimated aircraft cruise velocity of 50 mph. Thus, an ideal airfoil has a high Cl/Cd ratio at cruise and produces sufficient lift for takeoff. For low drag characteristics, the airfoil geometry must be considered, as it directly influences the pressure distribution over the airfoil surface and thus the $C_{D,I}$. This includes the thickness and camber of the airfoil as well as the point where the maximum values appear respective to the chord length. For example, the cambered airfoil has a higher drag than the uncambered airfoil at low C_L [10].

In addition to excellent aerodynamic characteristics, the wing had to be easy to fabricate. Especially high curvatures and sharp trailing edges are difficult to manufacture and can cause imperfections in the surfaces of an airfoil. These imperfections can have unpleasant impacts on airfoil performance. Therefore, simple airfoil designs are preferred over complex geometries. In case of turbulences and hard landings, the airfoil had to be well-tempered to compensate for loads above the maximum load limit and ensure the safety of the aircraft itself and its payload for M2 and M3. M3 represents a bottle neck for the maximum load limit, as the M3 payload must not be exposed to shocks greater than 25G in all spatial directions.

The airfoil analysis was conducted in XFLR5 [5] at a Reynolds number estimate of 340,000. Table 21 states the design and aerodynamic parameters of the most promising airfoils in alphabetical order: ClarkY, HQ3.0/12, NACA2412, MH114, and SD7062. Results were then plotted in MATLAB® [2] as depicted in Figure 9.

Table 21: Airfoil comparison

Parameter	ClarkY	HQ 3.0/12	MH114	NACA 2412	SD7062
Points	121	77	68	99	61
Max. thickness in %	11.71	11.98	13.06	12.00	13.98
Max. thickness at chord length in %	28.03	35.04	30.03	29.03	27.15
Max. camber in %	3.43	2.99	6.58	2.00	3.97
Max. camber at chord length in %	42.04	50.05	48.15	39.54	38.76
Max. lift coefficient	1.41	1.23	1.77	1.31	1.61
Min. drag coefficient	0.17	0.24	0.14	0.24	0.12
Crit. angle of attack in degrees	13.25	12.50	14.00	13.75	14.75
Max. lift/drag ratio	88.18	99.51	114.52	80.39	88.26
AoA at max. lift/drag ratio in degrees	4.00	4.75	4.75	5.75	6.75
Lift slope in degrees^{-1}	0.03	0.02	0.02	0.02	0.03
Zero lift angle in degrees	-3.75	-3.75	-10.00	-2.25	-4.00

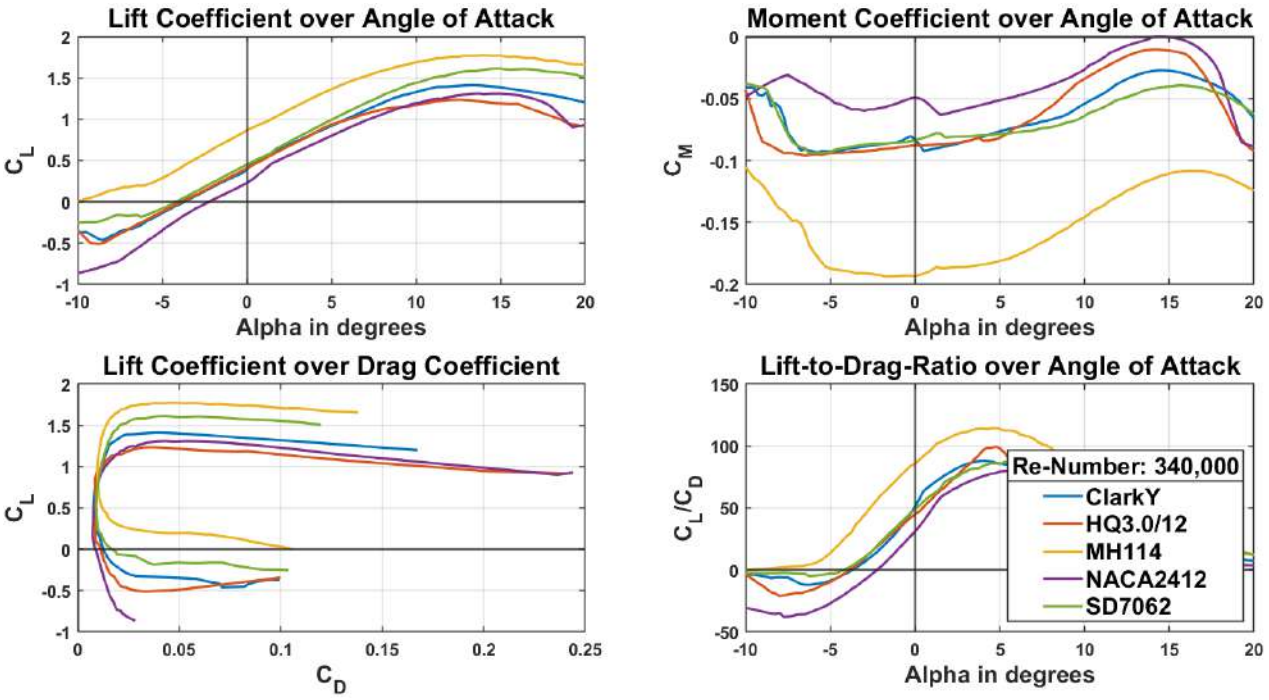

Figure 9: Airfoil comparison

Finally, the Selig/Donovan SD7062 (14%) airfoil (Figure 10) was selected, as it best met the design criteria. Its thickness-to-chord ratio and camber are 14% and 4%, respectively. Designed by Selig and Donovan, this profile is suitable for aircraft applications at low Reynolds numbers [12]. Especially, its high lift and soft stall behaviour are crucial for our application. Compared to all the considered airfoils, the SD7062 has the highest critical angle of attack at 14.75 degrees.

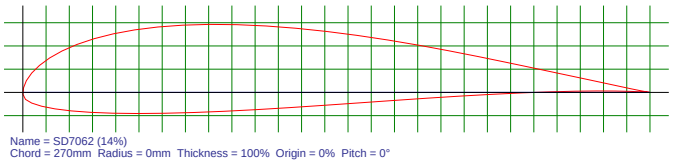

Figure 10: SD7062 airfoil geometry, 11 in chord [11, n.pag]

4.2.2.3 Preliminary Empennage Design and Sizing

The empennage was designed to withstand disturbances and control the aircraft. As defined in the conceptual design, a conventional tail configuration was selected. First thoughts on the design and sizing of the empennage were based on formulae by Raymer [13] and recommendations from the automotive and aeronautical engineering department of the Hamburg University of Applied Sciences (HAW Hamburg) [14]. The first step in designing the empennage was to estimate the surface reference areas (S_H and S_V) by assuming the tail volume coefficients (c_H and c_V) and the tail lever arms (l_H and l_V) according to Equation 4.6 and Equation 4.7. The tail volume coefficients were assumed based on tabular data for a home-built aircraft given in Raymer [13]. For the chosen conceptual aircraft configuration with the propeller in front of the fuselage, the tail lever arms were assumed to equal 60% of the estimated fuselage length of 5 ft.

$$S_H = \frac{c_H \cdot MAC_W \cdot S_W}{l_H} \quad (4.6) \qquad S_V = \frac{c_V \cdot b_W \cdot S_W}{l_V} \quad (4.7)$$

Based on the surface reference areas, it was possible approximating the span and the mean aerodynamic chord length (MAC) of the horizontal and the vertical tailplane by approximating the aspect ratios (AR_H and AR_V).

While the aspect ratio of the horizontal tailplane was assumed to equal about half of the aspect ratio of the wing, the aspect ratio of the vertical tailplane was assumed to be 1.5. When positioning the empennage, the horizontal tailplane had to be prevented by being affected by the slipstream of the wing. As the slipstream of sub-sonic aircraft is within smaller range, the position of the horizontal tailplane was chosen to be at the same height as the wing with sufficient distance to the trailing edge. For both, the horizontal and the vertical stabilizer the symmetrical airfoil NACA0010 was chosen. The preliminary design and sizing parameters for the empennage are summarized in Table 22.

Table 22: Preliminary empennage design and sizing parameters

Aerodynamic surface	Tail Volume Coefficient	Lever Arm	Area	AR	Span	MAC	Sweep Angle	Taper Ratio	Airfoil	Incidence Angle	Weight
Horizontal stabilizer	0.6	36 in	182 sqr. in	4	27 in	7 in	0	1	NACA0010	-1.5°	0.35 lb (5.6 oz)
Vertical stabilizer	0.03	36 in	50 sqr. in	1.5	9 in	6 in	14°	0.6	NACA0010	0	0.15 lb (2.4 oz)

4.2.2.4 Preliminary Control Surface Design and Sizing

The primary control surfaces consist of two ailerons, one elevator, and one rudder. Initial design and sizing were conducted following guidelines by Raymer [13]. The ailerons were designed based on the estimated roll moment coefficient and the preliminary wing dimensions. The total aileron span was assumed extending from about 50% to about 90% of the estimated wingspan. The chord length was then assumed based on a total aileron span-to-wingspan ratio of 0.4, an aileron chord-to-wing chord ratio of 0.27, and the estimated wing chord. With the assumptions made, one aileron reaches on each side of the wing from the wing tip with a span of 18 inches and from the trailing edge with a chord length of 3 inches. Both the rudder and the elevator were designed considering the preliminary empennage dimensions, the downwash of the wing, and relevant moment coefficients. To reduce the elevators' tendency to flutter and to facilitate the joint actuation of the elevators, the left and right elevator were combined into one single elevator. Therefore, it extends from one tip of the horizontal tailplane to the other, reaching along the estimated total span of the horizontal stabilizer. The rudder was sized and positioned to avoid the wake of the horizontal stabilizer with a span measuring approximately 90% of the vertical tailplane. The chord of the rudder and the elevator is about 30% of the tail chord. The preliminary design and sizing parameters for the primary control surfaces are summarized in Table 23.

Table 23: Preliminary control surface design and sizing parameters

Control Surface	Total span	MAC	Area	Max. upward deflection	Max. downward deflection
Ailerons	36 in	3 in	108 sqr in	35°	15°
Elevator	27 in	2 in	54 sqr in	15°	20°
Rudder	8 in	2 in	16 sqr in	10°	10°

4.2.2.5 Preliminary High-Lift Device Design and Sizing

Two flaps – one on each side of the wing – were implemented to increase the camber and surface area of the wing and thus the generated lift. For a large maximum lift coefficient, the flap span was defined as large as possible. The flaps are located near the root of the wing occupying the part of the wingspan inboard of the ailerons with an assumed total flap span and assumed chord length equal to the preliminary sizing of the ailerons (see Table 23). These sizing parameters are also based on the guidelines by Raymer [13]. The configured maximum deflection of the flaps is 40 degrees, which results in a 50% higher lift coefficient at a lower AoA compared to a wing without flaps. It is planned to use the flaps only during takeoff and landing.

4.2.2.6 Preliminary Winglet Design and Sizing

To improve the low speed-to-drag characteristics of the aircraft, the team introduced winglets to its design, as they maximize the lift and decrease the induced drag of the wing. Not only do winglets increase the wingspan from 0.6% to 0.75% with respect to the winglet's height and, therefore, the wing effective aspect ratio but they can also reduce the leakage of the airflow around the wingtip. The initially chosen geometry of the wing and the winglets was interactively adapted and further optimized with the help of several CFD simulations in Ansys CFX [6]. The wing geometries both with and without winglets were integrated into an isothermal flow simulation with respect to different angles of attack. In total, the *Aerodynamics & Stability* sub-team performed 52 individual simulations (50 continuous stationary and 2 transient flow simulations) in an angle of attack range from -5 up to +20 degrees. The general set-up and mesh remained the same for all simulations. A temperature of 77 °F and a Reynolds number of 340,000 were chosen. Figure 11 and Figure 12 indicate the mesh quality depicted on the left the defined fluid domain with its four sub-domains (inlet domain, domain of interest, outlet domain, and symmetry domain), and, on the right, the inflation layers around the wing profile.

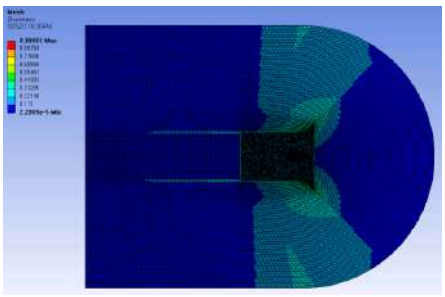

Figure 11: Skewness of the total mesh region

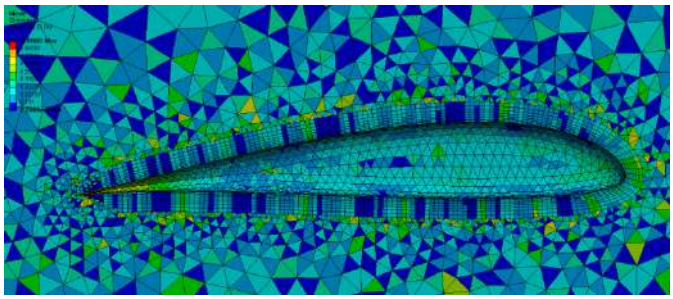

Figure 12: Inflation layers around the SD7062 profile

As output parameters, the normal force (F_N) and the tangential force (F_T) acting on the wing were specified. Based on these forces, the resulting aerodynamic forces and corresponding coefficients were calculated by applying the relations given in Equation 4.8 and Equation 4.9.

$$F_L = 2 \cdot (F_N \cdot \cos(\alpha) - F_T \cdot \sin(\alpha)) \qquad (4.8)$$

$$F_D = 2 \cdot (F_N \cdot \sin(\alpha) - F_T \cdot \cos(\alpha)) \qquad (4.9)$$

Based on the results obtained, the lift force, drag force, the corresponding coefficients, and the lift-to-drag ratio were determined over the defined angle of attack range. Furthermore, the critical angle of attack of the chosen wing geometry without winglets was found to be 14.98 degrees, which agrees with the 14.75 degrees given by XFLR5 [5]. Results above 15 degrees were identified to be invalid and not representative, as the wing begins to stall above the critical angle of attack. However, below the critical angle of attack, the wing with winglets proved to have better aerodynamic characteristics than the one without winglets. While both lift and drag increase with winglets, they lead to a significantly higher raise of lift.

4.2.3 Preliminary Landing Gear Design and Sizing

Based on certain aspects and advantages, the landing gear was designed as a tricycle landing gear. That configuration is ideal for taxiing and takeoff. It also reduces the risk of a ground loop. For M3, where the airplane is bound by the rules to stop in the drop-off zone for deployment, the landing gear is equipped with an electric brake system.

4.2.4 Preliminary Avionics and Propulsion Design and Sizing

The preliminary design for the avionics and propulsion system was sub-divided into the avionics system and the propulsion system, as two different battery configurations are required for the propulsion and other electronic components. Regarding the sizing of the power supplies, M3 was chosen as the limiting case because of the increased payload weight and the maximum number of laps to be completed. The maximum total operating time was derived from the targeted number of 5 laps to be completed in M3 which correspond to approximately 15 minutes. Based on the chosen battery configurations and the preliminary sizing of the aircraft an avionic harness was developed connecting the power supplies with all electrical components. In addition, safety components like fuses and arming plugs were integrated into the avionics and propulsion system for its faultless functionality.

4.2.4.1 Preliminary Avionics Design and Sizing

The preliminary avionics design served the purpose of identifying electrical components which are vital for the functionality of the aircraft. To successfully supply and operate the identified components, an adequate electronic power and control system had to be developed.

4.2.4.1.1 Servo motors and linkages

For the preliminary design a total number of eight servo motors were intended for actuating two ailerons, two flaps, the elevator, the rudder, the nose gear, and the hatch of the payload compartment. For the selection of the servo motor and the linkage type the maximum aerodynamic forces acting on the surfaces were considered. The maximum required torque (τ_{max}) was determined by inserting the assumed maximum speed (v_{max}) of 146 ft/s (100 mph), and the discussed control surface parameters in section 4.2.2.4 and section 4.2.2.5 such as the chord length (c), the span of the control surface (b_c), and the maximal control surface deflection ($S_{c,max}$), and the maximal servo deflection ($S_{s,max}$) into Equation 4.10.

$$\tau_{max} = 8.5 \cdot 10^{-6} \cdot \left[(v_{max})^2 \cdot c^2 \cdot b_c \cdot \sin\left(S_{c,max}\right) \cdot \frac{\tan\left(S_{c,max}\right)}{\tan\left(S_{s,max}\right)} \right] \tag{4.10}$$

It was found that, the two empennage control surfaces and the nose wheel encounter a smaller resistance than the flaps and ailerons. Based on the results obtained four KST X10mini V2 were chosen for operating the flaps and ailerons and three KST X08H Plus V5 servos for controlling the elevator, the rudder, and the nose wheel. In addition, the team decided to use glass fibre reinforced plastic (GFRP) control horns. As linkages 0.1 in threaded steel rods with clamps on both ends were implemented in the first prototype.

4.2.4.1.2 Avionics Power Supply

The avionics power supply must provide all system electronics with sufficient power during the operating time of the aircraft. Therefore, the total energy required was estimated by multiplying the total continuous current draw of all integrated system components with the assumed maximum operating time. The total energy required was estimated to be 2,000 mAh. To be safe a factor of 50% was added resulting in a total energy of 3,000 mAh.

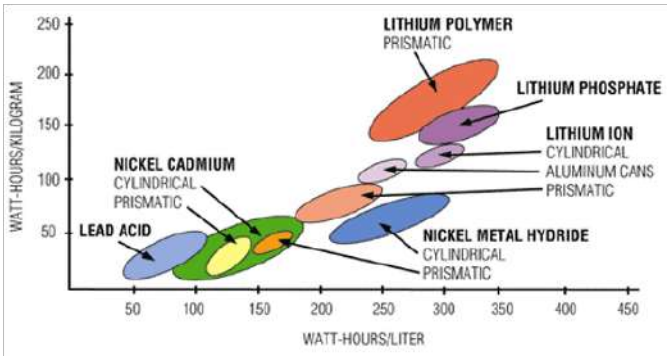

Figure 13: Energy densities of various battery types [**?**]

Having to choose one battery type for the aircraft's avionics system, Lithium-Polymer (LiPo) batteries were selected because they have a higher specific energy and provide a higher energy density than Nickel-Cadmium (NiCd) and Nickel Metal Hybrid (NiMH) batteries (see Figure 13). As stated by the official rules, the individual battery packs cannot exceed the FAA limits for hand carry on commercial air flights of a maximum total stored energy (P_{max}) equal to 100 watt-hours per battery pack [1]. Based on the fact, that the estimated total energy required was lower than this limit, it was decided that one single LiPo battery pack should be sufficient for the avionics power supply.

4.2.4.2 Preliminary Propulsion Design and Sizing

The preliminary propulsion design was aimed at choosing a reasonable motor, motor controller, battery, and propeller combination for providing the necessary power for takeoff and a respectable performance during flight. Based on the chosen conceptual propulsion placement and configuration (single tractor motor), a suitable combination for the motor, battery and propeller was calculated using the application eCalc [4]. At takeoff the motor, battery, and propeller combination must deliver sufficient thrust for lifting the aircraft with an estimated $MTOW$ equal to 16.55 lb within the maximum take off distance (s_{TO}) of 25 ft. To estimate the required total thrust, it was assumed that the aircraft takes off at a stall speed (V_{stall}) of 47 ft/s (32 mph), which was calculated with Equation 4.11. Based on this assumption, the required total thrust consists of the thrust component needed to accelerate the aircraft up to V_{stall} within the above stated s_{TO}, and F_T acting on the wing. The tangential force was directly derived from the previous described CFD simulation of the wing with winglets, and measures roughly 1 N at 2 degrees incidence angle of the wing. The second thrust component was calculated by inserting the V_{stall} into Newton's law of motion (Equation 4.12).

$$V_{stall} = \sqrt{\frac{2 \cdot MTOW \cdot g}{\rho \cdot S_{ref} \cdot C_{L,max}}} \qquad (4.11) \qquad F = m \cdot a = MTOW \cdot \left[\frac{(V_{stall})^2 - (v_0)^2}{2 \cdot s_{TO}}\right] \qquad (4.12)$$

With a resultant thrust force of 65 N, the motor, battery and propeller combination must produce a total thrust of approximately 66 N. For reasons stated above, LiPo batteries were also chosen for the battery type of the aircraft's propulsion system. As stated by the official rules, P_{max} for propulsion power cannot exceed 100 watt-hours [1]. Possible cell configurations could be determined using Joule's law (Equation 4.13), and knowing that a LiPo battery cell has a nominal voltage of 3.7 V [16].

$$P = U \cdot I \quad \longrightarrow \quad I = \frac{P}{U} \qquad (4.13)$$

Based on the results the two possible LiPo configurations depicted in Table 24 were up for decision.

Table 24: Propulsion battery pack options

Parameter	Option 1	Option 2
Maximum total energy	100 Wh	100 Wh
Nominal voltage per LiPo cell	3.7 V	3.7 V
Cell number	6S	8S
Nominal voltage	22.2 V	29.6 V
Nominal capacity	4,504.51 mAh	3,378.38 mAh

As 6S LiPo batteries with 4500 mAh (99.90 Wh) are rather common and nearly exploit the complete 100 Wh limitation, they were prioritized over the 8s which only were available in 3200 mAh (94.72 Wh).

Thus, the Hacker TopFuel ECO-X 6S LiPo with a nominal voltage of 22.2 V, a nominal capacity of 4,500 mAh, and a C-rating of 20 C was chosen for the preliminary propulsion battery pack. Knowing the propulsion battery configuration and the preliminary aircraft specifications a variety of motors and propellers was analyzed in eCalc [4]. With the results from eCalc [4] the *Avionics & Propulsion* team focused on motors by Hacker, Scorpion, and Dualsky, as these are known for their good performance. Finally, the choice fell on the Scorpion SII-4025-520 with 520 RPM per Volt because of its weight, size, static thrust, and its outstanding performance in the last year's DBF competition. With the chosen LiPo configuration, the motor can spin at 11,544 RPM, which equals the maximum angular frequency of around 1,209 s^{-1}. Additionally, three propellers to be tested in the further design process were selected. For speed control of the motor, a brushless electronic speed control (ESC) which met the current and voltage requirements of the motor was chosen. The preliminary propulsion package is summarized in Table 25.

Table 25: Preliminary propulsion package

Motor	ESC	Battery	Propellers		
Scorpion SII-4025-520	RCE-BL100A ESC 10A BEC	Hacker TopFuel ECO-X LiPo 6S 22,2/4500 20C MTAG	APC 14x10	APC 14x8.5	APC 15x8

4.2.4.3 Wiring Harness and Connectors

The wiring harness connects all sub-components of the avionics and propulsion system with their corresponding power supply. For the design of the wiring harness, several aspects such as the placement and the total weight of the wires were considered. The main design driver for the wiring harness was its influence on the flight characteristics as a poor design can lead to unnecessary additional weight or affect the induced aerodynamic moments. To mitigate the effects of the wiring harness on the aircraft's flight characteristics, it was decided that the total weight of the wires must be minimal and that the wiring must be designed symmetrical to the roll axis of the aircraft. Regarding weight reduction measures, wires with the same function were combined into one to avoid duplicated wiring and thus, unnecessary weight. For example, individual wires supplying several servos in the same wing section were combined into a single wire. For the choice of wires, the supply voltage of the main power supplies and the required supply voltage of each sub-component were considered. Based on the American wire gauge (AWG) system following minimal wire thicknesses were taken into account: AWG10 for main power routes, AWG14 for receiver to ESC, AWG18 for receiver to consumers, AWG25 for receiver to servos implemented in the wing, and AWG27 for receiver to servos placed inside the fuselage.

4.2.4.4 Fuses and arming systems

The implementation of safety components such as fuses and arming systems was considered to protect the avionics and propulsion system by disconnecting the battery packs in case that their normal current rating is exceeded. According to the official rules [1] each LiPo battery pack is required to have an individual fuse in line with the positive terminal. The selection of the fuse type was limited to the maximum continuous current rating, which had to be below the maximum continuous discharge current rating of the LiPo battery pack. The maximum allowable current (I_{max}) of one battery pack was calculated with Equation 4.14. Thus, for the envisaged LiPo batteries with a capacity of 4,500 mAh and a nominal discharge rate of 20 C I_{max} results as 90 A.

$$I_{max} = Capacity \cdot C\text{-}Rating = 4,500\,mAh \cdot 20\,C = 90A \tag{4.14}$$

First, bolt-down fuses were considered. However, bolt-down fuses are for single use only and were only available for 80 A applications. In contrast to bolt-down fuses, circuit breakers can be reset or disengaged at any time without

having to replace any component. Therefore, it was decided to implement circuit breakers. As additional safety factor the aircraft was required to have an externally accessible switch to turn on the radio control system and an independent mechanical motor arming system for the mechanical separation of the propulsion battery from the electric circuit. For both designs of the receiver (RX) switch, and the motor arming system it was decided, to adopt the design of last year's jA DBF aircraft with a RX toggle switch and a motor arming plug hard mounted on the outside of the fuselage.

4.2.4.5 Aircraft and deployment mechanism controls

For the remote control of the aircraft and the deployment mechanism one transmitter was considered to connect with one receiver. The receiver was determined to regulate the ESC, all servo motors, and a self-designed printed circuit board (PCB). Together with an on top mounted microcontrol unit (MCU), the PCB is designated to operate the brake system, and the stepper motor envisaged for the conveyor belt system.

4.3 Performance Prediction Methodology

The performance prediction methodology applied was based on a tabular mission model to simulate the flight performance, and the respective mission performance of the aircraft. Based on the preliminary design and with the help of the mission model the mission scores for M2 and M3 were estimated.

4.3.1 Description and capabilities

As the aircraft must complete the same flight course in each mission the flight can be divided into several flight phases. The overall performance can be estimated by assessing the performance of the aircraft in every flight phase. Altogether the following five phases, and representative parameters were defined:

- **Ground roll & takeoff**: For the first phase takeoff is assumed to be performed at maximum throttle setting using high-lift devices. It is possible to determine the required takeoff speed and distance of each mission considering the thrust-to-weight ratio. Additionally, the stall velocity is estimated based on the critical angle of attack.
- **Transition to climb & climb:** During the climb phase the aircraft is assumed to climb 100 ft above ground level with a static rate of climb.
- **Cruise:** The cruise phase was divided into straight cruise and level turns.
  - **Straight cruise:** Straight cruise is defined to be a level, constant-speed flight without any maneuvering apart from compensating for gusts. For each mission, the optimum cruise thrust setting is selected in order not to exceed the nominal battery capacity.
  - **Level turns:** For both types of turning maneuvers (two 180° and one 360° turns), the coordinated level turns are assumed to be completed with a constant radius and speed of approximately 66 ft/s (45 mph).
- **Descent & landing**: The descent and landing phase plays a vital role in M3 as the aircraft must land with every completed lap. A precise landing on the runway close to the designated vaccine vial package drop area saves precious mission time by reducing the taxi distance. Therefore, the required landing distance and touch down speed are considered to estimate M3 performance. On the contrary, this phase must not be considered for M1 and M2, because the landing is not part of the mission time window. Here the descent is initiated after passing the finish line on the last lap and therefore performed without time pressure.

Additionally, following assumptions were made. The total lap distance of the flight course described in section 3.1.2 was assumed with 3,000 ft. For the mission model following general formulas for the Reynolds number (Equation 4.15) and the fluid dynamic pressure at a temperature of 59 °F (Equation 4.16) were applied. As characteristic lengths the length L was considered for the fuselage and the mean aerodynamic chord (MAC) for all aerodynamic surfaces.

$$Re = \frac{\rho \cdot v \cdot L}{\mu} \tag{4.15}$$

$$q = \frac{1}{2} \cdot \rho \cdot v^2 \tag{4.16}$$

4.3.2 Uncertainties

Following uncertainties of the performance prediction methodology were determined: In general, the mission model applied does not depict the real world performance of the aircraft, as the model was mainly built upon assumptions, empirical methods, and numerical computations. Firstly, the assumed flight phases, and thus the representative parameters will slightly deviate for every lap in every flight mission. Secondly, the predicted takeoff distances were slightly underestimated because of inaccuracies of the rolling friction coefficient and takeoff drag coefficient. However, as the takeoff distance estimates had a large margin for error they were considered within safe bounds. Thirdly, the predicted flight distance does not represent the actual flight distance of the flight course, as deviations due to pilot error, and the turn radius of the aircraft were not considered. Additionally, the absolute score of the best performing team was a vague estimate, and is likely unattainable in practice. Lastly, and in addition to the previous aspects, environmental conditions, such as temperature, air density, and wind, may interfere with the actual performance due to geographical and seasonal differences. While flight tests were performed in the Austrian winter season, the contest is flown in Wichita during spring season, leading to uncertainties in the propeller efficiency, battery pack endurance, and thus in the maximum power from the propulsion system, and overall flight endurance. Geographical and seasonal differences identified between the location of design, manufacturing, and testing, and the contest location are listed in Table 26.

Table 26: Comparison of the design, manufacturing and test location with the contest location

Uncertainty	Graz, Styria, Austria, Europe	Wichita, Kansas, USA, America
Season of the year	Winter	Spring
Temperature	40 °F	59 °F
Wind	8 ft/s	27 ft/s
Gusts	No wind gusts	Regular wind gusts
Terrain	Alps, mountains	Flat land
Elevation of airfield	1,296 ft	1,378 ft

4.4 Aerodynamics and Stability Prediction

Estimates of the aircraft lift, drag, and stability characteristics were obtained through several analyses conducted in XFLR5 [5], Ansys CFX [6], and MATLAB® [2]. Empirical results were compared to observations from flight tests, and used to continuously improve the design of the *Hornet*. For validation purposes results obtained by the empirical method were compared to typical values found in literature and those gained through the CFD computation described in section 4.2.2.6.

4.4.1 Lift and Drag Prediction

A preliminary lift and drag analysis was conducted in MATLAB® [2] based on semi-empirical methods according to Raymer [13] and the automotive and aeronautical engineering department of the Hamburg University of Applied Sciences (HAW Hamburg) [14].

4.4.1.1 Lift Prediction

For predicting the lift of the aircraft the lift coefficient was estimated as the sum of the zero lift coefficient ($C_{L,0}$), and the lift curve slope ($C_{L,\alpha}$) multiplied with the angle of attack, Equation 4.17. The $C_{L,0}$ value for the SD7062 airfoil was derived with 0.45 from the database airfoil tools [17].

$$C_L = C_{L,0} + C_{L,\alpha} \cdot \alpha \tag{4.17}$$

To estimate $C_{L,\alpha}$ the Polhamus formula as given in Equation 4.18 was applied. The mach number term was neglected due to the low cruising speeds expected. The airfoil efficiency (η) was estimated with 95% [13].

$$C_{L,\alpha} = \frac{(2 \cdot \pi \cdot AR)}{2 + \sqrt{4 + \frac{AR^2}{\eta^2} \cdot \left(1 + (\tan \Lambda_{50})^2\right)}} \tag{4.18}$$

The resulting lift at the cruise and stall speed was then computed with Equation 4.1 given in section 4.2.2.1. Table 27 summarizes all relevant lift parameters. For the operating point an AoA of 2 degrees was chosen, as this is the angle of the wing inclination.

Table 27: Estimated lift parameters of the aircraft

	Mission 1	Mission 2	Mission 3
C_L at $\alpha = 2°$	0.6217	0.6223	0.6205
$C_{L,max}$	1.5660	1.5699	1.5585
Lift at chosen cruise speed and $\alpha = 0°$	106.05 N	130.92 N	64.15 N
Lift at chosen cruise speed and $\alpha = 2°$	146.51 N	181.05 N	88.46 N

4.4.1.2 Drag Prediction

In general, the drag of an aircraft is composed of two main sources of drag: induced drag and parasite drag (Equation 4.19). The general formula for the drag force (F_D) is given in Equation 4.20.

$$F_{D,tot} = F_{D,0} + F_{D,I} \tag{4.19}$$

$$F_D = q \cdot C_D \cdot S_{Ref} \tag{4.20}$$

To estimate the minimum total drag of the aircraft, the drag contributions of fuselage, wing, empennage, and landing gear were summed up over a flight velocity (v) ranging from 0 to 525 ft/s (358 mph). The applied method assumes that the drag contribution of an individual component itself is the sum of pressure drag, skin friction drag, miscellaneous drag, leak and protuberance drag, and induced drag. Therefore, the minimum total drag coefficient results with given Equation 4.21. Extra components such as the static front and rear landing gear were accounted for in the $C_{D,misc}$ term. Additionally, an 8% margin was added for leak and protuberance drag, $C_{D,L\&P}$.

$$C_{D,min} = C_{D,0} + C_{D,I} \quad with \quad C_{D,0} = C_{D,P} + C_{D,misc} + C_{D,L\&P} \tag{4.21}$$

As shown in Equation 4.22, the pressure drag coefficient ($C_{D,P}$) can be computed as a function of the Reynolds, adjusted skin-friction drag coefficient ($C_{f,c}$), a component form factor (FF_c), a component interference factor (Q_c), the component wetted area ($S_{wet,c}$), and the wing reference area (S_{ref}). During cruise flight the induced

drag coefficient ($C_{D,I}$) can be estimated assuming that the lift force is in equilibrium with the drag force ($F_L = F_D$). Therefore, $C_{D,I}$ for cruise flight results, when inserting the MTOW into the formula for the lift coefficient, as given in Equation 4.23. With an assumed MTOW of 16.50 lb, the induced weight force F_{MTOW} equals approximately 74 N. All computed drag coefficients were scaled to the wing reference area.

$$C_{D,P} = \frac{\sum (C_{f,c} \cdot FF_c \cdot Q_c \cdot S_{wet,c})}{S_{ref}} \qquad (4.22)$$

$$C_{D,I} = \frac{1}{k} \cdot \left(\frac{2 \cdot F_{MTOW}}{\rho \cdot v^2 \cdot S_{ref}} \right)^2 \qquad (4.23)$$

As stated in Equation 4.24 a turbulent flow was considered over all aerodynamic surfaces, and the fuselage.

$$C_{f,turb} = \frac{0.455}{\log(Re)^{2.58}} \cdot 1.144^{-0.65} \qquad (4.24)$$

As stated above the mach number term was also neglected for the calculation of C_f. Table 28 lists the estimated drag components for every mission in accordance to the assumed cruise speed. In addition, the percentage composition of different drag types is illustrated in Figure 14. As expected the wing contributes to most of the drag because of its large sizing. The assumed decrease of cruise velocity resulted a in higher induced drag for M3.

Table 28: Estimated drag parameters of the aircraft

	Mission 1			Mission 2			Mission 3		
Cruise speed	82 ft/s (56 mph)			91 ft/s (62 mph)			64 ft/s (44 mph)		
	$C_{D,norm}$	D (N)	D $(\%)$	$C_{D,norm}$	D (N)	D $(\%)$	$C_{D,norm}$	D (N)	D $(\%)$
Component	**Pressure drag**								
Fuselage	0.0053	1.2533	16.43	0.0052	1.5192	15.99	0.0056	0.7924	14.51
Wing	0.0122	2.8737	37.67	0.0122	3.5414	37.27	0.0123	1.7471	31.99
Horizontal stabilizer	0.0025	0.5867	7.69	0.0025	0.7226	7.60	0.0025	0.3573	6.54
Vertical stabilizer	0.22	0.5073	6.65	0.0021	0.6246	6.57	0.0022	0.3092	5.66
	Miscellaneous drag								
Gear	0.0032	0.7614	9.98	0.0032	0.9386	9.88	0.0032	0.4625	8.47
Linkages and plugs	0.0028	0.6508	8.53	0.0028	0.8034	8.45	0.0028	0.3937	7.21
	Leakage and protuberances drag								
Estimated 8% margin	0.0023	0.5307	6.96	0.0022	0.6520	6.86	0.0023	0.3250	5.95
	Induced drag								
Wing	0.0020	0.4656	6.10	0.0024	0.7014	7.38	0.0075	1.0751	19.68
	Total minimum drag								
Total estimate	0.0324	7.6295	100	0.0327	9.5030	100	0.0383	5.4622	100

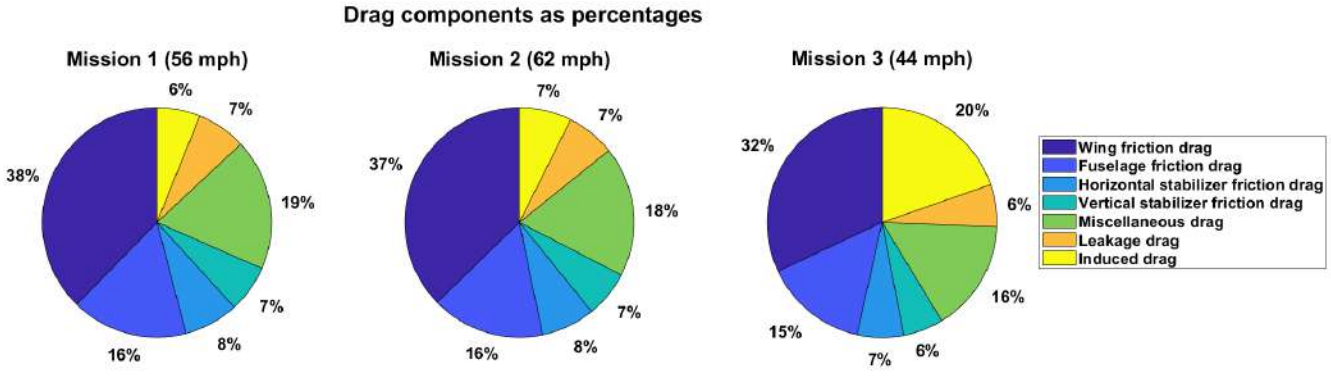

Figure 14: Graphical representation of the drag distribution

4.4.2 Stability Prediction

To ensure that the aircraft is stable during all three missions, several analyses on the static stability, the dynamic stability, and the stability and control have been conducted in XFLR5 [5]. M1 was simulated without payload. For the analysis of M2 and M3 the aircraft was examined having almost same weight, but a different weight distribution. As M3 payload gets unloaded at the end of every lap, the aircraft becomes lighter in every lap, and undergoes a weight shift. Due to the automatic unloading regulations, the team was not able to manually relocate the batteries during M3 flight tests to compensate for a shift in the CG. Thus, the weight distribution for M3 had to be checked with every deployment of a vaccine vial package. The team managed to compensate for the CG shift by shifting the payload with the conveyor belt after the deployment and at the beginning of every new lap. However, the difference between the CG of a fully loaded M3 configuration (Figure 15) and the empty M3 configuration (M3e) (Figure 16) could not be compensated for. Therefore, a weight shift had been considered when designing the plane and for the stability and control analysis. The three missions were analyzed with the following masses:

- M1: 13.25 lb
- M2: 16.50 lb
- M3 empty: 13.25 lb
- M3: 15.75 lb

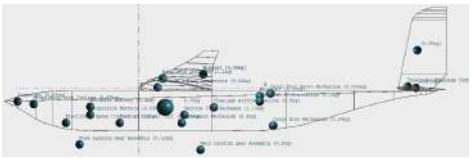

Figure 15: M3 weight distribution

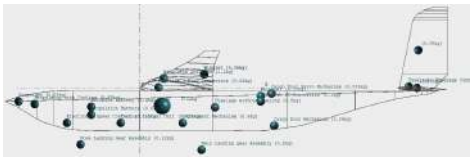

Figure 16: M3 empty weight distribution

The mass was distributed according to the Figures above establishing the CG at 1/3 of the chord length. The *Hornet* was designed to fit the typical tolerance range for transport aircraft which is 25% to 35% of the mean chord length from the leading edge of the wing [13, p.675].

4.4.2.1 Static Stability

As can be seen in the moment coefficient (C_M) over angle of attack plot depicted in Figure 17, the aerodynamic stability can be determined as stable. The aircraft's operating point in M1 is at C_M equal to zero. Figure 17 shows that alpha measures -1.15 degrees at the operating point. The higher slope resulting for M3 empty indicates a higher stability force [18]. Figure 18 indicates the value of the lift coefficient at the operating point being 0.4.

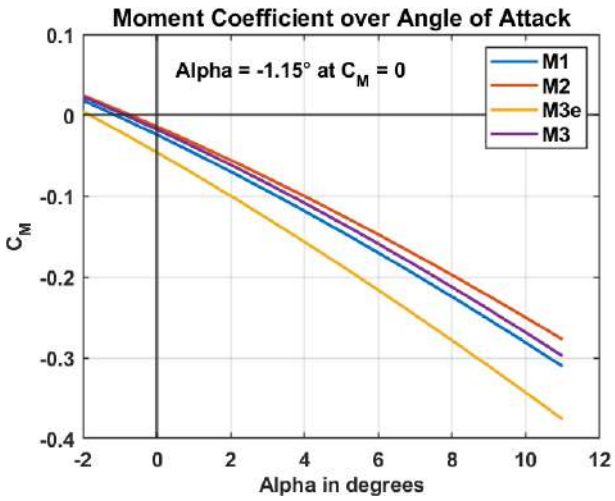

Figure 17: Moment coefficient over angle of attack

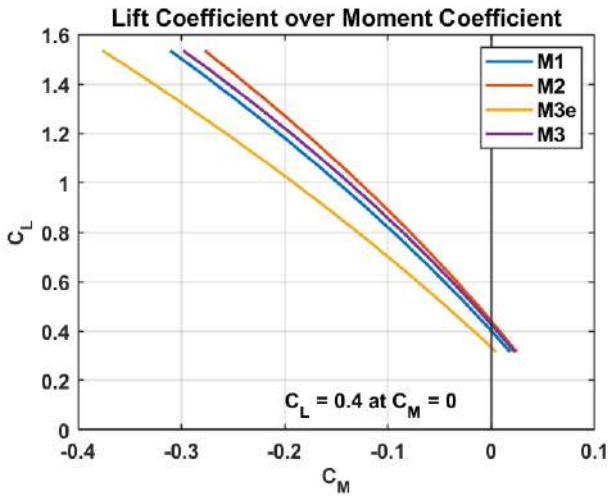

Figure 18: Lift coefficient over moment coefficient

4.4.2.2 Dynamic Stability

The dynamic behavior of the *Hornet* was analyzed in XFLR5 [5]. Table 29 list the available modes in XFLR5 [5]. For the longitudinal stability, and the lateral stability four modes can be analyzed each. The longitudinal stability consists of two symmetric phugoid modes and two symmetric short period modes, depicted in Figure 19, and Figure 20. The lateral stability features the spiral mode, the roll damping mode and two dutch roll modes, shown in Figure 21, and Figure 22.

Table 29: Dynamic stability modes

Mode type	Longitudinal stability	Lateral stability
Mode 1	Short period	Roll damping mode
Mode 2	Short period	Dutch roll mode
Mode 3	Phugoid	Dutch roll mode
Mode 4	Phugoid	Spiral mode

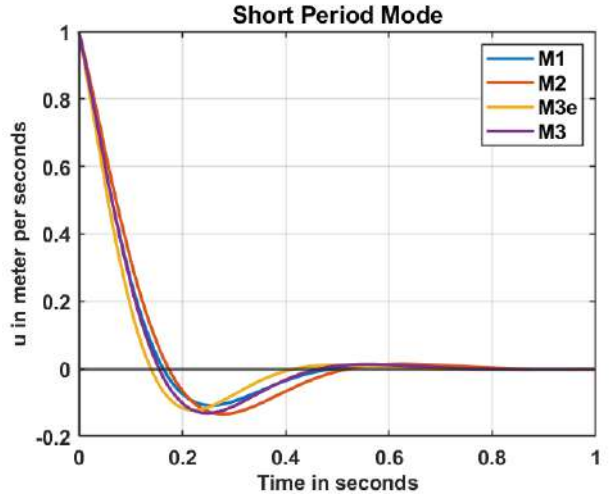

Figure 19: Time response plot of the short period mode

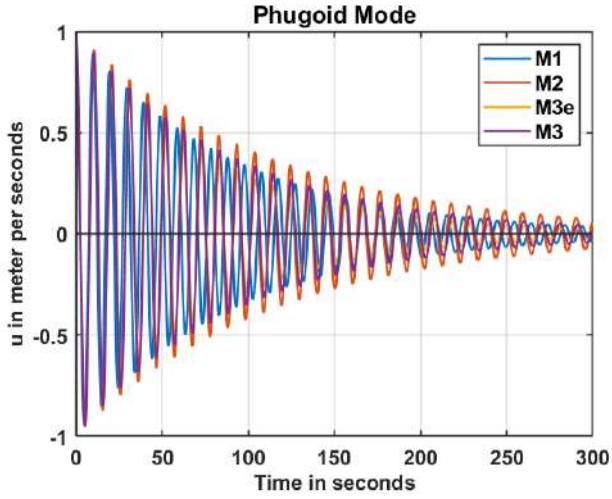

Figure 20: Time response plot of the phugoid mode

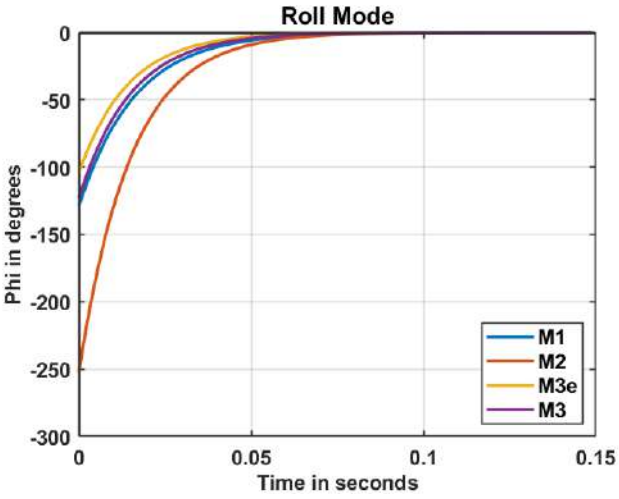

Figure 21: Time response plot of the roll mode

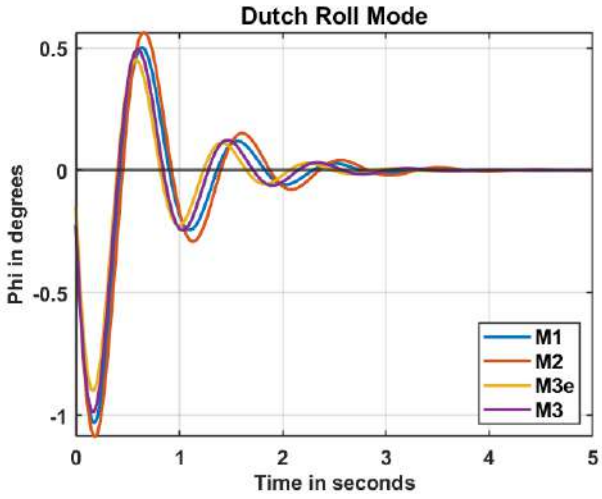

Figure 22: Time response plot of the dutch roll mode

During flight tests a yawing instability was noticed. A deeper analysis of the root locus plot shown in Figure 23 proved that the aircraft is generally stable, but unstable in one lateral mode. The spiral mode depicted in Figure 24 mode was found to be slightly unstable. The real value calculated with XFLR5 [5] measures 0.026, which additionally indicates instability. An instability in the spiral mode is congruent with the flight test observations and results. The *Aerodynamics & Stability* team identified a possible cause for the yawing during a steep turn at an increased angle of attack, being the disturbed air at the vertical stabilizer. The stall tests showed a tendency of the wing to shake when reaching stall speed, leading to a stall over the right wing, and finally forcing the aircraft to enter a spin. Upon this observation, the *Aerodynamics & Stability* team examined the tail geometry, and realized that only 1/8 of the rudder is unblocked from the disturbed air, and effective. However, according to Raymer [13] the minimum desired unblocked rudder is 1/3. In addition, the team believes that the winglet geometry based on the SD7062 airfoil becomes effective at steep turns, and thus, intensifies the yawing. Furthermore, at takeoff a left yaw immediately after the rotation of the aircraft was noticed. To mitigate this effect, the thrust angle was set a few degrees to the right. Moreover, when inflight and with maximum thrust applied, the airplane tends to climb. The down-thrust angle was increased to overcome this issue. Additionally, a slightly forward CG was observed at the dive test performed during flight tests. In general, the spiral mode is unstable and easier to control for the pilot because the response time is longer than that of the dutch roll mode [19].

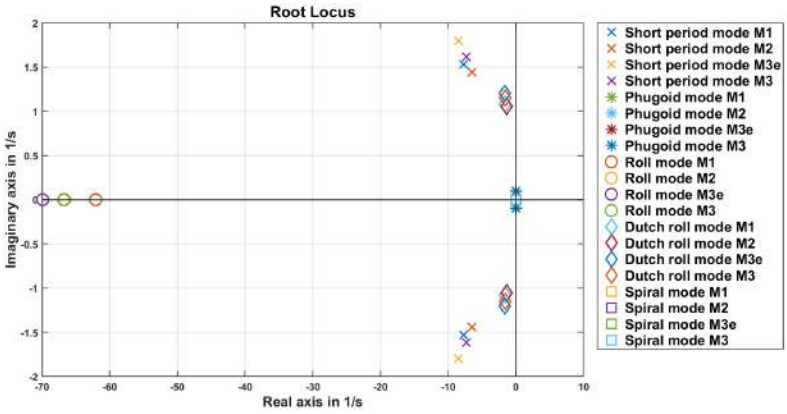

Figure 23: Root locus plot of the dynamic Eigenmodes

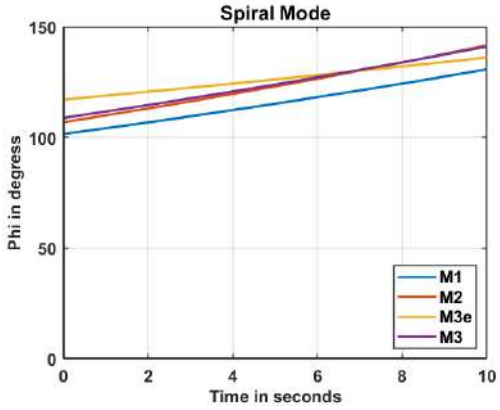

Figure 24: Spiral mode

4.5 Mission Performance Estimation

The aircraft mission performance was estimated based on the predicted aircraft performance considering lift, drag, and stability characteristics. To decrease the required takeoff and landing distance, fully deployed flaps at a maximum deflection of 40 degrees were considered during the first and the last flight phase. By assuming fully deployed flaps, it was possible to reduce the stall velocity around 10%. Figure 25 depicts the final takeoff distance and the remaining margin to the 25 ft for all mission configurations. To determine the optimal cruise speed for all missions, the drag over velocity was considered for the cruise phase. The goal was to fly in the velocity stable region above the point of minimum total drag, as gust loads have

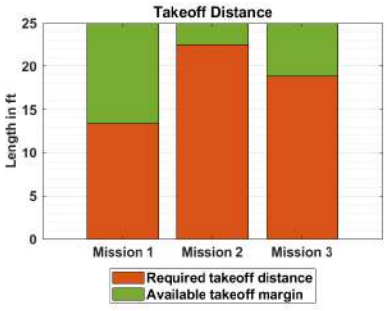

Figure 25: Takeoff performance

comparatively lesser influence on the aircraft's stability in this region. The approximated cruise speed, and the minimum total drag point are indicated in Figure 26 for M1, in Figure 27 for M2, and in Figure 28 for M3.

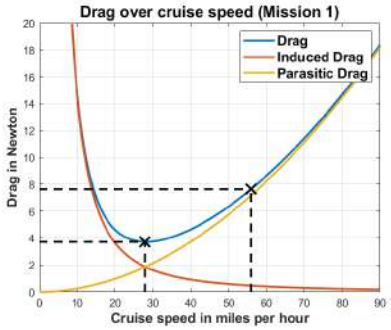

Figure 26: Drag over speed (M1)

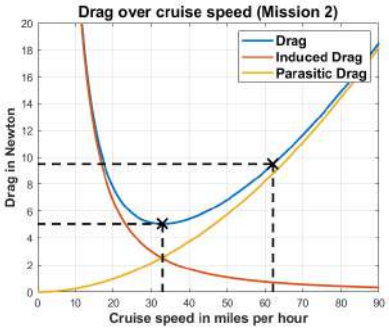

Figure 27: Drag over speed (M2)

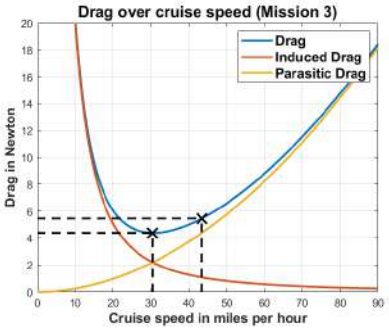

Figure 28: Drag over speed (M3)

Results for the estimated aircraft mission performance are summarized in Table 30.

Table 30: Aircraft mission performance estimation

	Mission 1	Mission 2	Mission 3
Number of M2 payload	-	80	-
Number of M3 payload	-	-	5
Payload weight	-	3.25 lb (52 oz)	2.5 lb (40 oz)
Takeoff gross weight	13.25 lb (212 oz)	16.50 lb (264 oz)	15.75 lb (252 oz)
Takeoff distance	14 ft	22 ft	19 ft
Stall speed with flaps deployed	30 ft/s (20 mph)	32 ft/s (22 mph)	32 ft/s (22 mph)
Average cruise speed	82 ft/s (56 mph)	91 ft/s (62 mph)	64 ft/s (44 mph)
Lap time	37 s	33 s	120 s
Mission duration	40 s	100 s	600 s
Number of laps	1	3	5
Absolute personal mission score	1	80 syringes / 100 s	5 successful deployments
Absolute best team theoretical score	1	120 syringes / 120 s	7 successful deployments
Normalized personal mission score	1	1.8	2.71
Total personal flight mission score	**5.51**		

5 Detail Design

The detail design phase was the final phase before finishing the competition aircraft. During this phase small enhancements of the second prototype eventually lead to the final design of the *Hornet*. Structural build ups of the fuselage, wing, empennage, and landing gear were continuously improved before the structural assembly of the final aircraft. Throughout the process final components were selected for the payload storage configuration, the deployment mechanism, and the avionics and propulsion system. These systems, and sub-systems were integrated into the final aircraft after its structural assembly.

5.1 Dimensional Parameters of the Final Design

The characteristic dimensional parameters used for the final design of the *Hornet* are listed in Table 31.

Table 31: Final aircraft parameters

Aerodynamic surfaces								
	Airfoil	**Span**	**MAC**	**Area**	**AR**	**Sweep angle**	**Taper ratio**	**Incidence angle**
Wing	SD7062	7.38 ft	10.63 in	6.53 ft^2	8.34	0°	1	2°
Horizontal stabilizer	NACA0008	2.30 ft	7.09 in	1.357 ft^2	3.90	0°	1	-0.5°
Vertical stabilizer	NACA0006	1.00 ft	5.86 in	0.49 ft^2	2.04	15.57°	0.65	0°
Control surfaces								
	Span		**MAC**	**Area**	**Max. upward deflection**		**Max. downward deflection**	
Ailerons	2 x 11.54 in		2.56 in	59.08 in^2	30°		20°	
Elevator	27.56 in		1.97 in	54.29 in^2	20°		15°	
Rudder	12.05 in		1.97 in	23.74 in^2	20°		20°	
High lift devices								
Flaps	2 x 23.11 in		2.56 in	in^2	0°		40°	
Fuselage								
Total length	**Nose**	**Avionics**		**Payload**	**Tail**	**Max. height**	**Max. width**	**Incidence angle**
5.57 ft	8.98 in	6.30 in		18.50 in	22.44 in	5.91 in	5.51 in	3°
Avionics								
Battery	**Battery**		**Motor**		**Receiver**		**Transmitter**	
6S LiPo 1,500 mAh	6S LiPo 1,500 mAh		Nema17 SY42STH47-1684A		Spektrum AR8020T		Spektrum DX8	
Propulsion								
Battery			**Motor**		**ESC**		**Propeller for all missions**	
6S LiPo 4,500 mAh			Scorpion SII-4025-520		RCE-BL100A ESC 10A BEC		17x10	

5.2 Structural Characteristics

In this chapter, the structural characteristics of the fuselage, wing, empennage, and landing gear are explained. Advanced materials such as aramid, carbon and glass fiber were used in different varieties to build a light and strong structure. In addition, plywood was used as reinforcement in load absorbing locations.

5.2.1 Structure Layout

The main goal for the structural layout was ensuring the aircraft withstands all loads occurring during the flight missions. The main loads result from aerodynamic and inertia forces acting on the wing and empennage, the motor pulling the aircraft forward and the impact on the landing gear when touching down on the runway. Therefore, the aim was to redirect all occurring forces from the wings along the main spar, and from the empennage along the tail into the main load bearing components of the fuselage. Frames and reinforced sections of the fuselage also damp loads induced by the motor and the impact from the landing gear during the landing.

5.2.2 Detailed Fuselage Design

The detailed inner fuselage design is depicted Figure 29. Preliminary analyses resulted in the design of a single, monocoque fuselage which incorporates the avionics systems as well as the deployment mechanism in the payload compartment of the hull. All corners of the rectangular body are rounded, and the tail is tapered to improve the aerodynamic behaviour of the fuselage. The skin is manufactured from two negative molds and consists of a carbon fiber and aramid honeycomb sandwich structure. Carbon fibre reinforced Airex frames support the skin and internal structures as well as one carbon fibre reinforced wooden frame in the front of the hull, where the nose gear is mounted. Loads are introduced into the carbon fiber coating of the support

Figure 29: Detailed fuselage design

elements, whereas the Airex core contributes to lightweight characteristics. On the top of the hull, two hatches were implemented to access the avionics compartment and the cargo compartment for loading and unloading the syringes and vial packages. A single brushless motor is mounted to the streamlined front, rendering the drag as small as possible. To ensure enough ground clearance for the propeller of the aircraft, the cowling is tapered upwards with an opening for the motor.

5.2.3 Detailed Wing Design

For the manufacturing of the wing the team has designed it as a composite sandwich structure using two different kinds of polystyrene foam as the core material and reinforcing those with one layer of carbon fibre. The carbon fibre functions as the tensile stress absorbing part and the polystyrene foams absorb the compression force. Both kinds of foam differ by density and manufacturing method, which are 1.25 lb/ft^3 for the expanded polystyrol (EPS) and 1.87 lb/ft^3 for the extruded polystyrol (XPS). The wing parts are cut by an electrically powered hot wire which is controlled by a 4-axis computer numerical control (CNC) machine. Following the cutting process of the hard foams, the parts are bonded together with two component adhesive. The main spar is based on a square cross section XPS core with a side length of 1.4 in which is the maximum height without an influence on the airfoil's surface. To withstand the bending moment of the wing under the aerodynamic and inertia forces one 78.70 in long and one 39.40 in unidirectional carbon fibre strip is placed centered on the top of the foam core. Similar strips are placed on the underside. To encounter the torsion load, a braided carbon fibre sleeve over the foam core is used. To validate this construction, a finite element analysis was conducted. The main spar was meshed with 25,200 mesh elements in Altair Hyperworks [20]. With this amount of elements, the constraints of the spar were realistically simulated. For the analysis, the area load was calculated with 6G maximum load for M2, as it is the one where the takeoff mass is highest. The carbon layers of the spar were represented as virtual laminate. As seen in Figure 30 a deformation of 0.25 in can be observed in z-axis direction. This value was perceived within the allowable range.

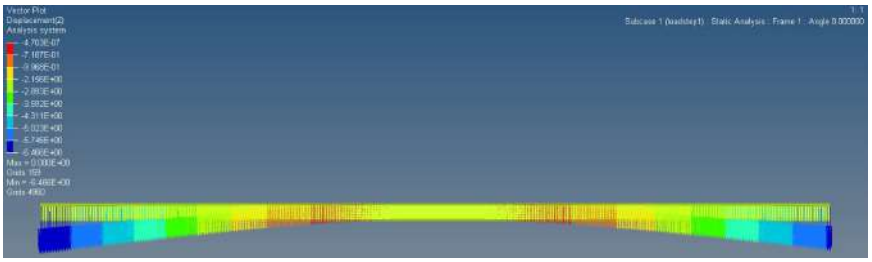

Figure 30: Deflection of the main spar at 6G

Figure 31: Detailed wing design

The final coating of the wing was one layer of bidirectional carbon fibre. Dedicated spots were incised to implement servo motors for aileron and flap movements . Both ailerons and flaps were cut out, their corners rounded and tapped back to the wing using rudder tape. The fuselage-wing adapter is 3d-printed out of light weight polymerized lactic acid (LW-PLA) which foams during extrusion. By adopting just this 3d-printed part changes in the incident angle (0° to 8°) can be archived with low production and design effort. In order to bolt the wing to the fuselage a 3d-printed carbon reinforced wing mount is bonded into the wing foam core. To withstand the high local compression the 3d-printable polymerized lactic acid carbon (PLA-Carbon) which consists of micro carbon fibres is used. The final wing design with its four connection bolts is depicted in Figure 31.

5.2.4 Detailed Empennage Design

The empennage was manufactured in a similar way as the wing. For the stabilizer, only XPS hard foam was used as the core. Both the vertical and horizontal stabilizer were cut with a hot wire and reinforced with one layer of bidirectional carbon fibre. All control surfaces were subsequently cut out of the stabilizers and reconnected with rudder tape. Chamfering the connection sides of the rudder's and the elevator's control surfaces ensured a suitable ruder deflection. The empennage connection to the wing is based on 3d-printed parts out of PLA-Carbon seen in Figure 32. The vertical stabilizer is bonded into the form fitting stabilizer adapter, which is bonded form fitting onto the horizontal stabilizer. The horizontal stabilizer mount is bonded into the XPS core of the horizontal stabilizer to withstand the high local compression of the two bolts that connect the empennage assembly to the fuselage. A 3d-printed counterpart with threat inserts is bonded to the upper inner side of the fuselage to evenly distribute the empennage loads into the fuselage structure .

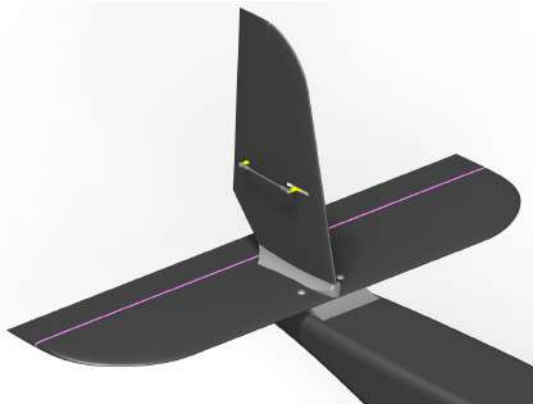

Figure 32: Detailed empennage design

5.2.5 Detailed Landing Gear Design

One steering nose gear and two rear wheels form the conventional tricycle configuration, illustrated in Figure 33. It was decided to use a conventional RC nose gear kit with a bearing pedestal that is mounted on the reinforced wooden frame inside the fuselage. A servo motor connected with the nose gear through a rod enables steering. The rear wheels are designed to endure load introductions during landing. In order to maintain structural integrity the landing gear is made from 20 layers of twilled GFRP with unidirectional CFRP strips on the outside. Inside the fuselage, lock nuts mounted to a plywood plate ensure a sufficient load distribution and establish the connection between the main landing gear and the fuselage.

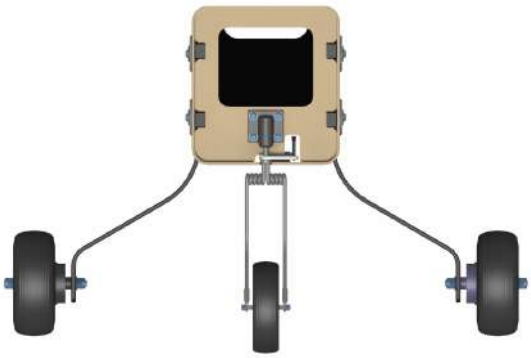

Figure 33: Detailed landing gear design

5.3 Systems and Sub-Systems Selection, Integration and Architecture

The final storage configuration for M2 and M3 payload, the final deployment mechanism, and the final avionics and propulsion set-up are described in detail in the following chapters.

5.3.1 Detailed Payload Compartment Design

The payload compartment for M2 and M3 payload lays in between the avionics compartment and the tail section of the fuselage. It houses the majority of the avionics system, the system for the deployment mechanism, and depending on the mission either 80 syringes or 5 vaccine vial packages. During all missions the deployment mechanism is a fully integrated part of the payload compartment.A removable hatch in the top section of the fuselage skin enables a fast and secure loading and unloading of M2 and M3 payload for the ground mission. For the remote deployment of M3 payload a hatch door is implemented at the rear bottom skin of the fuselage.

5.3.1.1 Syringe Storage Configuration

The syringes are stored partially loosely and partially restraint in packages. The packages are secured by special velcro restraining belts that partially connect to the fuselage structure. These secured packages of syringes wedge together with the loose syringes to prevent a CG shift.

5.3.1.2 Vaccine Vial Package Storage Configuration

The vaccine vial packages are carried on the conveyor belt system with rubber nobs as spacers in between.

5.3.2 Detailed Deployment Mechanism Design

Resulting from the preliminary design phase, a conveyor belt system was chosen for the deployment of the vaccine vial packages. A detail view of the mechanism is depicted in Figure 34. Two 3d-printed U-shaped shells out of PLA guide the vial packages along the deployment direction. A stepper motor fixing position is located on the first shell. The stepper motor is mounted inside the shell to save space in the fuselage. 3d-printed Gears out of PLA-Carbon were implemented to transmit the rotation and the moment of the stepper motor on to the drive belt. One gear is directly connected with the stepper motor, whereas the second gear transmits the rotation onto a rod. For both gears a transmission ratio of 1:1 is utilized. Both drive belts interlock with two gears, positioned on each end of the U-shaped shells. Special attention was paid to the payload restraint. Both shells have walls that are high enough to secure the vial packages in y-direction of the body system. Securing the packages along the x-direction was established with spacers on the drive belt. The spacers were positioned on the drive belts according to the box alignment. In order to avoid vertical shifting of the vial packages, a conventional rod was placed above the vial packages, which can be moved to the side for M2. To prevent the boxes from jamming, the walls and the rod were lined with teflon tape. A slide was realized for the package transfer between the conveyor belt and the hatch of the fuselage. The slide is crucial for a smooth transition of the boxes between the conveyor belt and the ramp.

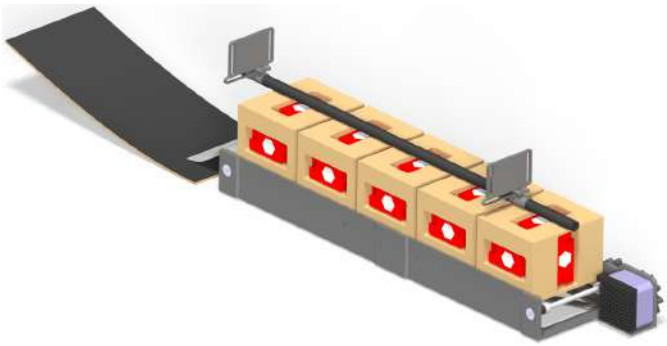

Figure 34: Detailed deployment mechanism design

5.3.3 Detailed Avionics and Propulsion Design

The final avionics and propulsion system consists of two subsystem, the avionics system and the propulsion system. While each subsystem features a wiring harness with fuses and an arming system, both subsystems are regulated by the overall control system.

5.3.3.1 Detailed Avionics Design

The final avionic system consists of following sub-components: two batteries serving as power supply and eight servo motors actuating the aerodynamic surfaces, the wheel gear and the hatch of the payload compartment.

5.3.3.1.1 Avionics Power Supply

The avionics power supply consists of two parallel connected 6S LiPo batteries with a nominal capacity of 1,000 mAh. After frequent flight testing the preliminary battery configuration discussed in section 4.2.3.1.3 proved to be oversized.

5.3.3.1.2 Servomotors and Linkages

Overall, 8 servo motors are built into the wing, empennage and fuselage. To provide a sufficient response time and torque for all control surfaces and flaps, two different types of servos were selected. Four KST X10mini V2 were installed in the wing, actuating the flaps and ailerons. All control surfaces on the empennage, the elevator and the rudder, the nose wheel, and the hatch door of the payload compartment are actuated with one KST X08H Plus V5 servo each. The implemented control horns are made of GFRP and the linkages of m2 in threaded steel with clamps on both ends. In contrast to the preliminary design, thinner linkages proved to be sufficient.

5.3.3.2 Detailed Propulsion Design

The finally selected propulsion system consists of the in section 4.2.3.2 described motor-ESC-battery configuration including the Scorpion SII-4025-520 motor, the RCE-BL100A ESC 10A BEC speed controller, and one 6S LiPo battery with a nominal capacity of 4,500 mAh. The motor-ESC-battery configuration chosen in the preliminary design proved to be sufficient during flight testing. For all flight missions a 17x10 propeller was chosen.

5.3.3.3 Wiring Harness and connectors

The wiring harness for the avionics and propulsion system consists of two main independent electric circuits each supplied an individual power source. For CG reasons both main power supplies (propulsion battery and auxiliary batteries) are placed behind the motor mount at the front of the fuselage. An adapter with a two pole XT90 connector links the batteries with their corresponding electric circuit. The propulsion power line runs from the propulsion battery pack to the 90 A circuit breaker, to the arming plug, and then to the ESC which is connected to the motor. The second main electric circuit gets fed by two auxiliary batteries and supplies all other electrical components. The auxiliary batteries are each connected to one 7.5 A circuit breaker, to a self-designed PCB with three implemented DC-DC converters. The receiver being placed at the rear of the fuselage and is fed with 5.5 V from the DC-DC converter. From the receiver four servo motor cables are fed through the 3D-printed fuselage wing adapter. Two of these cables then run through a cable channel in the foam of of the wing to the corresponding aerodynamic control surface (ailerons, flaps). The servo motor cables for elevator and rudder directly run from the receiver to the rear of the fuselage. All power lines inside the fuselage are lead through a spiral coiled tube. Furthermore, the avionics and propulsion wiring harnesses are connected with a common ground to ensure that both circuits are working on the same electrical potential. This ensures that the receiver on the avionics circuit can control the ESC on the propulsion circuit. The complete carbon composite structure of the aircraft is also connected to the common ground to prevent different electric potential.

5.3.3.4 Fuses and arming systems

Several fuses (circuit breeaker) and two arming systems, one for the receiver and one for the motor, were implemented for safety reasons. The implementation of a 90 A circuit breaker at the positive terminal of the propulsion battery pack and a 7.5 A circuit breaker for the avionics battery pack protects the electrical circuits from high currents. Both circuit breakers were placed, so that they can be pulled into the off position when connecting battery packs, loading and unloading cargo or working on the aircraft. Additionally, the receiver can be mechanically switched off by a toggle switch installed at the side of the fuselage. Furthermore, the propulsion circuit can be mechanically interrupted by the arming plug installed at the front of the fuselage in the skin besides the avionics compartment. The arming plug connects into gold contact plugs which interrupt the positive power supply line.

5.3.3.5 Aircraft and deployment mechanism controls

For the remote control of the aircraft and the deployment mechanism the transmitter Spektrum DX8 is used in combination with the Spektrum AR8020T receiver. Together they control the ESC, the aerodynamic surfaces, the brake system and the conveyor belt system. All of the eight available PWM signals of the receiver are allocated with specific functions. To help the pilot manoeuvring the aircraft in the air as well as on the ground, the rudder servo and nose gear servo share one access point. The channel allocation is summarized in Table 32.

Table 32: Selected control components and channel allocation

Component	Description	Connection or channel allocation
Transmitter	Spektrum DX8	Receiver
Receiver	Spektrum AR8020T	Transmitter and the channels listed below
ESC	RCE-BL100A ESC 10A BEC	Channel 1
Aileron servo (right)	KST 10mini V2	Channel 2
Elevator servo	KST X08 Plus V5	Channel 3
Rudder servo and nose wheel servo	KST X08 Plus V5	Channel 4
Flap servos	KST 10mini V2	Channel 5
Aileron servo (left)	KST 10mini V2	Channel 6
PCB	Self-designed	Channel 7
PCB	Self-designed	Channel 8
-	Not allocated	XBus Channel
Wheel brakes	Electromagnetical brake KAVAN	PCB
MCU	ATmega8U2-MU AVR	PCB
Hatch door servo	KST X08 Plus V5	MCU
Stepper motor	Nema17 SY42STH47-1684A	MCU

The deployment mechanism is handled through a MCU on a dedicated PCB, depicted in Figure 35 and Figure 36. The microchip ATmega 8U2-MU AVR acts as the core of the mechanism regulating two stepper-driver integrated circuits (ICs) and the servo for the hatch door. The stepper-drivers control the stepper motor of the conveyor belt system. A trigger signal on the s-bus connector starts a sequence to fully autonomously deploy one package at a time. Furthermore, the control sequence also maintains the aircraft's CG by moving the remaining packages back to the front. For the control of the wheel brakes two metal–oxide–semiconductor field-effect transistors (MOSFETs) are implemented on the PCB. The wheel brakes can either be controlled by the MOSFETS or by a PWM signal directly send by the receiver. A small section of the avionics system is shown in Figure 37.

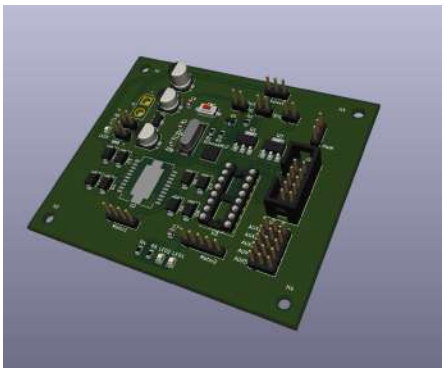

Figure 35: Rendering of the PCB

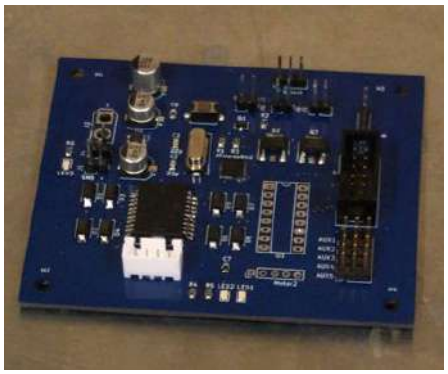

Figure 36: Manufactured PCB

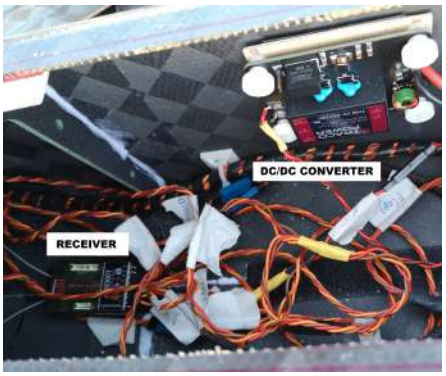

Figure 37: Avionics detail

5.4 Weight and Balance

For a weight and balance analysis the CG location for each aircraft component is estimated with the help of the CAD software CATIA V5-6R2012 [7]. During the detail design all structural component of the final design are integrated in an assembled CAD model. The weights are generated through estimation based on component volumes with known densities, measured component masses, and experiences from previous jA DBF aircraft. The CG position is then calculated in the CAD program. Table 33 shows the computed CG position of the final aircraft, empty and with each possible payload configuration. The positive x-axis is measured from the main wing leading edge towards the tail and the positive z-axis is measured up from the center of the main fuselage spar.

Table 33: Weight and balance table of the *Hornet* for all flight missions

Component	Weight (lb)	CG_x (in)	CG_y (in)	CG_z (in)
Fuselage without cowling	1.76	31.50	0	-0.87
Propulsion with cowling	1.21	2.76	0	-0.39
Wing with avionics	2.65	23.43	0	2.95
Winglets	0.26	27.17	0	3.94
Fuselage and wing connection	0.09	20.47	0	2.05
Fuselage and empennage connection	0.10	57.09	0	2.17
Horizontal stabilizer with avionics	0.33	58.27	-0.39	2.36
Vertical stabilizer with avionics	0.18	58.27	0	7.09
Main landing gear assembly	1.10	26.77	0	-7.09
Nose landing gear assembly	0.26	9.06	0	-6.30
Propeller	0.09	0	0	0
Deployment mechanism	1.32	24.02	0	-3.15
Cargo door mechanism	0.09	37.40	0	-3.54
Cargo door servo mechanism	0.08	37.01	2.36	1.18
Electronic speed control	0.25	7.09	0	-3.15
PCB with DC/DC converters	0.22	35.43	-2.36	0.00
Central control unit	0.08	14.96	0	-3.15
Receiver	0.04	35.43	0	0.79
Empty weight excl. batteries	10.12	24.43	-0.05	-0.55
Mission 1				
Propulsion battery	1.39	13.78	0	-1.97
Avionics battery	0.37	13.78	0	-0.79
Aircraft total weight	11.88	22.85	-0.04	-0.73
Mission 2				
Propulsion battery	1.39	8.66	0	0
Avionics battery	0.88	8.66	0	0
Vaccination syringes	2.78	28.74	0	0
Aircraft total weight	15.17	22.86	-0,03	-0,37
Mission 3				
Propulsion battery	1.39	13.78	0	-1.97
Avionics battery	0.88	13.78	0	-0.79
Vaccine vial packages	2.50	24.41	0	-1.97
Aircraft total weight	14.89	22.80	-0.03	-0.94

5.5 Final Flight Performance

Based on the tabular mission model described in section 4.3 "Aircraft Performance Prediction Methodology" the final flight performance of the competition aircraft is estimated with its final design parameters. To be able to compare the final performance estimation with the preliminary performance estimation, the same representative parameters are considered. Table 34 indicates the estimated final flight performance of *Hornet* in all missions. Obtained results were validated by flight tests.

Table 34: Flight performance of the final design

	Mission 1	Mission 2	Mission 3
Takeoff gross weight	11.88 lb (190 oz)	15.17 lb (243 oz)	14.89 lb (238 oz)
Takeoff distance	12.8 ft	18.8 ft	20.4 ft
Stall speed with flaps deployed	30 ft/s (20 mph)	31 ft/s (21 mph)	32 ft/s (22 mph)
Average cruise speed	99 ft/s (67.5 mph)	113 ft/s (77 mph)	77 ft/s (52.5 mph)
Lap time	30 s	27 s	100 s
Mission duration	35 s	80 s	500 s

5.6 Final Mission Performance

The final mission performance of *Hornet* is estimated based upon the final aircraft configuration parameters and the derived final flight performance. Assumed scores of the best-performing team correspond to these presented in section 3.6 "Final Conceptual Design Configuration" of the conceptual design chapter. Table 35 presents the calculated mission performance of the final design. Throughout the iterative design process, it was possible to increase the estimated total personal mission score by a total of 0.56 points.

Table 35: Mission performance of the final design

Aircraft	GM	M1	M2		M3
	Time in seconds		#Syringes	Time in seconds	#Successful Deployments
The *Hornet*	144	1	80	80	5
Assumed best	30	1	120	120	7
Personal mission score	0.21	1	2		2.71
Total personal mission score	**5.92**				

5.7 Drawing Package

The following four pages illustrate the detailed CAD drawings of *Hornet* derived from the assembled model in CATIA V5-6R2012 [7]. On the first page, a three-view drawing with the main measurements including relevant dimensions of all configurations is depicted. The second sheet shows the structural arrangement of all major components as an explosion view. Afterwards, the layout and location of the electrical system is displayed on the third sheet. Last, the payload accommodation for M2 and M3 including the deployment mechanism are contained on the fourth sheet of the drawing package.

Front view

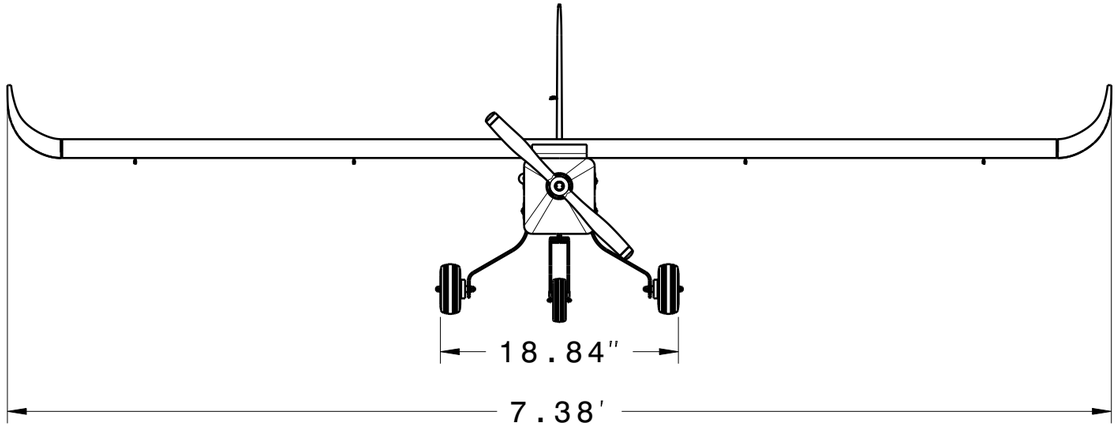

Left view

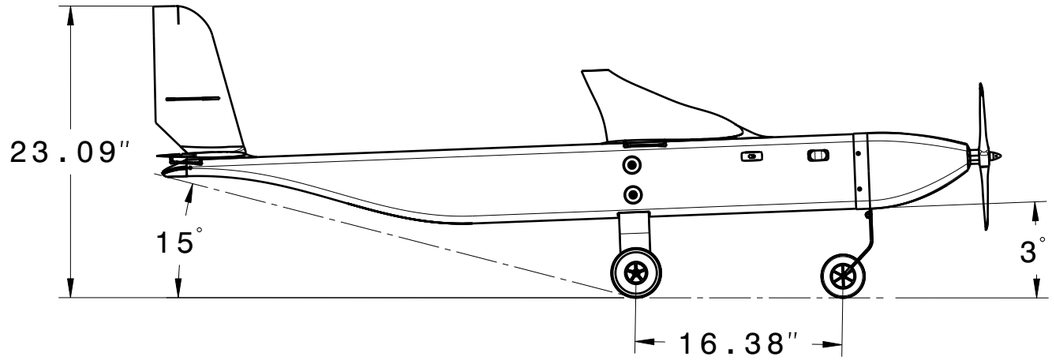

Top view

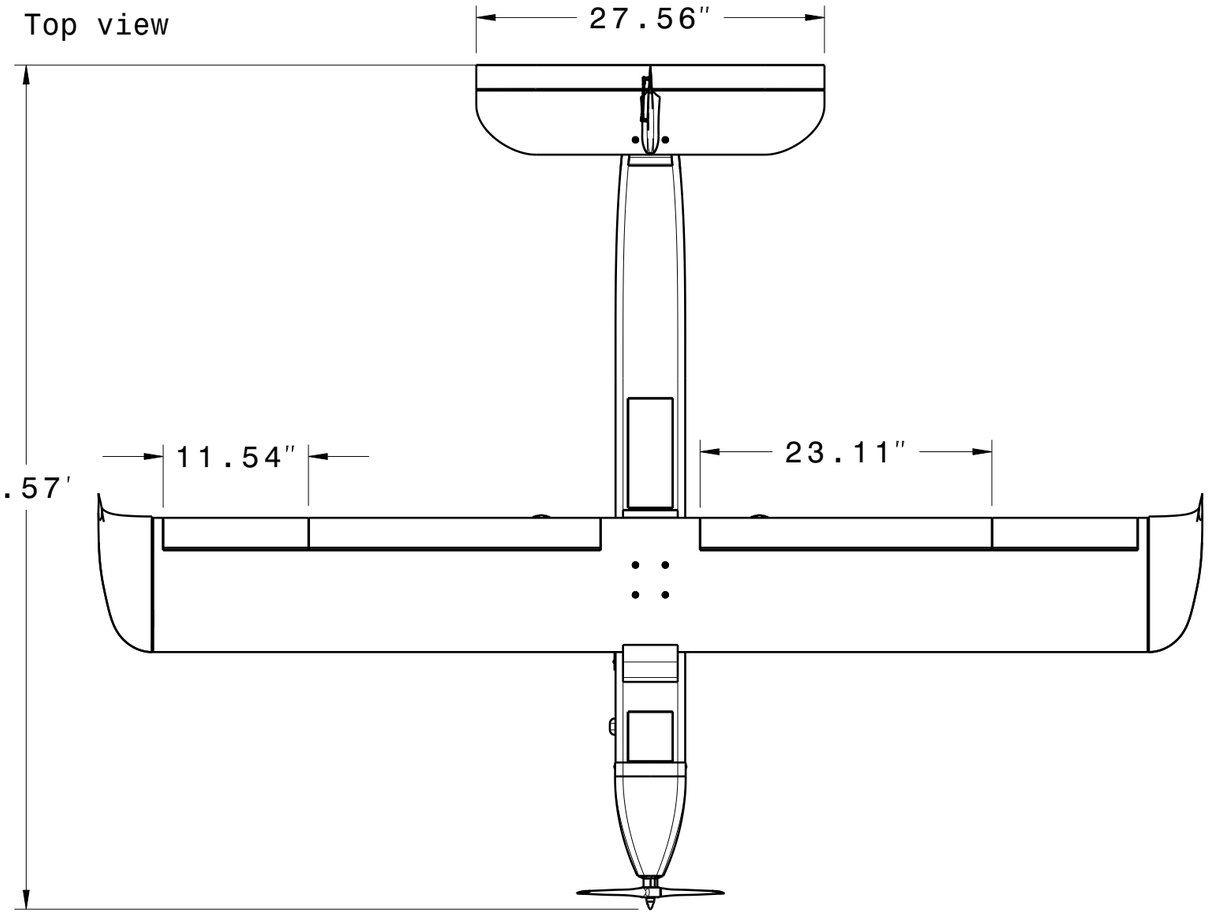

Isometric view
NTS

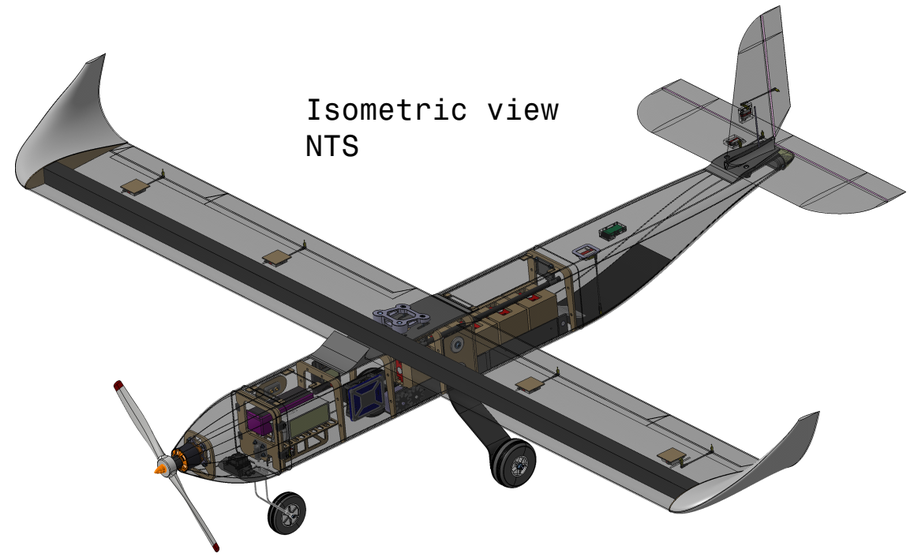

General Note:
Composite skin of fuselage, wing and empennage omitted for visibility

joanneum AERONAUTICS
Alte Poststraße 149
8020 Graz
Austria
joanneum-aeronautics.at

DRAWN BY: Gabriel	DATE: 23.02.2022	DRAWING TITLE: Three-View Drawing	
CHECKED BY: Teichmeister	DATE: 24.02.2022	SIZE: B	General Tolerances: ISO 2768-1 m — REV: A
DESIGNED BY: Schmedler	DATE: 21.02.2022	SCALE: 1:1	WEIGHT(lb): 15.17 — SHEET: 1/4

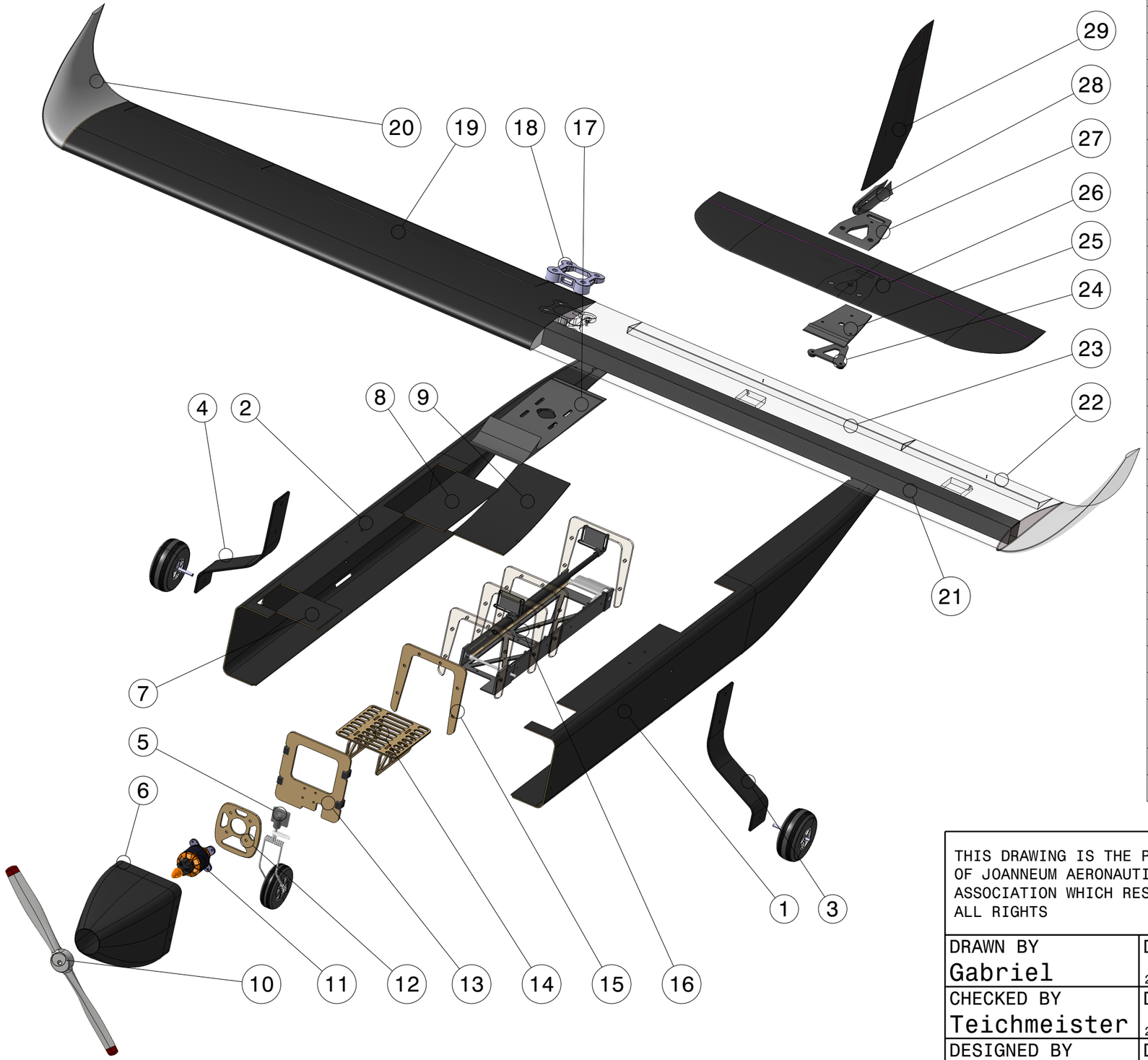

Item	Qty	Part Name	Material
1	1	Fuselage Skin Left	CFRP/Aramid
2	1	Fuselage Skin Right	CFRP/Aramid
3	1	Main Landing Gear Left	CFRP/GFRP
4	1	Main Landing Gear Right	CFRP/GFRP
5	1	Front Landing Gear	Aluminium
6	1	Cowling	CFRP
7	1	Service Door	CFRP/Aramid
8	1	Cargo Door	CFRP/Aramid
9	1	Cargo Ramp	CFRP/Aramid
10	1	Propeller	Composite
11	1	Electric Motor	-
12	1	Motor Mount	Plywood
13	1	Nose Gear Frame	CFRP/Plywood
14	1	Battery Mount	Plywood
15	5	Supporting Frame	CFRP/Airex
16	1	Unloading Mechanism	PLA
17	1	Fuselage Wing Adapter	LW-PLA
18	1	Wing Mount	PLA-Carbon
19	1	Wing	EPS Foam
20	2	Winglets	GFRP/LW-PLA
21	1	Main Spar	CFRP/XPS Foam
22	2	Aileron	CFRP/EPS Foam
23	2	Flap	CFRP/EPS Foam
24	1	Empennage Mount	PLA-Carbon
25	1	Fuselage Empennage Adapter	PLA-Carbon
26	1	Horizontal Stabilizer	CFRP/XPS Foam
27	1	Horizontal Stabilizer Mount	PLA-Carbon
28	1	Stabilizer Adapter	PLA-Carbon
29	1	Vertical Stabilizer	CFRP/XPS Foam

DRAWN BY Gabriel	DATE 23.02.2022	
CHECKED BY Teichmeister	DATE 24.02.2022	
DESIGNED BY Schmedler	DATE 21.02.2022	

joanneum AERONAUTICS
Alte Poststraße 149
8020 Graz
Austria
joanneum-aeronautics.at

DRAWING TITLE
Structural Arrangement

SIZE	General Tolerances	REV
B	ISO 2768-1 m	A

SCALE	WEIGHT(lb)		SHEET
NTS	15.17		2/4

Isometric view

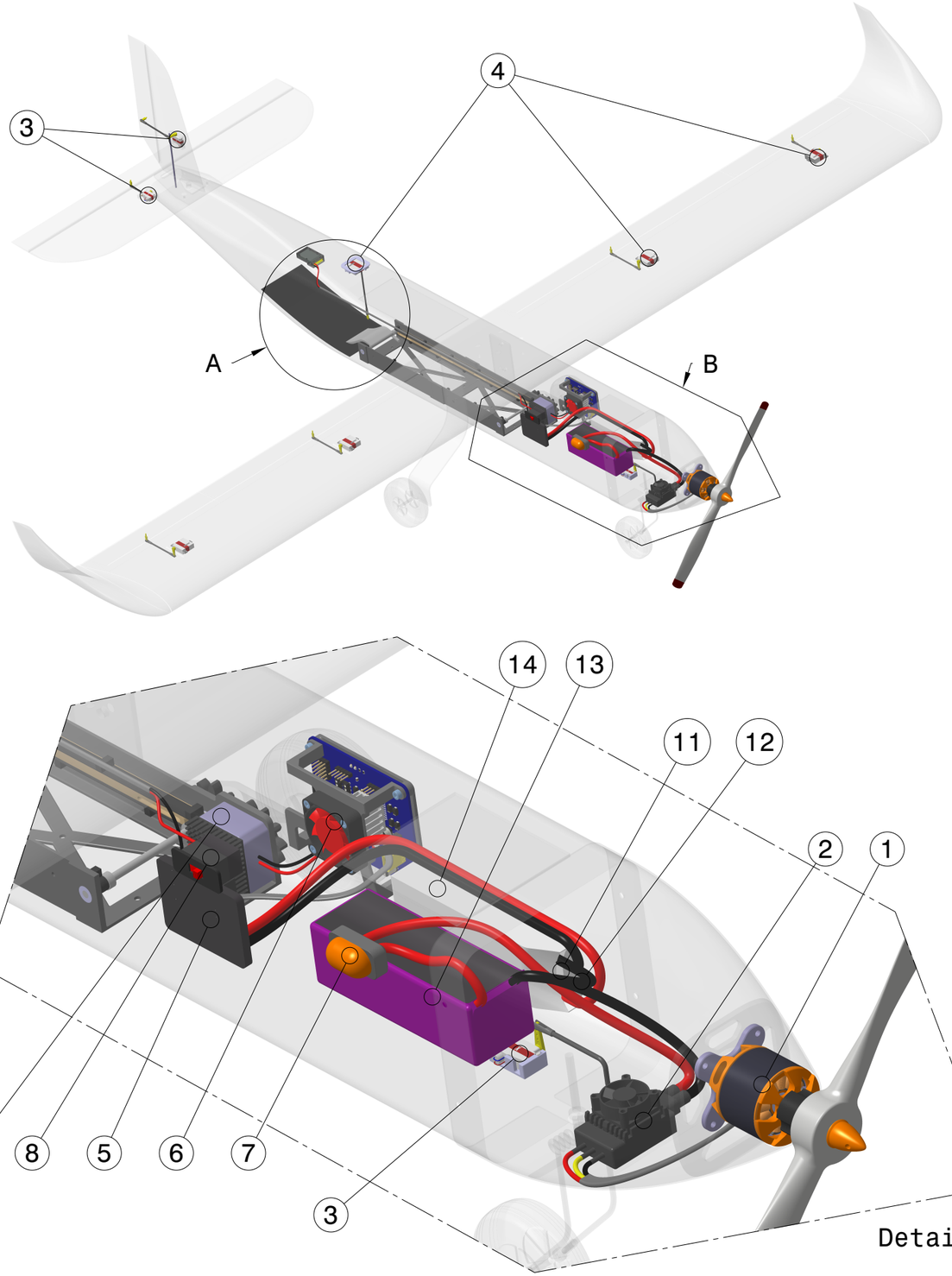

Detail A

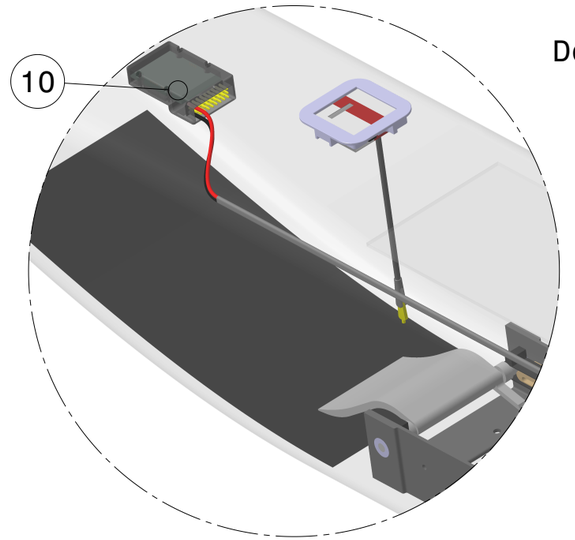

Item	Qty	Part Name	Description
1	1	Electric Motor	Scorpion S2-4025
2	1	Electronic Speed Controller	RCE-BL100A
3	3	Servo KST X08H	Empennage and Front Landing Gear
4	5	Servo KST X10	Flaps, Ailerons and Cargo Door
5	1	DC-DC Converter	20W at 5.5V, 4.5W at 9V
6	1	Deployment Controller Board	Integrated Circuit for deployment and breaks
7	1	Arming Plug	Gold Plug (0.315 inch)
8	1	Receiver Power Switch	Robbe Switch
9	1	Stepper Motor	NEMA 17
10	1	Receiver	Spektrum AR8020T
11	1	Safety Fuse Propulsion	Circuit Breaker 90A
12	1	Safety Fuse Avionics	Circuit Breaker 7.5A
13	1	Propulsion Battery	6S 4500 mAh
14	1	Avionics Battery	6S 3000 mAh

joanneum AERONAUTICS
Alte Poststraße 149
8020 Graz
Austria
joanneum-aeronautics.at

DRAWN BY: Gabriel	DATE: 23.02.2022	DRAWING TITLE: Systems Layout	
CHECKED BY: Teichmeister	DATE: 24.02.2022	SIZE: B	General Tolerances: ISO 2768-1 m — REV: A
DESIGNED BY: Schmedler	DATE: 21.02.2022	SCALE: NTS	WEIGHT(lb): 15.17 — SHEET: 3/4

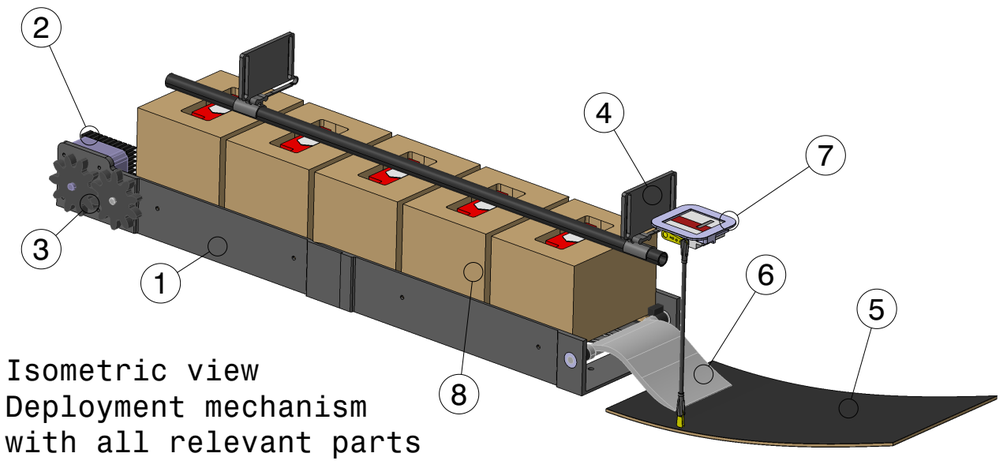

Isometric view
Deployment mechanism
with all relevant parts

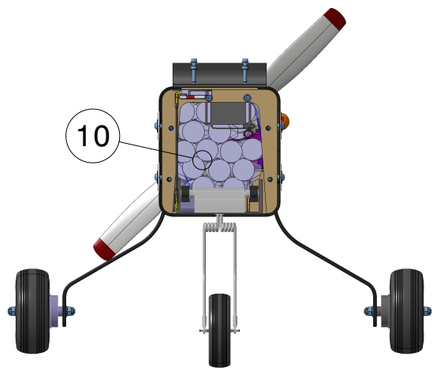

Isometric view
Rear view of loaded syringes

Isometric view
Aircraft loaded with syringes

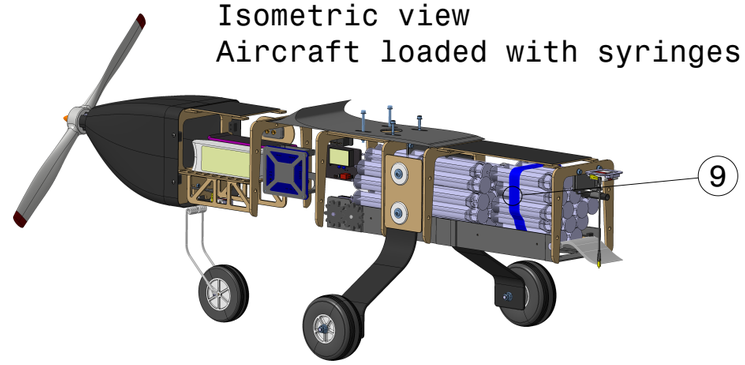

Item	Qty	Part Name	Description
1	1	Conveyor Belt Mechanism	Mostly PLA, consists of multiple parts
2	1	Stepper Motor	NEMA 17
3	1	1:1 Transmission Gears	PLA, Stepper motor (2) to conveyor belt mechanism (1) connection
4	1	Vertical Fixation	To hold the vial packages (8) in place
5	1	Hatch	To deploy the vial packages (8)
6	1	Slide	PLA, Connection between conveyor belt mechanism (1) and hatch (5)
7	1	Hatch Opening Mechanism	To open and close the hatch (5)
8	5	Vial Packages	Wooden boxes with g-sensors
9	8	Restraining Belt	Velcro syringe restraining belt
10	80	Syringes	Syringes for vaccination

Isometric view
Deployment process of a package seen from the rear

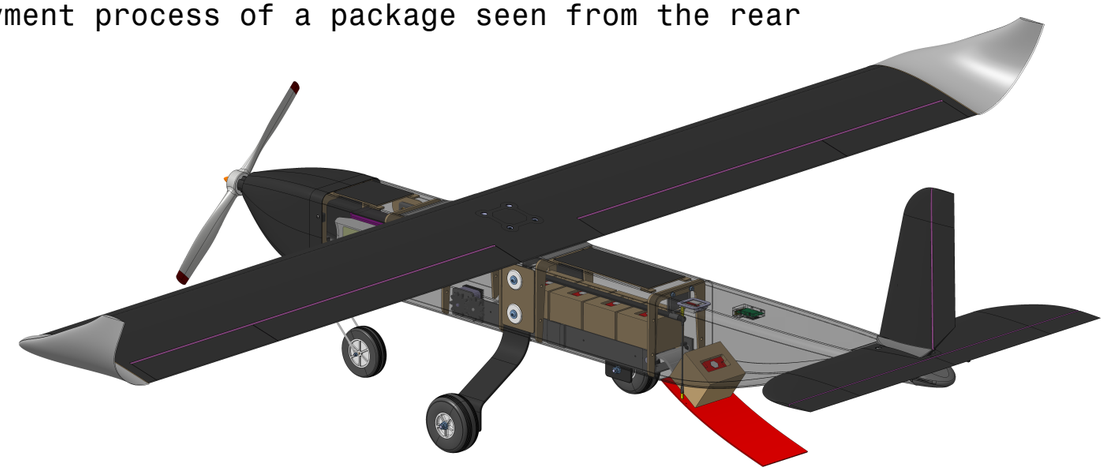

Isometric view
Deployment process of a package seen from a side view

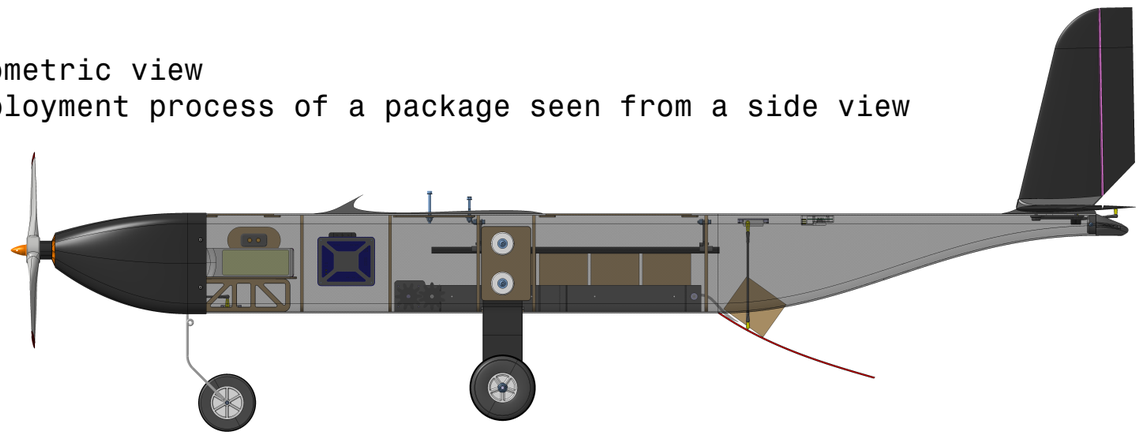

joanneum AERONAUTICS
Alte Poststraße 149
8020 Graz
Austria
joanneum-aeronautics.at

DRAWN BY Elzenbaumer	DATE 23.02.2022	
CHECKED BY Teichmeister	DATE 24.02.2022	
DESIGNED BY Schmedler	DATE 21.02.2022	

DRAWING TITLE
Payload Accommodation

SIZE	General Tolerances	REV
B	ISO 2768-1 m	A

SCALE	NTS	WEIGHT(lb)	15.17		SHEET	4/4

6 Manufacturing Plan

Different manufacturing processes were considered for different constructional elements of the aircraft. The wings, the fuselage, the empennage, the cowling, the landing gear and the deployment mechanism are the main elements taken into account. The most suitable processes were selected for each element.

6.1 Investigated Processes, Selection Process and Results

6.1.1 CNC-cutting/milling

CNC-cutting/milling is useful for manufacturing complex parts that require a high degree of precision. It allows the manufacturing of single parts as well as the cutting of one complex component. Also the ability to produce parts in a serial way enhances the advantage to manufacture spare parts. Composite molds are primarily cnc-milled

6.1.2 Composite Molding

Composite materials are very attractive for manufacturing aircraft components. Although composite molding is very time-consuming and expensive, it shows great advantages in terms of the strength-to-weight ratio. It also allows high precision manufacturing in combination with mold based vacuum bag lamination. Composite materials are also very durable but do not allow much deformation as fiber elongation is relatively poor and breaks instantly under too high load in comparison to metal that deforms much more before breaking.

6.1.3 Foam core composites

Foam is a very versatile material for manufacturing parts. A hot wire foam cutter allows easy shaping of the core material. Its light weight aspects and inexpensive acquisition contribute to its use for manufacturing the aircraft.

6.1.4 3d-Printing

3d-Printing is able to create complex geometries and components It is suitable for a cheap production of customized parts, prototypes, molds. Different modern materials increase the versatility extreme (e.g.LW-PLA, PLA-Carbon).

6.1.5 Balsa and Plywood

A structure made of balsa wood provides decent strength together with low weight mainly for structural elements. Single components can be manufactured with the help of handheld tools, a CNC milling machine, or a CNC laser cutter.

6.2 Selected Processes

The selection process of manufacturing methods was based on parameters such as costs, and weight-to-strength ratio of materials, experience needed, and the ease of manufacturing. Therefore, the team evaluated manufacturing methods and material properties through a FoM analysis. Table 36 shows the prioritised aspects for the selection.

Table 36: Figures of merit for manufacturing

FoM criteria	Score factor	Reasoning
Weight	5	Short takeoff and landing abilities
Strength	5	Reliability of the components during load exposure
Ease of manufacturing	4	Feasibility in manufacturing
Experience	3	Ensuring quality of the components
Cost	2	Limited budget
Repeatability of manufacturing	1	Lead time reduction and producing spare parts

As shown in Table 37, the above mentioned manufacturing methods were evaluated according to the score factor.

Table 37: Manufacturing methods evaluated

FoM criteria	Score Factor	CNC-cutting /Milling	Composite Molding	Foam core Composites	3d-Printing	Balsawood and Plywood
Weight	5	2	5	4	4	4
Strength	5	4	4	4	2	3
Ease of manufacturing	4	3	3	3	4	2
Experience	3	3	2	2	3	1
Cost	2	2	1	2	2	2
Repeatability of manufacturing	1	1	1	1	1	0
Total score		56	**66**	**63**	60	50

The evaluation through the FoM analysis highlighted two major manufacturing methods, which were selected to manufacture the main parts of the aircraft. The remaining methods were used to an extend that was necessary to manufacture the parts of the aircraft. The cowling, the hull, and the landing gear were manufactured through the combination of composite molding and the vacuum bag lamination process. Foam core composites were used for the wing and the empennage. In order to manufacture the deployment mechanism in a precise manner, the team decided to make use of the 3d-printing method.

6.2.1 Fuselage

The fuselage was built from composite materials by means of vacuum bag laminating. This method combines the advantage ensuring the structure's lightweight characteristics and necessary structural integrity. Firstly, negative molds were designed and customized for manufacturing the hull as well as the cowling element around the propulsion unit. The molds for the hull were milled out of a SikaBlock® M930. The molds for the cowling element were milled out of a SikaBlock® M700. In total four molds were milled for the fuselage. The molds were pretreated before use to smooth the surface. The pretreatment included sanding to exterminate faulty spots in the surface, impregnation with Chemlease MPP 712 EZ, and the application of priming wax in combination in combination with PVA release agent. This ensured a smooth surface of the hull and easier separation of the hull from the mold at the end of the process. The further process of vacuum bag laminating is shown in Figure 38 and Figure 39.

Figure 38: Fuselage laminating

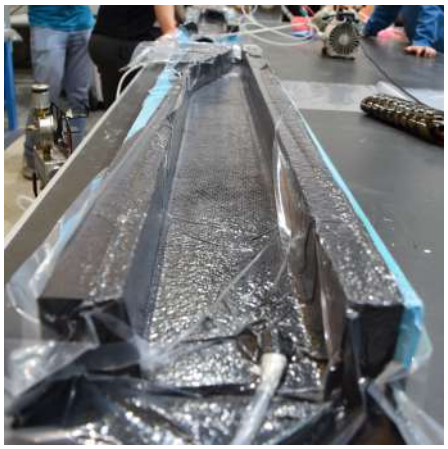

Figure 39: Fuselage vacuum bagging

Figure 40: Fuselage reinforcements

Manufacturing the hull was established using a sandwich structure. The outer and inner skin were manufactured from bidirectional carbon fiber reinforced polymer (CFRP) 2.36 oz/yd^2 plain weaved fabric for each side. In between the two layers of CFRP an aramid honey-comb structure of 0.079 in thickness was integrated for additional stability

and strength. Thereafter, the layers were impregnated with a mix of Epoxy resin and hardener. This ensured the bonding of the fibers and filled the spaces between the fibers. For enhanced adhesion between the layers, the honeycomb core was also impregnated. After impregnation, the mold was inserted into the vacuum bag for the vacuum bag lamination process. In the course of this process, excess Epoxy resin was sucked out of the composite to reduce weight and avoid unequal impregnation of the fibers. Once the Epoxy resin had dried and hardened the hull halves were tempered for extra strength for two days at 140 °F. For additional strength the inner fuselage was reinforced with spars, shown in Figure 40. The spars were bonded to one half before connecting the two hull halves. The spars were manufactured in sandwich structure out of an Airex foam core, and an inner and outer layer of 4.72 oz/yd^2 twilled CFRP fabric. CNC-cutting of the spars guaranteed a precise geometry. The spars were designed with an open lower part for a simplified implementation of the deployment mechanism into the fuselage. A plywood structure was used as the support element of the nose gear in form of a frame. Extra stability was established with one layer of carbon fiber on each side. The cowling element was manufactured in the same manner as the fuselage hull. Instead of the sandwich structure an outer layer and an inner layer of 4.72 oz/yd^2 twill CFRP fabric were applied, Figure 41. For the connection of the halves and extra strength the cowling halves were supported with four 2.95 oz/yd^2 unidirectional CFRP strips, shown in Figure 42. Thereafter, the molds were vacuum bagged, Figure 42, and tempered, Figure 43. A milled wooden structure serves as the engine mount inside the cowling element. The connection of the cowling element to the hull of the fuselage was realized with a 3d-printed and composite hybrid part. This element is bonded with the hull and provides a four-point screw connection for the cowling.

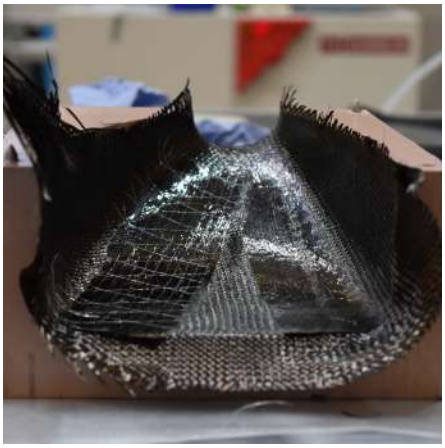

Figure 41: Unidirectional CFRP stripes

Figure 42: Cowling vacuum bagging

Figure 43: Tempered components

6.2.2 Wing

The wing of the aircraft was manufactured from two different positive hard foam cores, as seen in Figure 45. The two different foams were distributed over the wing in the following order: The leading edge was entirely made out of EPS hard foam, and the main spar of the wing was manufactured using XPS for the center section and EPS for the outer sections. The center section length is 31.49 in and the two outer sections are each 23.62 in long. XPS was used for the center part and the trailing edge behind the center part. This section needs to hold the connection element, which was 3d-printed and embedded in the XPS foam core. EPS was used for the rest of the wing and the outer 33.46 in of the trailing edge. The first element manufactured was the main spar. Pretreatment of the main spars through sanding ensured a smooth surface for the lamination process. The next step was to connect the three

main spar sections into one main spar using UHU Por. Through additional sanding, the main spar was customized to the necessary thickness. For giving the main spar extra strength, four 2.95 oz/yd^2 unidirectional CFRP strips were laminated to the main spar. Two unidirectional stripes of 39.37 in form the first layer in the middle of the main spar. Over those an additional layer of the same CFRP is then coated over the whole main spar. Once the layers had been added on both the upper and under side of the main spar, a CFRP tube was pulled over the main spar. After impregnation of the CFRP tube the main spar was put in a vacuum bag for the vacuum bag lamination process, as seen in Figure 44.

Figure 44: Spar

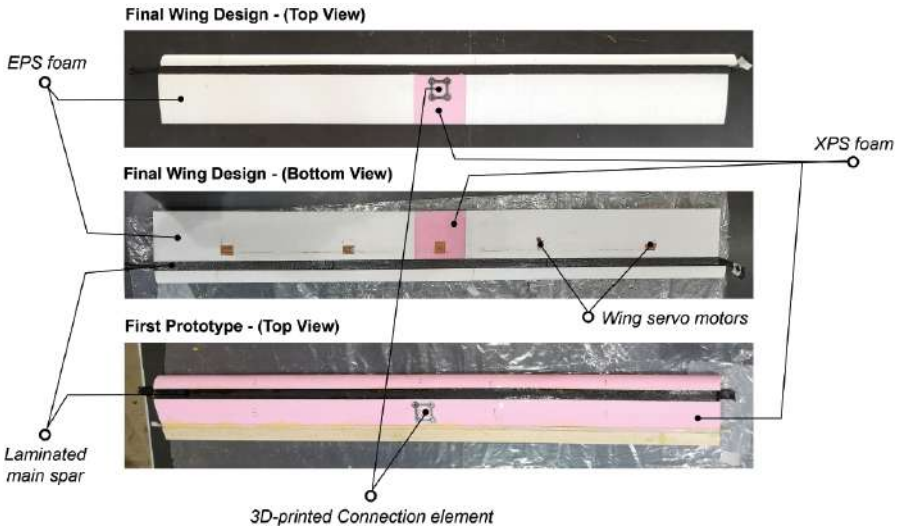

Figure 45: Structural wing layout

Once the resin dried the main spar was put into the oven for tempering. The main spar was then bonded to the rest of the wing with a quick curing resin. As soon as the connection had been established the wing was laminated with one layer of bidirectional CRFP 2.36 oz/yd^2 plain weave fabric, which was folded over the leading edge to ensure a faultless leading edge. Again, the vacuum bag lamination process was used for manufacturing the wing. Here the wing was also put in the oven after the vacuum bag process is completed. In the last step, the flaps and ailerons were cut, the servos were implemented and the winglets were connected to the wingtips. The winglet were 3d-printed with LW-PLA and afterwards coated with one GFRP layer for extra stiffness and stability.

6.2.3 Empennage

The empennage was manufactured in the same way as the wing, with the difference that only XPS was used as the core material. The foam core was cut with a hot-wire cutter and sanded as pretreatment of the surface. From here, the processes is done in the same matter as for the wings. Firstly, impregnating the foam core and the bidirectional CFRP 2.36 oz/yd^2 plain weave fabric ensured the adhesion of the CFRP to the core. In case the fabric forms folds or bubbles it is necessary to eliminate those in order to get a smooth surface and avoid delamination of the fabric from the core. Another priority is a smooth leading edge at the vertical stabilizer and the elevator. The vacuum bag method pressed the CFRP perfectly on to the core. Once hardened and tempered, a slanting cut was made at the base of the vertical stabilizer to guarantee space for the elevators deflection movement. The connection of the vertical stabilizer and the elevator was realized through a 3d-printed part, where a resin/hardener mix with glass bubbles supplementary, cotton flocks and thixotropic agent are applied for a strong connection. The implementation of the servos and the connection part is the last step for completing the empennage.

6.2.4 Landing gear

The landing gear was manufactured in the same way as the fuselage. Firstly, a mold had to be milled out of a SikaBlock® 700. The pretreatment of the mold is identical to that of the fuselage molds. Reduction of the lead time was realized with a wide mold. This allowed the manufacturing of one wide landing gear leg, which is then cut into the needed width of the main landing gear legs. Layering the landing gear was done in the following order: The first layer laid into the mold was a twilled CFRP fabric. The second layer consisted of an unidirectional CFRP. The core of the landing gear was formed by 20 plys of GFRP. Adding another unidirectional CFRP stripes to the core, allowed for higher load introduction into the landing legs. The layup was finished with another layer of twilled CFRP fabric, contributing to a good torsion resistance of the landing gear. The connection of the landing leg to the fuselage was established by two holes in the upper leash of the landing leg. For the wheel mounting the lower leash was provided with a hole. The wheels were mounted with an M6 tapered rod, M6 nuts, washers, and the brake system.

6.2.5 Deployment Mechanism

The deployment system was created, using the 3d-printing method. Two U-shaped shells, and a slide, at the end of the conveyor belt, were manufactured additive with polyactic acid (PLA).

6.3 Manufacturing Schedule Plan

For the purpose of the coordinating manufacturing efforts, the team developed a milestone plan depicting the most important achievements integrated into a timetable. Figure 46 shows the manufacturing milestones chart depicting the planned and actual schedule of processes. The chart was divided into three different component groups or main tasks, for prototype 1, prototype 2 and the competition aircraft respectively.

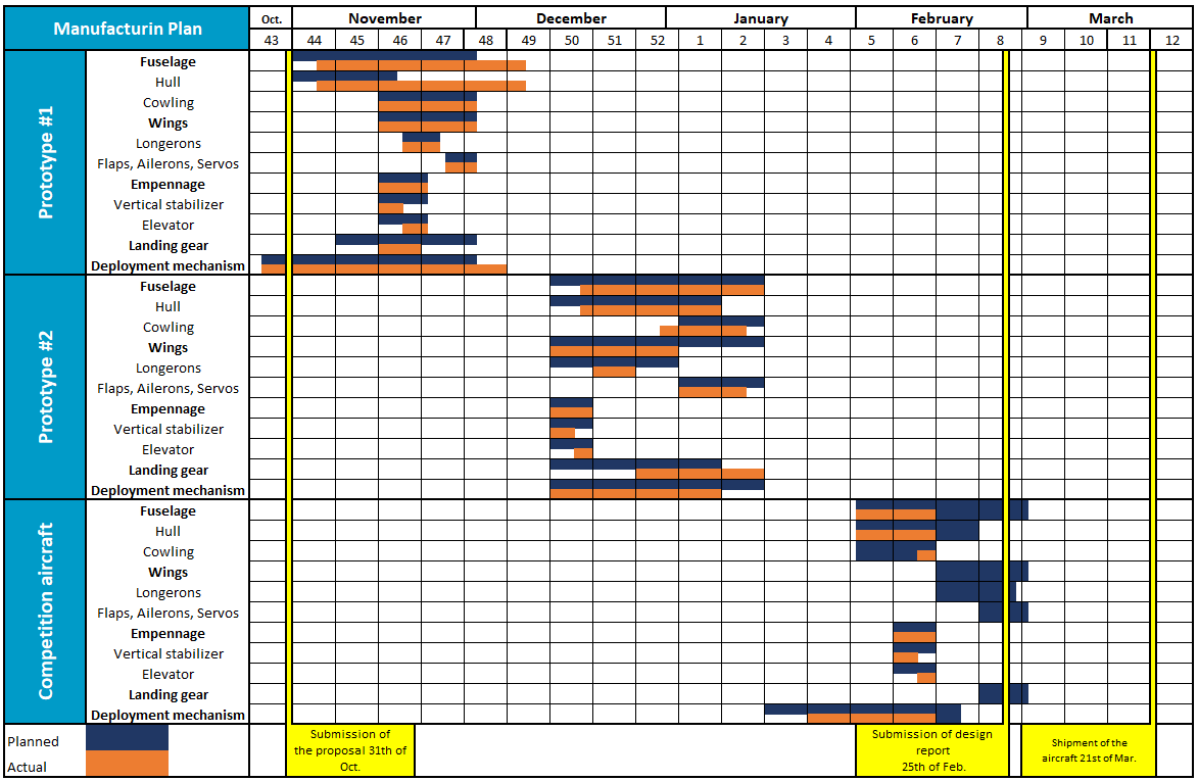

Figure 46: Manufacturing schedule plan

7 Testing Plan

The aircraft's components and mechanisms were tested in the course of flight and ground tests. The main goal was to validate the functionality of all systems as well as the proper operation of the aircraft in flight through data acquisition. Based on the acquired data, the final design of the aircraft was established.

7.1 Objectives and Schedule

The planned testing schedule is depicted in Figure 47. To efficiently conduct all necessary tests, a time schedule was generated for all ground and flight tests. The ground tests include two structural tests, one of the wing structure, and one of the landing gear, a static thrust test, a ground mission simulation, and a functionality test to prove the flawless operation of the deployment mechanism. In addition to the ground test, flight tests were conducted to evaluate the aircraft's performance. The main goal, that was simulating the contest conditions and maximizing the performance for every mission. Another goal was to detect possible design flaws, to continuously improve the design, and to achieve the maximum performance of the aircraft.

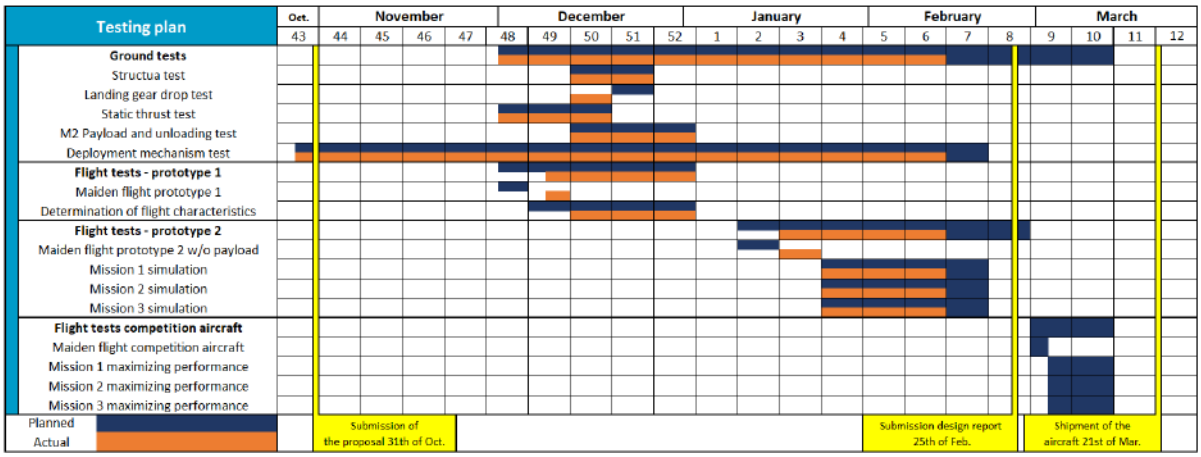

Figure 47: Testing schedule

7.2 Ground Tests

In order to establish the basic functionality of the subsystems, a series of tests were carried out in the ground testing phase. The main aspects were functionality, reliability and quality of the individual components and systems. Additional structural tests were conducted to verify the endurance and strength of the major components.

7.2.1 Structural Tests

For testing the structural properties of the aircraft, a wingtip test and a landing gear drop test were conducted. The wing tip test was implemented by suspending a weight of up to 25 kg at the CG before lifting it up. At the maximum load, both wing tips faced a loading of 150 N which results from the empty weight and the attached weight, as shown in Figure 48. The wingtip test was carried out to determine and validate if the wing design is sufficient enough to withstand loads reaching

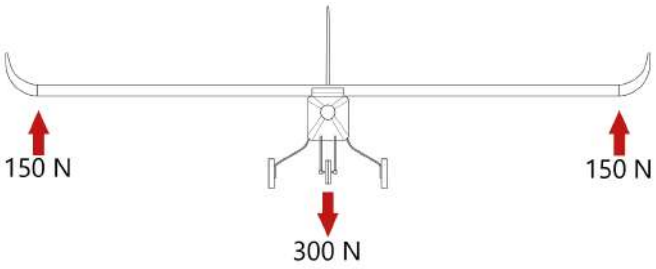

Figure 48: Wing tip test set up

and exceeding 5G. In addition, to the wing tip test a landing gear drop test was conducted to verify the materials implemented. The aircraft was dropped from several heights to test the landing gear in its stability and load absorption. Simultaneously this test showed if the damping abilities of the landing gear were sufficient, and determined the allowed touchdown conditions.

7.2.2 Static Thrust Test

The measurements of the static thrust were conducted for gathering data on the propulsion system. The thrust force measured for an electric current interrelationship with different propellers was showed in a Newton/Ampere curve and helped the team to verify level-flight thrust as well as take off thrust settings. Further tests concerning the battery pack temperature provided first estimations for the flight time. Additional tests displayed the operating voltage behaviour and electric current peaks. The static thrust set up is depicted in Figure 49.

Figure 49: Static thrust test set up

7.2.3 M2 Payload Loading and Unloading Test

Testing the loading and unloading of the syringes showed how many syringes fit in the payload compartment of the fuselage. Special attention was paid to the hatch, which is opening the payload compartment. If the hatch was causing difficulties during the loading and unloading of the M2 payload, it would be redesigned. Loading and unloading time of the syringes and the vial packages were measured and improved by every iteration. This testing phase did not only show possible improvements but also served as a solid training opportunity for the ground mission.

7.2.4 Deployment Mechanism Test

The testing of the deployment system was split into two phases. Firstly, the deployment mechanism was tested for its functionality. Several drive sequences were conducted in order to validate the function of the stepper motor and the transmission of the rotation motion to the drive belt. In the course of an endurance test, the engine was running 500 times in one direction for 2 seconds with a full load and then 500 times in the other direction. Securing the load in deployment direction was realized with rubber nobs that also serve as separators for the boxes. Because of the flexibility of the rubber nobs, another endurance test was conducted in order to determine which bonding method and adhesive should be used. 200 runs were made to test the durability of the connection between rubber nobs and the conveyor belt. For the second test phase, the deployment mechanism was implemented into the aircraft. The integrated system was tested in terms of unloading the boxes and the behaviour of the ramp with the unloading sequence. The set up for the deployment mechanism test can be seen in Figure 50.

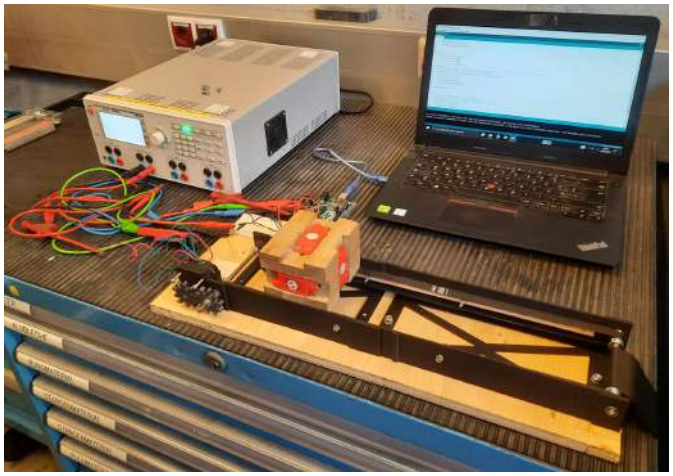

Figure 50: Deployment mechanism test set up

7.3 Flight Tests

Throughout each of the design phases, the team performed several flight tests in order to obtain the proof of concept for the aircraft's aerodynamics, stability, and controls. The first test flight was conducted with the first prototype to determine the flight characteristics and gain knowledge of the aircraft's behaviour. Based on the first test flights, weight reductions were made to the landing gear and wing to minimize the takeoff distance. The second prototype was used to simulate all three flight missions in order to determine the lap times and the flight behavior, both without and with payload. In the second test flight phase, the payload restrain for M3 was evaluated. Ensuring a reliable payload restrain was necessary to establish stability during flight and avoid false triggering of the shock sensors resulting from impact with other parts inside the fuselage. Acquired data from the test flights with the second prototype enabled the team to make detailed improvements for the contest aircraft. Extracting the best performance of the contest airplane was the priority goal for the team. Training the pilot and improving the lap times with the contest aircraft was the ultimate goal to be achieved in the course of the final test flights. In Figure 51 the *Hornet* can be seen successfully taking off during a flight test. One of the many completed approaches by the *Hornet* is depicted in Figure 52.

Figure 51: Successful takeoff during a flight test

Figure 52: Approach of the *Hornet* during a flight test

7.4 Checklists

Implementing checklists for all procedures prevents malfunctions during testing and reduces the risk that the aircraft of crashes because of missing connections or parts. It also helps to direct the attention to possible errors that might lead to the damage of the aircraft, other objects or injuries of people. Table 38 shows the checklists used during the testing phase and the flight tests. The checklists will also be used in the contest.

Table 38: Flight checklists

Pre-flight checklist:		
☐	Inspect aircraft exterior	NO DAMAGES
☐	Inspect landing gear	NO DAMAGES
☐	Inspect aircraft interior	STRUCTURE INTACT, NO DAMAGES
☐	Battery voltages (TX, RX, propulsion)	VERIFIED
☐	Batteries (RX, propulsion)	INSERTED AND ATTACHED
☐	Mission specified payload	PREPARED
☐	Center of gravity	CHECKED, WITHIN LIMITS
Deployment mechanism checklist:		
☐	Top lids	OPENED
☐	Conveyor belt	INITIAL POSITION
☐	Stepper motor	CONNECTED
☐	Servo motor	CONNECTED
☐	Battery	CONNECTED
☐	Shock sensors	INITIAL CONDITION, NOT TRIGGERED
☐	Vial packages	STORED
☐	Vertical securing beam	INSTALLED, LOCKED
☐	TX power	ON
☐	RX power	ON
☐	Top lids	CLOSED AND LOCKED
☐	Ramp	CLOSED AND LOCKED
Before takeoff checklist:		
☐	Wind and weather	FLYABLE
☐	Air and ground traffic	CLEAR
☐	TX power	ON
☐	RX power	ON
☐	Control surfaces	CHECKED, FREELY MOVING
☐	Mission specified payload	MOUNTED AND SECURED
☐	Propeller area	CHECKED, CLEAR
☐	Propulsion arming plug	INSERTED
☐	Propulsion	CHECKED, WORKING
After landing checklist:		
☐	Propulsion arming plug	REMOVED, SAFE
☐	RX power	OFF
☐	TX master switch	OFF
Post landing checklist:		
☐	Top lid	OPENED
☐	Batteries (RX, propulsion)	UNPLUGGED AND REMOVED
☐	Payload	REMOVED

Separate checklists were included for testing the propulsion and the range and fail-safe testing of the transmission. The purpose for those checklists is to pay attention during the testing of the propulsion and avoid any incidences and injuries of the testing personnel. Therefore strict compliance and supervision was mandatory. Table 39 and Table 40 show the parameters to be checked and the wished condition.

Table 39: Propulsion test checklist

Propulsion test checklist:		
☐	Motor	SECURED, ROTATES FREELY
☐	Propeller	SECURED, NO DAMAGES
☐	Battery	CONNECTED, CHARGED
☐	ESC	CONNECTED, CORRECT SETTINGS
☐	Control unit	CONNECTED
☐	Wiring connected properly	CHECKED
☐	Measuring instruments	CONNECTED, ACTIVE
☐	Propeller area	CLEAR
☐	Personal protection equipment	APPLIED

Table 40: Range and fail-safe test checklist

Range and fail-safe checklist:		
☐	TX power	ON
☐	Range check mode	ACTIVATED
☐	RX power	ON
☐	Controls working	CHECKED
☐	Propulsion arming plug	INSERTED
☐	Distance to aircraft	ACCORDING TO TX MANUAL
☐	Controls working	CHECKED
☐	TX power	OFF
☐	Controls in fail-safe position	CHECKED
☐	TX power	ON
☐	Controls working	CHECKED

8 Performance Results

This chapter presents the performance results of the aircraft and its subsystems as obtained through the ground tests and the flight tests.

8.1 Performance of Key-Subsystems

The performance results of all relevant subsystems are described in the following sections. The static thrust test provides the chosen propeller diameters and the results of the conducted test. Structural test show the conducted wingtip test, and the deployment mechanism test concludes the outcome for the chosen deployment components.

8.1.1 Static Thrust Test

To ensure a takeoff within 25 feet of the start-finish line testing and evaluating the propulsion system was necessary. The tests made by the *Avionics & Propulsion* subteam consisted of three different propellers for analyzing the thrust force and energy consumption to decide on the best propeller for each mission. Due to a higher weight in M2 and M3 the efficiency and thrust force was a decisive factor. As seen in Figure 53 the propellers 15x8, 17x8 and 17x12 were compared. In the thrust plot the 17x8 propeller has the highest thrust force with a maximum of 55N. It uses less energy than the 17x12 propeller as seen in the Current plot. The 17x12 propeller would have drawn more than 80 A if the power supply would not have been limited to a maximum of 80 A. Therefore, the PWM value never reached 100. Otherwise the 17x8 would have a bigger power output. From the tests the team got to the result that the best fitting propeller is a 17-inch propeller with a pitch of 10 to get more thrust at takeoff. This propeller configuration has almost no difference to the power output to the 17x8 but is seen more suitable for the short takeoff requirements. During the testing phase, the team has agreed, that the Scorpion SII-4025-520 will be the motor powering the aircraft. This motor suits the chosen battery for the propulsion and showed the best performance capabilities with the chosen propeller dimension of 17x10. The combination of the motor with the corresponding battery and propeller dimension proved to be best for the short takeoff requirement.

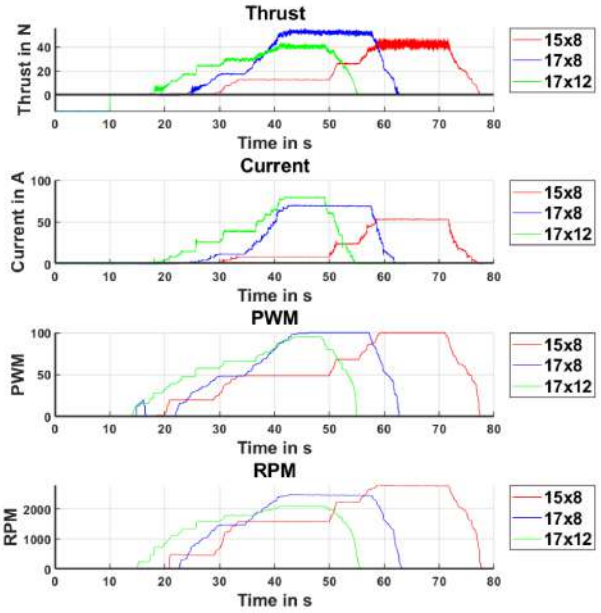

Figure 53: Force curve and ampere curve over the time

8.1.2 Structural Tests

The structural test was conducted in the form of a wing tip test as seen in Figure 54. The wing tip test evaluated the aircraft's ability to withstand multiple loads occurring during flight. To simulate the in-flight conditions on the ground the team has lifted the aircraft with the M2 payload at its wing tips and put on extra weight at the bottom of the fuselage. The extra weight is used to simulate the 2.5G load acting on the whole aircraft. In order to prevent damages to the wing and the aircraft, the extra weight has been increased gradually.

Figure 54: Wing tip loading test of the final design aircraft

8.1.3 Deployment Mechanism Test

The deployment system was tested in terms of endurance of the stepper motor and the conveyor belt. The tests showed that the choice of the NEMA 17 stepper motor and conveyor belt is sufficient for the deployment of the vial packages. After the system was integrated into the aircraft, to evaluate the functionality for the whole procedure, it showed that the system was running as planned. Figure 55 shows the deployment system during the ground test.

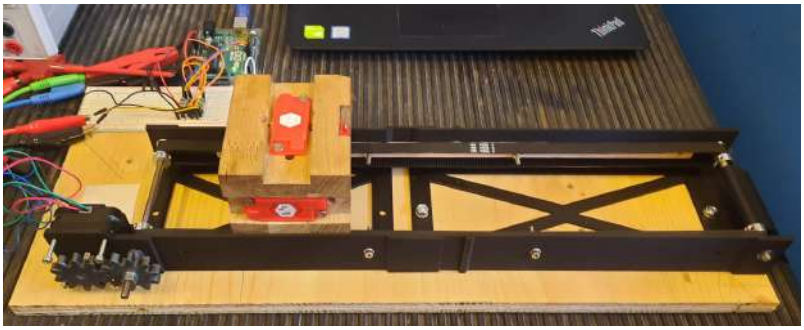

Figure 55: Deployment mechanism detailed view

8.2 System Performance

Conducting live and timed simulations of the ground mission, the flight missions and the radio fail-safe check validated the aircraft's performance. Table 41 depicts the final configuration for the competition aircraft. Resulting from the simulation runs for the ground mission, validated times are displayed for every activity in Table 42.

Table 41: Configuration of the final aircraft

Parameter	Specification
Battery propulsion	1x LiPo 4,500 mAh 6S
Battery pack M1	1 x LiPo 1,500 mAh 6S
Battery pack M2 & M3	2 x LiPo 1,500 mAh 6S
Receiver battery control 1	Traco Power THM 20-2411WI
Receiver battery control 2	TRS 0.5-2490
Electric motor	Scorpion SII-4025-520
Speed control	RCE-BL100A ESC
Propeller M1 & M2 & M3	17x10
Empty weight	11.88 lb
Total maximum weight	15.17 lb

Table 42: Ground mission test results

Activity	Time
Syringes loading time	65 s
Syringes unloading time	60 s
Loading vial packages	9 s
Deployment of the vial packages	10 s

Table 43, Table 44, and Table 45 depict the mission simulations with the most relevant values for the team. It turned out that the lap times were even better than predicted in the preliminary design phase.

Table 43: Flight test results for M1

Flight Mission 1				Weight:
Lap	Average speed [ft/s]	Distance flown [ft]	Lap time [s]	Comment
1	98.43	2,430	24.69	Takeoff within 25 ft successfull
2	99.56	2,416	24.27	
3	101.33	2,413	23.81	
Total:		7,259	72.77	Time below 300 s

Table 44: Flight test results for M2

Flight Mission 2				Weight:
Lap	Average speed [ft/s]	Distance flown [ft]	Lap time [s]	Comment
1	93.78	2,487	26.52	Takeoff within 25 ft successfull
2	92.61	2,425	26.19	
3	93.44	2,422	25.92	
Total:		7,334	77.63	Time below 300 s

Table 45: Flight test results for M3

Flight Mission 3				Weight:
Lap	Average speed [ft/s]	Distance flown [ft]	Lap time [s]	Comment
1	90.65	2,487	101.52	Takeoff within 25 ft successfull
2	88.38	2,425	101.43	
3	89.11	2,422	99.29	
4	87.45	2,421	100.77	
5	87.93	2,412	101.02	All vial packages deployed safely
Total:		12,167	504.03	Time below 600 s

8.3 Differences to Predictions and Improvements

Due to testing some aspects were changed to improve the performance of the handling of the aircraft. In the preliminary design phase it was intended to have an incidence angle of -1.5° for the vertical stabilizer. It became clear that counter trimming the angle was not tolerable so the incidence angle was changed to -0.5°. Concerning the propellers for each flight mission the team has verified a change of dimensions from the preliminary design. All three missions are flown with a propeller dimension of 17x10. During the flight testing an instability in the yawing was noticed. From the root locus plot, Figure 23 in section 4.4.2.2, it is seen that the Spiral mode is slightly unstable. The real value calculated with XFLR[5] resulted in 0,06 which shows instability. The yawing could also be triggered by an increased Angle of Attack in a steep turn where the wing blocks the clean air which is desired at the vertical stabilizer. The SD7062 airfoil used at the winglet could intensify the yawing and would become effective at steep turns. The noticed left yaw after rotation shows that the thrust angle could be set a few degrees to the right. When inflight and maximum thrust is applied the airplane tends to climb so also the down-thrust angle could be increased. During the assembly of the foam cores and the main spar of the first prototype wing, a lot of manufacturing inaccuracies and dents formed. These have been compensated by filling these imperfections with a mixture of epoxy resin and cotton flocks. This in combination with too high tolerances at the bonding gaps lead to an overall too high mass of the foam core assembly of the first prototype wing. More mindful handling of the thin foam parts and smaller tolerances for the bonding gaps decreased the mass of the second wing by about 30%.

Bibliography

[1] American Institute of Aeronautics and Astronautics (AIAA), “2021–2022 Design, Build, Fly Rules,” [online document], final version, AIAA DBF, 01 November 2021, URL: https://www.aiaa.org/docs/default-source/uploadedfiles/aiaadbf/dbf-rules-2022.pdf, [retrieved November 2021]

[2] MATLAB©, MathWorks, Inc., R2021b, Natick, Massachusetts, USA, 2021.

[3] American Institute of Aeronautics and Astronautics (AIAA), “2021-22 Design, Build, Fly Q&A #1,” [online document], AIAA DBF, 29 November 2021, URL: https://www.aiaa.org/docs/default-source/uploadedfiles/aiaadbf/resources/dbf-2021-22-q-a-1.pdf, [retrieved November 2021]

[4] Müller, M., “eCalc,” [online tool], URL: https://www.eCalc.ch/, [retrieved December 2019]

[5] Deperrois, A., “XFLR5”, [open source software], URL: https://xflr5.com/xflr5.htm, [retrieved December 2021]

[6] ANSYS©, ANalysis SYStem, Release 18.1, ANSYS, Inc., Canonsburg, Pennsylvania, USA, 2019

[7] CATIA©, Computer Aided Three-Dimensional Interactive Application, V5R16, Dassault Systems. Velizy-Villacoublay, France, 2019

[8] Meyers, K., “Wing Cube Loading (WCL),” SEFSD, [online]. URL: http://www.sefsd.org/generalinterest/wing-cube-loading-wcl/, [retrieved January 2022]

[9] Sadraey, Mohammad, "Chapter 5 Wing Design," Daniel Webster College, 2015, [online document]. URL: http://wpage.unina.it/fabrnico/DIDATTICA/PGV_2012/MAT_DID_CORSO/09_Progetto_Ala/Wing_Design_Sadraey.pdf, [retrieved January 2022]

[10] Mason, W.H., "6. Subsonic Aerodynamics of Airfoils and Wings," [online document]. URL: http://www.dept.aoe.vt.edu/ mason/Mason_f/ConfigAeroSubFoilWing.pdf, [retrieved January 2022]

[11] airfoiltools, [online tool]. URL: http://airfoiltools.com/plotter/index, [retrieved January 2022]

[12] Worasinchai, S., and Ingram, G., and Dominy, R., "A low-Reynolds-number, high-angle-of-attack investigation of wind turbine aerofoils," [online document], SAGE, 9 March 2011, URL: https://windharvest.com/wp-content/uploads/2017/03/A-Low-Reynolds-Number-High-Angle-of-Attack-Investigation-of-Wind-Turbine-Aerofoils-S-Worasinchai-G-Ingram-and-R-Dominy-SAGE-and-Institution-of-Mechan.pdf, [retrieved January 2022], doi: 10.1177/0957650911405411

[13] Raymer, D.P., *Aircraft Design: A Conceptual Approach*, 6th ed., AIAA, USA, 2018.

[14] Scholz, D., "Empennage General Design," *Aircraft Design*, [online document], Hamburg Open Online University (HOOU), 27 May 2017, URL: https://www.fzt.haw-hamburg.de/pers/Scholz/HOOU/AircraftDesign_9_EmpennageGeneralDesign.pdf, [retrieved February 2022]

[15] Yost, B., “The Energy Densities of Various Battery Types,” [online figure], National Aeronautics and Space Administration (NASA), 6 November 2019, URL: https://sst-soa.arc.nasa.gov/03-power, [retrieved December 2021]

[16] GensTattu, "Lipo Battery Guide," [online article], 2022, URL: https://www.genstattu.com/bw/, [retrieved January 2022]

[17] airfoiltools, [online tool], URL: http://airfoiltools.com/, [retrieved December 2021]

[18] Deperrois, A., "About stability analysis using XFLR5," [online document], revision 2.1, November 2010, URL: http://www.xflr5.tech/docs/XFLR5_and_Stability_analysis.pdf, [retrieved January 2022]

[19] Dauntless Aviation, "Spiral Instability," *FAATest.com*, 2022, [online article], URL: http://www.faatest.com/books/FLT/Chapter17/SpiralInstability.htm, [retrieved January 2022]

[20] Altair Hyperworks, Altair Engineering Inc., V2017.2, Troy, Michigan, USA, 2019

Massachusetts Institute of Technology

MIT AEROASTRO

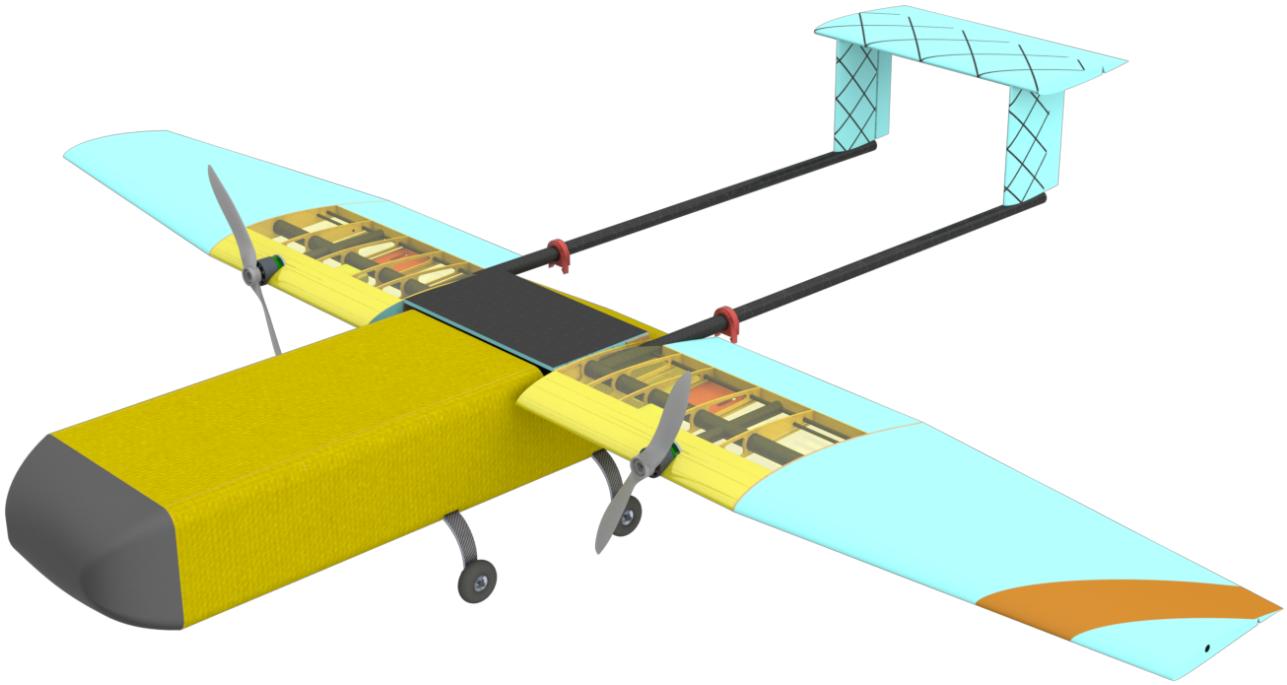

Massachusetts Institute of Technology

Spitzfire

2021-2022 Design Build Fly Competition

Raytheon Cessna AIAA

Table of Contents

1 Executive Summary

This report documents the design, manufacturing processes, and testing conducted by the Massachusetts Institute of Technology (MIT) Spitzfire team for entry in the 2021/2022 AIAA/Cessna/Raytheon Design/Build/Fly Competition. The team's objective is to produce an electric, remote-control aircraft that will achieve the highest total score: a combination of the written report score and the mission scores.

1.1 Design Overview

To maximize the scoring function for this year's competition, the team sought to maximize the number of vaccine vial packages deployed, maximize the number of syringes carried, and minimize loading time. All major aircraft structures and mechanisms required to accomplish these goals underwent rigorous manufacturing process selection and testing iteration to minimize the weight while maintaining reliability.

The amount of payload able to be carried while sustaining a high cruise velocity was determined to be a primary competitive differentiator between teams. An optimization model considering the aircraft weight, the scoring function of missions, speed, and estimated performance of competing aircraft was created to make initial aerodynamic design decisions and determine the optimum number of vaccine vial packages and syringes to carry.

Maximizing payload capacity and speed while minimizing structural weight were our main design drivers. In order to maximize the thrust and allow for a short takeoff, a dual motor configuration was chosen. A high wing was chosen to increase aerodynamic performance and allow for ease of vaccine vial deployment. A quadricycle landing gear configuration was chosen to be able to sustain multiple landings while allowing for maximum control when taxiing the aircraft. Due to the takeoff distance constraint and an emphasis on a large amount of payload, the wing was designed to be high lift with the addition of flaps while still performing well during cruise.

1.2 System Performance and Capabilities

The aircraft has a maximum cruise velocity of 25 m/s in Flight Mission 2 and a maximum cruise velocity of 20 m/s when fully loaded in Flight Mission 3. The aircraft can carry 200 syringes during Mission 2 and can deploy 8 vaccine vial packages during Mission 3. It accomplishes all flight missions under the allotted amount of time using no more than 100 W-h of propulsive energy. This high performance is achieved by employing lightweight composite construction techniques and an airframe and propulsion system designed through parameter analysis, optimization, and flight testing.

Flight tests of the aircraft show that it is stable and responsive for each of the flight missions, and the aircraft is capable of the 25 ft takeoff field length for all three missions. The prototyping and testing schedules of critical components resulted in multiple rapid design and fabrication iterations, which in turn led to a robust design. Ground mission tests demonstrate that the vaccine vial packages are reliably deployed without setting off the sensors, and both the packages and the syringes can be quickly loaded within the airframe.

2 Management Summary

The 2022 MIT team is composed of 20 undergraduates and 2 graduate students. The team has 5 seniors, meeting the DBF competition rule that one third of the team must be Freshmen, Sophomores, or Juniors.

2.1 Team Organization

The team is student run with people assigned to both technical and administrative roles. The assigned roles give specific responsibilities to ensure the proper management of the team, and there is a large amount of knowledge sharing and collaboration between members of different roles. Our faculty advisor and graduate advisor help us interact with our department while reviewing the design as necessary. The President and Vice President handle trip planning, fundraising, recruitment, and any other administrative tasks along with ensuring that all technical milestones are met in a timely fashion. The Chief Engineer finalizes design choices and collaborates with the subteam leads in order to design the system and ensure smooth integration. The social chair organizes events within the team and with other engineering teams to encourage collaboration and foster community. The subteam leads, Chief Engineer, social chair, and administrative team together form our executive board, which makes key decisions about the team. This overall team structure is depicted in Figure 2.1 below.

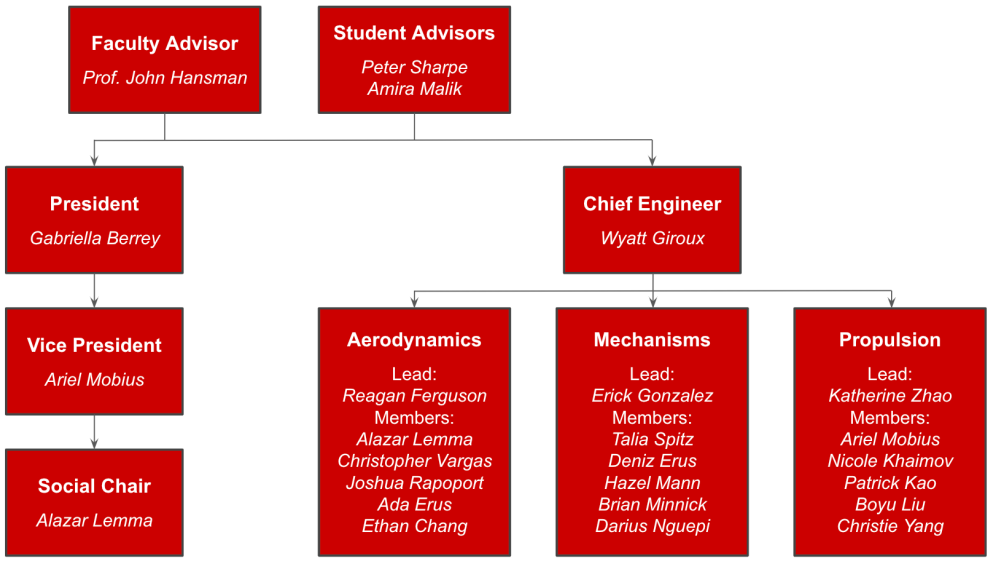

Figure 2.1: Team organization.

2.2 Schedule and Planning

The Executive Board developed a timeline for the important phases of the project, referencing it throughout the year to ensure the schedule was maintained. The team expects to complete and test the final aircraft in time for competition in late April. The timeline displayed in Figure 2.2 outlines the original schedule and compares it to the team's actual progress.

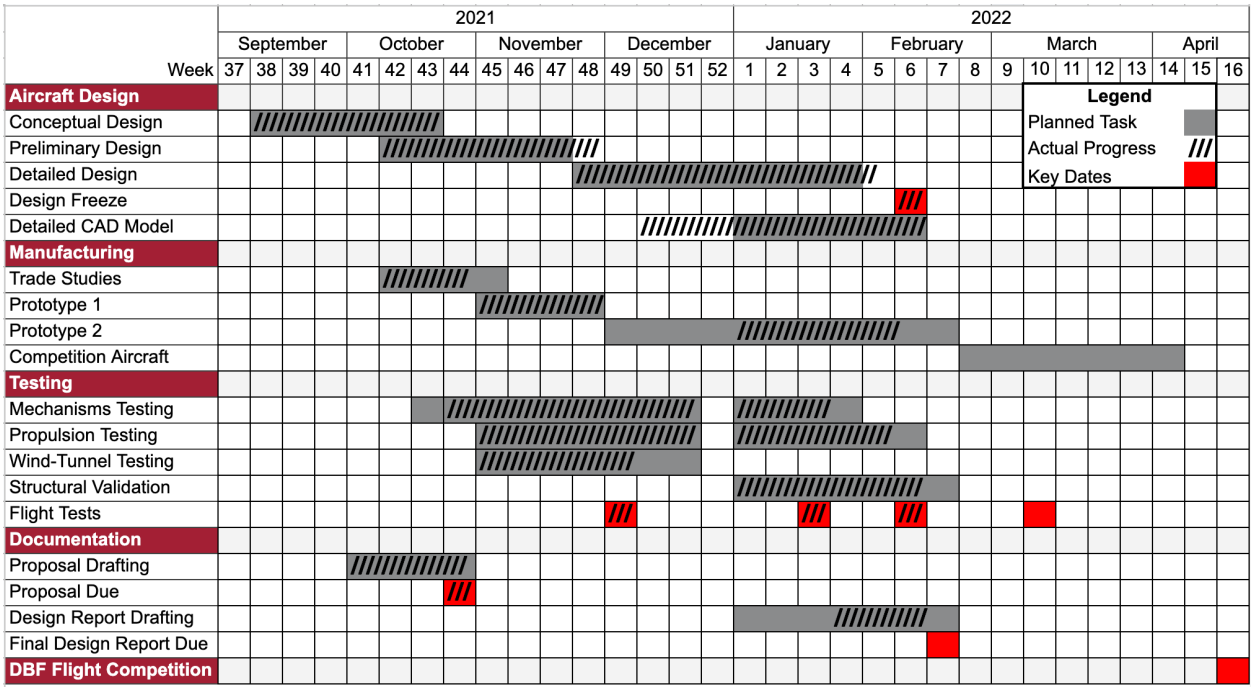

Figure 2.2: Planned schedule compared to actual progress.

3 Conceptual Design

In the conceptual design phase, the team analyzed the competition rules, mission requirements, and scoring function to identify the primary design drivers and objectives. Airframe configurations, vaccine package deployment mechanism designs, and flight control schemes were generated, rapidly prototyped, tested, and selected based on these objectives.

3.1 Mission Requirements

Based on the three flight missions and ground mission, an analysis was performed to determine the system parameters critical to all four missions.

3.1.1 Flight Mission Requirements

All of the flight missions are to be flown on the course depicted in Figure 3.1.

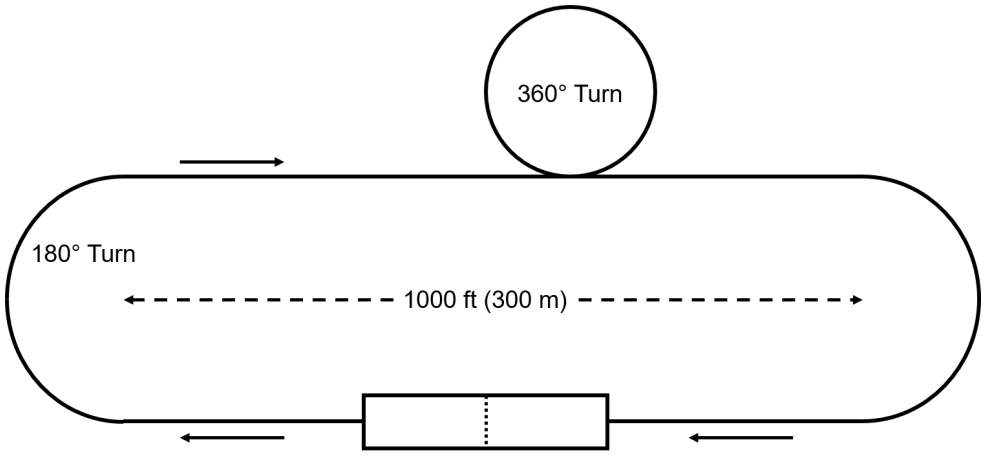

Figure 3.1: Course Layout [1].

Flight Mission 1 ***(Deployment Flight)***

The first flight mission is flown without payload. The aircraft must enter the staging box in flight configuration and take off within 25 ft. It must then fly three laps within five minutes, with time starting at initial throttle-up. Laps are counted whenever the aircraft passes the start/finish line in the air. The aircraft must then successfully land; however, landing time is not included in the five-minute window. For scoring, one point is awarded for successful completion of Mission 1.

Flight Mission 2 ***(Staging Flight)***

This mission's payload is at least ten vaccine syringes, with no maximum set. The aircraft must take off within 25 ft, fly three laps within a five-minute window, then successfully land. This mission score is calculated as the ratio of syringes carried to flight time, divided by the largest ratio obtained by any team, plus one point.

Flight Mission 3 ***(Vaccine Deployment Flight)***

This mission's payload is vaccine vial packages. The aircraft must carry at least one vial package and at most the lesser of either 1) the maximum declared during Tech Inspection or 2) the maximum number of syringes flown successfully in Mission 2 divided by ten, rounded down to the nearest integer. The aircraft must take off within 25 ft and will fly the standard mission profile each lap. After the downwind turn of a given lap, the aircraft will land on the runway and taxi to anywhere within 25 ft prior to the starting line up to the starting line. If the aircraft lands such that it cannot taxi, the ground crew member may approach, safe the propulsion system, place it on the runway, rearm the system, and return to the flight line, after which the pilot may resume. Once the aircraft has reached the designated zone, it must remotely deploy one vaccine vial package. After this, the aircraft will taxi back across the starting line, stop fully, and repeat the process from takeoff, dropping one package per lap for up to ten minutes, ending the mission with a successful landing. During each lap, the ground crew member will retrieve the package for evaluation of shock sensors and, if no sensors are triggered, the package is added to the number successfully deployed. The score for Mission 3 is the number of successfully deployed packages divided by the maximum number achieved by any team with two points added for mission completion.

3.1.2 Ground Mission Requirements

This mission is a demonstration of Flight Missions 2 and 3 on the ground within the 10' x 10' mission box. The mission begins with the aircraft inside the mission box in flight configuration, unloaded, alongside the max number of vial packages declared at Tech Inspection and a number of syringes equal to ten times the number of packages. When the ground mission official says "GO," the assembly crew member must run to the aircraft from the start/finish line and load the full Mission 2 payload. They must then run back to the start/finish line, at which point time will stop, resuming only when the ground mission official says "GO" again. The assembly crew member must then return to the mission box to remove the Mission 2 payload and install the Mission 3 payload, after which they must run back to the start/finish line with time stopping again when they cross the line. With time stopped, the pilot must remotely deploy *all* the Mission 3 payloads one at a time, with the ground crew retrieving packages between deployments. The scoring of this mission is the minimum time achieved by any team divided by our time.

3.1.3 General Aircraft Requirements

In addition to the specific missions, the aircraft is required to fulfill outside criteria. These include:

Design: The largest linear dimension of the aircraft, defined as the maximum of either the largest spanwise or chordwise measurements, must be no more than eight feet. It can use either NiCad/NiMH or Lithium Polymer (LiPo) batteries with a maximum total of 100 W-h of energy. It must be AMA legal, use commercially-produced propeller blades, and use commercial electric motors.

Payload: The aircraft must be equipped to carry both vaccine syringes and vaccine vial packages. The syringes will be standard 30-milliliter plastic syringes. Vaccine vial packages will be wooden blocks with three axis-aligned 25G shock sensors. They will weigh 8.00 +/- 0.10 oz and will have dimensions specified in Figure 3.2. For each mission, the payload must be carried in the internal space of the aircraft.

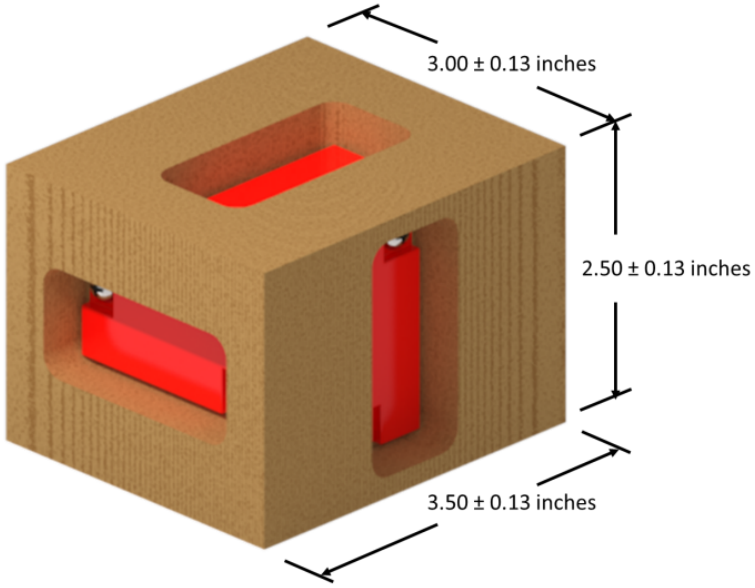

Figure 3.2: Vaccine vial package dimensions *[1].*

3.2 Score Analysis

The overall score is the product of the Written Report Score (WRS) and the Total Mission Score (TMS), shown in Equation 3.1. The Total Mission Score is the sum of the Flight Mission scores (M1, M2, M3) and the Ground Mission score (GM), shown in Equation 3.2.

$$Score = WRS * TMS \quad \text{(Eq. 3.1)}$$

$$TMS = M1 + M2 + M3 + GM \quad \text{(Eq. 3.2)}$$

Flight Mission 1's score is either one or zero for a success or failure, respectively. Flight Mission 2's score is one plus the ratio of syringes carried divided by flight time ($N_{syringes}/time$), divided by the maximum ratio achieved by any team. Flight Mission 3's score is two plus the number of successful package deployments ($N_{deployed}$) divided by the maximum number of packages deployed by any team. The Ground Mission's score is the minimum time achieved by any team divided by our team's time. The scoring functions for each mission are summarized in Table 3.1.

Mission	Scoring Equation	Maximum Score
M1 (Deployment Flight)	$M1 = 1$	1
M2 (Staging Flight)	$M2 = 1 + \frac{N_{syringes/time}}{Max_{syringes/time}}$	2
M3 (Vaccine Deployment)	$M3 = 2 + \frac{N_{deployed}}{Max_{deployed}}$	3
GM (Ground Mission)	$GM = \frac{Min_{time}}{N_{time}}$	1

Table 3.1: Scoring Function Table

Assuming all Missions are completed successfully, the Total Mission Score is:

$$TMS = 4 + \frac{N_{syringes/time}}{Max_{syringes/time}} + \frac{N_{deployed}}{Max_{deployed}} + \frac{Min_{time}}{N_{time}} \quad \text{(Eq. 3.3)}$$

3.2.1 Sensitivity Study

From Equation 3.3, it is known that variable elements of the scoring function are evenly weighted between the achieved performance on Flight Missions 2 and 3 as well as the Ground Mission. All of these are reliant on the maximum achieved score over all teams, so preliminary estimates of these values needed to be estimated.

Mission 3 depends on the number of packages a team can successfully deploy in the ten-minute window. In order to deploy as many packages as possible during the allotted time, a team must have 1) a fast cruise speed, 2) a pilot with the ability to land close to the landing zone to minimize taxi time, and 3) a rapid deployment mechanism. Due to the likelihood of pilot error in making precise, targeted landings, the time spent on the ground per lap becomes difficult to estimate. Based on input from previous team pilots and the assumption of a near-instantaneous deployment mechanism, we assumed that a good aircraft would spend 20 seconds on the ground per lap on average. Given the 100 W-h constraint on total energy, the average propulsive power during the mission is approximately 600 W. Assuming a 50% propulsive efficiency and a drag coefficient of 0.048 (determined with preliminary numerical drag models), we determined the maximum number of packages possible to deploy to be approximately 9.

Next, we estimated the maximum M2 score. Mission 2 performance is proportional to the payload mass (via #_syringes) divided by the flight time. Due to the low mass/volume fraction of a single 30 mL syringe, the total quantity of payload on a given aircraft will likely be constrained by volume instead of mass. Given the cross-section area of a syringe, historical data on teams using large fuselages, and an assumed packing fraction of 0.8 (slightly below the max achievable for circles of ~0.9) *[2],* we calculated the maximum number of syringes carried by a team to be approximately 400. Using our flight speed estimate from the M3 analysis, we obtain a flight time of 120 s. This yields a maximum theoretical Mission 2 syringe to time ratio of 3.3 1/s.

Finally, based on our testing, we estimated that the fastest ground mission time would be 20 seconds, based on a minimum payload of 10 syringes and 1 vaccine vial package. Using these estimates, an

optimization model of basic aerodynamics, propulsion, takeoff, mass modeling, and scoring was developed using the AeroSandbox optimization framework *[3]*. This model provided our baseline parameters: number of syringes = 265, number of vial packages = 8, M2 speed = 25 m/s, M3 speed = 20 m/s. A sensitivity analysis was then performed on these parameters to determine the most optimal way to vary these values in future design iterations. The results of this analysis are shown in Figure 3.3. Notably, M3 speed is not shown, as the number of packages and flight speed in Mission 3 are very strongly correlated.

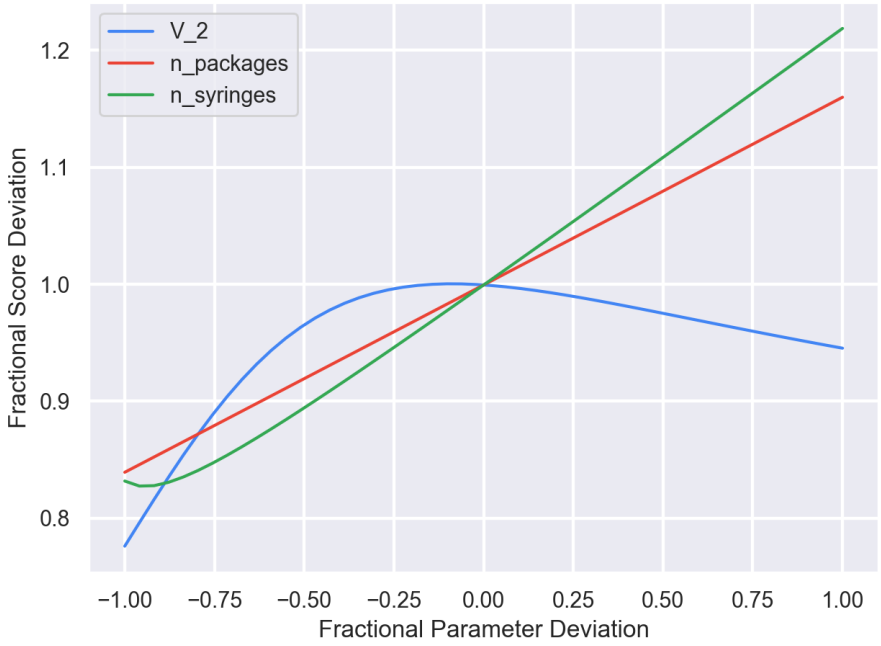

Figure 3.3: Sensitivity of Score to Design Parameters

It is apparent from this analysis that increasing the payload of each variable-score mission would lead to an increase in overall score while small variations in Mission 2 speed will have little effect. More intensive analytical design and empirical testing needed to be used to verify the optimizer models and determine an optimal overall design. It is possible that, due to the lower fidelity of the preliminary models, our code was limited by hard boundaries set by the competition rules that, in actuality, would have more margin (e.g. propulsive energy, takeoff requirements, etc.).

3.2.2 Design Drivers Conclusion

From the sensitivity analysis and optimization conducted based on the mission requirements and scoring functions, it was apparent that maximizing payload in both missions would be critical. Due to the short 25-foot takeoff distance, the low energy limit of 100 W-h, and the requirement to perform repeated landings/taxis in M3, it was determined that maximizing cruise speed, stall-C_L, and payload fraction alongside development of strong landing gear capable of rapid and precise taxiing would be critical to achieve the highest possible score. These considerations drove the design during the conceptual design phase.

3.3 Design Requirements

3.3.1 Structural Requirements

The aircraft must have a maximum linear dimension of 8 ft, and must fit inside a hypothetical 8' x 8' square. Additionally, the weight of the aircraft must be less than 55 lbs. Based on our mission requirements, it should have a high strength-to-weight ratio to maximize cruise speed. The fuselage will bear significant loads from the payloads, mechanism, wing, tail booms, and landing gear; these factors all necessitate greater structural integrity.

The aircraft must not bounce off the runway nor obtain "significant" damage while landing, as determined by the Flight Line Judge. Flight Mission 3 also requires multiple landings, followed by the aircraft taxiing to a vaccine vial package drop area. As a result of these requirements, the landing gear must be strong enough to land multiple times with a heavy payload without failure. It must also be able to have sufficient steerability and braking.

The aircraft will undergo many high-G maneuvers during the course and must have a strong wing as a result. The wing must be able to survive a wing tip load test with the battery pack and the maximum number of vaccine vial packages that the team declared for Flight Mission 3, to ensure the aircraft will survive turning maneuvers. Likewise, the empennage structure must be strong and stiff to transfer the load of the horizontal and vertical tail.

3.3.2 Payload Requirements

The aircraft is required to carry a payload for Flight Missions 2 and 3. A payload of at least 10 syringes is required for Flight Mission 2, where a syringe will weigh 18 g with a length of 13.77 cm and a diameter of 2.59 m. We anticipate carrying 200 syringes, with a total weight of approximately 3.6 kg.

For Flight Mission 3, the aircraft is required to carry at least 1 vaccine vial package. The vaccine vial packages are made of wood blocks, which weigh approximately 226.8 g. They have a maximum dimension of 6.35 cm x 7.62 cm x 8.89 cm, and within the maximum dimension the packages will contain three 25G shock sensors in the vertical, lateral and longitudinal directions. We anticipate carrying 8 vaccine vial packages, with a total weight of approximately 1.814 kg.

All payloads are required to be carried internally, and for Flight Mission 3 the aircraft is required to remotely deploy one vaccine vial package after each lap. In response, the team has decided to carry all the payloads, restraint, and deployment mechanisms inside the fuselage.

3.3.3 Propulsion Requirements

The propulsion system is carefully selected to provide optimal performance on both Mission 2 and Mission 3, while accounting for the takeoff distance constraint of 25 feet for all three flight missions. Both Mission 2 and Mission 3 require the propulsion system to be efficient with high speed and high thrust due to the heavy payloads. This is especially relevant given the 100 W-h restriction imposed by the rules. Since the system must provide enough static thrust to achieve takeoff, while also staying within this power limit, large propellers and high torque motors are needed. Due to their higher specific energy and specific power, lithium-polymer batteries should be used instead of NiMH batteries for propulsion.

3.4 System Design Concepts

The full design space for the aircraft is summarized in Table 3.2. The team evaluated, prototyped, and analytically analyzed various wings, empennages, fuselages, landing gears, and propulsion system configurations. Design points were evaluated and selected based on weight, estimated performance benefits, score impact, and manufacturability. These evaluations are discussed in the following sections.

Subsystem	Configurations		
Wing	High Wing	Low Wing	Biplane
Fuselage	Continuous	Pod + Single-Boom	Pod + Twin-Boom
Empennage	Conventional	Inverted V-Tail	T-Tail
Payload and Mechanism	Pitching Conveyor	Two-Belts	Belt and Rail
Propulsion System	Single Tractor	Twin Tractors	Push-Pull
Landing Gear	Tricycle	Quadricycle	Tail-Dragger

Table 3.2: Aircraft Design Space

3.4.1 Wing

Potential wing configurations are summarized in Table 3.3 below.

	High Wing	Low Wing	Biplane
Image	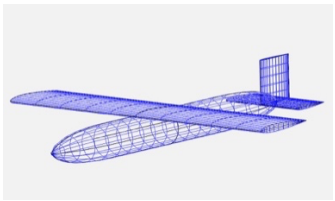	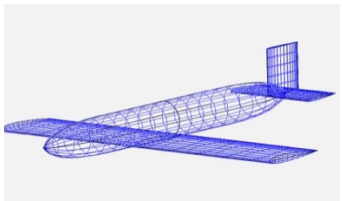	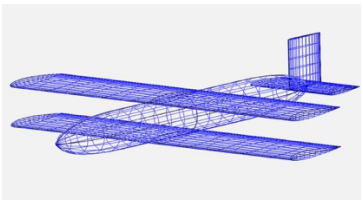
Pros	- Greater prop clearance - More lateral stability - Easier to attach - Continuous upper surface	- Better lift for ground effect - Easy to load payload	- Can handle larger wing loading
Cons	- Hard to access the fuselage interior	- Harder to deploy payload - Cannot get prop core below wing	- Aerodynamically less efficient than monoplane variations - Would require heavier wing-fuselage connections

Table 3.3: Wing Configurations

A high wing configuration allows for greater propeller clearance, greater lateral stability, and a continuous upper surface, giving better aerodynamic performance. However, the high wing makes it harder to access the interior of the fuselage, making maintenance and payload access on the aircraft more cumbersome. A low wing experiences better lift from the ground effect, and the payload is easier to load in the Ground Mission as one can open the top of the fuselage and access the payload. The biplane configuration allows for larger lift distributions than monoplane designs, but it creates more drag and would require more materials for reinforcement, especially at the wing-fuselage connection.

3.4.2 Fuselage

Due to the large amount of payload necessary for Missions 2 and 3, a rectangular pod and boom fuselage was decided on for its efficient use of volume and ease of manufacturing, despite creating more drag than a continuous fuselage. The configurations considered were a single-boom or twin-boom connection to the empennage. A single-boom would be less mass, although a twin-boom provides more stiffness and support to a large empennage. For this reason, the twin-boom configuration was chosen.

The dimensions of the fuselage were determined considering the payload and aerodynamics of the overall plane. Originally, the fuselage was made bigger than necessary. Its size was later decreased for greater stability and to concentrate the weight towards the front of the plane. A smaller fuselage also weighs less and provides less drag, so the fuselage volume was adjusted to be just big enough for the payload.

3.4.3 Empennage

We considered a twin-boom conventional tail, an inverted V tail, and a twin-boom T-tail for our design. The comparisons are summarized in the following Table 3.4.

	Twin-Boom Conventional	Inverted V-Tail	Twin-Boom T-Tail
Images	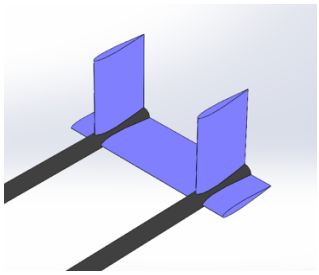	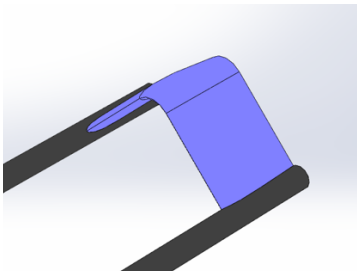	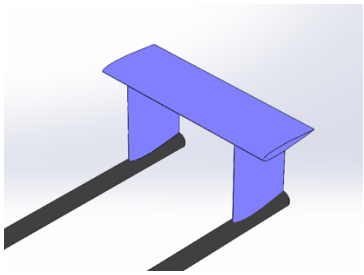
Pros	- Ease of manufacturing - Convenient to analyze	- Less drag - Ground clearance - Less weight	- Greater control authority - Great ground clearance - Greater pitching moment
Cons	- Less control authority	- Less control authority - More difficult to manufacture - More difficult to analyze	- Potential for deep stall - Greater weight

Table 3.4: Empennage Configurations

Ultimately, we chose the twin-boom T-tail configuration for our empennage. By placing the horizontal stabilizer above the fuselage, we avoid the viscous wake from the main wing and increase pitch authority. The improved pitch authority allows for control at higher angles of attack during take-off and landing.

3.4.4 Payload and Mechanisms

Different mechanism options for Mission 3 were considered including a pitching conveyor, two belts, and a belt and rail system. The pitching conveyor was a conveyor belt under the payload. During deployment the conveyor belt would pitch down to the floor. The conveyor belt would push the payload forward until one was deployed and pitch back up. The limitations were that this option would be very heavy due to motors required to pitch the bottom of the fuselage with the payload down and back up. It would also be hard to fabricate. The two-belt system would sandwich the payload between two belts. The belts would

spin in opposite directions to move the payload towards the trapdoor-slope component where they would be deployed. This method was not reliable since there had to be great tension for the conveyor belts to be able to move the payload. In the belt and rail system, rails are made under the payload and lubricated using clear packing tape and Teflon lubricant. This ensures that the boxes deploy correctly and prevents them from moving around during flight. A conveyor belt was put on top of the payload. The conveyor belt had bolts sticking out to push the payload forward. This method was chosen due to its consistent success in deploying the payload, ease of fabrication, and low weight.

	Pitching Conveyor Belt	Two-Belts	Belt and Rail System
Images	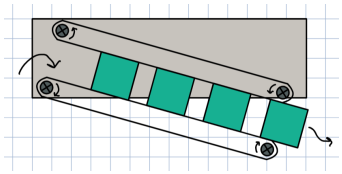	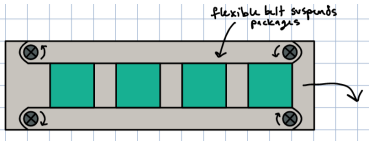	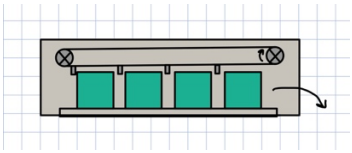
Pros	- Low chance of setting off sensor	- Easier to manufacture - Packages cannot get stuck	- Easy to manufacture - Low weight
Cons	- Heavy due to motors - Fuselage complications - Difficult to manufacture	- Potential to set off sensor - Unreliable due to the need for a high tension in the belts	- Potential for packages to get stuck on rail - Potential to set off sensor

Table 3.5: Mechanism Configurations

3.4.5 Propulsion System

The propulsion system was driven by the need to take off in a short distance while having limited power. Because a single motor would have trouble creating the amount of thrust required for the short takeoff and would require a very large propeller, a dual motor system was decided on. The push-pull configuration was ruled out, because it would be less efficient than the twin tractor configuration due to the disruption of airflow ahead of the rear propeller by the front propeller. Thus, a twin tractor configuration was selected for its high static thrust, relative efficiency, and the benefit of supporting differential thrust. Differential thrust also will help with the taxiing ability of the aircraft which is important for Mission 3. These design considerations are highlighted in Table 3.6 below.

	Single Tractor	Twin Tractors	Push Pull
Image			
Pros	- Simple to design and build - Greatest specific power	- Requires smaller propellers - Possibility of differential thrust	- Requires smaller propellers - Zero net angular momentum

		- Less trim drag due to zero net angular momentum - More thrust overall	- Less structural complexity than twin tractors
Cons	- Requires a larger propeller, adding weight and added ground clearance - Large angular momentum could lead to control issues	- Greater structural complexity - Lower specific power compared to single motor	- Less efficient than twin tractors - Tail boom clearance - Center of gravity shifts back

Table 3.6: Propulsion Configurations

3.4.6 Landing Gear

Landing gear was a major consideration due to the need to take off and land repeatedly, as well as taxi the plane multiple times during the third mission. The three configurations taken into account were tricycle gear, quadricycle, and tail dragger. The tail dragger configuration was ruled out due to the possibility of the deployed payload in Mission 3 interfering with the bottom of the empennage. Due to the size and weight distribution, the tricycle configuration proved to be unable to support the weight of the aircraft in prototype testing, so a quadricycle configuration was chosen. This configuration provides more stability on the ground and distributes the landing forces such that each wheel will take less stress. Additionally, the two back wheels will have separate brakes attached to them and the front wheels will be castor wheels to allow the plane to steer freely using differential braking when taxiing. The configuration comparisons are highlighted in Table 3.7.

	Tricycle	Quadricycle	Tail Dragger
Image	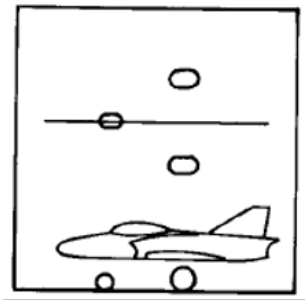	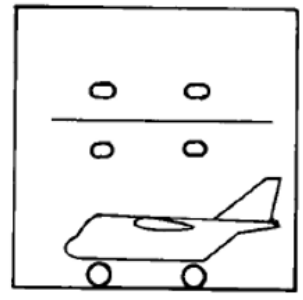	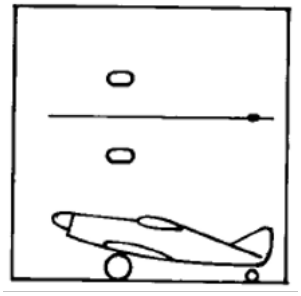
Pros	- Stable during taxi - Moderate weight/drag - Less chance of nose-over	- Most stable configuration in taxi - No chance of nose-over - Durable for multiple landings	- Lightest and least drag - No chance of tail strike - Pre-set angle of attack on takeoff
Cons	- Chance of tail strike - Requires rotation during takeoff	- Greatest weight & drag - Chance of tail strike - Requires rotation on takeoff	- Least stable on ground - Chance of nose-over - Interference with deployed payloads

Table 3.7: Landing Gear Configurations

3.5 Configuration Selection

3.5.1 Concept Weighting and Selection

Concepts for each subsystem were ranked based on four criteria: Weight, Drag, Performance, and Ease of Fabrication. Weight and drag are self-explanatory. Performance depends on the sub-system; for example, for the vaccine deployment system, performance is mainly measured by the ability of the device to quickly and reliably lower the package to the ground without exceeding the 25G maximum loading limit. The criteria were assigned weights according to the chart in Table 3.8.

Criteria	Weight
Weight	0.25
Drag	0.25
Performance	0.6
Ease of Fabrication	0.2

Table 3.8: Concept Selection Criteria

Each concept within a subsystem was ranked in inverse order, i.e., higher numbers are better, and assigned a score based on the weighted sum of their ranks within each category. In the case of a tie between ranks, both concepts receive the higher rank. Concept ranking and scoring is shown in Table 3.9.

Subsystem	Concept	Rankings				Final Score
		Weight	Drag	Performance	Ease of Fabrication	
Wing	Low Wing	3	2	1	3	2.45
	High Wing	2	3	3	2	**3.45**
	Bi Wing	1	1	2	1	1.9
Fuselage	Continuous	2	3	1	1	2.05
	Pod + Single-Boom	3	2	1	2	2.25
	Pod + Twin-Boom	2	2	3	2	**3.2**
Empennage	Twin-Boom Conventional	3	2	3	3	3.65
	Inverted V-Tail	4	3	2	2	3.35
	Twin-Boom T-Tail	3	2	4	3	**4.25**
Vaccine Deployment	**Belt and Rail**	4	4	3	4	**4.6**
	Twin Belts	3	4	2	3	3.55
	Pitching Conveyor	1	4	4	1	3.85
	Elevator	2	4	1	2	2.5
Propulsion	Single Tractor	3	3	1	3	2.7
	Twin Tractor	1	2	3	2	**2.95**
	Push-Pull	2	1	2	1	2.15
Landing Gear	Tricycle	2	2	1	2	2
	Quadricycle	1	1	2	2	**2.1**

Table 3.9: Concept Ranking and Scoring

3.5.2 Final Morphological Chart

Based on the results of the selection process, the configuration summarized in Table 3.10 and Figure 3.4 was selected.

Wing	Fuselage	Empennage
High Wing	Pod + Twin-Boom	Twin-Boom T-Tail
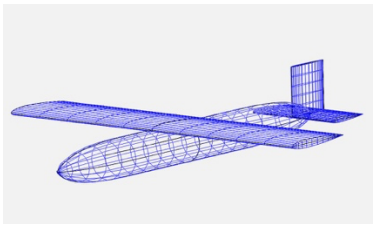		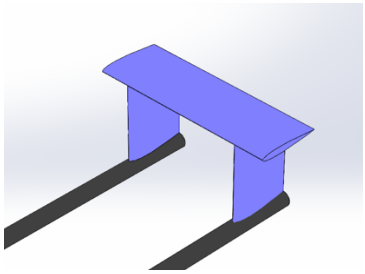
Package Deployment Mechanism	**Propulsion**	**Landing Gear**
Belt and Rail System	Twin Tractor	Quadricycle
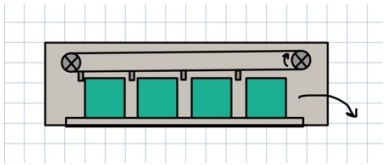		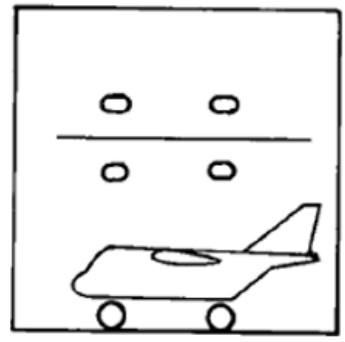

Table 3.10: Final Conceptual Configuration of the Aircraft

Figure 3.4: Final Concept Sketch

4 Preliminary Design

With the aircraft conceptual design and configuration determined, extensive analysis and trade studies were carried out to validate optimization models and determine the aircraft parameters which would maximize the scoring function. The preliminary design phase involved conducting design/sizing trades, validating a whole-system model in Python to estimate aircraft performance, conducting aerodynamic analysis using XFLR5 [c4], and collecting experimental performance data to verify our choices.

4.1 Design Methodology

In order to break down the problem of optimizing the aircraft performance, the preliminary design was carried out in stages. Our design methodology is summarized in Figure 4.1.

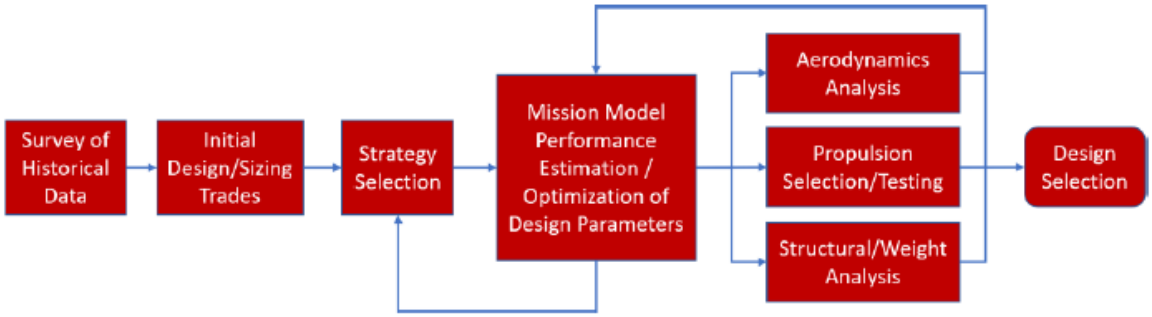

Figure 4.1: Design Methodology Flowchart

With historic and initial sizing weighed during conceptual design and with a vehicle configuration chosen, the AeroSandbox Python optimization framework *[3]* was used to determine baseline aircraft geometry, aerodynamic/propulsive performance, structural stability, and score. From these base parameters, results were verified and iterated on using higher fidelity software packages such as XFLR5 *[4]* (aerodynamic calculations), eCalc *[5]* (propulsive calculations), and SolidWorks Finite Element Simulation *[6]*. Wind tunnel testing was performed to gather empirical data.

All of these factors were combined to refine our optimization model further in order to obtain a new design point. This procedure was iterated until a satisfactory design was achieved.

4.2 Trade Studies

Tradeoffs exist between performance on each mission, so determining the optimal strategy and aircraft parameters required in-depth trade studies. We focused on the short takeoff and minimizing the aircraft weight while looking at the following parameters:

Chord

With a maximum wingspan of 8 ft, the total planform area of our wing was almost entirely dependent on the mean aerodynamic chord of the wing. A larger chord would help distribute wing loading and increase maximum lift, allowing for better takeoff and turning performance, at the cost of higher weight of the aircraft. However, due to the inverse relationship between chord and aspect ratio, increasing chord length would decrease our overall efficiency.

Syringes

Our Mission 2 score is directly proportional to the number of syringes we can carry. Due to their low density, our main constraint on the number of syringes we can carry is based on the internal volume of the fuselage. Increasing fuselage volume comes with an increase in fuselage weight, which drives up the wing area requirements, increasing overall drag.

Vaccine packages

Our Mission 3 score is directly proportional to the number of vaccine packages we can carry. Increasing the number of packages quickly drives up our Mission 3 weight, increasing the wing area and decreasing performance. Vaccine package count is directly tied to syringe count both in terms of constraints and in terms of mass reduction. In order to maintain a lower internal volume, the fuselage should only be as big as the mechanism, meaning increasing the number of syringes and vaccine packages will happen proportionally.

Propulsion sizing

The major constraints of our propulsion system were on the 25 ft takeoff distance and our 100 W-h energy constraint. Our propulsion system needed to have a high enough static thrust to accommodate a short takeoff, as each mission requires the takeoff distance constraint. Because of the different weights in each of the three missions, we need our propulsion system to be efficient within each of our operating speeds while also maintaining a low weight.

4.2.1 Primary Mission Model and Optimization

To obtain starting parameters for a design iteration, an optimization model was constructed in Python. This model, written using the AeroSandbox optimization framework *[3]*, consists of higher-fidelity estimates of a great number of parameters including airfoil performance, fuselage drag, propeller performance, static stability, and takeoff estimates. This simulation was iteratively updated to reflect experimental data from tests, as well as aerodynamics analysis from XFLR5 *[4]* and OpenVSP *[7]*. The critical models and their results are described in the following sections.

Aerodynamics

Airfoil performance was estimated using two curve fit models refined by iterations in XFoil *[8]*. The airfoil lift coefficient, C_l, was given a linear fit to model cruise while the profile drag coefficient, C_d, was modeled using a parabolic fit within the same operating angles of attack as the lift coefficient. These curve fits were discretely generated for a representative selection of Reynolds numbers within our operating envelope determined by first-order estimates. To estimate the 3-dimensional lift coefficient, we utilized aspect ratio (AR), the Prandtl-Glauert correction factor (β), and the assumed airfoil efficiency ($\eta = 0.95$).

$$\frac{C_L}{C_l} = \frac{AR}{2+\sqrt{4+(AR*\frac{\beta}{\eta})^2}} \quad \text{(Eq. 4.1)}$$

From this, overall drag coefficient could be estimated using the induced drag relation,

$$C_D = C_{d0} + \frac{C_L^2}{\pi\, AR\, e} \quad \text{(Eq. 4.2)}$$

where C_{d0} is the profile drag and *e* is the Oswald's span efficiency factor. Lift was constrained in the optimizer by ensuring that the condition for level flight was met by solution parameters. Namely,

$$mg = q_\infty S C_L \quad \text{(Eq. 4.3)}$$

Tail surfaces were estimated to be flat plates for the purposes of drag estimation and the fuselage was estimated to be a blunt body in flow.

Propulsion

Our propulsion models fulfilled two primary functions: to estimate the required thrust and to estimate the required power to produce that thrust in order to ensure our energy constraint (100 W-h) is not exceeded. To do this, the thrust is estimated using level flight conditions (thrust equals drag) with a safety factor of 1.5 multiplied to the cruise drag. Dynamic disk actuator theory modeled natively in AeroSandbox is then used to obtain required shaft power, and a motor efficiency estimate is used to obtain a required power of flight. The optimizer constrains the overall design space by ensuring that the required power does not exceed the average available power, equal to the energy of the battery divided by the mission time estimate.

Static Stability

To estimate static stability, the center of gravity (CG) and aerodynamic neutral point (NP) had to be estimated. To estimate the CG, historical surveys of previous team aircraft components were done to produce estimates of all component masses. These empirical masses were then placed on individual optimization variables and were given reasonable constraints (e.g. tails must be behind the wing, etc.). The neutral point was estimated using XFLR5 *[4]* after a first iteration without stability modeling, and was iterated to ensure accuracy. The static margin was calculated from this information and was generally constrained to between 5% and 15% to produce a weakly stable aircraft.

Takeoff

The takeoff model assumed constant static acceleration until takeoff, with values drawn from the team's library of thrust data from various motor/propeller configurations. Knowing this, the takeoff speed and distance were calculated to be

$$V_{to} = \sqrt{\frac{2mg}{\rho S C_{L,max}}} \quad \text{(Eq. 4.4)}$$

$$d_{to} = \frac{V_{to}^2}{2a_{static}} \quad \text{(Eq 4.5)}$$

where $C_{L,max}$ is the stall lift coefficient of the aircraft, and a_{static} is the constant static thrust. The takeoff distance was then given the constraint to be less than 20 feet (safety factor of 1.25) to ensure the aircraft can rotate in the allotted distance.

Initial Results

After initial evaluation, the optimizer model produced a set of results upon which future changes were based. To elaborate on the baseline parameters established in Section 3.2.1, the model returned initial critical parameter values enumerated in Table 4.1. These values were further analyzed and iterated until the final design was achieved, as is described in the following sections.

Parameter	Value	Units
Wingspan	2.43	m
Wing Area	0.9	m^2
Wing Aspect Ratio	6	—
Wing Taper Ratio	0.6	—
Number of Syringes (M2)	200	—
Number of Packages (M3)	8	—
Propeller Diameter	16	in
Propeller Pitch	10	in
Number of Motors	2	—

Table 4.1: Initial Optimizer Results

4.3 Aerodynamics

The airframe was design by analysis using XFoil [8] and XFLR5 [4]. XFoil [8] was used for the initial selection and analysis of the airfoils. Aerodynamic performance of the airfoil, wing geometry, and the static and dynamic stability derivatives were found using XFLR5 [4], which uses vortex-lattice method.

4.3.1 Airfoil Selection

A set of airfoils were chosen based on the requirement for a short takeoff and landing, requiring a high maximum lift coefficient. The airfoils considered were the NACA 4408, NACA 4410, NACA 5410, SD7032, and the SD3021. The analysis was conducted at alpha ranges of -10° to 15°, and at our target Reynolds number of 560,000. The analysis is shown in Figure 4.2 below.

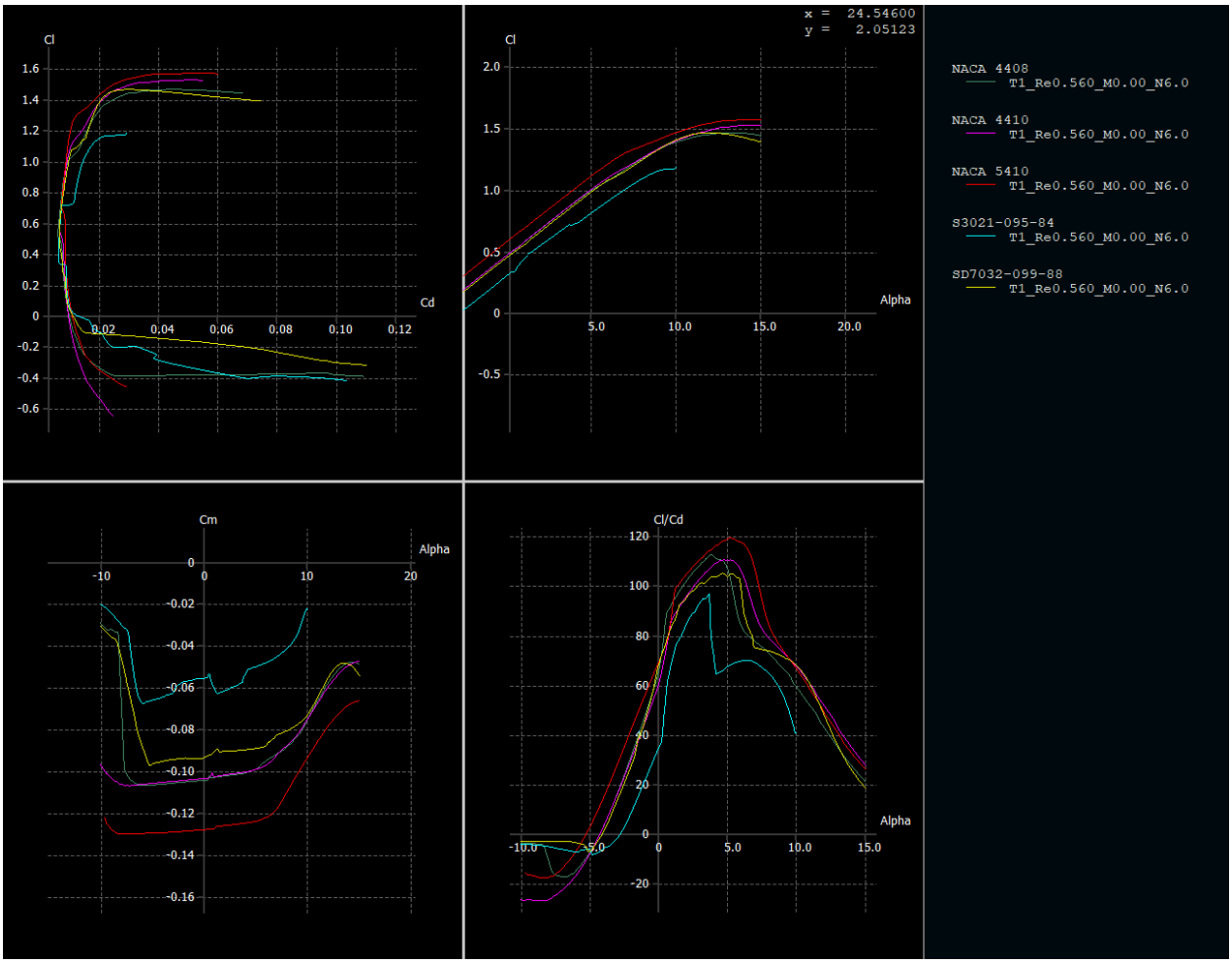

Figure 4.2: XFLR5 [4] Analysis of Candidate Airfoils

According to our analysis, the NACA 5410 performs the best given the flight requirements. A major drawback is that the camber of the NACA airfoils considered are too concave, such that manufacturing and structural reinforcements of the wing would prove a major concern. For our operating conditions, we found better performance from the SD7032 than from other airfoils considered. Thus, the SD7032 was selected for the final design.

4.3.2 Fuselage Aerodynamics

The fuselage was designed around being able to contain the mechanism, which occupies a large volume within the plane. In order to improve the aerodynamic performance of the fuselage, a rounded rectangular profile was selected, with a blunt nose and sharp trailing edge to streamline flow around it. Parasitic drag analysis in OpenVSP *[7]* showed there to be a C_{d0} of 0.00631 for the fuselage and 0.020964 for the entire aircraft.

4.3.3 Tail Sizing

The tail was sized for minimal structural weight while both maintaining stable flight during all missions and remaining within the eight-foot length maximum. Due to Mission 3's shifting CG from repeated vaccine vial package deployment, the tails were also sized to maintain stable flight for all package configurations. Aspect ratios for all tail surfaces were given a minimum value of 1 to ensure favorable aerodynamic characteristics. Stability of a given set of tail parameters was assessed using the horizontal and vertical tail volume coefficients, kept between 0.3 to 0.6 and 0.02 to 0.05 respectively to ensure ease of control of the aircraft. These tail volume coefficients are defined as:

$$V_h = \frac{S_h l_h}{Sc} \quad \text{(Eq. 4.6)}$$

$$V_v = \frac{S_v l_v}{Sb} \quad \text{(Eq. 4.7)}$$

The control surface sizing was set at 30% chord length for each aerodynamic surface. Both the tail volume coefficient ranges and control surface chord fraction were based on historic team flight testing results. Stability assessment from flight testing was the primary driver for following tail and control surface size iterations.

4.4 Stability and Control

4.4.1 Lateral Stability

Root locus stability analysis was performed in XFLR5 *[4]*. Figure 4.3 shows the lateral stability results for all three flight missions. The aircraft is expected to be stable in both the Dutch roll and roll subsidence modes for all missions, regardless of the payload variations. As payload mass increases in the order of Mission 1, Mission 3, Mission 2, the poles move further from the root locus origin. For Dutch roll, the dramatic motion of roots primarily in the imaginary direction indicates the lowering of the mode's damping, which will lead to longer yaw oscillations. The damping will reach a minimum in Mission 2 due to the forward shift in CG location due to high payload. Contrary to this, the roll disturbances recover faster as payload mass increases, maximizing recovery speed in Mission 2. Spiral mode is expected to be marginally unstable due to the aircraft's lack of dihedral. The time constant of the mode exceeds 20 seconds, meaning that a pilot would have ample time to correct for the mode before it could become problematic.

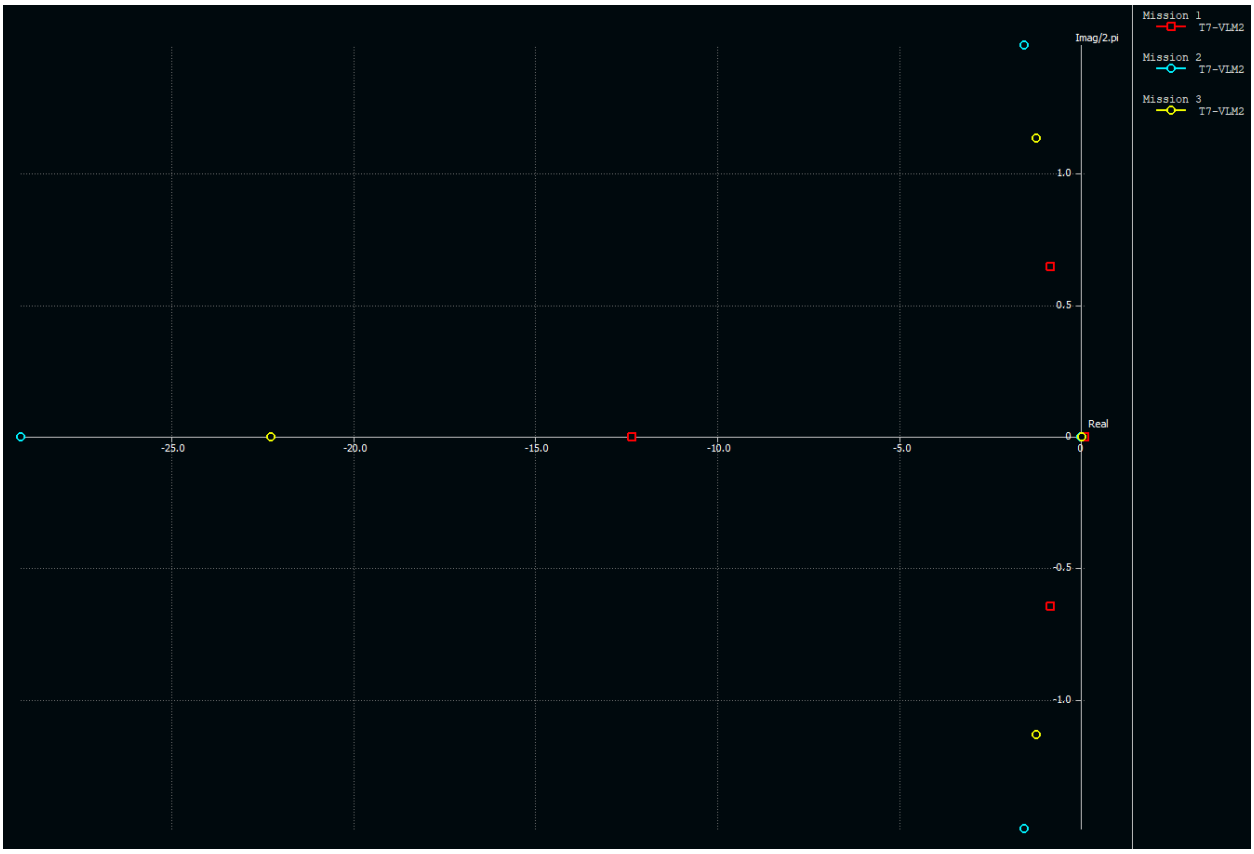

Figure 4.3: Lateral Stability Root Locus

4.4.2 Longitudinal Stability

Figure 4.4 shows the longitudinal mode root locus diagram, which indicates that the aircraft will experience a well-damped short period mode and a stable phugoid mode across all flight missions. While the phugoid characteristics for the missions are comparable, the short period mode grows more stable in order of Mission 1, Mission 3, Mission 2. Mission 2 exhibits the fastest short period recovery, due again to a forward shift in CG location caused by high payload mass.

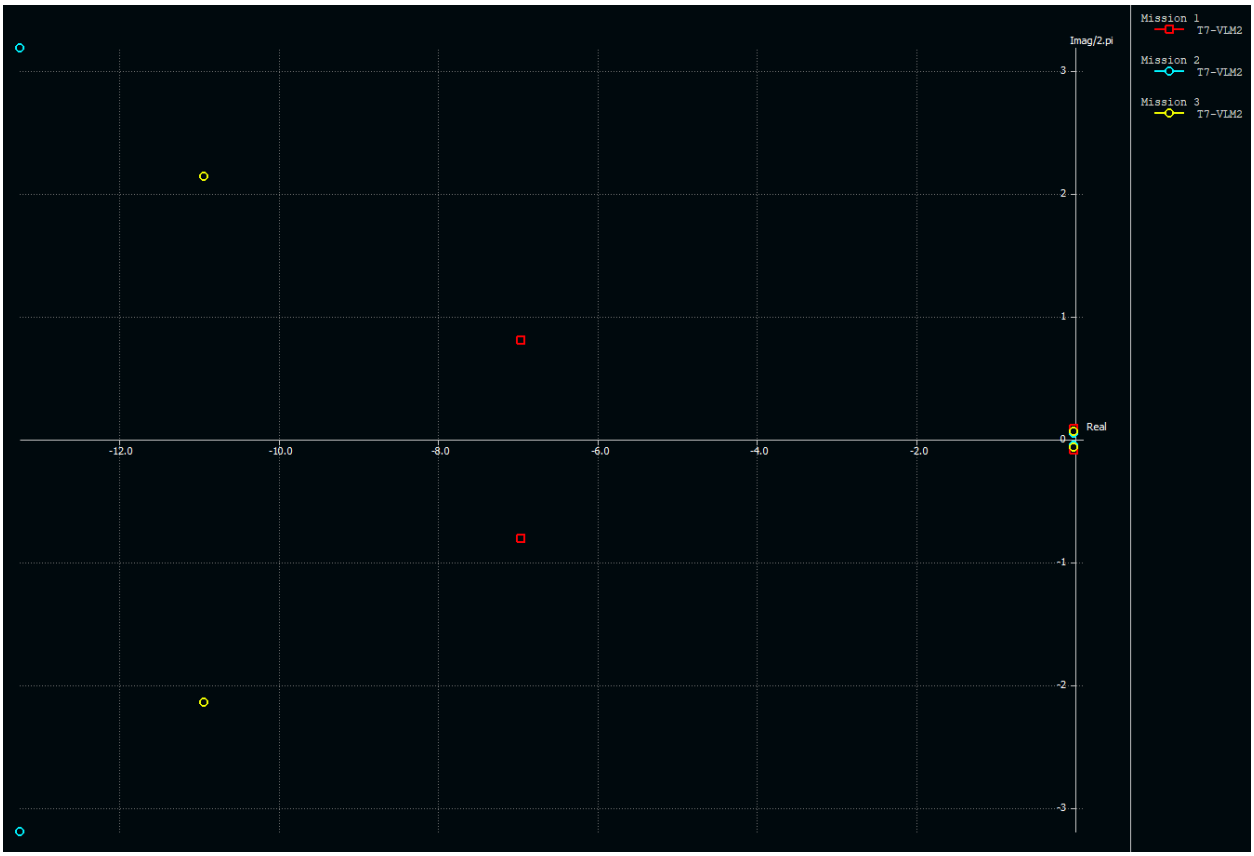

Figure 4.4 - Longitudinal Stability Root Locus

4.4.3 Center of Gravity

The neutral point of the aircraft, calculated using the XFLR5 model, was 0.169m. The aircraft's center of gravity was at 0.135 m from the leading edge for Mission 1, 0.100 m for Mission 2, and 0.113 m for Mission 3 with all 8 vaccine vial packages. Using this information, the static stability margin was calculated for each flight mission using Eq. 4.6 below. The static margin was 9.19% for Mission 1, 15.1% for Mission 2, and 18.6% for Mission 3. As packages are deployed in Mission 3, the CG will slowly return back to the CG of Mission 1, ensuring stable flight throughout Mission 3. These data and our flight tests indicate that the CG location is acceptable for controlling and handling the aircraft.

$$S.M. = \frac{x_{np} - x_{cg}}{c} \quad \text{(Eq. 4.6)}$$

4.4.4 Wing and Tail Incidence

XFLR wing and tail analysis showed an angle of incidence of 0° for both the main wing and the tail to be ideal. This is done to minimize the drag and to optimize the performance of the wing. The aerodynamic surfaces and masses were distributed so that no elevator deflection was required for proper trim.

4.5 Propulsion System

A twin-tractor propulsion system was selected for its negation of motor torque and high static thrust to power ratio. Since competition rules require commercial power system components, the design of the propulsion system revolves around selecting available batteries, motors, and propellers which can match

the ideal parameters as closely as possible. A battery cell type and count were chosen to provide the required energy and power while not exceeding 100 W-h. Then, several leading battery brands were compared based on discharge testing to select the one with the highest true capacity and the lowest resistance. Based on the pack voltage, motor and propeller combinations were chosen that would be able to match the optimal motor power and RPM determined by the performance optimization. Candidate system combinations were compared based off of calculated capabilities in this preliminary design process.

4.5.1 Batteries

To select batteries for the aircraft, we found the amount of energy required. Mission 3 was used to calculate this, as we wanted to account for the extra energy needed for multiple takeoffs and the maximum flight time of 10 minutes. To perform this calculation, we used the estimated takeoff velocity, historical drag data, and course length to calculate the thrust and power needed at both takeoff and steady flight. We determined that we needed at least 50N of thrust for takeoff and 10N of thrust for steady flight, assuming 0.6 propulsive efficiency. With the time limit of 10 minutes, we will need at least 60 W-h of energy.

The next step was to select a battery voltage. The 100 W-h energy constraint creates a tradeoff between battery capacity and voltage. Because low-KV motors use less current and consequently have lower resistive losses, we decided to use the maximum of 6 LiPo cells with 22.2V in total. We then selected a total capacity of 4500mAh that would maximize total energy to account for losses due to the fact that LiPo batteries normally discharge at a lower rate than expected. There were two options: two 6s batteries with around 2200mAh capacity or one 6s battery with 4500mAh capacity. Fitting two 6s batteries in a configuration that optimized energy storage, discharge, and capacity was more difficult than using one 100 W-h 4500 mAh battery, so we decided to use one battery. Two brands were selected as candidates: Zippy Compact 40C 4500mAh and Turnigy Nano-tech 45C 4500mAh. We used historical data in which each of these batteries were discharged under a 4A load until they reached 22V (approximately 80% discharged) by a West Mountain Radio CBA battery tester. These results show that batteries have approximately the same capacity. Since the Turnigy Nano-tech is 0.3 lbs. lighter, the Turnigy brand was preferred.

4.5.2 Propellers, Motors, and ESCs

The motor and propeller candidates are selected together to maximize system performance. To do this, the following procedure was followed:

1. Using the mission mode, propellers and motors were sized based on the necessity of short, repeated takeoffs on Mission 3 as well as the 100 W-h energy limit. We calculated the amount of thrust needed for the takeoffs and selected motor-propeller combinations that would achieve these requirements.
2. Based on the computed thrust and power requirements, candidate motors were selected by an aircraft configuration analysis tool called eCalc *[]* as well as a search through reliable motor manufacturers. eCalc *[5]* accounts for the motor's power output and power-to-weight ratios, based on first-order approximations of required aircraft power and thrust.
3. After determining candidate motors and corresponding propellers, candidates were compared by simulating their speed, power, and thrust using eCalc *[5]*. We looked for motors that would be able

to provide the required thrust without exceeding the 100 W-h energy limit, using a propeller with diameter at most 16 inches for manufacturing purposes. We then narrowed the search further by choosing the motor that maximized flight time and speed.

4. After determining the motor, candidate propellers were chosen based on data charts available on manufacturer websites, with the 16-inch maximum diameter in mind. Candidates were compared by testing their power output, efficiency, and thrust.

At the current phase of iteration, the Cobra 4130/20 300 KV is the most promising. The optimal propeller for use with this motor was determined to be an APC 15x10. After performance simulation and thrust testing described in sections 7 and 8, this motor-propeller combination was determined to be the most efficient over the aircraft's flight time and required thrust. This motor was found to draw a maximum of 52A according to the manufacturer website. Therefore, we selected the Phoenix Edge 75A ESC as a compatible ESC. At about 4.0 oz, this ESC is able to continuously provide the current required for our aircraft's system.

4.6 Estimated Performance

4.6.1 Aerodynamic Performance

The lift and induced drag forces were calculated in XFLR5 [4]. The parasitic drag of the aircraft was also accounted for in XFLR5 via computation of the zero-lift drag coefficient in OpenVSP [7]. The L/D plot in Figure 4.5 is a result of these methods. The solid curve represents the L/D with flaps up while the dashed curve represents the L/D with flaps down. This curve applies for all missions. The L/D curves for both missions are relatively flat over the range of angles of attack: flaps-up L/D peaking in the range of 12.5 to 13 from alpha 1.5 to 5.5 degrees, while flaps-down peaks in the range of L/D 6.5 to 7 from alpha 2.5 to 6.5.

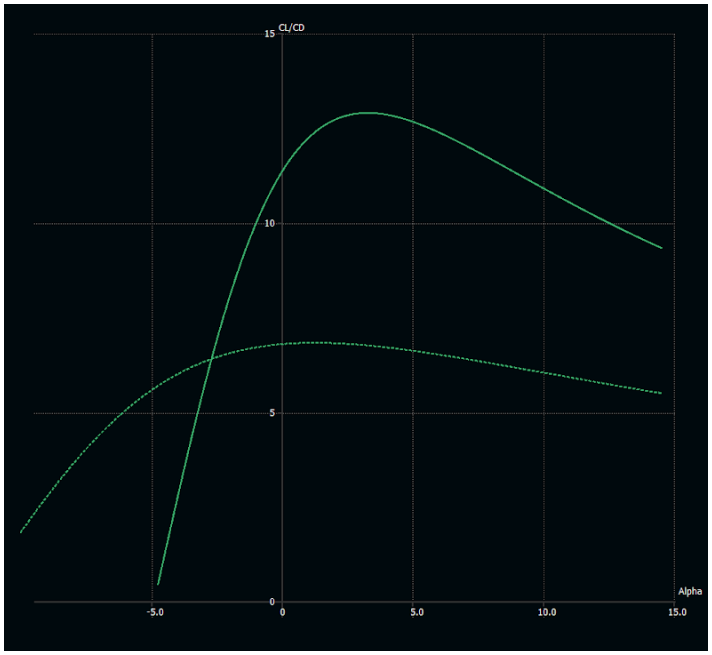

Figure 4.5 – L/D Plot. The solid line is with flaps up while the dashed curve is with flaps down.

4.6.2 Mission Performance

The estimated mission scores, given in Table 4.2, are determined from the optimization model detailed in section 4.2.2 with speed estimates refined by propulsion testing. During Mission 2, the aircraft is predicted to complete three laps in 150 seconds while carrying a payload of 200 syringes. During Mission 3, the aircraft is predicted to complete eight deployments with an average lap/landing time of 73 seconds. Based on ground mission time trials, we estimate the ground mission will take 91 seconds. With the estimated maximum mission scores calculated in section 3.2, our estimated score can be calculated.

Mission	Laps	Payload	Time	Estimated Best	Score
Flight Mission 1	3	-	-	-	1
Flight Mission 2	3	200 Syringes	150s	3.3 [1/s]	1.40
Flight Mission 3	10	8 Vial Packages	584s	9 packages	2.89
Ground Mission	-	-	91s	20 s	0.22
				Total Mission Score (TMS)	5.51

Table 4.2 - Predicted Mission Performance

5 Detail Design

5.1 System Dimensional Parameters

All critical dimensions for the MIT Spitzfire plane are summarized in Table 5.1.

General Airframe		Horizontal Stabilizer	
Length	1.97 m	**Airfoil**	NACA 0010
Span	2.44 m	**Chord**	0.25 m
Height	0.51 m	**Span**	0.50 m
Ground Clearance	0.08 m	**Planform Area**	0.125 m^2
Fuselage		**Aspect Ratio**	2
Body Shape	Rounded rectangle	**Tail Volume**	0.416 m^3
Length	1.12 m	**Angle of Incidence**	0.0 deg
Maximum Width	0.33 m	**Vertical Tails**	
Maximum Height	0.18 m	**Airfoil**	NACA 0010
Wing		**Chord**	0.15
Airfoil	SD7032	**Span**	0.225
MAC	0.340 m	**Planform Area**	0.03375 m^2

Span	2.44 m	**Aspect Ratio**	1.5
Planform Area	0.810 m^2	**Tail Volume**	0.016 m^3
Aspect Ratio	7.29		
Angle of Incidence	0.0 deg		

Table 5.1: Aircraft Dimensional Parameters

5.2 System Structural Characteristics

The aircraft's structure is broken up into the wing-tail assembly and the fuselage.

The wing is constructed from a central built-up section with a static foam leading edge and an actuated foam trailing edge. The foam trailing edges have been enhanced with a glass fiber composite cover to increase the stiffness and durability of the parts. Two motor mounts machined from aluminum are rigidly mounted to the carbon fiber spar running the length of this section of the wing in order to provide a hard point to mount the two Cobra Motors. Two glass fiber enhanced solid foam wing tips attach to the central wing section to bring the wing to its full 8 ft span. These outer wing sections also have ailerons on a separate control mechanism from the flaps on the built-up section of the wing for roll control of the aircraft. The wing tip extensions are mounted to the central wing section through two friction fit carbon fiber spars.

The twin tail booms fit to within carbon fiber tubes of the wing and are secured in by a bolt and 3D printed snap ring. The tail is made with a foam core and cross-hatching carbon fiber tow beneath a glass fiber composite layup. There are actuated control surfaces for both the rudders and the elevator.

The fuselage itself is constructed from interlocking laser cut plywood panels which are glued together. A layer of Kevlar over these panels increases the aerodynamic efficiency and structural integrity of the fuselage. The lightweight fuselage mounts to the wing assembly through a carbon fiber foam composite board spanning the width of the fuselage and is attached to the plywood panels with sections of carbon fiber cloth. Two nylon bolts and two pegs connect the wing assembly to the fuselage through this plate. The nose of the airframe is constructed from a solid foam block cut into an aerodynamic shape and the aft plywood panels are tapered. The fuselage also contains the Vaccine Deployment Mechanism which is further described in section 6.2.4. No significant structural amendments were required in order to fit the mechanism, save for the integration of two small doors in the underbelly of the fuselage. The landing gear is custom made out of foam core and carbon fiber and affixed to the underside of the fuselage using nylon bolts.

5.3 Subsystem Design and Architecture

The following section provides an overview of the design and integration of all major subsystems in the aircraft. The subsystem design was guided by the objectives of reducing structural weight while maintaining integrity and an ease of manufacturability. A structural engineering margin of 1.5 was employed where necessary to ensure that inflight and landing loads would be withstood.

5.3.1 Wing and Mount

The wing design consists of two sections, the midsection and the tapered wing tips. The tapered wing tip has a foam core, with a carbon spar running through the outer wing, mainly to resist the moment of lift along the whole wing. The midsection is built up, with ribs running throughout that section. Two spars run through the middle, and MONOKOTE covers the outside of the midsection to give the plane an aerodynamic profile and to reduce skin friction drag. To attach the wing tip and the midsection, a segmented tube ran in between the outer wing and midsection, allowing the outer wing to slot into the midsection. A figure of coefficient of lift and coefficient of pitching moment vs spanwise position of the wing is shown below, along with a CAD representation of the wing.

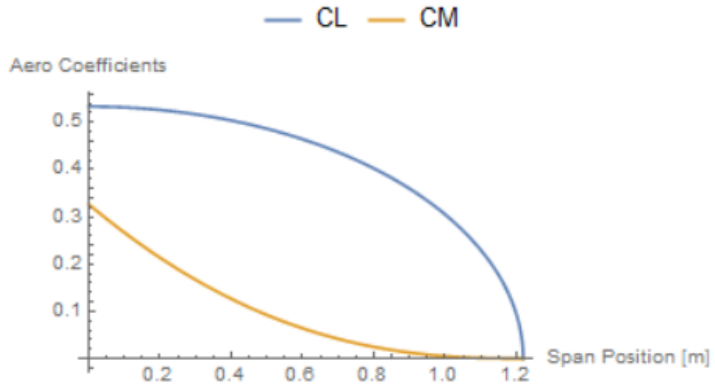

Figure 5.1: Force and Moment Distribution over the Wing

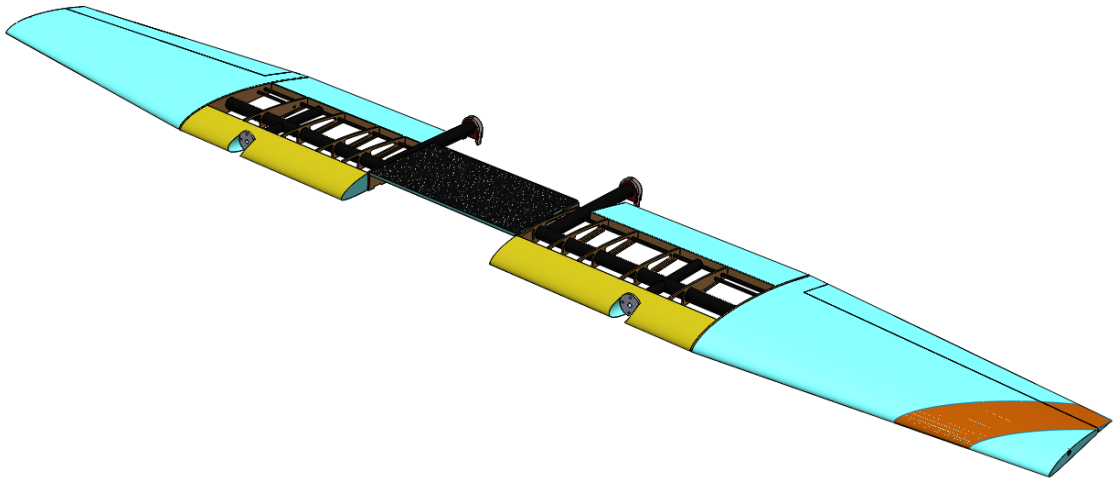

Figure 5.2: Wing Representation

To attach the wing to the fuselage, pegs are attached to the leading edge of the wing, and corresponding holes are cut out in the fuselage. The pegs will slot into the fuselage, and then will be bolted down into the fuselage to prevent any shifting from the wing. The location of this attachment is seen in Figure 5.3 below.

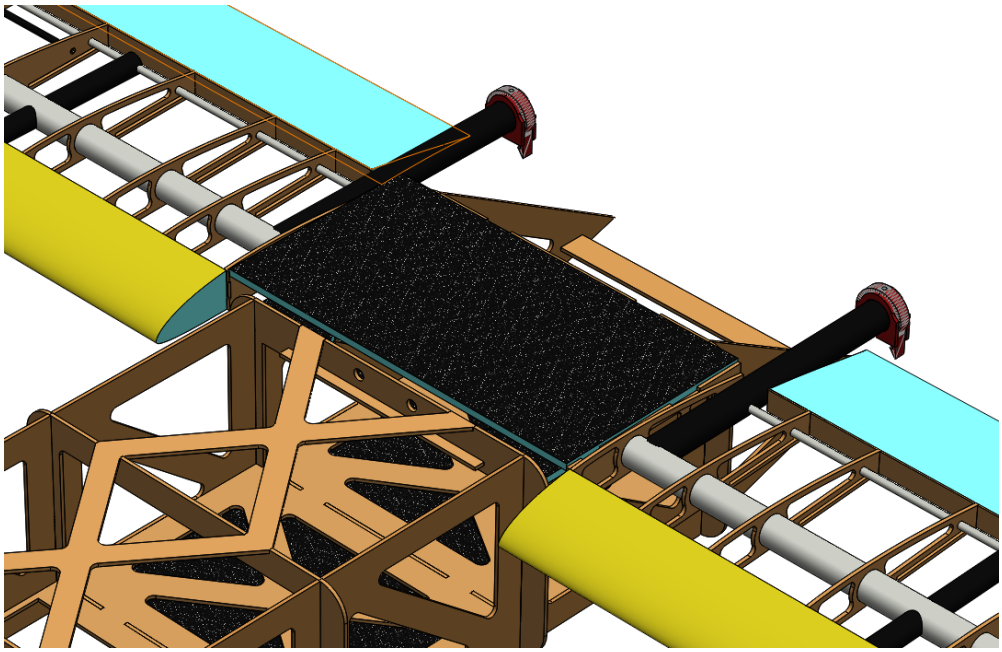

Figure 5.3: Wing and Fuselage Connection

5.3.2 Fuselage

The 1.12 m x 0.33 m x 0.18 m fuselage consists of built-up plywood reinforced by a series of carbon fiber foam core sandwich panels. The built-up structure was designed using splined cross sections to maximize the payload capacity while minimizing the drag effects. The carbon fiber sandwich panels extend across the fuselage to provide a strong point of attachment for the wings, landing gears and payloads. The exterior of the fuselage is covered by Kevlar and the foam nose is attached to provide structural and aerodynamic support. A representation of the empty fuselage structure and the fuselage with the built-in mechanism and electronics can be seen in Figures 5.4 and 5.5 below.

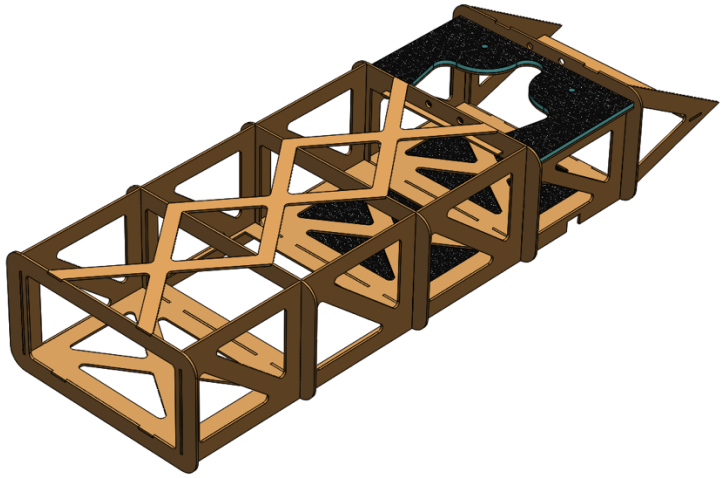

Figure 5.4: Empty Fuselage Structure

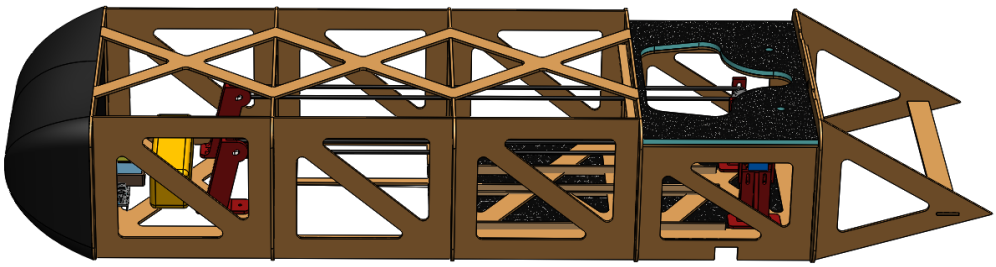

Figure 5.5: Fuselage with Mechanism and Electronics

5.3.3 Empennage

The final configuration of the empennage is composed of the horizontal stabilizer mounted atop two vertical stabilizers. Each vertical stabilizer is mounted onto a carbon fiber boom. The vertical stabilizers each have a span of 0.30m and a chord of 0.19m, while the horizontal stabilizer has a span of 0.61m and a chord of 0.29m. All the stabilizers have no sweep, and each is constructed with a foam core, wrapped in a crosshatch pattern of carbon fiber tow, and covered with fiberglass for torsional stiffness. The horizontal stabilizer is secured to the vertical stabilizers with a 45-45 carbon fiber wet lay. The full empennage can be seen in Figure 5.6 below.

The rudders and elevators both start at 70% chord length, with hinges designed for +/- 30 degree deflection. Servos for the control surfaces are embedded directly into the stabilizers to reduce the size of control linkages, with the servo wires routed along the booms into the fuselage.

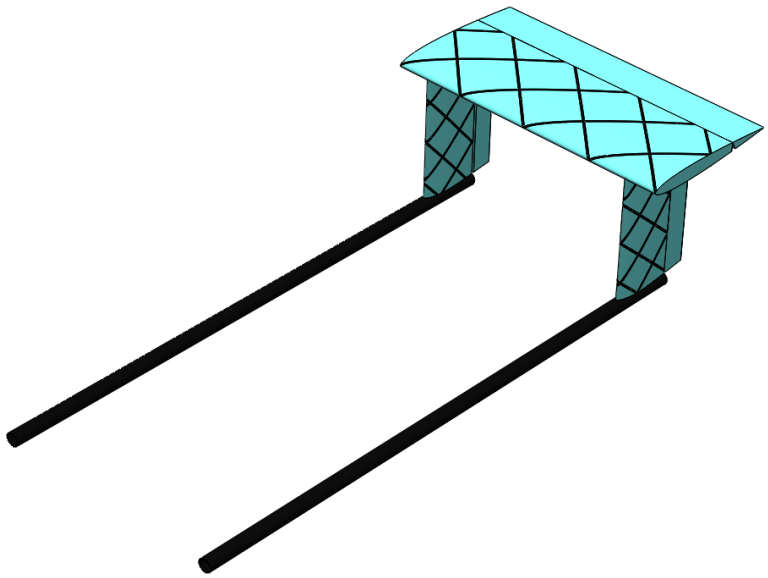

Figure 5.6: Empennage

5.3.4 Landing Gear

Custom landing gear struts were designed using finite element analysis (FEA) in SolidWorks®. The rear landing gear strut was designed to withstand a 10G vertical impact for the maximum aircraft weight, while the front landing gear strut was designed to withstand a 10G vertical impact with the weight distributed between the front and rear landing gear struts. The final results of the FEA for the rear landing gear strut are shown in Figure 5.7, with the maximum stress location shown to occur at the hole necessary for the wheel attachments. The landing gear was created by laying up unidirectional carbon fiber strips on a mold with a post processing wrap of a braided carbon fiber tube in order to prevent delamination or bursting between the layers of unidirectional carbon. The two landing gear struts are mounted to the aircraft's bottom payload bulkhead.

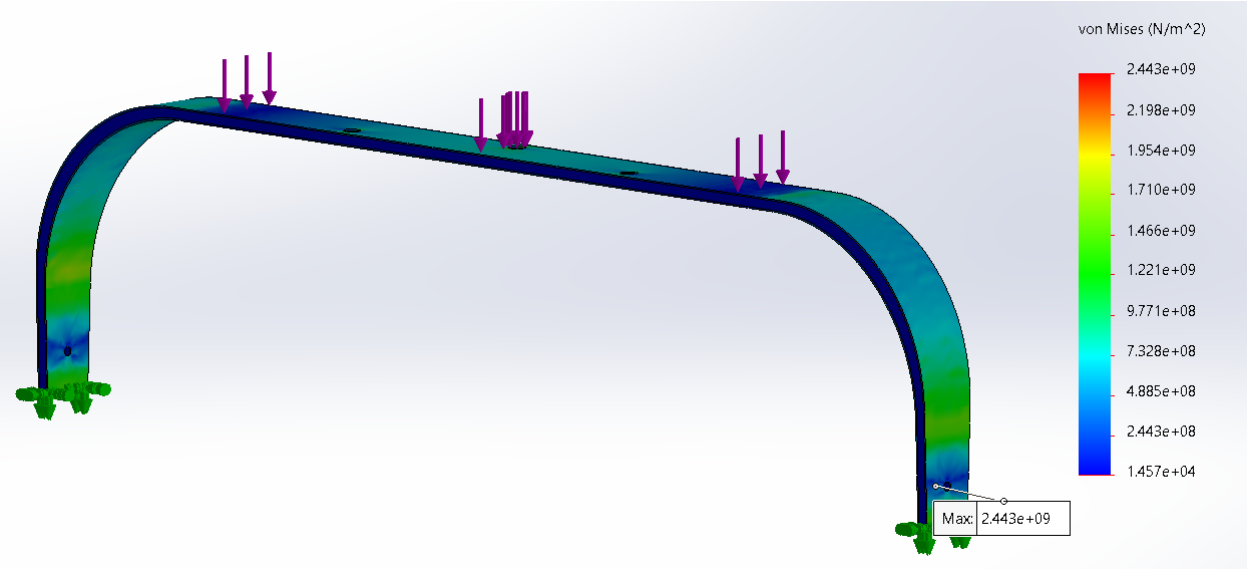

Figure 5.7: FEA of Landing Gear

5.3.5 Propulsion System

The chosen propulsion system for the competition aircraft is a dual-prop system consisting of two counter-rotating APC 15x10E and two Cobra C-4130-20 300kv motors each controlled by a Phoenix Edge 75A ESC. The system is powered by one 6-cell 4500 mAh lithium-polymer battery pack, rated for a discharge rate of 45C. The battery is stored in a compartment at the front of the fuselage. This configuration is depicted in Figure 5.8 below.

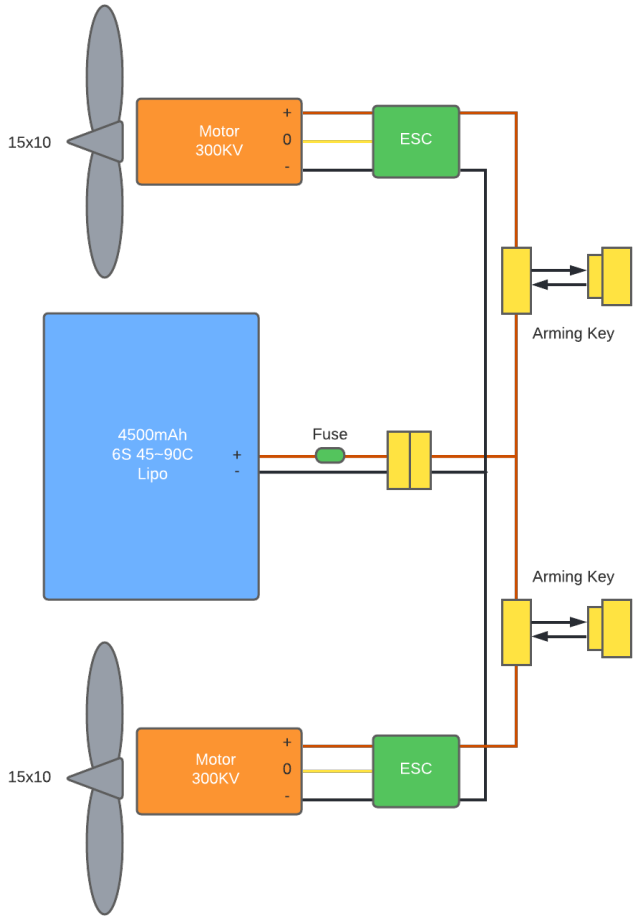

Figure 5.8: Propulsion System Wiring Diagram

The two motors are mounted on the left and right side of the plane, secured to the leading edge of the wing by a custom aluminum motor mount. Power wires extend from the battery compartment and route along the fuselage and wings and into the ESCs, which are mounted just behind the motors within the built-up wing.

5.3.6 Vaccine Deployment Mechanism

Vaccine vial packages will be in the fuselage, ordered in two rows. They will be standing on top of rails. A conveyor belt controlled by a servo connected to Arduino Nano sits on top of the packages. The conveyor belts have bolts sticking out that will push the packages forward along the rails once the system is activated. Two trap doors lined up with the end of the two rails are cut in the underbelly of the plane and are held shut with rubber bands. These rubber bands also act to dampen the impact of the vaccine packages as they slide off the rails and out of the plane. When a signal is sent from the receiver to the Arduino, one of the conveyor belts will push one row of packages forward, until one of them falls off the rails and onto the trap door. The weight of the package opens the trap door, turning it into a slide. The package slides down the slope and hits the ground lightly so that the 25G maximum loading limit is not exceeded. The isolated mechanism is depicted in Figure 5.9.

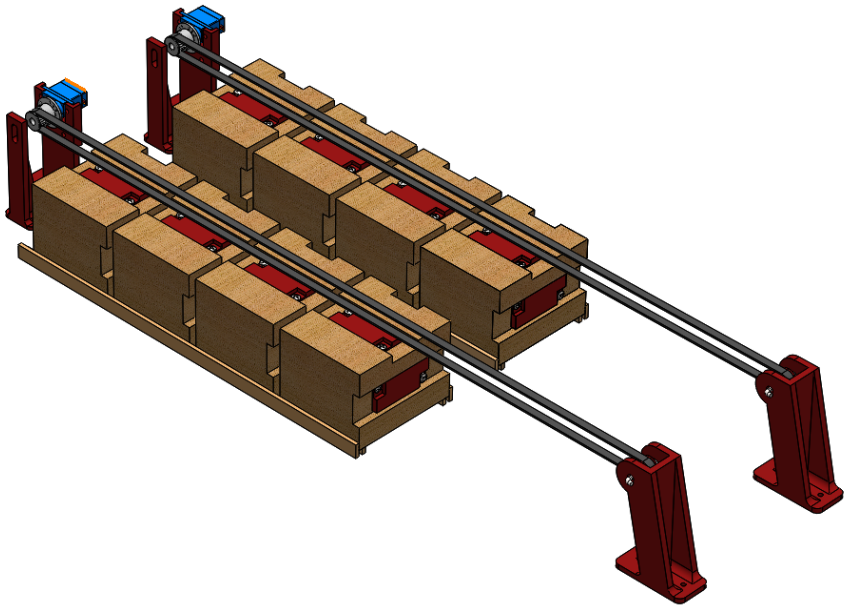

Figure 5.9: Deployment Mechanism with Payload

5.4 Weight and Balance

The competition aircraft is designed to have a minimal shift in stability margin between the fully loaded and empty configurations for all three of the flight missions. This was accomplished by placing the fuselage far up compared to the wing so that while the CG will shift between missions, more payload increases the static stability of the aircraft. The weights of the major aircraft components are outlined in the table below. The servos include the servos used for control along with the mechanism servos. The avionics includes ESCs, wiring, and the receiver. The tail includes both the horizontal and vertical tails, which are separate from the booms. The battery weight is the same for all three missions.

Aircraft Component	Weight	
	lbs	kg
M_1	12.13	5.49
Fuselage	1.54	0.7
Wing	3.86	1.75
Motors	1.75	0.79
Propellers	0.20	0.09
Servos	0.20	0.09
Landing gear	1.06	0.48
Avionics	0.16	0.07
Tail	0.99	0.45

Booms	0.35	0.16
Battery	1.59	0.72
Mechanism	0.43	0.19
M₂	20.51	9.29
Payload	8.38	3.80
M₃	16.13	7.3
Payload	4.00	1.81

Table 5.2: Aircraft Component Mass

The position of the center of gravity as measured from the leading edge of the wing is outlined in the table below. The X, Y, and Z axes are defined in the standard directions for aircraft: +X out the rear of the aircraft, +Y out of the right wing, and +Z out of the top of the aircraft.

	$W_{payload}$ (kg)	W_{total} (kg)	X_{CG} (m)
Mission 1	0.00	5.41	0.135
Mission 2	3.80	9.21	0.100
Mission 3	1.81	7.22	0.115

Table 5.3: Aircraft Center of Gravity from Wing Leading Edge

The aircraft neutral point, xnp, as calculated in XFLR5 *[4]*, is located 0.169 m behind the mean aerodynamic chord leading edge. The aircraft's static longitudinal stability with no payload (Mission 1 configuration) is calculated as follows:

$$S.M. = \frac{x_{np} - x_{cg}}{c} = \frac{0.169m - 0.135m}{0.37m} = 0.092 = 9.2\% \quad \text{(Eq. 5.1)}$$

And fully loaded, with CG furthest from the neutral point (Mission 2 configuration), the static margin is:

$$S.M. = \frac{x_{np} - x_{cg}}{c} = \frac{0.169m - 0.100m}{0.37m} = 0.186 = 18.6\% \quad \text{(Eq. 5.2)}$$

To ensure the static margin remained in the weakly stable region, around 15%, the location of payload for each mission was added as far rearward as possible, while the battery was placed within the fuselage to ensure minimal drift of the CG away from the neutral point.

5.5 Aircraft Flight Performance

Having sized the wings and tails, the total aircraft drag was modeled by the aerodynamic surface analysis done on XFLR5 [4]. Interference drag and miscellaneous protrusion drag caused by servo linkages, control horns etc. are negligible.

The total thrust as a function of airspeed was determined by curve fitting to wind tunnel testing data of dynamic thrust. The Mission 2 cruise velocity was calculated based on the intersection of thrust and drag curves to be 25 m/s. The Mission 3 cruise speed was constrained by the 100 W-h energy limit. In order for

the aircraft to sustain repeated takeoff and cruise for the full 10-minutes of Mission 3, we determined the cruise speed would have to be limited to 20 m/s through empirical testing.

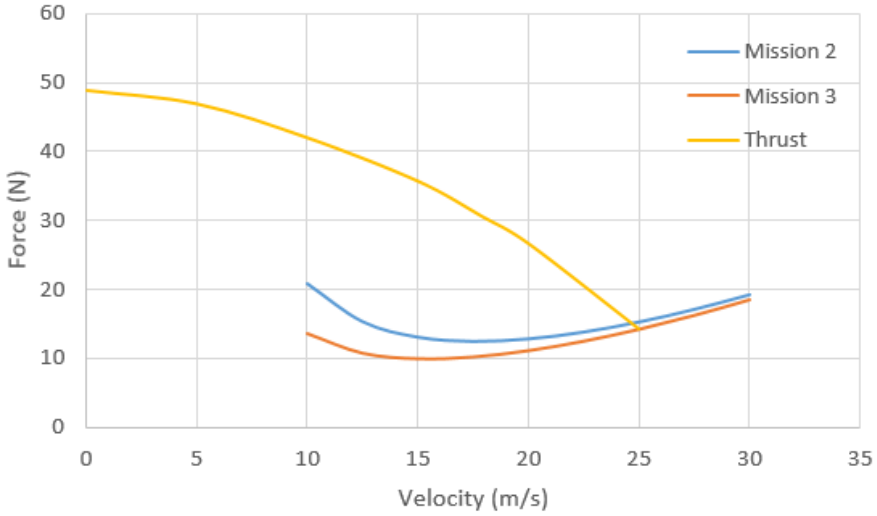

Figure 5.10 - Thrust and Drag Curves vs Flight Speed

For Mission 2, when the plane is fully loaded with vaccines, a maximum L/D of 11.7 was calculated at the cruise speed of 25 m/s. For Mission 3, when the plane is fully loaded with vaccine boxes, a maximum L/D of 10.8 was found at the cruise speed of 20 m/s. These were calculated using the equation below.

$$\frac{L}{D} = \frac{C_l}{C_d} = \frac{\frac{L}{0.5\rho V^2 S}}{C_{d0} + \frac{C_l^2}{\pi\, AR\, e}} \qquad \text{(Eq. 5.3)}$$

5.6 Aircraft Mission Performance

The estimated mission scores, given in Table 4.2, were updated from the original estimates given in Table 5.3 using the detailed propulsion and aerodynamic model results summarized in Section 5.5. During Mission 2, the aircraft is predicted to complete three laps in 141 seconds while carrying a payload of 200 syringes. During Mission 3, the aircraft is predicted to complete eight deployments with an average lap/landing time of 73 seconds. Based on ground mission time trials, we estimate the ground mission will take 91 seconds. With the estimated maximum mission scores calculated in Section 3.2, our estimated score can be calculated.

Mission	Laps	Payload	Time	Estimated Best	Score
Flight Mission 1	3	-	-	-	1
Flight Mission 2	3	200 Syringes	141s	3.3 [1/s]	1.43
Flight Mission 3	10	8 Vial Packages	584s	9 packages	2.89
Ground Mission	-	-	91	20 s	0.22
				Total Mission Score (TMS)	5.54

Table 5.3 - Predicted Mission Performance

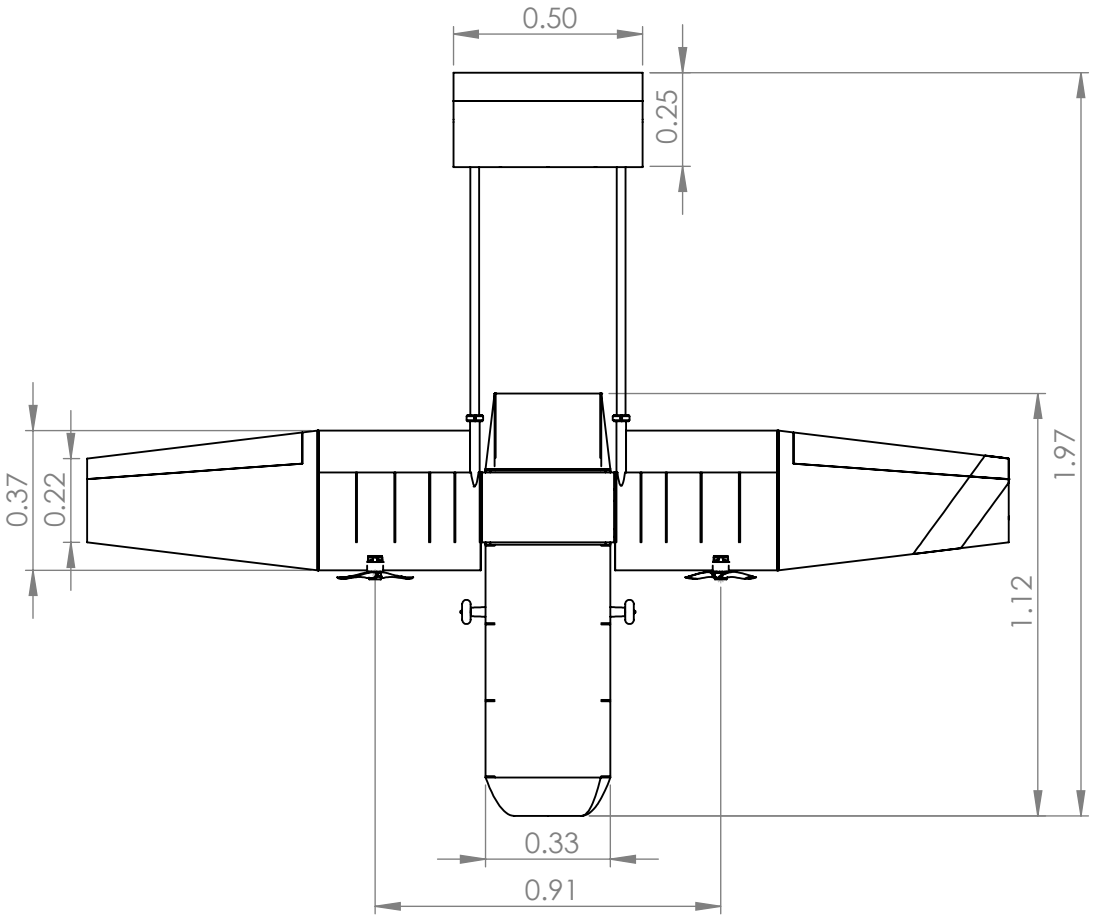

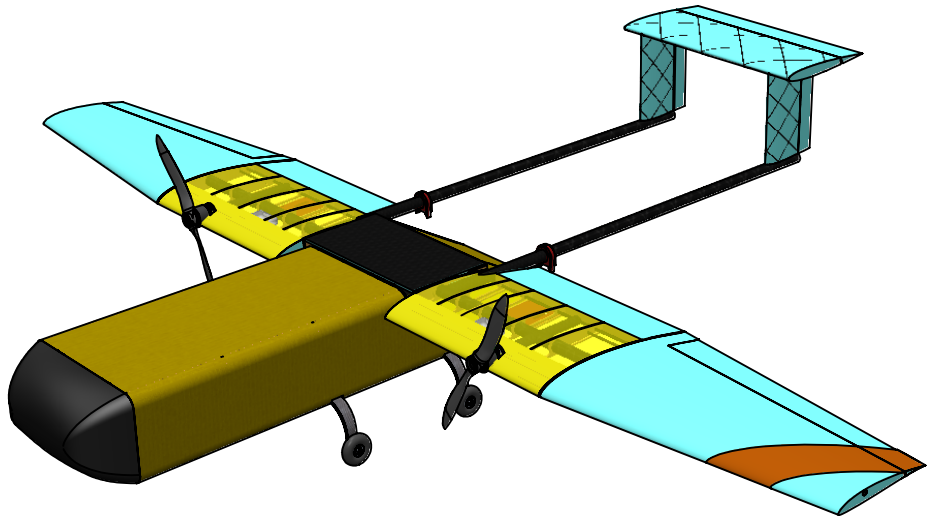

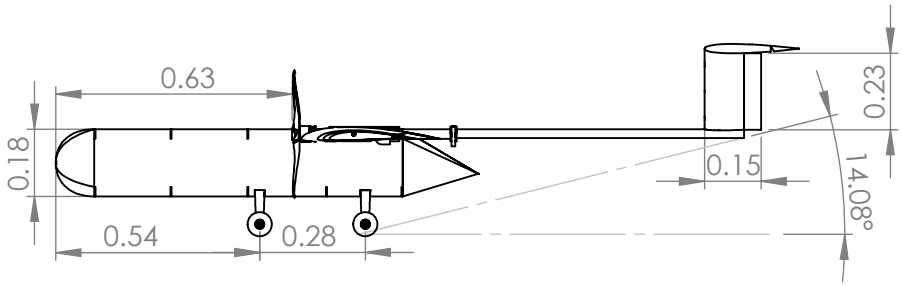

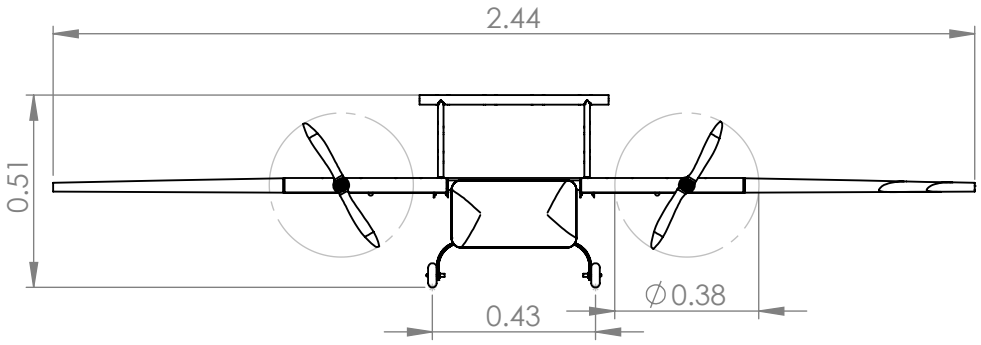

Design Build Fly
2022

TITLE:

3 View

Dimensions are meters unless otherwise specified.

PREP BY: T. Spitz

SCALE: 1:20

DATE: 2.25.2022

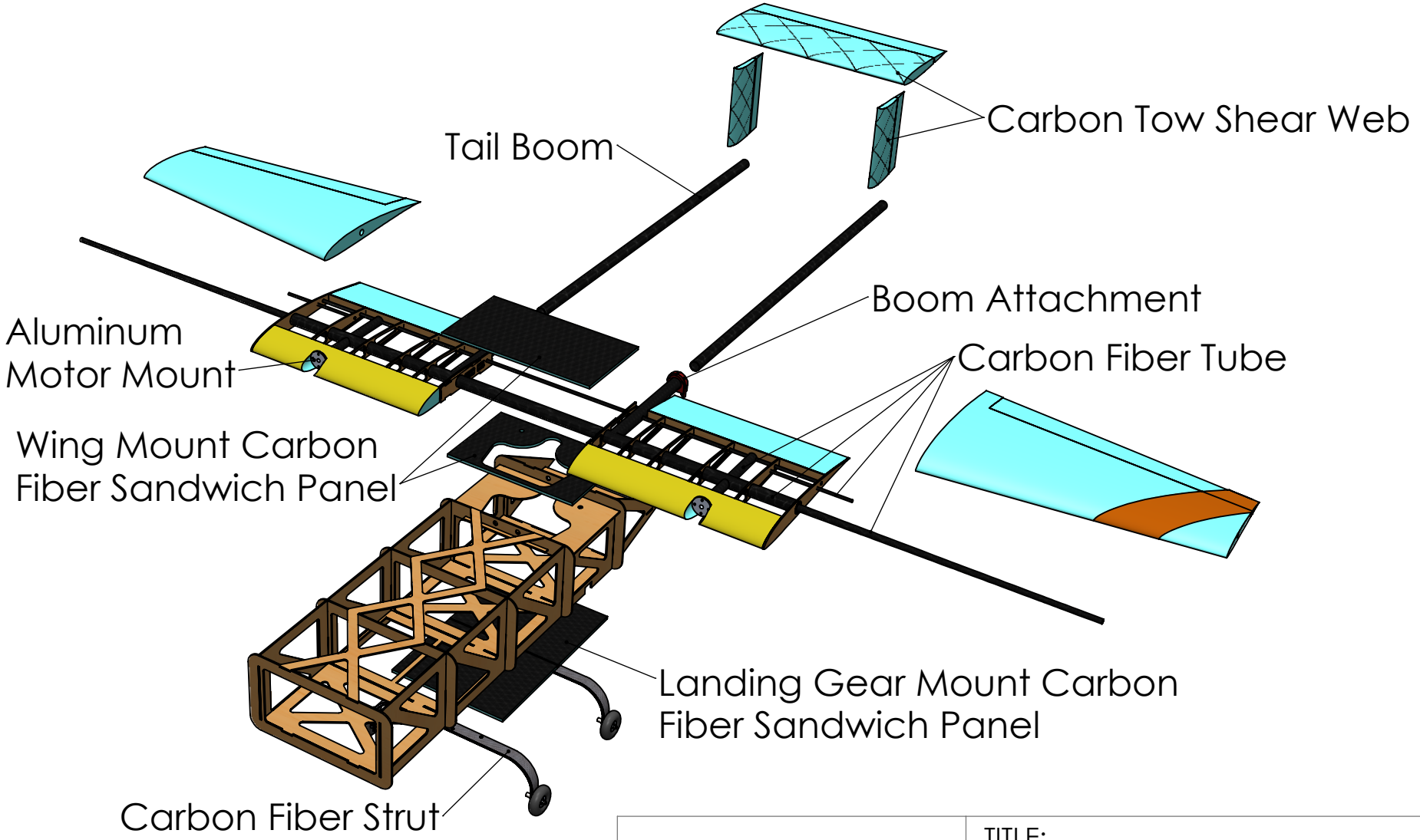

Design Build Fly
2022

TITLE:

Structural Arrangement

Dimensions are meters unless otherwise specified.

PREP BY: T. Spitz

SCALE: 1:8

DATE: 2.25.2022

Propulsion System

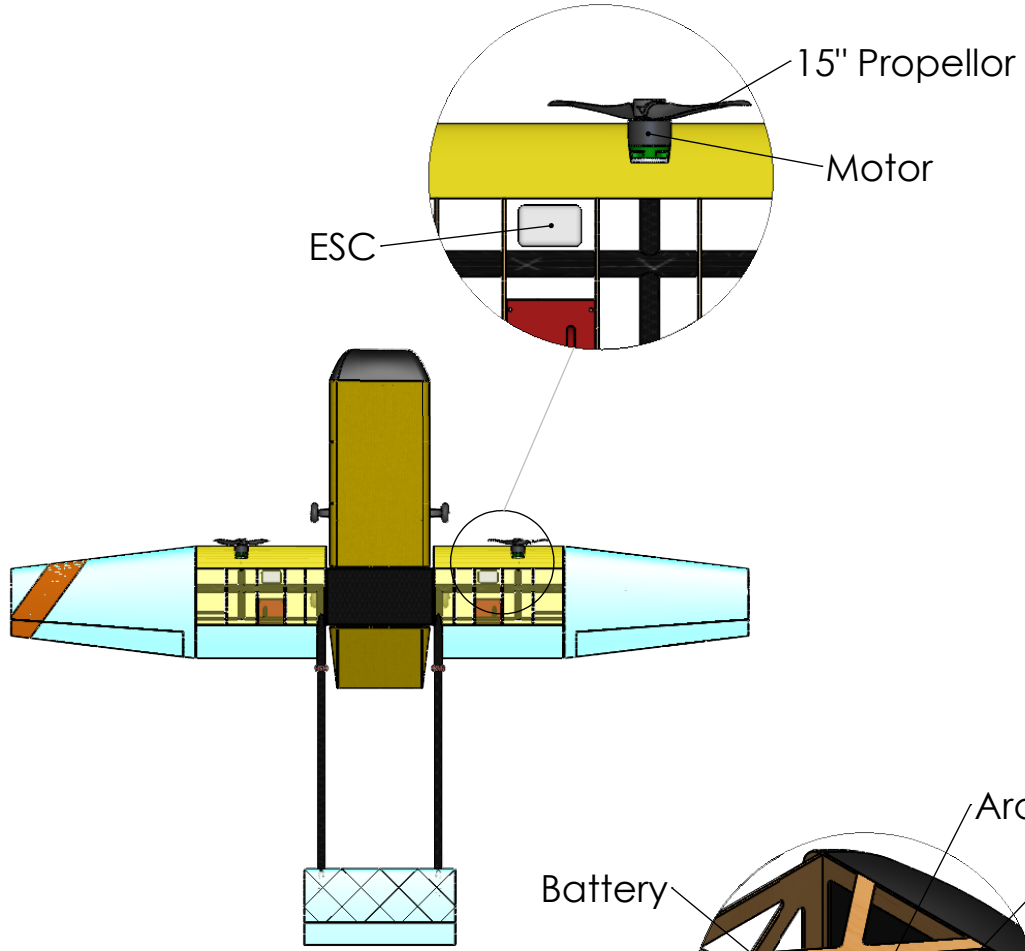

Payload Bay

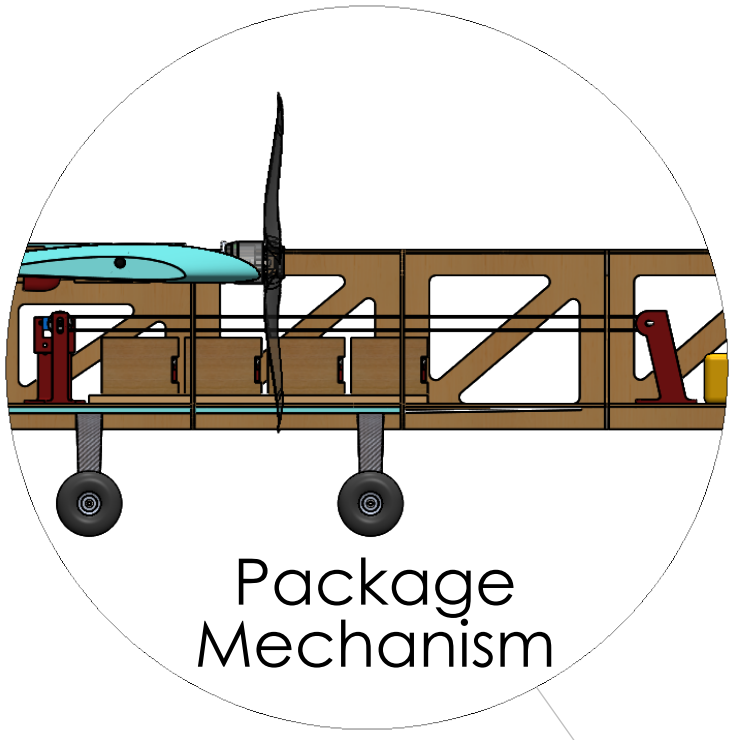

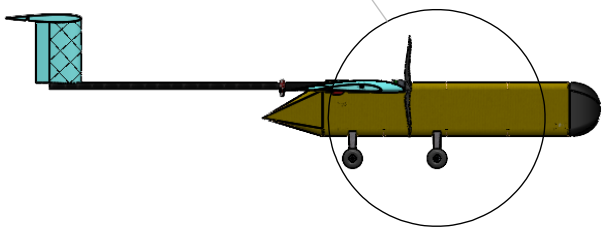

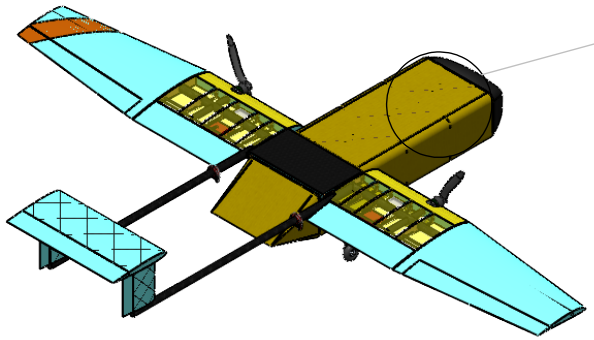

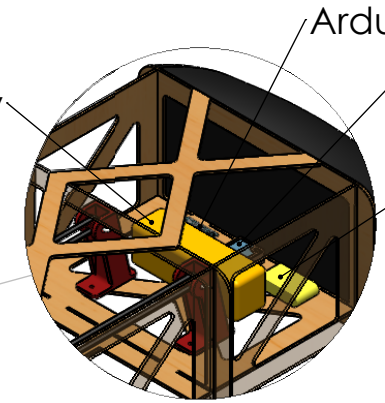

Electronics

SOLIDWORKS Educational Product. For Instructional Use Only.

Design Build Fly
2022

TITLE:
Aircraft Systems

Dimensions are meters unless otherwise specified.

PREP BY: T. Spitz

SCALE: 1:25 | DATE: 2.25.2022

Unloaded Payload

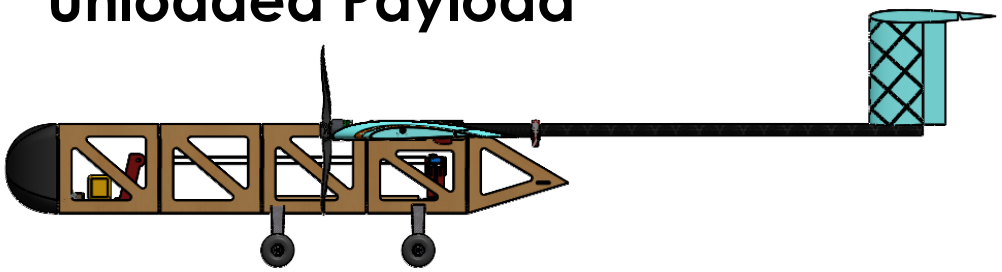

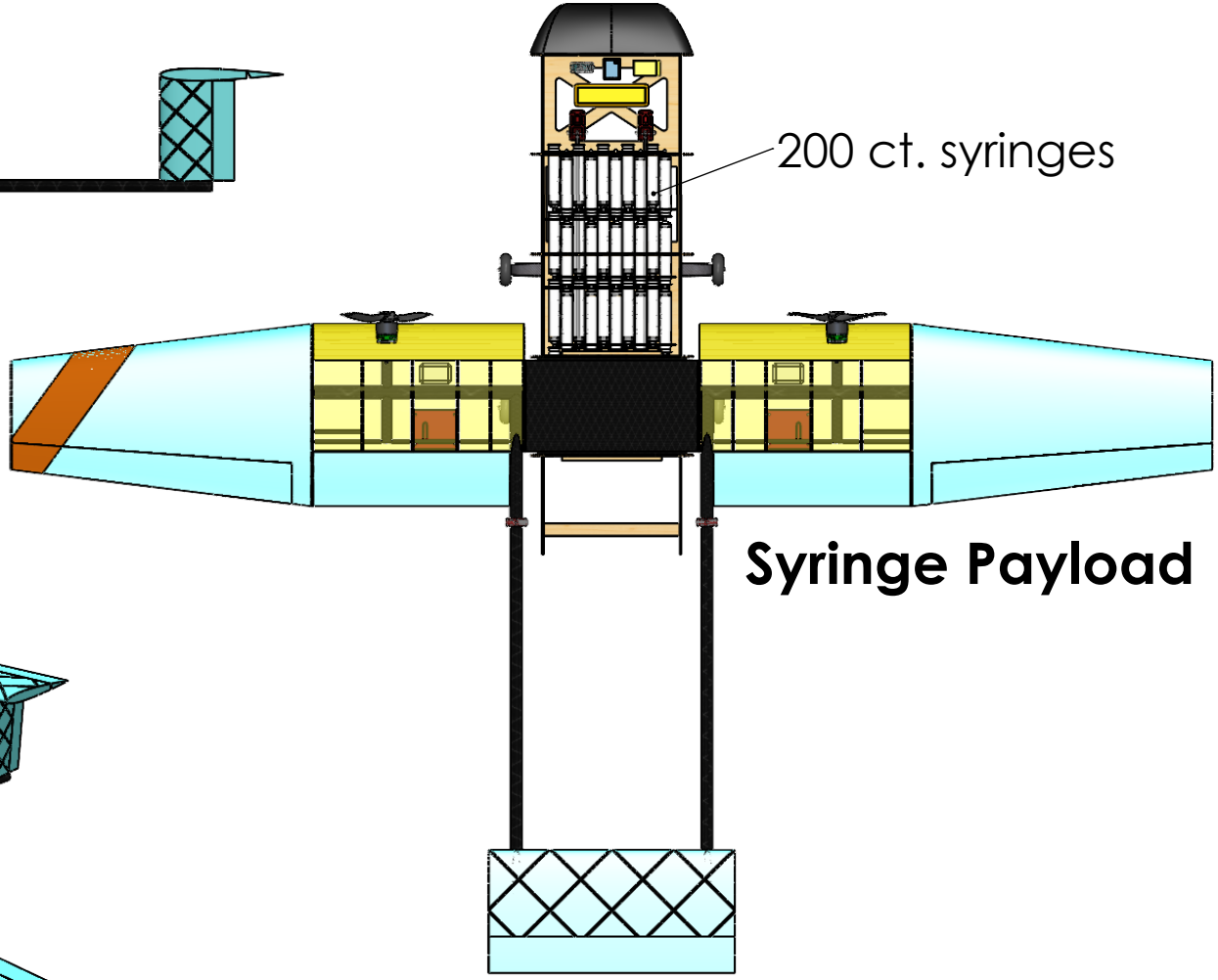

Syringe Payload

Package Payload

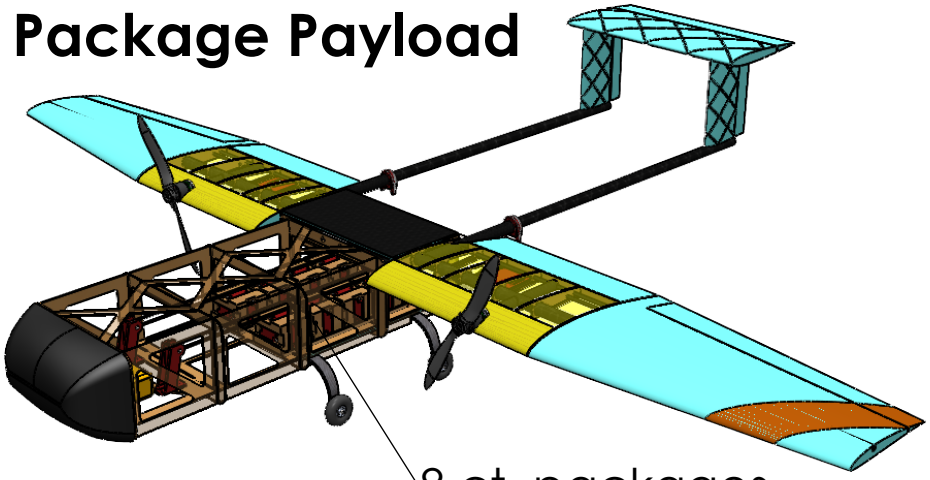

Design Build Fly

2022

TITLE:

Payload Configuration

Dimensions are meters unless otherwise specified.

PREP BY: T. Spitz

SCALE: 1:15

DATE: 2.25.2022

6 Manufacturing Plan

The team iterated through numerous manufacturing processes during the later phases of aircraft design. A summary of the processes, their advantages and disadvantages, and the final selection are outlined in the following section.

6.1 Manufacturing Processes Investigated

To be able to decide on the best manufacturing process for each aircraft component, the advantages and disadvantages of each available technique were investigated.

6.1.1 Foam Core

STYROFOAM HIGHLOAD-60 is a cheap material which is relatively easy to process using a hotwire foam cutter and sanding. Moreover, while it is very lightweight, it can become heavier than balsa, because composites are needed to provide structural support. In this case, the structural support comes from a fiberglass layup and a unidirectional pre-impregnated carbon spar. If necessary, cross-hatching of carbon tow can be used under the fiberglass to absorb torsional loads. The construction of wing surfaces with this method is simple but timely, and it is difficult to repair if heavily damaged in a crash.

6.1.2 Built-Up

Using a built-up design gives the team access to a broader array of structural materials and geometries at a lower weight when compared to other manufacturing techniques. A built-up structure is usually composed of several flat, laser cut plywood or balsa wood pieces connected together using cyanoacrylate glue or epoxy with Kevlar being added to high load areas as reinforcement. This structure is then covered with a heat shrinking material such as MONOKOTE. The rigidity, accessibility, and the ease of manufacture makes a built-up structure a good choice for low force, low weight structures such as the fuselage or wing. Furthermore, the low cost of these materials allows for fast and accessible prototyping. The main disadvantage is that it is difficult to repair and is susceptible to damage. Moreover, while it is easy to manufacture it is also time consuming.

6.1.3 Composite Molding

We investigated a lost foam molding strategy with composites. This involved cutting out a foam core wing section, cutting two slices through the foam mold to accommodate hexcomb spars with carbon fiber wrapping around, and one sheet of 45-45 carbon fiber wrapping around the entire wing section. Once the layup was complete, it was vacuum bagged for 24 hours, and then the foam was melted out with acetone. This composite molding technique was very time intensive and difficult to scale up for a full-size wing, although it provided a strong, continuous and lightweight wing once the foam was melted out.

6.1.4 Laser Cutting

Laser cutting allows for rapid prototyping thanks to its ability to quickly cut out parts for testing or use. It works especially well with plywood, and allows us to make lightweight panels and ribs to create built-up fuselage or wing sections with. The main drawback of laser cutters is the limited materials that can be cut with them, requiring composites to be added on later for improved strength of parts.

6.1.5 CNC Routing

CNC routing generally leads to more accurate parts than other machining options because material is not burned away and it is not constrained to 2 dimensional cuts. One downside is that for certain foams and softer materials, CNC routing is not ideal and will cause a rough finish. For parts where high tolerances are needed or for creating molds, CNC routing is the better alternative.

6.1.6 3D Printing

3D printing is a fast, cheap, and easy way to prototype parts. It offers high flexibility for part geometry with relatively low effort and time, as they can run unsupervised. The largest downside to 3D printing is its lack of part accuracy and the lack of a smooth finish on parts, which takes time to sand down. 3D printed parts can be very heavy if they are meant to be structural, and they have a high possibility of breaking even then, particularly in dynamic situations given the anisotropic structure of the final part. 3D printed parts should be used for non-structural applications or prototypes only.

6.2 Manufacturing Processes Selected

6.2.1 Wing

The wing has a built-up center and foam core outer sections reinforced with 0.7 oz fiberglass and a carbon spar. This method was selected due to its ease of repair, rapid manufacturability, and light weight. The outer sections of the wing are removable to allow for easier transportation of the large wing.

The built-up center of the wing is made by a framework of laser-cut ribs made out of plywood. Two carbon fiber spars go through the ribs for spanwise strength. A heat shrink skin of MONOKOTE covers the center of the wing. The wiring for the servos and the motors goes through the center of the wing and sits within the laser-cut ribs. The trailing edge flaps were made using foam laid up with fiberglass, and cuts were made to make room for the motors to sit within the leading edge.

The wing's foam outer sections were cut using a CNC hot wire foam cutter. Ailerons were cut out using box cutters. A unidirectional carbon spar was inserted into a slit at the quarter cord for spanwise strength. The foam parts were laid up with fiberglass in the 45-45 direction for torsional rigidity, after which the ailerons were reattached with tape enforced with Super 77 adhesive. Aileron servos were inserted in pocketed foam and all servos were connected to custom G10 control horns with threaded linkages.

6.2.2 Fuselage

The fuselage consists of a laser cut, Kevlar covered plywood frame supported by carbon fiber foam core sandwich panels and connected to a foam nose. Fuselage framing will be cut using a laser cutter, while the nose is cut using a hand-held foam cutter. All frame connections between the plywood sections are made with epoxy and cyanoacrylate glue and connections to carbon fiber sandwich panels are made with epoxy. Furthermore, load bearing connections are reinforced with carbon fiber. A carbon fiber sandwich panel was placed atop the fuselage, secured by carbon fiber and epoxy to provide a location to mount the wing. This method of construction was selected for its stability and emphasis on reinforcement near the wing to handle the increased load and ensure a stiff connection.

6.2.3 Empennage

To make the empennage, the horizontal and vertical tail cores are first CNC wire cut from foam, after which the elevator and rudder control surfaces are cut off. All of the foam parts are then laid up with 0.7 oz fiberglass, with the main foam part laid up with carbon fiber strips for torsional rigidity. After post-processing, the elevator and rudder control surfaces are re-attached with tape hinges adhered with Super 77 adhesive. To complete the tail assembly, the two vertical tail cores are epoxied to the horizontal tail core. The tail was strengthened using 45-45 carbon fiber patches between the vertical and horizontal stabilizers. Control surfaces were actuated using servos embedded in the foam with piano wire linkages and custom waterjet G10 control horns. The vertical stabilizers were affixed to the tail booms using 5-minute epoxy to align them, and carbon tow for added strength and rigidity.

6.2.4 Vaccine Deployment Mechanism

The vaccine deployment mechanism uses a simple belt and rail system to deploy the packages. Eight packages are stored inside the fuselage of the aircraft constrained laterally by a thin wooden rail and vertically by the gt2 timing belt. See Figure 6.1 for a cross section of this rail system.

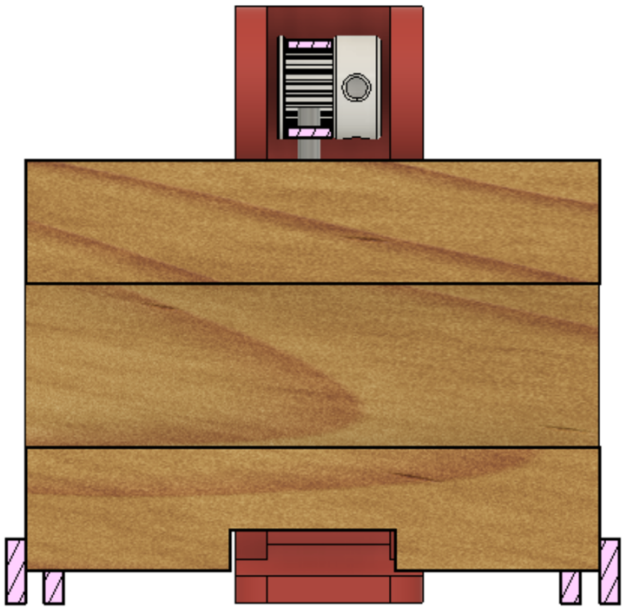

Figure 6.1: Cross Section View of the Vaccine Package Rail Mechanism. Pink areas show the wooden rails (bottom) and GT2 timing belt (top).

The timing belt above the packages also acts as the mechanism by which the packages are deployed. M3 bolts through the belt are spaced such that boxes can easily fit in between. When a continuous rotation servo drives a pulley at the aft of the airframe, the bolts push the boxes forward along the rails until they fall off the rail system and onto the impulse damping door on the underbelly of the airframe. The box comes to rest on the ground without exceeding the set maximum impulse requirements.

The continuous rotation servo mount, idler and pulley housings were 3D printed on a Lulzbot Taz 6 out of PLA (Polylactic Acid). This material was chosen for its ease of manufacture and impact durability relative to other polymers.

6.3 Manufacturing Milestone Chart

A general timeline for the important manufacturing phases for each aircraft iteration was developed at the beginning of the design process. The team expects to be able to complete the final aircraft in time for the competition in late April. The timeline shown in Figure 6.2 outlines the original manufacturing schedule and compares it to the actual manufacturing schedule.

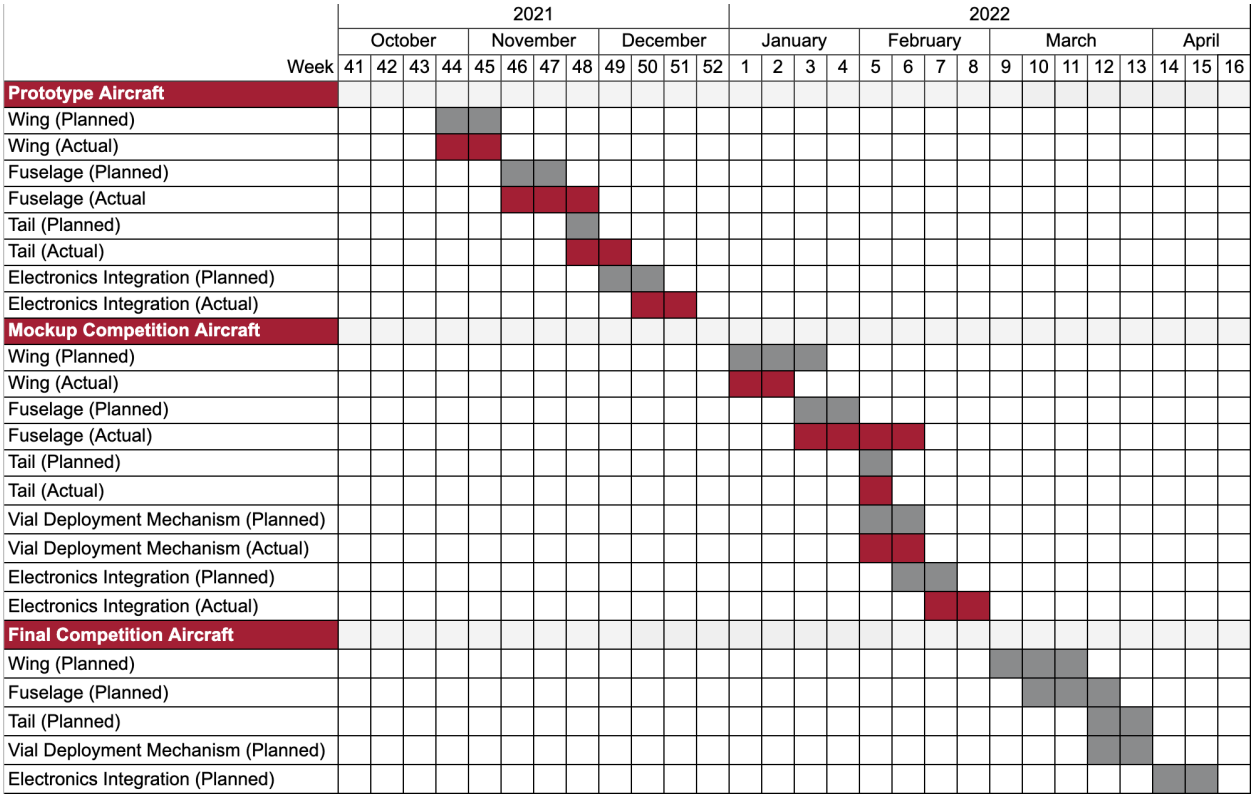

Figure 6.2: Manufacturing Milestone Chart. Proposed dates are shown in grey, while actual dates are shown in red.

7 Testing Plan

This section describes the test objectives and procedures used to confirm important subsystem performance and general flight characteristics.

7.1 Test Schedule

Test	Objective	Dates
Motor/Propeller Testing	Evaluate the thrust produced by the propulsion system while observing the voltage and amps drawn.	Dec 6 - Jan 14

Battery Testing	Ensure that the battery will be able to provide appropriate voltage for all three missions.	Jan 17 - Jan 21
Structural Testing	Determine maximum weight capacity of load-bearing structures.	Jan 17 - Ongoing
Mechanism Testing	Ensure that all payload mechanisms actuate properly and secure payload accordingly.	Jan 4 - Jan 28
Taxi Testing	Evaluate the controllability of the aircraft while taxiing on the ground.	Feb 1 - Ongoing
Flight Testing	Validate takeoff distance and top speed	Dec 5 - Ongoing

Table 7.1: Major Testing Objectives

7.2 Subsystem Tests and Objectives

7.2.1 Wing Structural Testing

The purpose of structural testing is to ensure that the wing is strong enough to withstand all the forces in flight without failing. To test the structural integrity of the middle built-up section of the wing, the midsection was placed between two tables and weights were loaded on top, as shown in Figure 7.1. We estimated a 2G force on the wing with a safety factor of 1.5, so we loaded the midsection with the appropriate weight and recorded the deflection at the tips. We also did a wingtip test with a full payload to see if the wing could withstand the aerodynamic forces during flight.

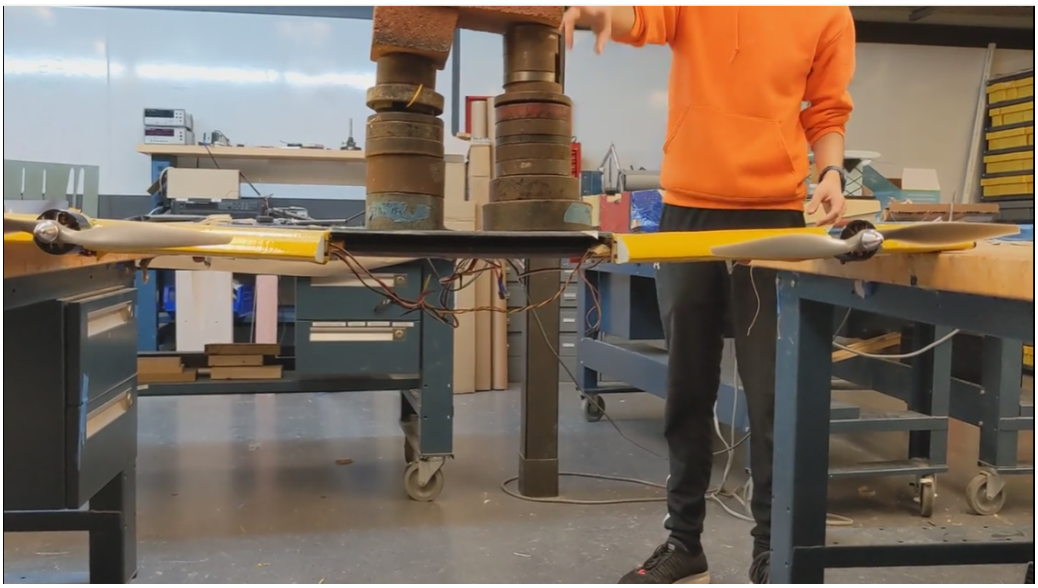

Figure 7.1: Wing Loading Test Setup

7.2.2 Propulsion Testing

Propulsion testing utilized an RCBenchmark 1580 thrust test stand to measure thrust output, power draw, and acceleration of our theoretically optimal motor/propeller combination. Testing was first done in static conditions utilizing a motor mounted on a test plane (see Figures 7.2 and 7.3), then in a wind tunnel using the test stand to simulate both static and cruise flight conditions at 40mph (see Figure 7.4). Calibrated load cells on the test stand were used to measure thrust and torque, while current and motor voltage were measured using onboard sensors in the RCBenchmark test stand. Testing was used to verify predicted levels of current draw in order to choose an ESC, confirm battery selection, and ensure that the motor and propeller combination would perform as expected. We were able to verify that the propulsion system was able to produce sufficient thrust for takeoff and cruise. In addition, by continuously running the motor until the battery was drained, we verified that the propulsion system had enough energy to sustain our target flight time for Mission 3.

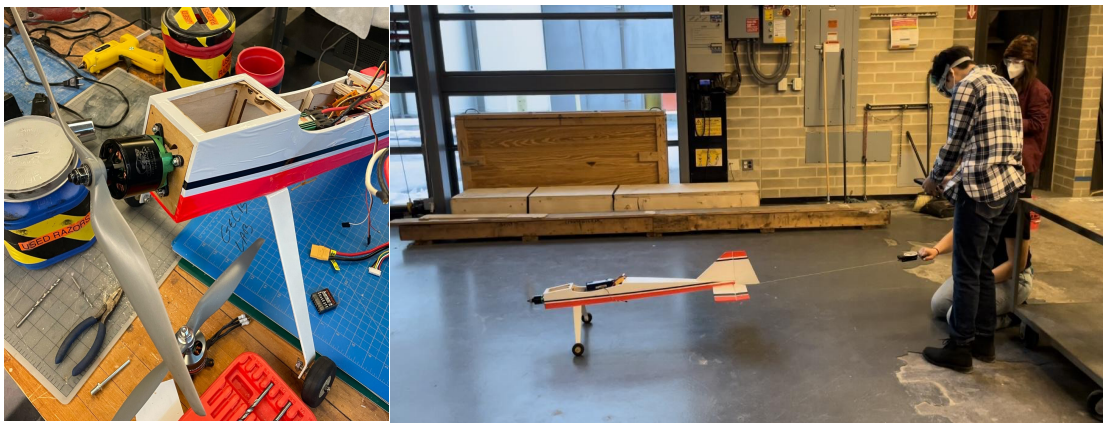

Figure 7.2 and Figure 7.3: Propulsion Testing (test plane)

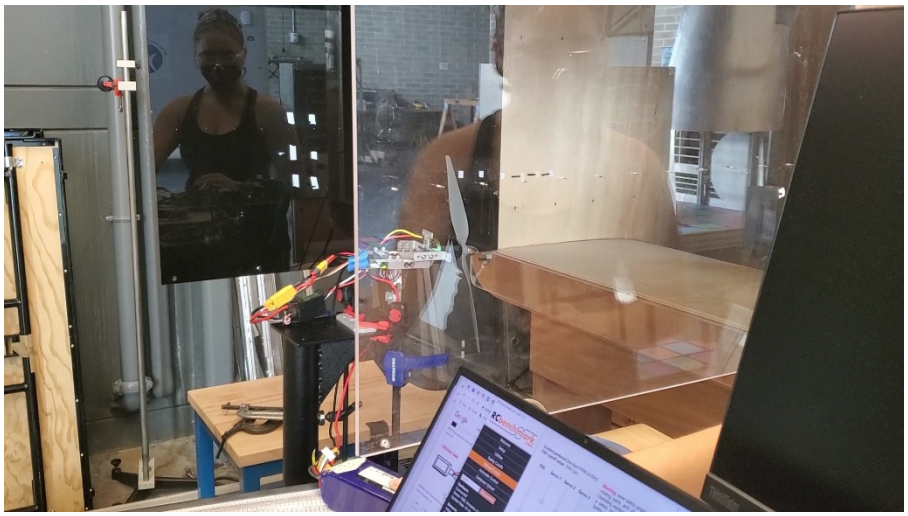

Figure 7.4: Propulsion Testing (wind tunnel)

7.2.3 Vaccine Deployment Testing

Before the construction of the full-scale vaccine deployment mechanism, several small-scale test articles were constructed to verify the function, material choice, and manufacturing method of the device. Tests were divided into two criteria: the functionality of the mechanism and the effectiveness of the impulse dampening of the trapdoor to bring the package to rest without exceeding the maximum impulse requirement of 25G. Tests in the first category showed that the deployment mechanism was successful, but the wooden rails must be covered in a low friction material in order to keep the packages from tipping over during deployment. This test setup is shown in Figure 7.5 below. The second category, however, was more problematic as it was discovered that common 9g servos do not have sufficient holding torque to keep the trapdoor closed if a package was deployed onto it given the specific configuration of the trapdoor and servo. In the final design, the trapdoors are held closed by the aerodynamic forces in flight as well as a highly compliant rubber band which acts to dampen the impact of the box on the trapdoor and lower it to the ground. With these modifications, the mechanism was deemed to be ready for integration on the final airframe.

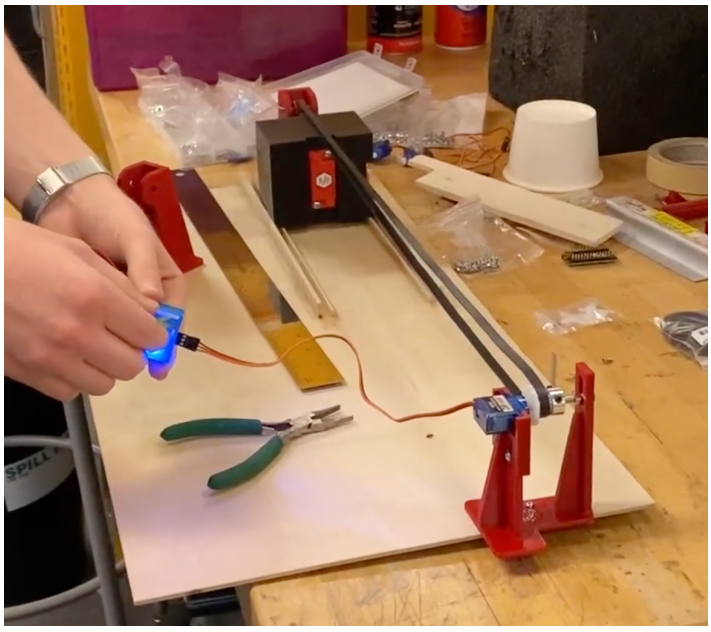

Figure 7.5: Mechanisms Testing

7.3 Flight Testing

Flight testing is conducted on a full-scale prototype to verify the predicted performance and functionality of the competition aircraft. The flight test pilot assesses the flight characteristics of the aircraft configured with and without payload as appropriate for all three flight missions. Flight tests are conducted at an open field to recreate the competition conditions as closely as possible. The flight readiness of the aircraft, respective portion of the ground mission, and runway constraints are assessed before each flight.

7.3.1 Flight Checklists

The flight checklist is split into two parts: the Preflight Checklist, shown in Table 7.2, and the Flight Test Checklist, shown in Table 7.3.

Item	Description	Completed?
Airframe		
CG Position	Verify proper CG location	□
Payload Restraint	Check respective payload for security, proper loading, & proper deployment conditions	□
Control Surfaces	Check for control surface attachment, proper range of motion, & slack	□
Structural Test	Ensure the airframe is fit to fly through a wing tip test along with a drop test to replicate landing	□
Propulsion		
Flight Battery	Verify propulsion pack voltage	□
Receiver Battery	Verify receiver pack voltage	□
Propellers	Balance the propellers, visually inspect for damage, verify prop nuts are secure	□
Motors	Verify opposite spin directions for motor pair and motors are secure to motor mounts	□
Failsafe	Cycle TX power; ensure proper failsafe actuation	□
Arming Plug	Insert plug & check operation	□
Field / Miscellaneous		
Range Check	Perform range check	□
Transmitter	Verify TX voltage: >9.6V	□
Flight Line	Clear flight line for takeoff	□

Table 7.2: Pre-flight Checklist

General					
Ground Mission Time Trial				□	
Live tracking of airspeed, propeller RPM, current, voltage, & GPS location				□	
First Flight (Flight Mission 1, Deployment Flight)		**Second Flight (Flight Mission 2, Staging Flight)**		**Third Flight (Flight Mission 3, Vaccine Delivery Flight)**	
Trim Aircraft	□	Record throttle – takeoff time delay	□	Record takeoff distance	□
Record takeoff distance	□	Record max dash speed	□	Record throttle – takeoff time delay	□
Establish stability & controllability	□	Record min turning time	□	Record dash speed	□
Record max dash speed	□	Record run time	□	Record turning time	□
Record min turning time	□	Record payload	□	Establish continued stability after deployments	□
Record run time	□	Ensure safe landing	□	Record successful vaccine vial package deployments	□
Ensure safe landing	□			Record run time	□
				Ensure safe landing	□

Table 7.3: Flight Test Checklist

7.3.2 Data Recorders

An EagleTree Pro flight data logger is used to track the propeller's RPM, current, and voltage throughout the flight. It is supplemented with a pitot tube and an EagleTree Pro GPS logger which monitors airspeed. Data is recorded for post flight analysis. The data from flight tests are compared with analytical calculations of velocity, acceleration, current draw, and thrust to ensure the aircraft performs as expected.

8 Performance Results

8.1 Subsystems Performance

8.1.1 Wing Structural Testing

The testing described in section 7.2.1 was carried out. The midsection of the wing was loaded with 66 pounds to simulate a total of 3Gs of force. The midsection was able to hold up the weight with minimal deflection and there were no cracks or failures in the structure. Additionally, a wing tip test with full simulated payload within the prototype aircraft demonstrated that the wing and the mount was capable of safe flight. This is shown in Figure 8.1 below. With this information, it was decided that the wing was sufficiently strong enough to support the aircraft on all three missions and for all maneuvers it would undergo.

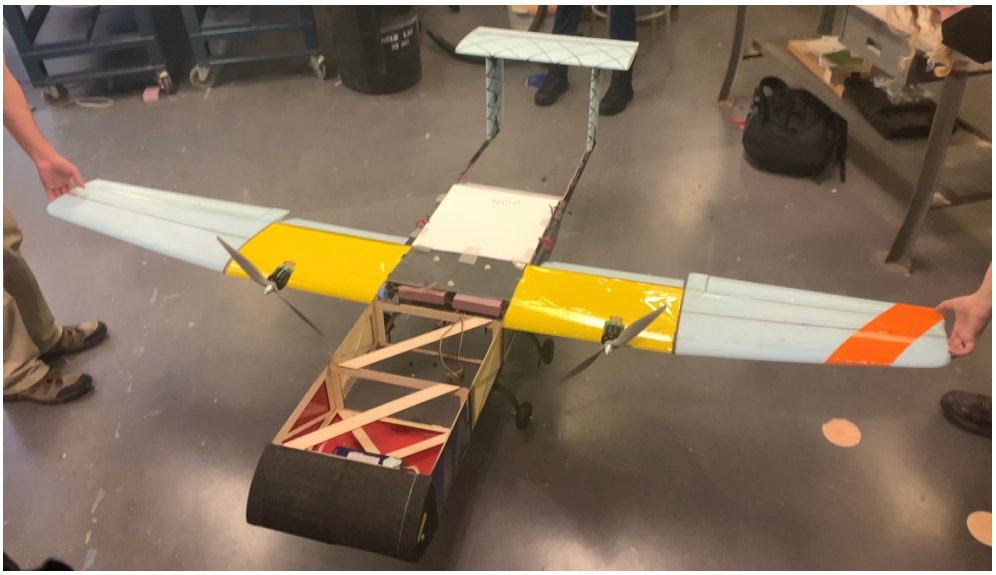

Figure 8.1: Wing Tip Test of Prototype

8.1.2 Landing Gear Testing

To test the landing gear, the strut was clamped down to a table. A load was applied to the struts to simulate a very rough landing. The deflection was small enough for the aircraft to have sufficient prop clearance upon landing. There were no visible cracks or failures on the landing gear, so it was concluded that the landing gear would absorb the necessary forces during landing. This setup is shown in Figure 8.2.

Figure 8.2: Landing gear testing setup

8.1.3 Propulsion Testing

The propulsion testing described in section 7.2.2 was conducted using two different methods. We first used a test plane and luggage scale for propeller selection, testing 16x10, 15x10, 15x9, and 14x10 propellers. We found that the 14x10 and the 15x9 propellers produced insufficient thrust. We selected the 15x10 propeller as it was more power-efficient than the 16x10 propeller while still providing sufficient thrust.

To confirm the validity of this decision, we ran the motor on full throttle with the 15x10 propeller until a significant power drop was observed from the battery. With calculated adjustments to account for the twin-tractor configuration, this power drop occurred outside the frame of our target flight time, confirming that the propulsion system would be able to sustain our performance goals.

We then used the RCBenchmark 1580 thrust test stand to obtain the data provided in Table 8.1 below.

Motor/Propeller Combination	Test Condition	Thrust (kgf)	Thrust (N)	Electrical Power (W)
Motor 1	Static	2.52	24.7	446
	Cruise	1.53	15.0	446
Motor 2	Static	2.63	25.8	473
	Cruise	1.58	15.5	483

Table 8.1: Propulsion System Testing Results

This table summarizes the results of testing our Cobra C-4130-20 300kv motors under static and cruise conditions. Both motors were tested using a 15x10 propeller. The test conditions are defined as follows:

Static: A full-throttle test at zero airspeed

Cruise: Full throttle at 40mph airspeed

Our target static and cruise thrusts were 21N and 5N respectively. Based on the results of this table, it was confirmed that both motors would provide sufficient thrust under both static and cruise conditions.

8.1.4 Vaccine Deployment Testing

The trap doors were initially controlled by servo motors; however, it was observed that the servo motors were not able to hold the trap doors up during take-off and landing. As a result, the servos were taken out and rubber bands were used instead to hold the trap doors up. Through testing, the optimal places and length of rubber bands were found.

Through repeated testing, it was confirmed that the trap doors would open with the weight of packages. The servo-driven belt deployment system was tested to make sure that the packages would deploy consistently from alternating sides when the signal was received by the Arduino. 3D printed packages of the correct weight distribution with sensors on three sides were dropped onto the slope created by the trap doors to validate the sensors would not be activated with the force of packages falling onto concrete. Several floor materials were tested to ensure that the packages did not exceed the 25G limit regardless of the hardness of the surface the packages were dropped on.

To improve the transport of packages through the conveyor belt system, rails under the packages were lubricated using clear packing tape and Teflon lubricant. The supports on each side of the rails were tested to see if they would be long/strong enough to hold the packages during turns. To do this, extreme bank angles of up to 90 degrees to each side were simulated while the airframe was shaken. This testing indicated that no packages would fall out of the mechanism even in these extreme conditions.

8.1.5 Subsystems Comparison

Flight tests of the mockup competition aircraft confirmed subsystem performance and allowed for the creation of a control scheme for the final competition aircraft. The prototype withstood a fully loaded wing tip test along with loaded competition flight maneuvers in flight tests. The landing gear, propulsion system, and mechanism performed as predicted.

8.2 Demonstrated Aircraft Performance

8.2.1 Aircraft Performance Results

A flight test of the prototype competition aircraft was performed to confirm critical performance values and verify the aircraft has adequate handling and stability properties. The takeoff was assessed by measuring maximum takeoff distance of 25 ft to ensure the aircraft was able to take off in the required distance. Takeoff was performed on packed snow without brakes. Even with these suboptimal conditions, takeoff was achieved within 25 ft and no other complications arose with takeoff, meaning that the propulsion system is sufficient for allowing the aircraft to take off in the 25 ft distance.

A second flight was performed in which a sharp banking turn was performed and a portion of the wing spar cracked. The aircraft continued flying and successfully landed, at which point the issue was identified. The method of joining the wing sections had concentrated the turn load on a thin section of the spar via a plywood rib. This, combined with the relatively thin wall of the spar section, caused it to crack under the high loading. This issue was addressed by increasing the wall thickness of the outermost spar sections.

Figure 8.3: Takeoff of Prototype during Flight Test

Figure 8.4: Aircraft right before landing, including an on-board view

8.2.2 Complete Aircraft Comparison

From the flight test, an average lap time of 45 seconds was measured for Mission 1. Due to the crack in the spar which occurred during the first flight test, we have not yet measured lap times for Missions 2 and 3, although based off of the flight we expect to be close to our predicted mission performance in Section 5.6. Differences in performance will most likely be due to an underestimation of turn radius and time, as well as potential error in package deployment during Mission 3. The data collected in the flight test was used to update the performance model and refine our manufacturing techniques.

8.2.3 Handling Evaluation

In flight, the aircraft exhibited slight pitch instability, which the team later deduced was caused by two factors: a faulty wing-to-fuselage mount which was not caught in the design process, and the omission of the fuselage in aerodynamic analysis. Both the mount design and fuselage were accounted for in the final aircraft design. Despite this slight pitch instability, the pilot remarked that the handling of the aircraft was otherwise reasonable. Landing and takeoff were both successful without much difficulty.

9 References

[1] AIAA, "Cessna Aircraft Company Raytheon Missile Systems AIAA Foundation - 2020/2021 Rules and Vehicle Design," 22 November 2020. [Online]. Available: https://www.aiaa.org/docs/default-source/uploadedfiles/aiaadbf/dbf-rules-2022.pdf. [Accessed 4 November 2022].

[2] “Circle Packing.” *Wikipedia*, Wikimedia Foundation, 16 Feb. 2022, [Online]. Available: https://en.wikipedia.org/wiki/Circle_packing. [Accessed 5 Feb 2022].

[3] Peterdsharpe. “Peterdsharpe/Aerosandbox: Aircraft Design Optimization Made Fast through Modern Automatic Differentiation. Composable Analysis Tools for Aerodynamics, Propulsion, Structures, Trajectory Design, and Much More.” *GitHub*, https://github.com/peterdsharpe/AeroSandbox. [Accessed 1 October 2020].

[4] André, “XFLR,”[Online]. Available: http://www.xflr5.tech/xflr5.htm [Accessed 9 October 2020].

[5] eCalc, "eCalc propCalc - Propeller Calculator," 15 February 2014. [Online]. Available: http://ecalc.ch/motorcalc.php?ecalc&lang=en. [Accessed 1 October 2020].

[6] Solidworks, “3D CAD Design Software.” *Solidworks*, https://www.solidworks.com/. [Accessed 10 January 2022].

[7] OpenVSP, “OpenVSP,” January 2012. [Online]. Available: http://openvsp.org/. [Accessed 23 October 2020].

[8] Drela, M. and Youngren, H., “XFOIL,” December 2013. [Online]. Available: http://web.mit.edu/drela/Public/web/xfoil/. [Accessed 9 October 2020].

Washington University in St. Louis

2021-2022 Design Report

Contents

Nomenclature

Abbreviations

AIAA	American Institute of Aeronautics and Astronautics	RC	Radio-controlled
AoA	Angle of attack	TOFL	Takeoff field length
AR	Aspect ratio	T-O	Takeoff
AUW	All up weight	VLM	Vortex lattice method
CA	Cyanoacrylate	VT	Vertical Tail
CAD	Computer-aided design	WU	Washington University
CBDM	Component drag build-up method	WUDBF	Washington University in St. Louis Design/Build/Fly
CF	Carbon fiber	**Symbols**	
CFD	Computational Fluid Dynamics	b	Span [m]
CG	Center of gravity	c	Chord [m]
DBF	Design/Build/Fly	C_D	Drag coefficient
FEA	Finite Element Analysis	C_L	Lift coefficient
GM	Ground Mission	Re	Reynolds number
HT	Horizontal Tail	S	Wing Area [m^2]
HQRS	Cooper-Harper handling qualities rating scale	T	Thrust [kgf]
KM Sim	Kinematic mission simulator	T/W	Thrust-to-weight ratio
LiPo	Lithium Polymer	V_{HT}	Horizontal tail volume
M1	Mission 1	v_{max}	Max cruise velocity [m/s]
M2	Mission 2	V_{VT}	Vertical tail volume
M3	Mission 3	W	Weight [kgf]
NACA	National Advisory Committee for Aeronautics	W/S	Wing loading [kgf/m^2]
NiMH	Nickel-metal hydride		

1. Executive Summary

The Washington University in St. Louis Design/Build/Fly (WUDBF) 2021-22 Design Report describes the design, testing, and manufacturing of the *Pflyzer*, the team's entry in the American Institute of Aeronautics and Astronautics (AIAA) 2022 Design-Build-Fly competition. For the competition, the aircraft must be able to complete three flight missions and one ground mission. The first flight mission (M1) is a deployment mission that verifies the function of the aircraft. The second mission (M2) is a staging flight; during this mission the aircraft must carry a payload of syringes while flying the course as fast as possible. The third mission (M3) is a vaccine delivery flight involving repeated takeoff/landing with package deployment following each landing. The ground mission (GM) serves as a timed demonstration of the aircraft.

The *Pflyzer* has been designed to meet all mission requirements while maintaining a high level of reliability and minimizing risk. The aircraft consists of a conventional, single motor, taildragger, low-wing aircraft with a dihedral of 5°. These characteristics were chosen during the conceptual design phase in response to the stated requirements. The taildragger configuration gives the plane an initial 11.02° angle of attack on takeoff, which helps decrease takeoff length. The low-wing configuration allows for payloads to be easily installed, which is ideal for the GM. The dihedral was added to improve the stability characteristics of the low-wing configuration. A sensitivity analysis performed during the conceptual design phase indicated that a M2 payload of 40 syringes and a M3 payload of 4 packages was optimal given size constraints and WUDBF's desire for a low-risk design.

During the preliminary design phase, the aircraft was further refined via detailed aerodynamic and propulsion design. Lift, drag, and stability analyses were performed to size the aircraft and set the outer geometry. The wingspan was set at 2400 mm with a wing loading of around 6 kgf/m^2. Package placement was also determined such that center of gravity shifts are minimized following deployment. A propulsion system was then selected that gives the aircraft a 1.52 thrust-to-weight ratio and a predicted maximum cruise velocity of 22.5 m/s.

During the detail design phase, the internal structure of the aircraft was defined. A two stage-deployment mechanism consisting of a servo-controlled release stage and a ramp-based lowering stage was also designed to safely deploy the packages without tripping the shock sensors.

Based on subsequent performance simulations, the aircraft was able to takeoff in less than 12 ft, well below the 25 ft requirement. The aircraft was predicted to be able to complete M2 in 2.192 minutes, well within the time limit and yielding a score of 1.616. For M3, the aircraft was predicted to fly for a total of 3.784 minutes while completing four scoring laps, yielding a predicted score of 1.667. Endurance estimates aligned well with both the M2 and M3 flight times. Adding on the predicted M1 and GM scores, the *Pfylzer* is estimated to score competitively with a total score of 6.283 points out of a possible 7. Thorough ground and flight testing confirmed that the aircraft could meet all predicted performance goals.

2. Management Summary

2.1 Organization

WUDBF consists of 40 members organized into an Administrative Wing and a Technical Wing, both supported by a Faculty Advisor. The Administrative Wing, led by the Administrative President, is responsible for handling resource allocation, purchasing, public relations, and other administrative tasks. The Technical Wing is responsible for the design, manufacture, and testing of the competition aircraft. Within the Technical Wing, five subteams each handle separate aspects of the aircraft design (see Table 2.1 for details). Each subteam is led by a subteam lead and populated with general members. The Technical President oversees the entire Technical Wing to ensure effective collaboration and communication between the different subteams.

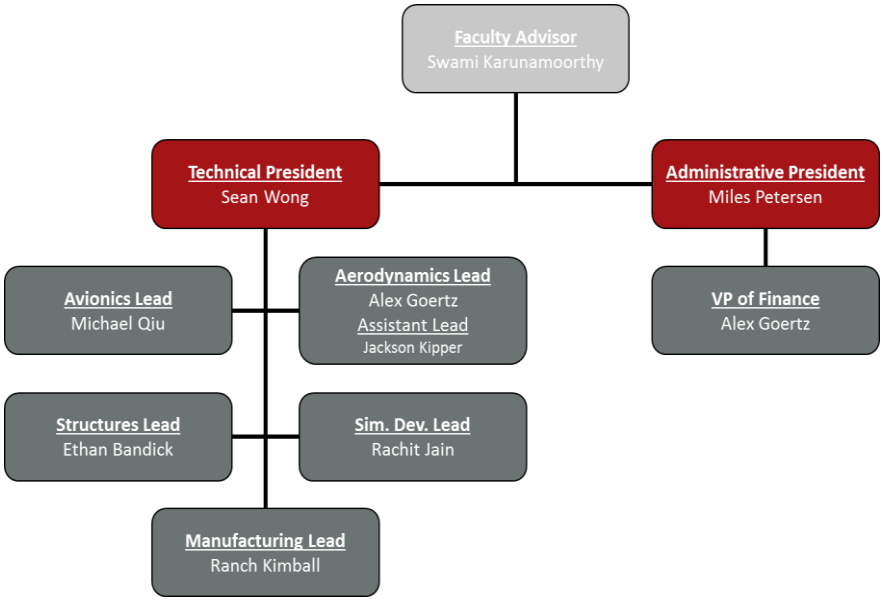

Figure 2.1: Team Hierarchy

Table 2.1: Subteam Roles and Skills

	Aerodynamics	Structures	Manufacturing	Avionics	Simulation Development
Roles	• Design of the exterior geometry of the aircraft • Aircraft sizing	• Design and modeling of the aircraft structure	• Assembly of the aircraft	• Design of the propulsion package • Install of electrical components	• Development of simulation tools • Programming of flight controllers
Skills	• Aircraft stability and control optimization • CFD analysis	• CAD • Structural FEA • Mass properties analysis	• Laser cutting, 3D printing, machining • Balsa RC aircraft construction	• Propulsion theory and analysis • Electrical design • Soldering	• MATLAB/Simulink • Python • Real Flight 8

2.2 Schedule

WUDBF uses a Gantt chart to ensure the team stays on track and meets major deadlines. The Gantt chart for the 2021-22 competition year is shown in Figure 2.2 below. Due to university regulations leading to a delayed start of the Spring semester, WUDBF had to slightly modify the originally planned schedule as January prototype test flights had to be delayed. Despite this, WUDBF still remains on track to arrive at competition with a successful aircraft.

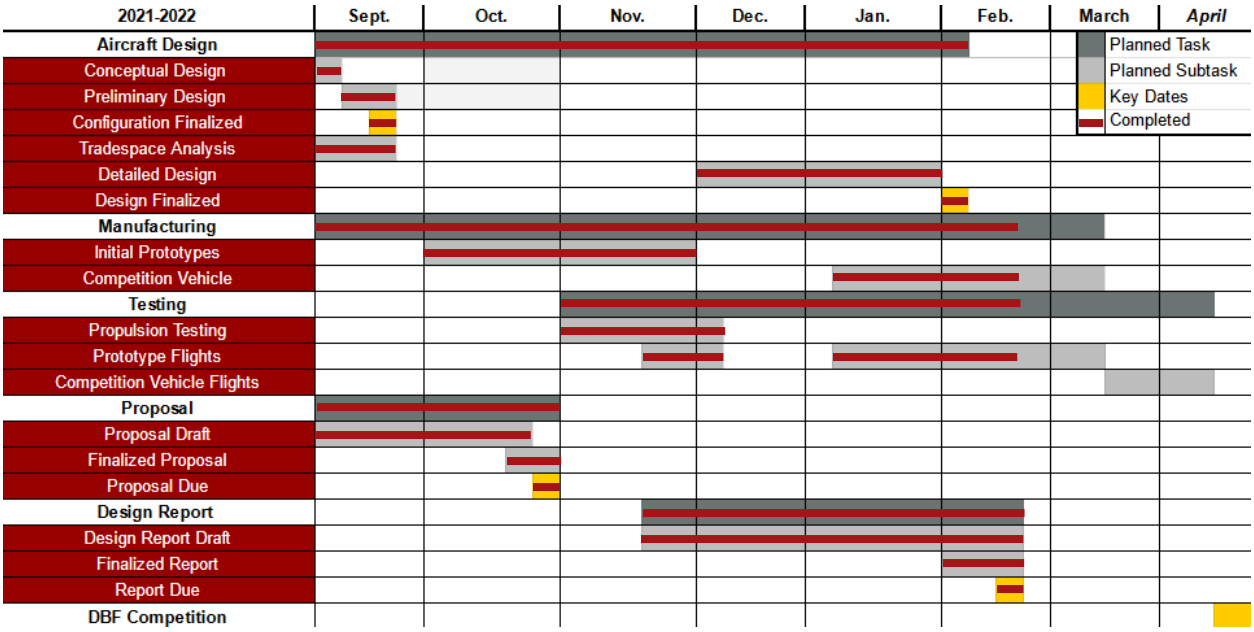

Figure 2.2: WUDBF Gantt Chart for 2021-2022 Competition

3. Conceptual Design

For the 2021-22 DBF competition, the AIAA has set the objective to design and build an aircraft to deliver vaccination components in a humanitarian mission scenario. The aircraft must be capable of transporting vaccination syringes, delivering environmentally sensitive vaccine vial packages, and taking off using short runways (less than 25 feet in length).

Upon receipt of the competition rules, WUDBF began the conceptual design phase starting with identification of key mission requirements and translation of those mission requirements into design requirements, followed by a scoring sensitivity analysis and configuration selection via a series of decision matrices.

3.1 Mission Requirements

A total of four missions are called for in the 2021-22 competition including three flight missions and one ground mission. The competition course layout (used for all flight missions) is shown in the figure below.

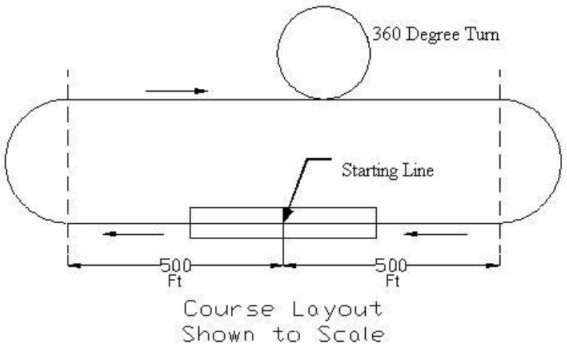

Figure 3.1: Competition Course Layout

3.1.1 Mission 1 – Deployment Flight

Mission 1 takes place with no payload. The aircraft must takeoff within a TOFL of 25 feet and complete 3 laps within a 5 minute flight window. A lap is considered completed when the aircraft passes over the start/finish line. Landing of the aircraft can occur outside of the 5 minute flight window, but a successful landing must be completed in order to receive a score. Scoring for Mission 1 is as follows:

$$M1 = 1.0 \tag{3.1}$$

The maximum achievable score for Mission 1 is **1.0 point**, which is earned upon completion.

3.1.2 Mission 2 – Staging Flight

Mission 2 is the syringe transportation flight. The minimum payload is ten syringes (there is no maximum). Based on syringes obtained by WUDBF, each syringe weighs ~0.65 oz (~0.02 kg). The aircraft with payload must takeoff within a TOFL of 25 feet and complete 3 laps within a 5 minute flight window. Landing of the aircraft can occur outside of the 5 minute flight window, but a successful landing must be completed in order to receive a score. Scoring for Mission 2 is as follows:

$$M2 = 1 + \frac{\left(\frac{\#syringes}{time}\right)_{WUDBF}}{\left(\frac{\#syringes}{time}\right)_{Max}} \tag{3.2}$$

where $\#syringes$ is the number of syringes flown during the mission, $time$ is the time required to complete the mission, and the $WUDBF$ and Max subscripts indicate the $(\#syringes/time)$ score received by WUDBF and the highest $(\#syringes/time)$ received by any team respectively. The maximum achievable score for Mission 2 is **2.0 points** with 1.0 point earned for completion and up to an additional 1.0 point earned for performance.

3.1.3 Mission 3 – Vaccine Delivery Flight

Mission 3 is the vaccine vial package delivery flight. The minimum payload is one package. The maximum payload is the maximum number of syringes flown in a successful Mission 2 divided by ten (rounded down to the nearest whole number). Each package consists of a wood block containing three 25G shock sensors. The weight of each package will be ~8.00 oz (~0.23 kg). The aircraft with payload must takeoff

within a TOFL of 25 feet. There is a 10 minute flight window for Mission 3 in which to complete as many laps as possible. Following completion of one flying lap, the aircraft must land on the runway and taxi to the designated vaccine vial package drop area. Once within the designated area, the aircraft must remotely deploy one package. After successfully deploying a package, the aircraft must then taxi across the start/finish line and takeoff again within 25 feet, complete another flying lap, and deploy a single package until all packages are deployed or the flight window expires. Landing of the aircraft can occur outside of the 10 minute flight window, but a successful landing must be completed in order to receive a score. Scoring for Mission 3 is based on the number of successful vaccine vial packages deployed within the designated drop area without tripping the shock sensor:

$$M3 = 2 + \frac{(\#successful\ deployments)_{WUDBF}}{(\#successful\ deployments)_{Max}} \tag{3.3}$$

where $\#successful\ deployments$ refers to the number of packages successfully deployed (i.e. without tripping the shock sensor) and the $WUDBF$ and Max subscripts indicate the $(\#successful\ deployments)$ achieved by WUDBF and the highest $(\#successful\ deployments)$ received by any team respectively. The maximum achievable score for Mission 3 is **3.0 points** with 2.0 points earned for completion and up to an additional 1.0 point earned for performance.

3.1.4 Ground Mission – Operational Demonstration

The Ground Mission serves as a timed ground demonstration of the aircraft's Mission 2 and 3 capabilities. The mission begins with the aircraft in the "mission box" with the maximum declared number of vaccine vial packages and the required number of syringes (ten times the maximum number of packages). The mission is divided into three phases. In the first phase, the mission official will say "GO" upon which time will start. An assembly crew member will then run from behind the start/finish line to the mission box. Once there, they will load the full Mission 2 payload (the syringes) and run back to the start/finish line; time stops when they cross the line. The second phase starts when the official says "GO" again and time restarts. The assembly crew member will then run back to the mission box, remove the Mission 2 payload, install the full Mission 3 payload (the packages), and run back to the line where time will stop. The timed portion concludes with the second phase. In the third phase, all packages will then be deployed remotely one at a time to validate functional performance. All packages must be deployed for the Ground Mission to count. Scoring is as follows:

$$GM = \frac{(time)_{Min}}{(time)_{WUDBF}} \tag{3.4}$$

where $time$ is the time required to complete the timed portion of the Ground Mission (phases 1 and 2 as described above) and the $WUDBF$ and Min subscripts indicate the time achieved by WUDBF and the fastest ground mission time achieved by any team respectively. The maximum achievable score for the Ground Mission is **1.0 points** based on performance.

3.1.5 Total Competition Score

The Mission 1, Mission 2, Mission 3 and Ground Mission scores will be combined to give the Total Mission Score:

$$Total\ Mission\ Score = M1 + M2 + M3 + GM \tag{3.5}$$

The maximum achievable Total Mission Score is **7.0 points** with 4.0 points earned based on completion and 3.0 points earned based on performance. The Total Mission Score is then multiplied by the Design Report Score to give the Total Competition Score (SCORE):

$$\text{SCORE} = Design\ Report\ Score \times Total\ Mission\ Score \tag{3.6}$$

3.1.6 General Mission Requirements

In addition to the requirements specific to each mission, there are also a number of other rules of note that apply to the competition aircraft during all missions:

- The aircraft cannot exceed 8 feet in any linear dimension.
- All payloads must be carried internally to the aircraft. No part of any payload can be part of or protrude outside of the airplane external surfaces or features.
- Any device used to load, store, or deploy a payload must remain installed on the aircraft during all flight missions and be included during all phases of the Ground Mission.
- The aircraft may utilize either NiCad/NiMH OR Lithium Polymer (LiPo) batteries for propulsion, but the total propulsion power total stored energy cannot exceed 100 watt-hours.
- The flight missions must be flown in order; a new mission cannot be flown until the team has obtained a successful score for the preceding mission.

3.2 Translation to Design Requirements

Based on the mission requirements outlined above, WUDBF formulated design requirements for each mission. These design requirements are broken down in the table below.

Table 3.1: Translation of Mission Requirements into Design Requirements

Mission	Mission Requirement	Design Requirement
All	25 ft TOFL	Low W/S, high $C_{L,max}$, high T/W
M2	Minimize lap time	High cruise velocity, high T/W, low drag
	Maximize payload	Large wing area, sufficient internal volume
M3	Maximize payload	Large wing area, sufficient internal volume
	Remote payload deployment	Electronic deployment mechanism
GM	Minimize loading time	Optimized payload storage configuration, easy access to internal storage
General	Complete every mission	Low risk design, high stability
	Max propulsion energy of 100 watt-hours	High efficiency, constrains maximum propulsion power
	Max linear dimension of 8 ft	Constrains wingspan

3.2.1 Analysis of Design Requirements

TOFL: The short takeoff imposes a number of major design requirements. In order to achieve the 25 ft TOFL, the aircraft must have some combination of low wing-loading, high $C_{L,max}$, and high thrust-to-weight ratio. These are critical design requirements since no flight mission can be completed without meeting the 25 ft TOFL requirement.

Mission 2: In order to maximize Mission 2 score, the aircraft must be designed to maximize payload while minimizing lap time. These two mission requirements lead to somewhat opposing design requirements. Increasing the payload requires an increase in the overall size of the aircraft; the wing area must increase to maintain a reasonable wing-loading. This however increases the drag on the aircraft, decreasing the cruise velocity. Thus, the aircraft must achieve a balance between these two sets of design requirements in order to maximize score.

Mission 3: Scoring in Mission 3 is based entirely on the number of successful deployments. Thus, the primary design requirement is for a large wing area and internal volume to maximize the number of packages that can be carried. It is important to note, however, that designing for Mission 3 impacts Mission 2 as well, since designing for increased Mission 3 payload would also decrease Mission 2 cruise velocity. Increasing payload also impacts takeoff ability.

Ground Mission: In order to minimize the Ground Mission time and increase score, the payload storage configuration must be optimized to allow for easy loading/unloading of Mission 2 and 3 payloads. For the same reason, the fuselage of the aircraft should allow easy access to the storage compartment via a hatch or door.

Minimal Risk: From previous experience and the results from past competitions, WUDBF determined that only a fraction of teams successfully complete every flight mission. Successfully completing every mission is critically important in order to maximize score, especially for this year's competition where over half of the points are awarded for completion. Consequently, WUDBF prioritized designing a reliable, stable aircraft that minimizes risk.

Constraints: The 100 watt-hour maximum propulsion energy limit imposes a hard constraint on the design of the aircraft. This limits the maximum power of the propulsion system and creates a need for a high efficiency design. The 8 ft maximum linear dimension constrains the wingspan of the aircraft.

3.3 Scoring Sensitivity Analysis

Based on the design requirements formulated above, WUDBF determined that there was no single obvious design direction. Prioritizing Mission 2 cruise velocity to minimize lap time drives the design towards a smaller, faster aircraft. Prioritizing increased payload in Missions 2 and 3 drives the design towards a larger, slower aircraft. Therefore, WUDBF conducted a scoring sensitivity analysis to determine which design direction maximizes total score.

3.3.1 Scoring Model

To construct a scoring model, WUDBF first identified the key scoring variables in the scoring equations: M2 time, number of syringes flown in M2, number of deployments in M3, and GM time. A sensitivity analysis could be conducted using all four scoring inputs. However, WUDBF determined that these variables are not all independent and could be linked together. Increasing M3 payload requires increasing the M2 payload (since the number of syringes flown in M2 must be at least ten times the number of packages flown in M3). Increasing the payload increases the weight of the aircraft, which in turn impacts the maximum cruise velocity in M2 and M2 time. GM time is also affected, since increasing the payload increases the time required to load/unload it.

Thus, WUDBF constructed a scoring model using the **number of deployments in M3** as the sole input variable. Various equations were then developed to link it to M2 time, the number of syringes flown in M2, GM time, and ultimately Total Mission Score. A diagram depicting the full scoring model is shown in Figure 3.2. In order to implement the model, a number of simplifying assumptions had to be made. These assumptions and their associated justifications are detailed in Table 3.2.

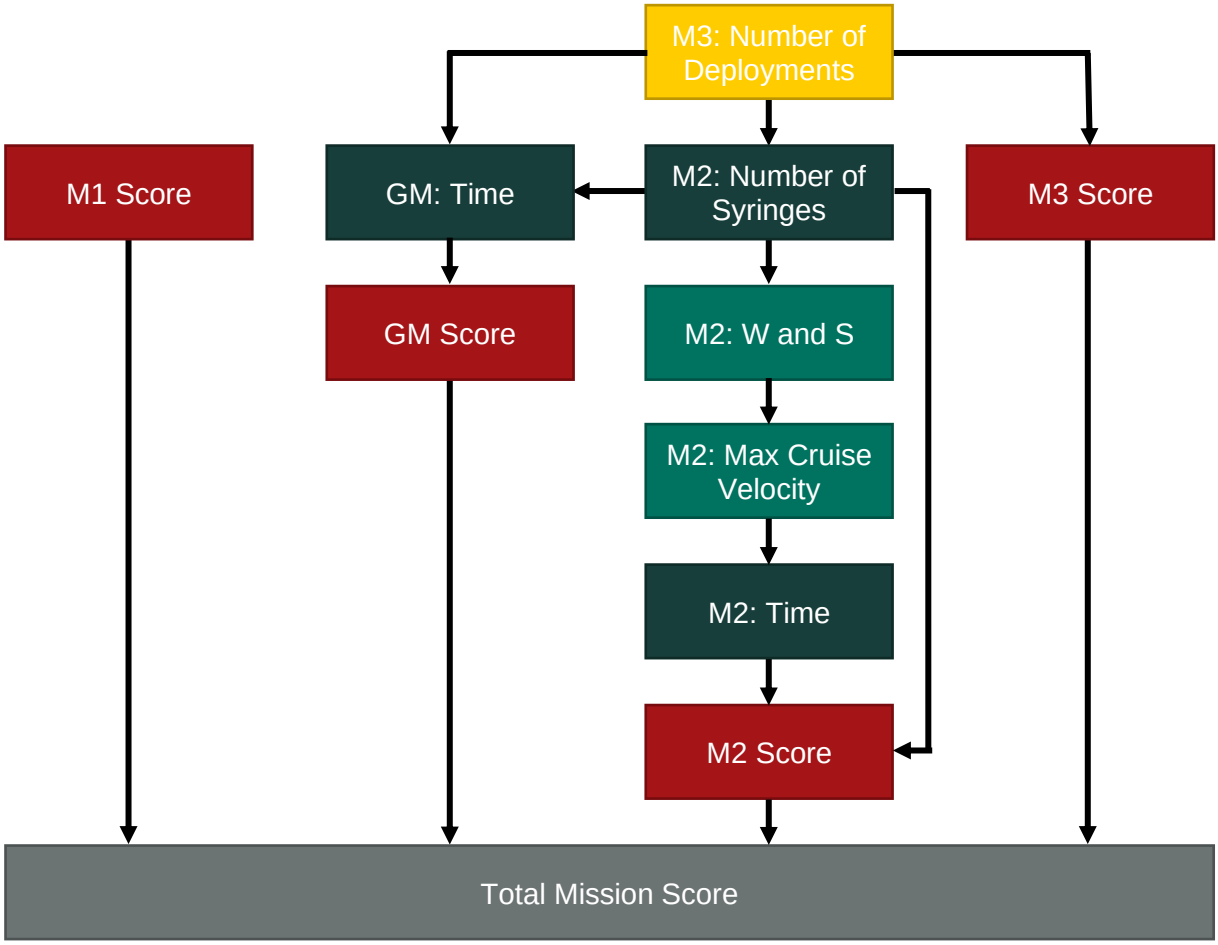

Figure 3.2: Scoring Model Flowchart

Table 3.2: Table of Key Assumptions and Justifications for Scoring Model

Assumption	Justification
10 syringes weigh the same as 1 package and take up approximately the same volume.	Based on empirical testing done by WUDBF.
The number of syringes carried in M2 is 10x the number of deployments in M3.	Based on the minimum amount required by the rules. Theoretically, more syringes could be flown in M2 than required, but for simplicity that possibility is ignored in this model. Furthermore, since 10 syringes weighs about the same and takes up the same volume as 1 package, it does not make sense to design an aircraft that can carry a significantly greater M2 payload than M3 payload.
GM time increases linearly with the number of syringes/deployments.	Based on empirical testing done by WUDBF.
M2 all-up weight (W) increases linearly with the number of syringes carried in M2.	Based on experience from previous DBF competitions. The amount of structural mass required to support each additional payload is approximately constant.
The aircraft has a wing-loading of 6.5 kg/m^2	Based on experience from previous DBF competitions. An aircraft with this wing-loading is likely to be able to take-off within 25 ft.
The aircraft has an AR of 5.5.	Based on minimal risk requirement. It is generally agreed that an AR of between 5:1 and 6:1 is ideal for an easy flying aircraft [1].
Max cruise velocity can be estimated from all-up weight (W) and wing area (S).	Max cruise velocity can be determined by iteratively solving the following equation [2, p. 878]: $\rho S C_{Dmin} {V_{max}}^3 = \eta P + \sqrt{(\eta P)^2 - 4W^2 {V_{max}}^2 C_{Dmin} k}$
Lap length is approximately 2500 feet.	Based on course diagram.

3.3.2 Results of Scoring Sensitivity Analysis

Using the scoring model developed above, WUDBF varied the number of deployments in M3 in order to determine which value maximizes total score. Figure 3.3 below shows how intermediate variables in the scoring model including all-up weight, wing area, GM time, and wingspan varied with the number of deployments in M3.

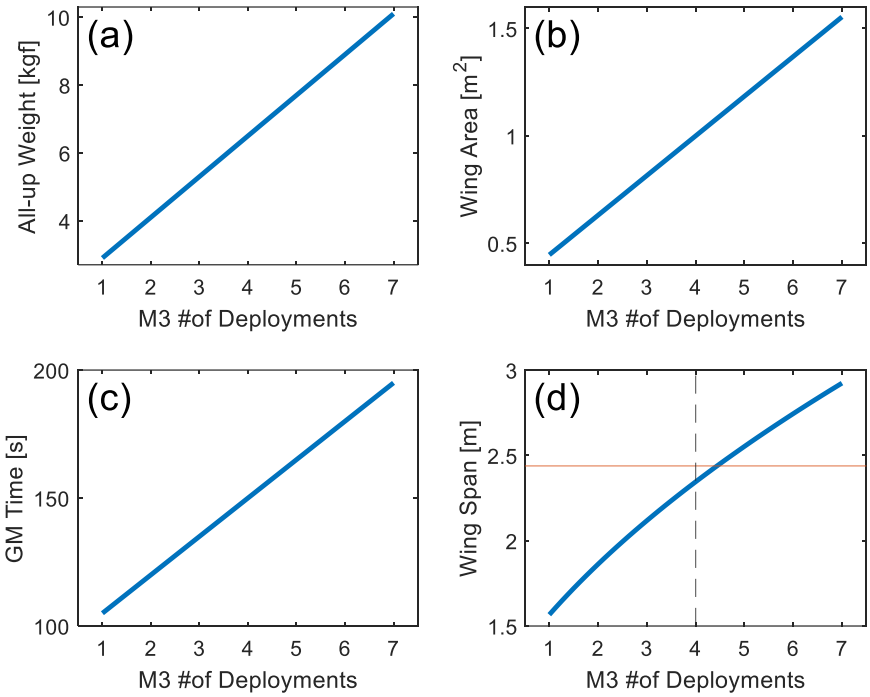

Figure 3.3: Plots of Intermediate Variables in Scoring Model

The plot in Figure 3.3d sets an important constraint on the scoring analysis. Since wingspan cannot exceed 8 ft (2.44 m), based on this model the maximum number of deployments in M3 that can be safely achieved is four. Note that by increasing the assumed wing loading or decreasing the assumed AR, more deployments could be achieved within the 8 ft wingspan constraint. However, WUDBF prioritized a minimal risk design and stuck with the assumed values. The resulting scoring calculations are shown in Figure 3.4 below.

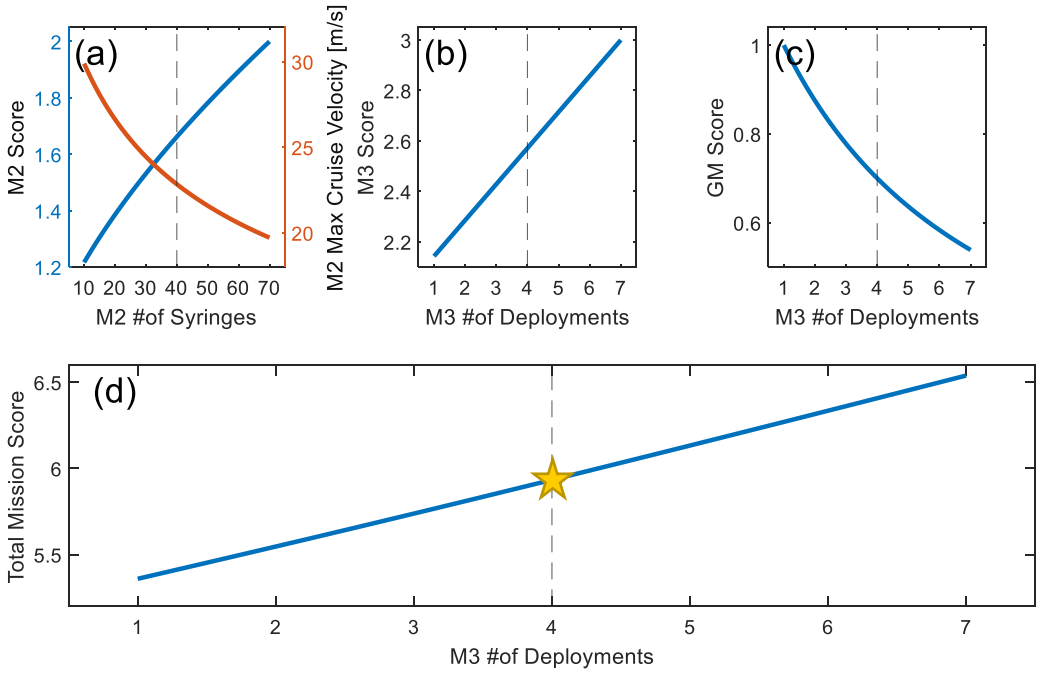

Figure 3.4: Plots of Mission Scores in Scoring Model

For M2, max cruise velocity decreases with increasing number of syringes, which increases lap time. However, the overall M2 score still increases with increasing number of syringes despite the increase in lap time. For M3, score increases linearly with the number of deployments, as expected. For the GM, score decreases with the number of deployments since more time is needed to load the additional payload. Summed together, Figure 3.4d shows that Total Mission Score increases with the number of deployments in M3. Thus, this scoring sensitivity analysis indicates that the optimal design is one that maximizes M2 and M3 payload, while sacrificing cruise velocity and GM time.

Since the maximum number of deployments in M3 is four (based on the wingspan constraint), WUDBF chose four deployments in M3 as the desired design point. From this, the following initial design targets were identified using the plots in Figures 3.3 and 3.4:

Table 3.3: Initial Design Targets

Design Specification	Initial Target Value
Number of deployments in M3	4
Number of syringes in M2	40
Max M2 cruise velocity [m/s]	22.5
GM Time [s]	150
M3 All-up weight [kgf]	6.50
Wing area [m^2]	1
Wingspan [m]	2.35

These design targets were used to guide the initial conceptual design and were further refined in the preliminary design phase.

3.4 Configuration Selection

Once initial design targets were determined, decision matrices were then used to select the overall aircraft configuration as well as the configuration of major subsystems. All decision matrix weights were determined based on design goals and competition requirements. Individual criterion scores were then determined based on team knowledge and experience from previous competitions. The individual criterion scores were multiplied by the weights and summed together to determine the total weighted score for each configuration. A selection was then made by comparing the total weighted score.

3.4.1 Overall Aircraft Configuration

WUDBF first considered three overall aircraft configurations including the monoplane, biplane, and blended body configurations. Key design criteria included aerodynamic efficiency, stability and control, wing area, and feasibility. The highest weights were assigned to aerodynamic efficiency and stability control, as those are the main drivers of overall aircraft design. Based on these criteria, the following conclusions were made.

- **Monoplane:** Provides good aerodynamic efficiency, stability and control, and is likely the most feasible configuration. However, available wing area within the span limitation is the lowest of the considered configurations.
- **Biplane:** Potentially allows for more lift within the span limitation by maximizing available wing area. However, the increased drag and added structural weight associated with the configuration decreases efficiency.
- **Blended Body:** Allows for increased wing area while still maintaining relatively good aerodynamic efficiency. However, the complex geometries of the blended-body reduces design and manufacturing feasibility. Additionally, the blended body configuration would have limitations in regard to stability and control.

Translating these judgments to the decision matrix resulted in the Table 3.4 below:

Table 3.4: Aircraft Configuration Decision Matrix

		Score		
			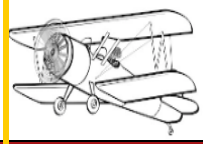	
Criteria	**Weight**	Monoplane	Biplane	Blended Body
Aerodynamic Efficiency	9	5	3	4
Stability and Control	9	5	3	2
Wing Area	5	3	5	4
Feasibility	7	5	3	1
	Total:	140	100	81
	Normalized:	**1.000**	**0.714**	**0.579**

Ultimately, the monoplane configuration was selected due to its superior total weighted score, efficiency, stability, and feasibility. While the monoplane configuration did not offer any advantages with regards to increased wing area, it was thought that the 8 ft wingspan limitation allowed for a large enough wing area to meet mission requirements with a monoplane design.

3.4.2 Wing Placement

WUDBF next considered wing placement by comparing high-, mid-, and low-wing configurations. Stability and control and takeoff capability were weighted highest followed by feasibility, payload loading, and payload capacity.

- **High-Wing:** Possesses the best stability and control due to its tendency to self-correct. Also is the most feasible configuration since WUDBF used it successfully in the past. However, access to the fuselage from above is restricted, increasing payload loading complexity and GM time.

- **Mid-Wing:** Has stability and control characteristics between that of the low- and high-wing configurations. However, this configuration necessitates that the structural support for the wing runs through the center of the fuselage. This results in a decreased payload capacity and potentially increased payload loading complexity.
- **Low-Wing:** Potentially reduces takeoff length due to ground effects. Because the low-wing configuration allows for easy access from above, it has superior payload loading capability. However, is the least stable configuration due to the CG being above the wing.

The resulting decision matrix is shown in Table 3.5 below:

Table 3.5: Wing Placement Decision Matrix

		Score		
				
Criteria	**Weight**	High-Wing	Mid-Wing	Low-Wing
Stability and Control	9	5	4	3
Takeoff Capability	8	3	4	5
Payload Loading	6	2	3	5
Payload Capacity	6	5	3	5
Feasibility	7	5	4	3
	Total:	146	132	148
	Normalized:	**0.986**	**0.892**	**1.000**

Ultimately, the low-wing configuration was chosen due to its superior takeoff and payload loading capabilities. WUDBF determined that concerns with stability and control could likely be mitigated by adding dihedral to the wing.

3.4.3 Empennage Configuration

WUDBF then selected the empennage configuration out of the conventional tail, the T-tail, the H-tail, and the V-tail. The main design criteria for empennage configuration were determined to be stability and control, flutter, drag, wake interference during takeoff, and feasibility.

- **Conventional:** Simple to design and manufacture. Also possesses good stability and control and flutter characteristics.
- **T-tail:** Keeps the HT in undisturbed air, which would reduce the drag. However, the high-mounted HT can also generate low flutter speeds and asymmetric lift and yaw which induces high torsional loads. Additionally, having the HT at the tip of the VT introduces additional complexity into the structure and manufacturing process.

- **H-tail:** Offers increased HT efficiency due to the endplates. However, the flutter speed of the H-tail is reduced due to the weight of the VTs being located at the tips of the HT. Additional control and structural complexity is introduced by having two VTs, decreasing feasibility.
- **V-Tail:** Possesses good flutter characteristics and reduces the wake interference at takeoff. However, the V-tail control system is significantly harder to design and implement.

Based on these judgments, the decision matrix in Table 3.6 was constructed.

Table 3.6: Empennage Configuration Decision Matrix

		Score			
					
Criteria	**Weight**	Conventional	T-Tail	H-Tail	V-Tail
Stability and Control	9	5	4	3	3
Flutter	8	5	3	2	4
Drag	6	4	5	3	2
Wake Interference at T-O	4	3	5	3	4
Feasibility	7	5	3	3	1
	Total:	156	131	94	94
	Normalized:	**1.000**	**0.840**	**0.603**	**0.603**

Ultimately, the conventional tail was chosen because it was considerably more feasible than the other configurations and provided improved stability/control and flutter characteristics with comparable wake interference.

3.4.4 Landing Gear Configuration

The landing gear was then chosen based on ground maneuverability, payload deployment, drag, and structural strength. Using these criteria, the following configurations were compared in Table 3.7.

- **Tricycle:** Three struts or fairings independently connected to the fuselage. Provides good ground maneuverability and provides the option to allow the landing gear to retract into the fuselage. However, the structural strength of the front landing gear and takeoff capability of this configuration is a concern.
- **Bow Tricycle:** One front independent strut and two rear wheels which are connected to the fuselage via a common strut or fairing. This configuration allows good ground maneuverability while also increasing structural strength by adding bowed support to the two rear wheels. However, the structural strength of the front landing gear and takeoff capability are a concern.

- **Strut Tail-dragger:** Two front wheels connected independently to the fuselage and one rear wheel connected to the tail. This configuration increases takeoff capability and potentially eases payload deployment by lowering the rear of the aircraft closer to the ground. However, it provides limited ground maneuverability and offers limited structural strength.
- **Bow Tail-dragger:** Two front wheels connected to the fuselage via a common strut or fairing and one rear wheel connected to the tail. Offers the same improved takeoff capability and payload deployment as the strut tail-dragger, while also providing better structural support. Ground maneuverability of this configuration is limited.

Table 3.7: Landing Gear Configuration Decision Matrix

		Score			
					
Criteria	**Weight**	Tricycle	Bow Tricycle	Strut Taildragger	Bow Taildragger
Takeoff Capability	8	3	3	5	5
Payload Deployment	8	3	3	4	4
Structural Strength	7	3	4	3	4
Ground Maneuverability	6	5	5	3	3
Drag	4	3	3	4	4
Feasibility	7	3	4	3	5
	Total:	132	146	148	169
	Normalized:	**0.781**	**0.864**	**0.876**	**1.000**

Despite poor ground maneuverability, the bow tail-dragger configuration was chosen because of the takeoff advantages offered by the increased initial AoA, the improved payload deployment capability, and the added structural integrity provided by the bowed front gear.

3.4.5 Propulsion Configuration

The propulsion system was chosen based on its efficiency, thrust, weight, component interference, and drag. The following propulsion configurations were considered and the constructed decision matrix is shown below in Table 3.8.

- **Tractor:** Single motor on the front of the aircraft. Provides the highest efficiency, lowest weight and drag, and is the most feasible. Ground clearance could be a concern depending on the required propeller size and height of front landing gear.
- **Pusher:** Single motor aft of the fuselage. Provides low weight and drag but has a decreased ground clearance (especially during rotation) and low efficiency due to fuselage interference.

- **Twin:** Two motors which are mounted on the wings. Provides improved ground clearance due to reduced propeller size and reasonable efficiency. Also offers torque balancing and is reasonably feasible. However, drag is increased resulting from the placement of the motors on the leading edge of the wing. Weight is also a concern because of the additional electronics and structural strength needed to support the second motor.
- **Push/Pull:** One motor at the front and aft of the fuselage. Offers low weight and drag. However, is the least efficient due to propwash interference, has the same ground clearance concerns as the tractor and pusher configurations, and is the least feasible. Weight is also a concern because of the additional electronics and structural strength needed to support the second motor.

Table 3.8: Propulsion Configuration Decision Matrix

		Score			
			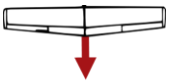	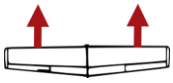	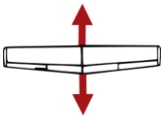
Criteria	**Weight**	Tractor	Pusher	Twin	Push-Pull
Efficiency	8	5	3	4	2
Weight	8	5	5	4	4
Ground Clearance	7	4	2	5	2
Drag	6	5	5	3	4
Feasibility	4	5	3	4	2
	Total:	158	120	133	94
	Normalized:	**1.000**	**0.759**	**0.842**	**0.595**

The tractor configuration was ultimately chosen because it was thought to maximize efficiency while minimizing weight and drag. Additionally, the tractor configuration is the most feasible design and is one that WUDBF has successfully employed in the past.

3.4.6 M3 Payload Configuration

The M3 payload configuration was chosen based on longitudinal weight distribution, lateral weight distribution, vertical weight distribution, ease of payload deployment, and available fuselage space. The following payload arrangements were compared in Table 3.9.

- **4 in-line:** Payloads on one horizontal plane lined up in the longitudinal direction. Minimizes lateral and vertical CG shifts and would make payload deployment reasonably simple. However, this configuration results in the largest longitudinal CG shift and necessitates a long fuselage.
- **Planar 2 by 2:** Payloads on the same plane, arranged in two longitudinal and two lateral rows. This configuration minimizes the vertical CG shift while balancing the longitudinal and lateral CG

shifts. This arrangement also improves payload deployment but necessitates a fuselage wide enough to fit two payloads side-by-side.

- **2 on 2 in-line:** Payloads stacked on two horizontal planes and arranged into one row running longitudinally along the fuselage. This configuration minimizes lateral CG movement while balancing longitudinal and vertical CG shifts. However, this arrangement increases payload deployment complexity due to the stacked payloads.
- **2 on 2 side-by-side:** Payloads arranged on two horizontal planes and two lateral rows to minimize longitudinal CG shifts while balancing vertical and lateral shifts. Like the 2 on 2 in-line, this configuration also increases payload deployment complexity.

Table 3.9: Payload Configuration Decision Matrix

		Score			
		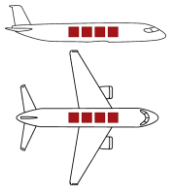	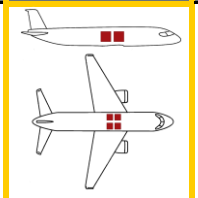	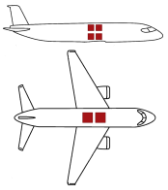	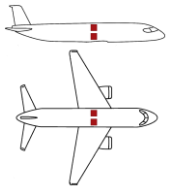
Criteria	**Weight**	4 In-Line	Planar 2 by 2	2 on 2 In-Line	2 on 2 Side-by-Side
Longitudinal CG Shift	9	1	3	3	5
Vertical CG Shift	8	5	5	2	2
Lateral CG Shift	6	5	2	5	2
Payload Deployment	6	3	5	2	1
Fuselage Size	4	3	3	4	4
	Total:	109	121	101	95
	Normalized:	**0.901**	**1.000**	**0.835**	**0.785**

In the end, the planar 2 by 2 was chosen because it is equally efficient in both the longitudinal and lateral directions. Thus, it does not require an extraordinarily wide fuselage, and does not induce large CG shifts as the payloads are deployed. Additionally, it does not require more than one horizontal plane of stacking, which simplifies payload deployment.

3.5 Final Conceptual Design

The final conceptual design consists of a low-wing, monoplane, tail-dragger aircraft with a conventional tail and a propulsion system in the tractor configuration. The aircraft is designed to carry an M2 payload of 40 syringes and a M3 payload of 4 packages. The targeted max cruise velocity in M2 is 22.5 m/s .

4. Preliminary Design

During the preliminary design phase, the initial aircraft concept and configuration from the conceptual design phase was further developed. Key aspects of the design including the overall sizing, wing geometry, airfoil, and propulsion package were refined following a number of trade studies.

4.1 Design Methodology

The full design methodology employed by WUDBF is outlined in Figure 4.1 below.

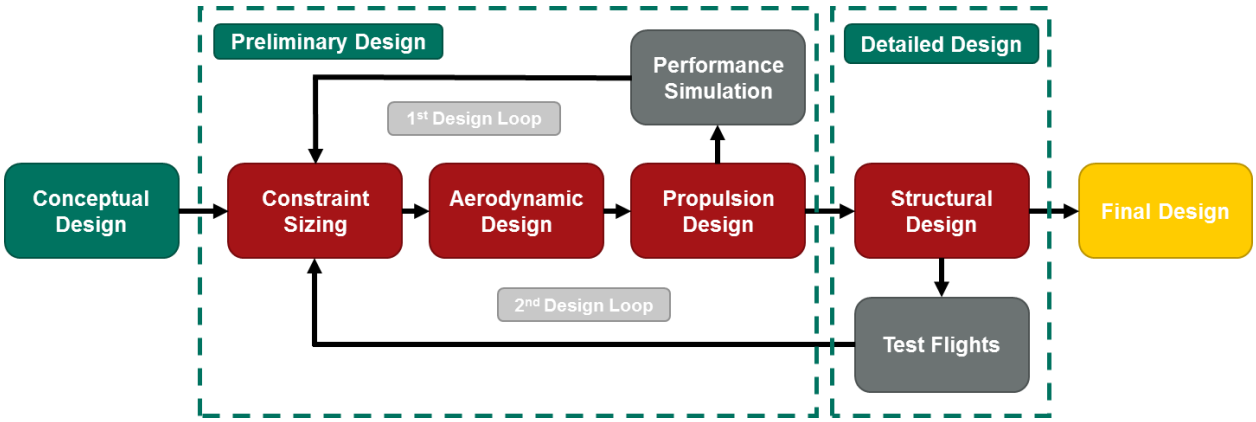

Figure 4.1: WUDBF Design Methodology

For the preliminary design phase, WUDBF utilized an iterative process focused on the performance of the fully loaded aircraft (i.e. with 4 packages in M3). This was done because 1) the AUW for M2 with 40 syringes is expected to be close to that of the fully loaded aircraft in M3 and 2) aircraft are typically designed for the fully loaded case. Initial design targets from the conceptual design phase were used as a starting point. A constraint analysis was performed to size the overall aircraft and to determine the desired wing-loading and required T/W and power. The chosen wing-loading was then used to guide aerodynamic design, from which the airfoil, wing geometry, and tail sizing were determined. The performance and stability characteristics of the aircraft were analyzed using the vortex lattice method in the analysis tool XFLR. The drag polar of the aircraft was determined using induced drag data from XFLR and the component drag build-up method. Following aerodynamic design, propulsion design took place using the required T/W, the required power, estimated AUW, and the drag polar as a starting point. The online tool eCalc was used to sort through a database of components to identify candidate propulsion system combinations. Data from eCalc was then used to select the optimal system, and performance was confirmed using WUDBF's time domain propulsion simulator written in MATLAB.

In order to iterate the design, WUDBF employed two design loops. Following the first design iteration, the preliminary design was tested using KM Sim, a kinematic mission simulator developed by WUDBF. Performance estimates from KM Sim were then used to iterate the preliminary design. Once the design met desired performance goals in KM Sim, the design moved into the second design loop. Structural

design took place to create a detailed CAD model of the aircraft. This model was used to build a prototype aircraft. Flight test data from the prototype were then used to inform changes to the preliminary design. Ultimately, the final design developed as the culmination of several iterations, with each iteration improving on performance and mission scores.

4.2 Constraint Sizing

An initial constraint sizing was performed by plotting the required thrust-to-weight ratio (T/W) to achieve a 25 ft takeoff and cruise at 22.5 m/s for a range of wing-loadings (W/S) using the equations developed in Gudmundsson [2, ch. 3]. These plots are shown in Figure 4.2a. Since the aircraft must be propeller driven using an electric motor, it is useful to convert T/W to required electrical power using initial estimates of weight, mechanical efficiency, and propulsive efficiency. This also allows for the setting of an upper power constraint of 2500 W (estimated from previous experience and past competition aircraft). The resulting power required curves are plotted in Figure 4.1b.

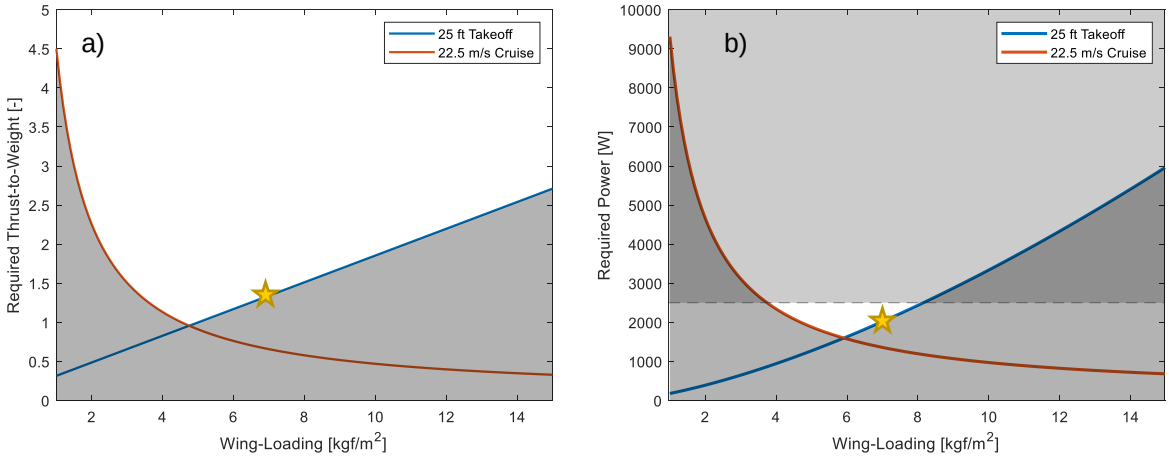

Figure 4.2: Plots of Required T/W and Power vs. Wing-Loading

From Figure 4.2b, the viable design space is limited to a small region of wing-loadings between 3.5 kgf/m^2 and 8 kgf/m^2. Note that the assumed wing-loading of 6.5 kgf/m^2 used for the scoring sensitivity analysis in Section 3.3 falls within this range, further justifying the assumption.

Ultimately, a wing-loading of 7.0 kgf/m^2 was selected for the design point as a conservative choice. During past competitions, the final WUDBF aircraft has consistently exceeded the designed weight. Thus, designing an aircraft with a wing-loading on the higher end of the acceptable range allows for a larger structural weight margin (given that propulsion and payload weight are essentially constant).

From the chosen wing-loading of 7.0 kgf/m^2, the minimum required power was set at ~2100 W and the minimum required T/W ratio at ~1.4 (as indicated by the stars in the figures above). Note that from the plots, the required T/W and power values are determined by the takeoff constraint; the required power at

cruise is only ~1400 W. Thus, the propulsion system could be designed to cruise at a lower throttle setting to increase endurance.

4.3 Initial Weight Estimation

The AUW of the aircraft was estimated using a breakdown of individual components. The weight of the wing, HT, VT, and fuselage were estimated using previous aircraft, which were built with similar methods and materials. Battery, motor, servo, electronics, central CF rod, and landing gear weights were determined by weighing representative components already possessed by WUDBF. The weight of the deployment mechanism was estimated using those built by WUDBF for recent competitions. The M3 payload weight is based on that given in the rules document. The full breakdown of estimated weights is shown below in Table 4.1.

Table 4.1: AUW Estimate Breakdown

Component	Weight (kgf)
Wing	2.15
HT	0.20
VT	0.13
Fuselage	0.50
Battery	0.75
Motor	0.61
Servos	0.08
Electronics	0.20
Central CF Rod	0.082
Front Landing Gear	1.0
Rear Landing Gear	0.10
Deployment Mechanism	0.20
M3 Full Payload	0.907
Total:	6.909

Based on this analysis, the predicted AUW of the fully loaded aircraft during M3 is 6.909 kg. Using the wing-loading of 7.0 kgf/m^2 determined in 4.2, that sets the desired wing area at around 0.987 m^2.

4.4 Aerodynamic Performance

The aerodynamic design of the aircraft was iteratively improved to ensure that it is stable, controllable, and achieves maximum aerodynamic performance. XFLR5 and MATLAB were the primary tools used for aircraft aerodynamic analysis. The size and shape of the main wing and stabilizers were driven by iterative static and dynamic stability analyses. Control surfaces and high lift devices were dimensioned to improve handling characteristics and minimize takeoff distance, respectively.

4.4.1 Aspect Ratio

Based on the desired wing area determined in 4.3 of 0.987 m^2, the required wingspan for different AR could be plotted as shown in Figure 4.3 below.

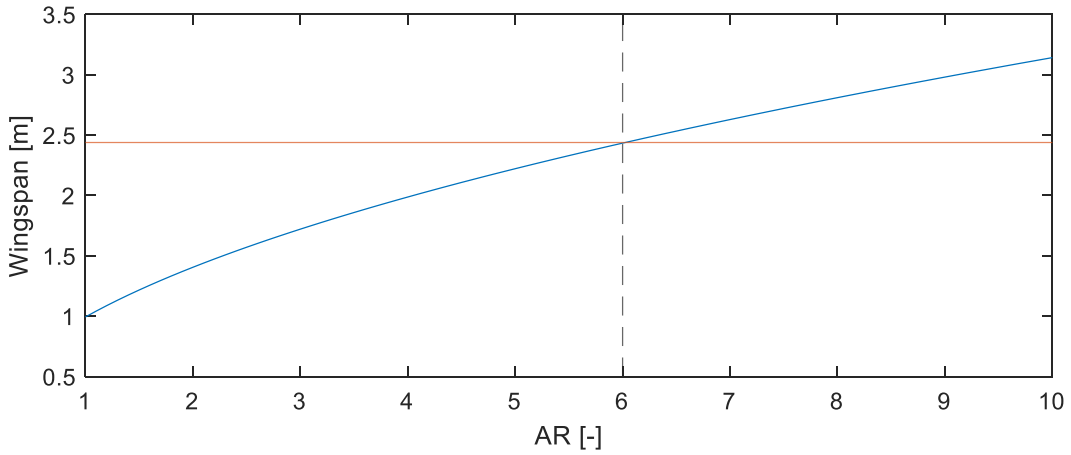

Figure 4.3: Required Wingspan for Varying AR

Based on the maximum 8 ft (2.44 m) wingspan limit, the viable AR ranges from 1-6. Generally, wings with an AR on the lower end of the range have the advantage of increased maneuverability due to increased stall AoA and low roll damping. Lower AR wings also require less structural weight. However, they are inefficient due to high induced drag and are generally more difficult to design and fly. Wings with an AR closer to 6 are more stable with good roll response and limited adverse yaw. They also benefit from improved efficiency due to lower induced drag [2, p. 310]. It is generally agreed that an AR of between 5 and 6 is ideal for an easy flying aircraft [1].

Ultimately, WUDBF chose the highest possible AR of 6 in order to maximize section lift and minimize induced drag. This choice also prioritizes safety, stability, and feasibility over maneuverability, which is in line WUDBF's stated design requirements.

4.4.2 Main Airfoil Selection

In order to select the main airfoil, the predicted Re of the aircraft was first calculated, using Equation 4.1:

$$Re = \frac{cV_\infty}{\nu} \tag{4.1}$$

where c is the mean aerodynamic chord [m], V_∞ is the freestream velocity [m/s], and ν is the kinematic viscosity of air [m²/s]. Kinematic viscosity was calculated from the average temperature in April (14 ℃) and altitude (400 m) in Wichita which yielded a kinematic viscosity of 1.498×10^{-5} m²/s. These conditions yielded a Reynold's number of 626,384.

Airfoil selection was then performed by selecting several different airfoils with maximum C_L/C_D near a Reynold's number of 500,000. Additionally, the search was restricted to airfoils with a minimum thickness of 10% and a maximum camber of 8% to ensure that the airfoil could accommodate structural and system integration and be reasonably manufactured with the processes available. Five promising airfoils were selected for comparison as shown in the table below:

Table 4.2: Airfoil Selection Options [3]

	Max. C_L/C_D at Re = 500 000	Max. Thickness [% of chord]	Max. Camber [% of chord]
Clark K	102.7	11.7	3.3
Clark Y	98.7	11.7	3.4
NACA 1412	73.5	12	1
NACA 2412	87.3	12	2
USA-35B	106.0	11.6	4.1

Once these potential airfoils were identified, analysis of each airfoil was performed in XFoil and XFLR to determine which provided a favorable lift coefficient, lift-to-drag ratio, and drag bucket at a Reynold's number of 626,000.

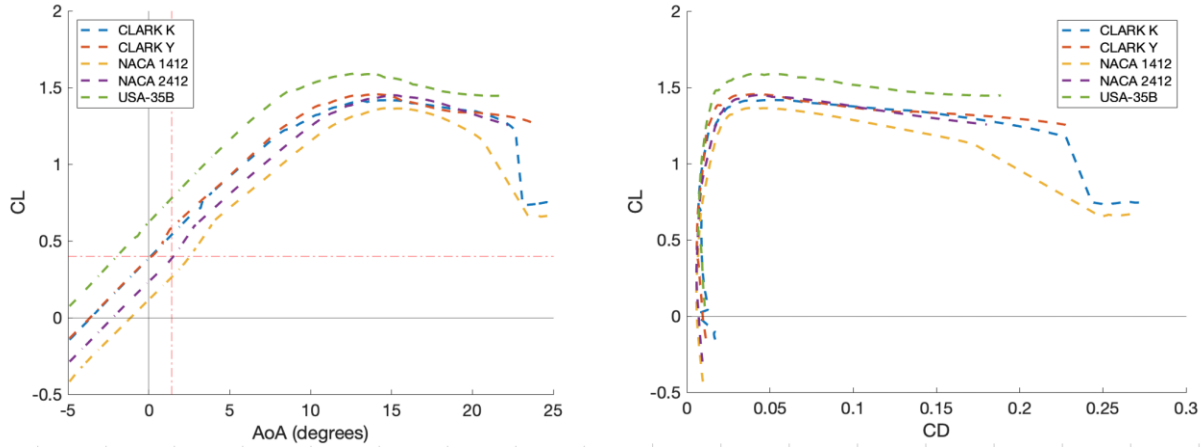

Figure 4.4: Airfoil C_L vs AoA (left) and C_L vs C_D (right)

As shown in the Figure above, the USA-35B possessed the highest lift coefficients and widest drag bucket. While the lift generated from this airfoil would improve T-O performance, it would also produce excessive lift at the target cruise velocity of 22.5 m/s, meaning the aircraft would have to fly slower resulting in longer lap times. Similarly, the Clark Y airfoil would also generate more lift than necessary at the target cruise velocity. While the NACA 2412 did not have the highest lift coefficients, it was found to provide sufficient lift at T-O and appropriate lift to meet cruise requirements. The NACA 2412 also had a drag bucket which comparable to the Clark Y. Thus, the NACA 2412 airfoil was chosen because it had the lowest C_{Dmin}, a wide drag bucket, and the desired lift characteristics at the target cruise velocity.

4.4.3 Empennage Sizing

Stabilizer airfoils are generally symmetric as they may either provide upforce or downforce, depending on the final trim state of the aircraft. WUDBF selected the NACA 0010 airfoil as it is common for stabilizers

and used successfully in past WUDBF projects [4]. Initial sizing of the empennage for stable flight began by investigating the vertical tail (VT) and horizontal tail (HT) volumes for aircraft of the same class. For a single-engine aircraft, the initial estimate was set at around V_{HT} = 0.70 and V_{VT} = 0.04 [5]. Initial horizontal and vertical tail areas were then solved for using Equation 4.2 and 4.3 as shown below [2, p. 513]:

$$S_{HT} = \frac{V_{HT} * S_{ref} * c_{ref}}{I_T} \tag{4.2}$$

$$S_{VT} = \frac{V_{VT} * S_{ref} * b_{ref}}{I_T} \tag{4.3}$$

Where S_{HT} is the horizontal tail area [cm^2], V_{HT} is the horizontal tail volume [cm^3], S_{VT} is the vertical tail area [cm^2], V_{VT} is the vertical tail volume (in cm^3), S_{ref} is the main wing area [cm^2], c_{ref} is the mean geometric chord [cm], b_{ref} is the span of the main wing [cm], and I_T is the optimal tail arm length [cm]. Based on these calculations, the VT and HT planform areas were set at 1285.4 cm^2 and 2236 cm^2 respectively. An initial assumption was made that the AR of the HT would be equal to about half the AR of the main wing and that the AR of the VT would be about 2 [6]. Initial estimates for the span of the VT and HT were then made using Eq 4.4 and 4.5 as shown below [2, p. 513]:

$$b_{HT} = \sqrt{AR_{HT} * S_{HT}} \tag{4.4}$$

$$b_{VT} = \sqrt{AR_{VT} * S_{VT}} \tag{4.5}$$

Where b_{HT} is the horizontal tail span (in cm), and b_{VT} is the vertical tail span (in cm).

During the design process, however, it was determined that using the method outlined by Gudmundsson was not feasible as optimal tail arm length is determined by considering the fuselage as a frustrum. Since it was decided that the fuselage would not extend the length of the tail early on in the design phase to save weight, the frustrum approximation was not reasonable for the design (see figure below). Thus, initial estimates for the tail arm using Gudmundsson's method were found to be sub-optimal.

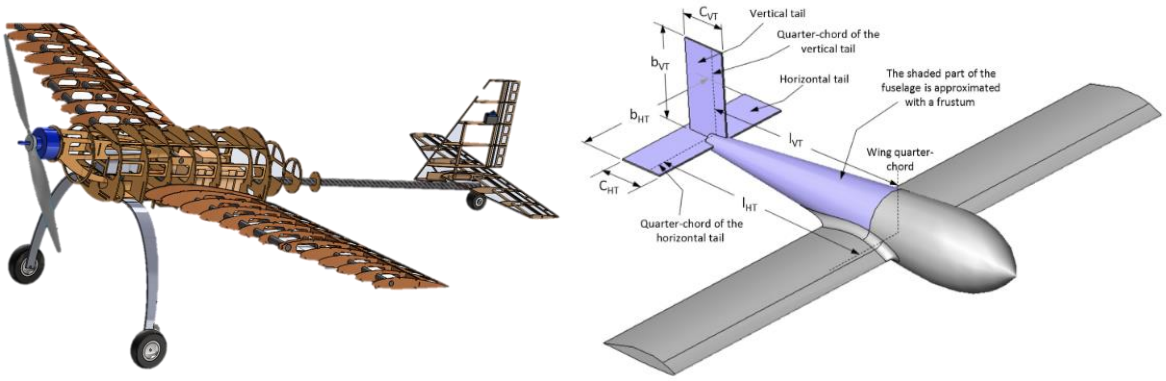

Figure 4.5: Initial Configuration of the Pflyzer (left) vs. Simplified Aircraft Layout used by Gudmundsson (right) [2].

To correct for this, the tail arm, CG locations and horizontal and vertical tail areas determined above using Gudmundsson's method were iterated on throughout the entire design process based on dynamic stability analysis and static margin. In the end, the resulting VT had a planform area of 1209.5 cm² and the HT had an area of 1845.0 cm².

4.4.4 High Lift Devices

Winglets were implemented to increase lift performance and were sized according to Gudmundsson and previous testing done by WUDBF [4]. Tests concluded that the additional lift generated as a function of winglet area hits a plateau beyond a certain point. Since a 5° dihedral angle was added to the wings, ground clearance was not a concern in this design. This allowed the area of the winglet to be larger than it would have been otherwise. The final winglet area was set at 230 cm². The Manufacturing and Structures subteams determined that this design is feasible and the additional lift generated outweighs the increased manufacturing complexity.

4.4.5 Control Surface Sizing

Given the traditional design of this aircraft, all control surfaces (rudder, elevator, and ailerons) were designed using rule-of-thumb parameters from Gudmundsson [2, p. 419]. Control surface sizing was verified using Equation 4.6 (see below) from Gudmundsson [2, p. 953], previous WUDBF aircraft, and prototype performance.

$$C_{l_{\delta_a}} = \frac{c_{l_{\delta_a}} C_R}{Sb}\left[(b_2^2 - b_1^2) + \frac{4(\lambda - 1)}{3b}(b_2^3 - b_1^3)\right] \tag{4.6}$$

Where $C_{l_{\delta_a}}$ is the aileron authority, $c_{l_{\delta_a}}$ is the change in lift coefficient with aileron deflection, b is the wing span [m], S is the wing area [m²], C_R is the root chord [m], and λ is the taper ratio.

Plain flaps were chosen to simplify the manufacturing process. The hinge point of the flaps was placed at the center of the leading edge arc to minimize large gaps and overhangs when the surfaces are deployed. The flaps were given a chord fraction of 25%, and a span of 40% of the wing. The ailerons had a chord fraction of 25% and a span of 60% of the wing. Both the flaps and the ailerons were designed to deploy at a 25° angle. Using data taken from XFLR, Figure 4.5 shows the plotted lift coefficient versus AoA with the flaps deployed at 25° and with no flaps. Chord fractions for the control surfaces on the empennage were 30% for the elevator, and 40% for the rudder. The Rudder was designed to deflect a maximum of 25°, while the elevator was designed to deflect a maximum of 25°.

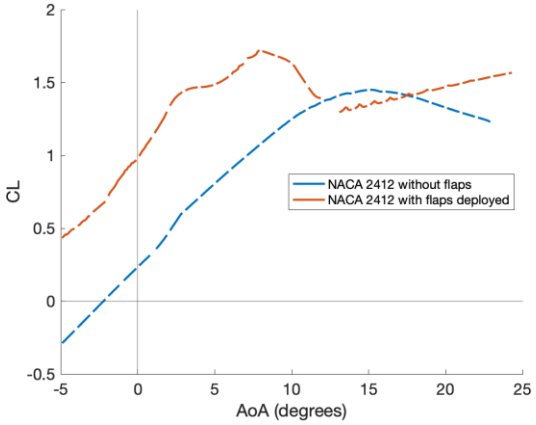

Figure 4.6: C_L vs AoA With and Without Flaps

4.4.6 Dynamic Stability Analysis

The dynamic stability characteristics of the aircraft were analyzed using XFLR. The Root Locus plot below in Fig 4.7 shows the dynamic stability modes when the aircraft is loaded with four packages in M3 (red) and when it is empty (blue). Based on the weight of the packages, the stability when loaded with four packages in M3 is nearly identical to M2 stability when loaded with syringes. Thus, the dynamic stability characteristics of the M3 fully-loaded configuration were comparable to M2, so M2 is not shown. As packages are deployed in M3, the CG shifts, which negatively impacts dynamic stability. However, the dynamic stability characteristics with 1, 2, and 3 packages are still acceptable, with values between those for the fully loaded and empty aircraft. Thus, the 1, 2, and 3 package configurations are also not shown.

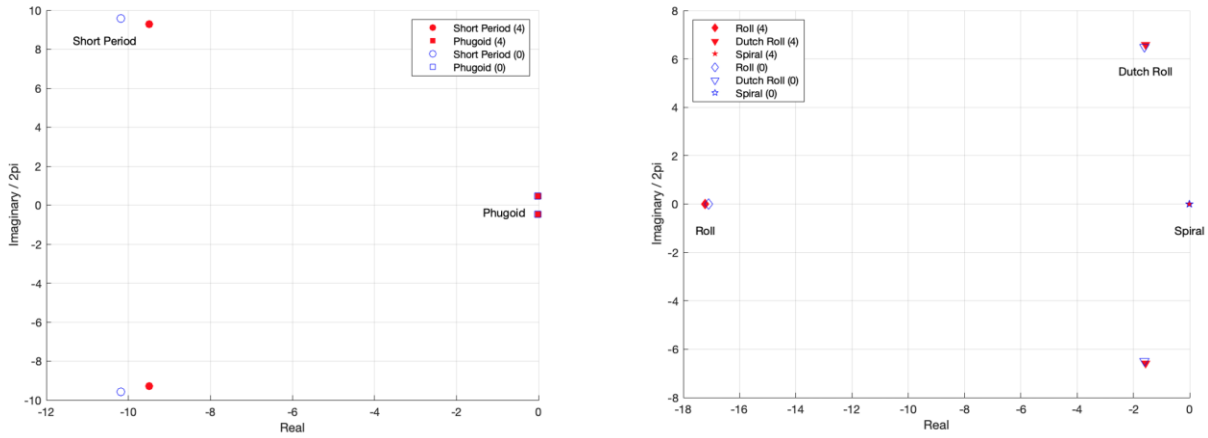

Figure 4.7: M3 Root Locus Longitudinal plot (left) and Lateral plot (right)

Based on the root locus plots, all modes were stable for both loading conditions. The design goal of this aircraft was to satisfy the level 1 flying qualities of a Class 1 aircraft described in MIL-F-8785C [7]. The dynamic stability characteristics from XLFR when the aircraft was loaded with 4 packages are shown below in Table 4.3 with MIL-F-8785C requirements in parenthesis. Similarly, the stability characteristics of the aircraft when empty are shown below in Table 4.4.

Table 4.3: Dynamic Stability Table for M3 Fully Loaded

Mode	ζ	ω_n [rad/s]	$\zeta\omega_n$ [rad/s]	τ [s]
Short Period	0.714 (0.35 < ζ< 2.00)	13.2889	9.4883	-
Phugoid	0.028 (ζ>0.04)	0.4712	0.0132	-
Roll	-	-	-	0.058 (τ<1.4)
Dutch Roll	0.232 (ζ > 0.19)	6.7669 (>1.0)	1.5699 (>0.35)	-
Spiral	-	-	-	119.728

Table 4.4: Dynamic Stability Table for Empty Aircraft

Mode	ζ	ω_n [rad/s]	$\zeta\omega_n$ [rad/s]	τ [s]
Short Period	0.728 (0.35 < ζ< 2.00)	13.9864	9.4883	-
Phugoid	0.032 (ζ>0.04)	0.4775	0.0153	-
Roll	-	-	-	0.058 (τ<1.4)
Dutch Roll	0.239 (ζ > 0.19)	6.7669 (>1.0)	1.6173 (>0.35)	-
Spiral	-	-	-	82.198

With the exception of the phugoid damping ratio and the short period natural frequency, all modes satisfied the MIL-F-8785C level 1 requirements. The phugoid damping ratio did satisfy MIL-F-8785C level 2 requirements and pilot evaluation during test flights. The short period frequency fell just outside of level 2, but satisfied pilot evaluation during test flights.

4.4.7 Drag Analysis

Total aircraft drag was calculated using the *component drag build-up method* (CDBM) as described by Gudmundsson [4]. The method models the total drag C_D as the sum of the minimum drag C_{Dmin} and the lift induced drag $C_{D,i}$. The minimum drag coefficient, C_{Dmin}, AKA the zero-lift or parasitic drag coefficient was calculated using the following expression:

$$C_{Dmin} = \left(\frac{1}{S_{ref}}\sum_{i=1}^{N} C_{f_i} \times FF_i \times IF_i \times S_{wet_i} + C_{D_{misc}}\right) \times \left(1 + \frac{CRUD}{100}\right) \tag{4.7}$$

Where S_{ref} is the reference area (in cm^2), C_f is the skin friction coefficient, FF is the form factor, IF is the interference factor, S_{wet} is the wetted area of the component (in cm^2), and $C_{D_{misc}}$ is the drag coefficient from miscellaneous components other than the fuselage, HT, VT, and main wing.

The skin friction coefficient for the main wing was determined using Young's method for mixed laminar-turbulent flow [2, p. 679]. The FF for the main wing was found using Raymer's method with the compressibility correction term set equal to one [5]. Finally, the IF was found by using a typical IF for an un-filleted low wing. The skin friction coefficients for the HT and VT were also determined using Young's method for mixed laminar-turbulent flow, and the FFs were found using Jenkinson's method [2, p. 701]. A typical IF for a conventional tail was used. The skin friction coefficient for the fuselage was determined by considering a 100% laminar boundary layer. The FF of the fuselage was then estimated using the method suggested by Hoerner [8, p. 6-17] for bodies in airflow Re > 10^5. Air inlet vents and winglet endplates were accounted for in the C_{Dmisc} term using equivalent parasitic coefficients. To ensure that the drag estimate remained conservative, drag reduction from winglet endplates was ignored. To include drag contributions that could not otherwise be accounted for, a CRUD factor of 25% was applied as

recommended by Gudmundsson (see Equation 4.7). From these calculations, the minimum drag coefficient was found to be 0.1553. The full parasitic drag breakdown is presented below:

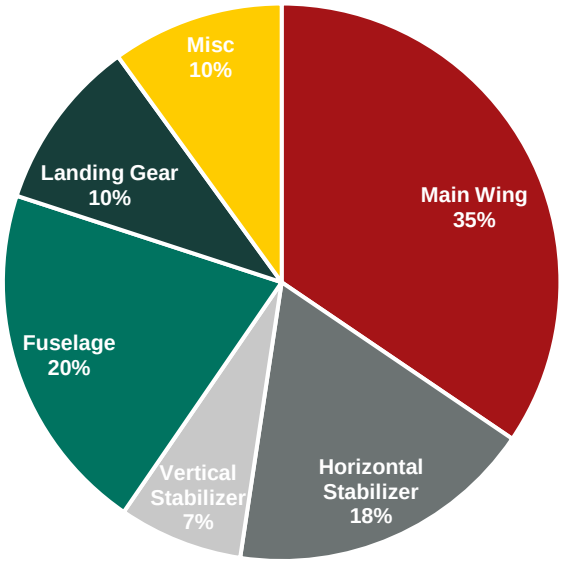

Figure 4.8: Parasitic Drag Breakdown

Table 4.5: Parasitic Drag Breakdown

Component	$C_{Dmin,i}$
Main Wing	0.04280
Horizontal Stabilizer	0.02220
Vertical Stabilizer	0.00894
Fuselage	0.02536
Landing Gear	0.01240
Misc	0.01239
C_{Dmin} w/o CRUD	0.12410
C_{Dmin} w/ CRUD	**0.1553**

As expected, the fuselage and main wing were the largest contributors to parasitic drag. The parasitic drag was then added to the lift induced drag, calculated using XFLR, to give the total drag polar, as shown in the figure below.

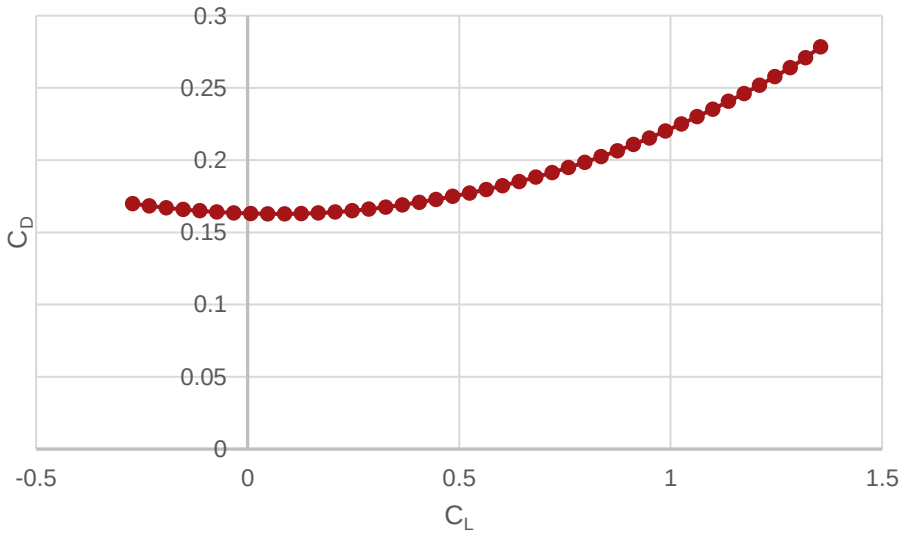

Figure 4.9: Total C_D vs. C_L

4.5 Propulsion

Design of the propulsion system centered on meeting a number of requirements set earlier on in the design process. In particular, a required T/W of ~1.4 for T-O, required electrical power of ~2100 W and ~1400 W for T-O and cruise, respectively (see Section 4.2), a desired cruise velocity of 22.5 m/s (see Section 3.3), and enough endurance to complete four laps (and four takeoffs) in M3. Additional considerations included maximizing efficiency, especially during cruise, and minimizing overall propulsion system weight.

4.5.1 Battery Selection

The DBF rules allow for the use of either LiPo (Lithium Polymer) or NiMH (Nickel-Metal-Hydride) batteries for propulsion. While NiMH batteries tend to be more robust and safe, LiPo batteries offer higher energy density, power to weight ratio, discharge rate, efficiency, and reliability. LiPos also tend to take up less space for a given energy capacity. Thus, WUDBF chose to use LiPo batteries for the propulsion pack.

LiPo's are commonly available in 3s, 4s, 5s, 6s, and 8s packs. For an aircraft of this size, LiPos below 6s are unlikely to provide the performance required. For 8s LiPos, there are not many (if any at all) available below the 100 Wh (3378.38 mAh for 8s) limit. Thus, WUDBF chose to use 6s LiPos, since they are readily available below the 100 Wh (4504.50 mAh for 6s) limit and have been used in the past to power competition aircraft of a similar size to this year's design.

In order to size the battery, WUDBF focused on M3, the mission that requires the greatest endurance. WUDBF plans to perform 4 deployments, meaning four laps and four takeoffs. Based on a desired cruise velocity of 22.5 m/s and a lap distance of 762 m (2500 ft), the aircraft must be able to fly for 2.26 minutes during M3. In order to account for takeoffs and to add a factor of safety, WUDBF set the desired M3 endurance at 3.5 minutes. Based on the earlier constraint analysis, the estimated power required at cruise is ~1400 W and at takeoff is ~2100 W. WUDBF estimated that the plane will spend approximately 5% of a lap under "takeoff" conditions and 95% under "cruise" conditions, yielding a weighted power requirement of 1435 W. Flying for 3.5 minutes with a 1435 W power consumption gives a required energy of 301.35 kJ. For a 6s LiPo (22.2 V nominal), assuming 85% max discharge, the required capacity is therefore 4436.05 mAh. See equation below for full calculation.

$$3.5\ min \times \frac{60\ s}{1\ min} \times 1435\ \frac{J}{s} \div 22.2\ \frac{J}{C} \times \frac{1\ mAh}{3.6\ C} \div 0.85 = 4436.05\ mAh \tag{4.8}$$

Based on this calculation, WUDBF chose to use a 6s LiPo with a capacity of 4500 mAh, which is just below the 100 Wh limit. The Turnigy Nano-Tech 4500 mAh 6s LiPo battery was selected to serve as the propulsion pack since it met the capacity requirement. Additionally, the Nano-Tech battery also possessed high discharge rates of 45C-Constant and 90C-Burst, which allows for a stronger throttle punch and improved takeoff performance.

4.5.2 Motor and Propeller Selection

In order to identify possible motor-propeller combinations, WUDBF employed the online propulsion design tool eCalc [9]. Using the parameters listed in the table below, WUDBF searched through the eCalc database for motor-propeller combinations that met the stated performance requirements.

Table 4.6: eCalc Search Parameters

Parameter	Value	Reasoning
Max Power [W]	~2100	See Section 4.2
T/W	~1.4	See Section 4.2
Max Cruise Velocity [m/s]	22.5	See Section 3.3
Endurance [min]	3.5	See Section 4.5.1
Battery	6s, 4500 mAh	See Section 4.5.1
Max Prop Diameter [in]	24	Estimated max ground clearance

From this search, a list of over 50 unique motor-propeller combinations were identified. This list was then further refined by limiting the possible motors to only those from trusted manufacturers (based on past experience and general online consensus) that were available, in-stock, at the time of the search. This narrowed the possibilities down to the four motor-propeller combinations shown in Table 4.7:

Table 4.7: Possible Motor-Propeller Combinations

Motor	Prop	Elec. Power @ Max [W]	Current @ Max [A]	RPM (Static)	Static Thrust [kgf]	T/W	Torque [N·m]	Flight Time [min]	Drive Weight [kgf]
SunnySky X7025-30cc-270	24x12	2258.5	112.94	4836	10.821	1.52	4	4.3	1.627
Scorpion SII-4035-330	22x13	2304.6	115.53	5101	10.042	1.45	3.4	4.1	1.439
Hacker A60-5S V4 28-Pole	23x10	2083.7	103.22	5280	9.460	1.33	3.35	4.3	1.615
Hacker A60-7XS V4 28-Pole	22x11	2204.3	109.9	5461	9.742	1.4	3.3	4.2	1.462

All four choices met or nearly met all of the stated requirements. Thus, in order to further evaluate each combination, plots of electrical efficiency vs. throttle, endurance vs. throttle, and thrust vs. electrical power were generated using data from eCalc:

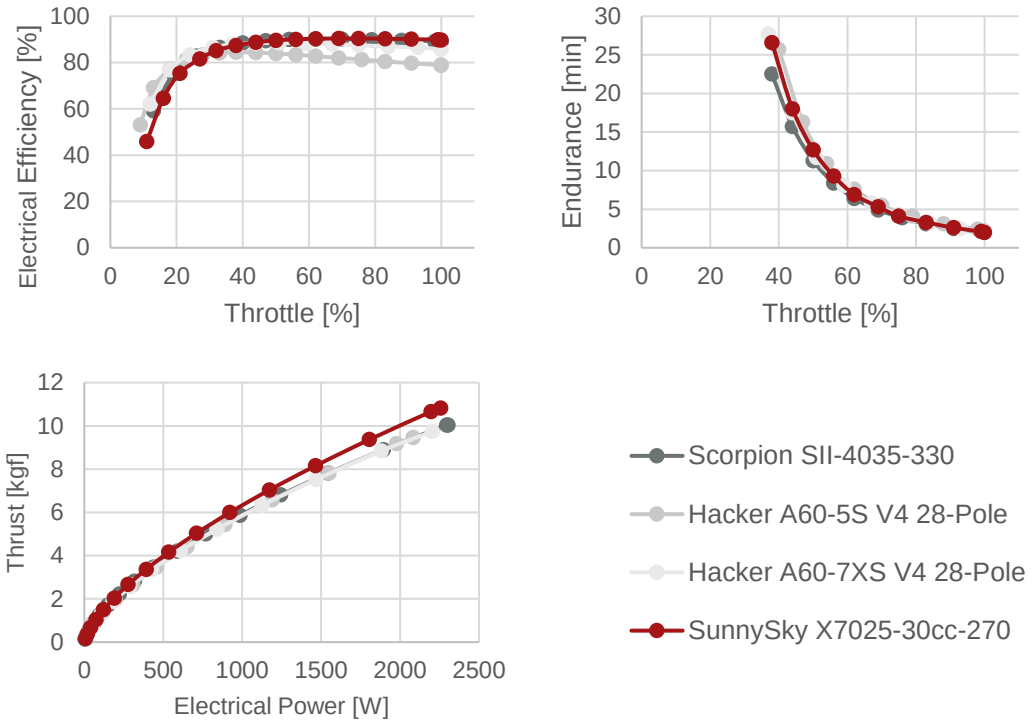

Figure 4.10: Performance Data for Motor-Propeller Combinations

From Figure 4.10, the SunnySky X7025-30cc-270 motor with a 24x12 propeller had the greatest electrical efficiency over relevant throttle settings (60-100%). This motor-propeller combination also provided superior thrust-to-power performance and endurance that was comparable to the other choices. From Table 4.7, the SunnySky did have the highest drive weight, but it still provided the greatest T/W. Based on these factors, the SunnySky X7025-30cc-270 motor with a 24x12 propeller was ultimately chosen for the aircraft's propulsion system. The top right plot in Figure 4.10 shows that an endurance of 5 minutes can be achieved at 70% throttle. Since M3 scoring does not depend on time, and the 10 minute flight window is more than enough to achieve the desired four scoring laps, 70% throttle will be used during M3 to ensure adequate endurance.

4.5.3 ESC Selection

Given the predicted max current of 112.94 A for the chosen propulsion system (see Table 4.7), WUDBF chose to use the AeroStar Advance 150A HV (6~12S) as the ESC. The AeroStar can handle 150 A continuous and 180 A burst current, which provides an adequate safe margin. Additionally, the AeroStar possesses a large aluminum heat sink case for optimal cooling.

4.5.4 Refinement for M2

Given that the propulsion system was designed primarily with M3 in mind, WUDBF next considered whether it could be refined to improve M2 performance (since the competition rules allow for the propeller and battery to be swapped out for different missions).

Starting with the battery, WUDBF considered whether the propulsion pack could be downsized for the M2 to save weight and increase performance. While four laps are required for M3 (to complete WUDBF's goal of four deployments), M2 only requires three laps with a single takeoff. Using a modified version of the calculation described in 4.5.1, WUDBF estimated that the required capacity to complete M2 was 2534.89 mAh. This allows for the use of the Turnigy Graphene Panther 3000mAh 6S 75C battery for M2, saving approximately 0.25 kgf of weight over the Turnigy NanoTech selected for use in M3.

WUDBF next considered whether the propeller could be optimized to increase cruise velocity during M2. In general, increasing propeller pitch increases pitch speed, which increases efficiency at higher velocities and allows for higher cruise velocity. This comes with the sacrifice of efficiency at low airspeeds, negatively impacting static thrust and takeoff performance [5]. In part because there are not many choices for commercially available propellers above a diameter of 22 in suitable for electric aircraft, WUDBF could not find a propeller that increased cruise velocity without decreasing the static T/W and/or endurance below acceptable levels. Thus, the 24x12 propeller was selected for use in both M2 and M3.

4.5.5 Required vs. Available Thrust Analysis

The dynamic performance of the propulsion system was evaluated to verify eCalc's predicted performance and to determine the aircraft's speed envelope. eCalc does not output dynamic thrust data, so this data was instead obtained from the APC Propellers website (the chosen propeller manufacturer) [10]. The APC performance data was generated based on vortex theory using actual propeller geometry and the NASA Transonic Airfoil Analysis Computer Program to estimate section lift and drag. Predicted RPM values from eCalc were used to query the APC dataset at velocities up to 30 m/s, with the corresponding dynamic thrust values calculated using an interpolation script written in MATLAB. The resulting dynamic thrust curve was then plotted along with the required thrust curve (calculated based on the drag polar in Figure 4.9) as shown below:

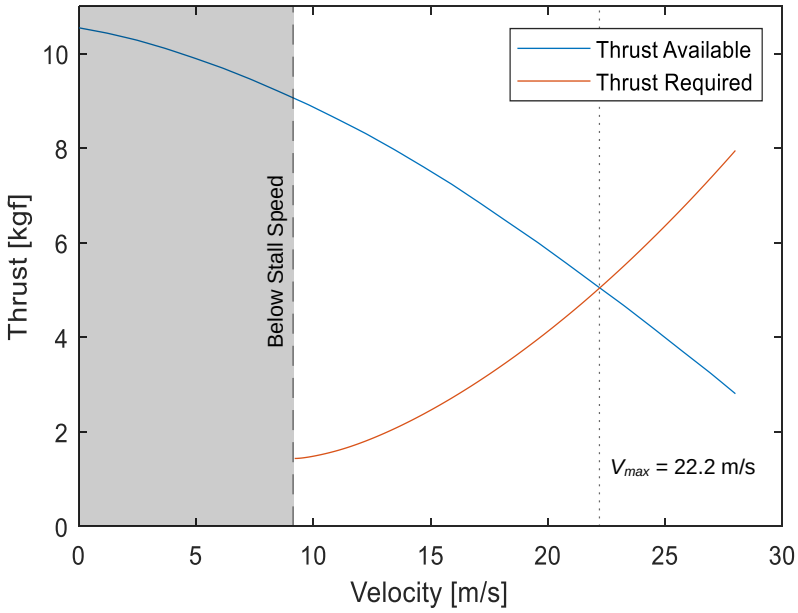

Figure 4.11: Required vs. Available Thrust Curves for Fully Loaded Aircraft

Based on this analysis, the estimated max cruise velocity for the fully loaded aircraft (in both M2 and M3) is 22.2 m/s. This is very close to the designed max cruise velocity of 22.5 m/s. The static thrust predicted using the APC data is 10.54 kgf, giving a T/W ratio of 1.51. This agrees well with both the desired static thrust and the static thrust predicted by eCalc, again confirming that the propulsion system meets the stated performance goals.

4.6 Predicted Aircraft Performance

In order to integrate the various aspects of the preliminary design and predict overall aircraft performance, WUDBF utilized Km_sim, an in-house kinematic mission simulator written in MATLAB [11].

4.6.1 Brief Explanation of Km_sim

Km_sim works by simulating an aircraft's performance as it flies through a mission profile. Each mission profile consists of a series of functions based on simple kinematics and Newton's 2nd Law describing the motion of the aircraft during a particular phase of flight (e.g., takeoff, climb, cruise, etc.). Specific mission profiles were written for M1, M2, and M3. Aerodynamic and propulsion data from Sections 4.4 and 4.5, respectively, were used to generate aerodynamic and propulsion performance look-up tables. These tables allow the simulation to determine the lift, drag, and thrust of the aircraft at any particular time point. During a simulation, Km_sim steps through each mission phase, numerically integrating the relevant equations of motion using ode45 and the look-up tables, while keeping track of changes in the state variables. At the end of the simulation, plots are generated displaying how the state variables change over time as shown in the figures below. For a complete explanation of Km_sim and the source code see [11].

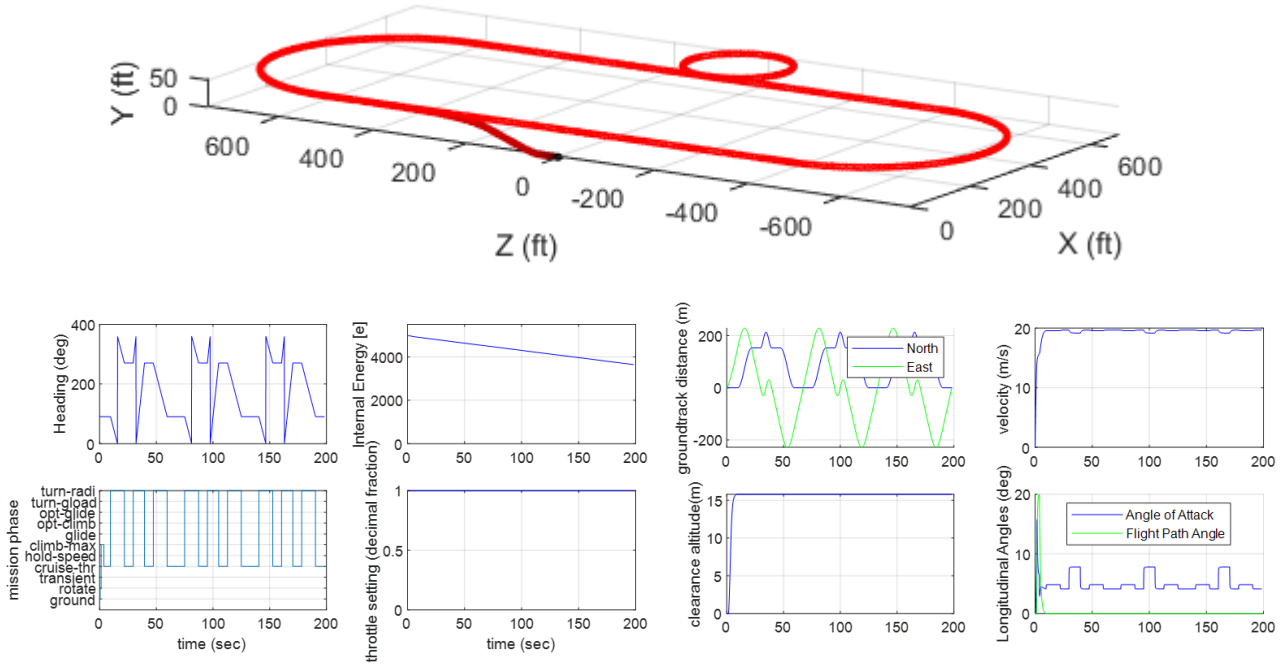

Figure 4.12: Example outputs from Km_sim including a trajectory plot (TOP) and an eight-panel results summary (BOTTOM) showing how state variables changes over time.

4.6.2 Km_sim Results

From simulations of the preliminary aircraft in Km_sim, WUDBF extracted the following aircraft performance predictions. To obtain normalized scores, best scores for M2 and M3 were estimated based on the analysis in Section 3.3.

Table 4.8: Predicted Aircraft Performance

	Mission 1	Mission 2	Mission 3			
Inputs						
All-Up Weight [kgf]	6.020	6.757	6.9072	6.7004	6.4736	6.2468
Payload Weight [kgf]	-	0.7370	0.9072	0.6804	0.4536	0.2268
Wing Loading [kgf/m^2]	6.044	6.784	6.935	6.727	6.500	6.272
$C_{L,max}$	1.44	1.44	1.44			
Static Thrust [kgf]	10.54	10.54	10.54			
Cruise Throttle	1	1	0.7			
Turn Load Factor	2.5	2.5	2.5			
Outputs						
Ground Roll [m]	3.364 (11.04 ft)	3.417 (11.21 ft)	3.511 (11.52 ft)	3.508 (11.51 ft)	3.502 (11.49 ft)	3.499 (11.48 ft)
$C_{L,cruise}$	0.409	0.409	0.394	0.394	0.394	0.394
$C_{D,cruise}$	0.1559	0.1559	0.1566	0.1566	0.1566	0.1566
Cruise Velocity [m/s]	21.68	21.67	20.36	20.38	20.38	20.39
Number of Laps	3	3	4			
Lap Time [s]	48.51	43.97	57.85	57.54	57.53	56.88
Mission Time [min]	2.426	2.198	3.830 (excluding ground phase)			
Scoring						
WUDBF Score	1	18.20	4			
Normalized Score	1	1.614	2.667			

4.7 Uncertainties

The design tools and analysis methods used throughout the preliminary design process all possessed a certain level of uncertainty. The lift and induced drag of the aircraft was computed in XFLR using the vortex lattice method (VLM). Using VLM, lifting surface thickness and air viscosity were neglected. Additionally, the fuselage was excluded from the analysis. Based on previous WUDBF designs, however, it was determined that the decreased lift due to neglecting viscosity is approximately equal to the lift gained by excluding the fuselage. It has also been verified that the contribution of drag associated with wing thickness was small compared to total drag calculations. Therefore, the lift and induced drag of the actual aircraft was expected to be approximately equal to the XFLR predicted lift using the VLM. The parasitic drag estimate using Gudmundsson's method were also subject to a certain level of uncertainty, but that uncertainty was mostly accounted for by the 25% CRUD factor.

eCalc and the APC propeller performance database were the two primary tools used for propulsion design. These third-party tools both carry a certain level of uncertainty owing to the fact that it is not entirely clear how they calculate their outputs. However, this uncertainty is mitigated by the fact that this method of propulsion design has been used successfully by both WUDBF and other DBF teams in the past with an acceptable level of accuracy.

Finally, Km_sim, while a very useful tool, makes a number of assumptions in its performance calculations. For instance, the simulation assumes that the pilot flies the plane on a perfect trajectory. The effects of wind are also neglected in the simulation. Since Km_sim relied on data from the aerodynamic and propulsion designs, any uncertainties from those processes were carried over into the simulation.

Ultimately, the nature of the iterative process meant that the uncertainty associated with any particular design tool was mitigated by ensuring that every aspect of the design agreed with the rest.

5. Detail Design

Following completion of the preliminary design, the structure and external geometry of the aircraft were finalized during the detail design stage. The electronics and package deployment mechanism were also developed during this process. Throughout, structural strength, reliability, weight, and mission performance were considered to refine the competition aircraft.

5.1 Dimensional Parameters

A CAD model of the final aircraft is shown in the figure below. Table 5.1 summarizes the key dimensions of the final aircraft design.

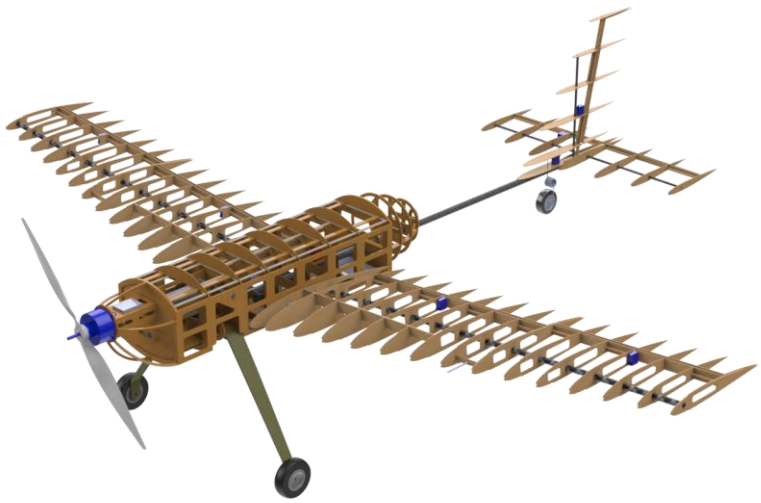

Figure 5.1: CAD Model of Final Aircraft Design

Table 5.1: Key Dimensions of Final Aircraft Design

Vertical Stabilizer		Horizontal Stabilizer	
Span [mm]	820.0	Span [mm]	700.0
Mean Chord [mm]	294.0	Mean Chord [mm]	264.0
Area [m^2]	0.121	Area [m^2]	0.185
AR	2.78	AR	2.64
Wing		**Overall Aircraft**	
Span [mm]	2402.5	Length [mm]	2051.7
Mean Chord [mm]	414.0	Width [mm]	2402.5
Area [m^2]	0.996	Prop Clearance [mm]	165.0
AR	5.78	Initial AoA	11.02°
Dihedral Angle	5°	Empty Weight [kgf]	5.68

5.2 Structural Characteristics and Design Methodology

WUDBF's primary structural design goals were to maximize strength and stability, maximize accessibility to the electronics and payload compartments, minimize weight, and simplify the manufacturing process. The overall structure is designed to direct loads from each subsystem into the major load bearing components of the aircraft. The fuselage consists of wooden formers with a central CF rod running through each former to resist bending moments. The fuselage structure is bolted into the central rod at key points to provide resistance to torsional loads. Wooden side panels also provide torsional resistance and structural stiffness. Propulsive loads from motor thrust and torque that can cause bending, torsion, and vibrations are directed through a wooden motor mount into the fuselage. Ground loads from the landing gear are directed through the fuselage structure and into the central CF rod. The wing consists of wooden ribs connected by stringer and spars, which provide bending and torsional stiffness. Aerodynamic loads from the wing are transferred to the side panels, where they are then distributed across the fuselage structure and the central CF rod. The empennage is directly connected to the central CF rod via CF spars, distributing loads into the central rod and the fuselage.

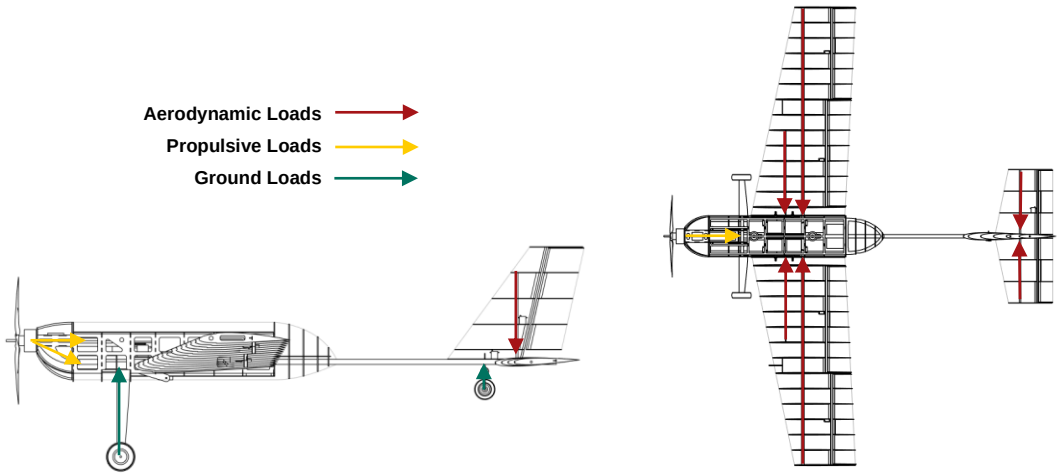

Figure 5.2: Load Path Diagram

5.3 Subsystem Design

5.3.1 Fuselage

The fuselage was designed to house the electronics, carry payloads, and connect to the wing and tail. The main structure is made up of basswood and birch plywood formers as shown in Figure 5.3. A CF rod runs lengthwise through the fuselage to increase stiffness and provide a mounting point for the tail. This is the main CF rod through which all loads are directed to. Plywood panels form the sides of the fuselage, providing an attachment point for the wing and helping to transfer wing loads to the main CF rod. An aluminum rod bent at 10° is also integrated into the fuselage to connect the two wing halves. The top of the fuselage was designed to be detachable for easy access to the battery, payload, and electronics compartments. The bottom of the fuselage acts as a ramp that can be lowered for package deployment in M3. A basswood motor mount runs through the nose and connects to the main lengthwise CF rod as well as an additional horizontal CF rod for added support.

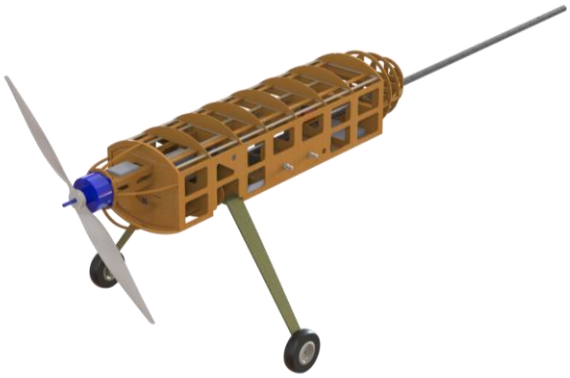

Figure 5.3: Aircraft Fuselage

5.3.2 Wing

Each half-wing is made of 15 ribs with a rear CF spar and a front wooden spar for support. The CF spar was designed to run the full length of the wing to take most of the aerodynamic bending load. The second wooden spar was included to resist twisting of the wing. The spars are angled at 5° to achieve the desired dihedral, and all outer ribs are oriented perpendicular to the spars. The innermost rib on each wing is oriented perpendicular to the ground plane in order to create flush contact with the side panels of the fuselage. The half-wings are designed to be bolted to the side panels. This allows for loads to be transferred into the side panels, while still allowing the half-wings to be detached for transport. The CF spar was designed to extend past the innermost rib to interface with the bent aluminum rod integrated into the fuselage, which provides added support against bending. The leading edge of the wing will be wrapped with balsa wood to increase stiffness and achieve the correct curvature. Servo and control surface attachment points were also included in the wing structure as shown in Figure 5.4 below.

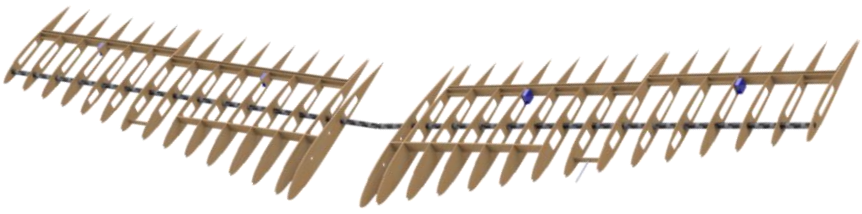

Figure 5.4: Aircraft Wing

5.3.3 Empennage

The empennage was designed using the same techniques as the main wing. The HT and VT are made of ribs supported by a CF spar and a wooden spar. The CF rods intersect directly with the tail boom. This allows tail loads to be transferred directly to the central CF rod. The tailwheel spring also intersects the main CF rod and is secured in place using a collar. Mounting plates for control servos and the rudder and elevator hinges are also integrated into the rib structure. The full empennage structure is shown in Figure 5.5.

Figure 5.5: Aircraft Empennage

5.3.4 Main Landing Gear

Since WUDBF did not have the equipment to manufacture the main landing gear, a set of CF landing gear was purchased online. The type and placement of the main landing gear were chosen based on three conditions: a takeoff AoA between 12°-15° (to aid in takeoff), a vertical angle with the CG of 16°-25° (based on rules-of-thumb [5]), and a ground clearance of at least 12.5 in (to accommodate the 24 in prop). Based on these criteria, the JTC-S24 standard style CF landing gear was chosen. The main landing gear is supported by two basswood plates on top and bottom. These plates intersect the first three formers to transfer loads to the main fuselage structure. Bolts running through the plates and the landing gear secure the gear to the fuselage. Additional structures that run perpendicular to the basswood plates give added compressive strength as shown in the figure below.

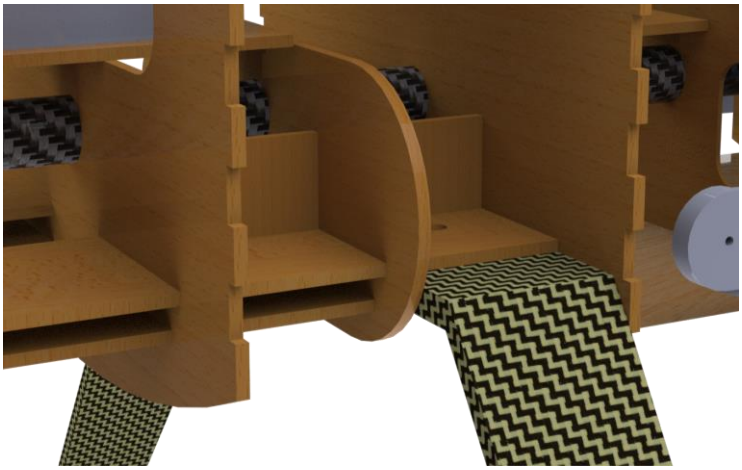

Figure 5.6: Closeup of Landing Gear Attachment

5.3.5 Payload Storage

The payload storage compartment is located within the fuselage just above the wings. This placement was chosen to minimize CG shifts during package deployment in M3. Figure 5.7 shows a close up of the payload compartment filled with four packages. Formers, the fuselage sidewalls, and the top lid contain the packages to minimize shift during flight. Based on empirical testing, WUDBF determined that 10 syringes can fit within the same space occupied by one package. Thus, for M2, the 40 syringes will be split into groups of ten and inserted into the package slots.

Figure 5.7: Payload Storage Compartment

5.3.6 Package Deployment Mechanism

The package deployment mechanism was designed to be as simple as possible in order to improve reliability and save weight. Because of the need to not trip the 25G shock sensors, the deployment mechanism was designed as a two-stage system with a servo-operated release mechanism and a ramp based lowering mechanism.

The release mechanism consists of servos attached directly to the walls of the payload storage compartments. Aluminum servo arms extend out beneath the packages to support them during flight. Because the packages are supported perpendicular to the servo's axis of rotation, the weight of the package acts primarily on the servo body and mount and not on the servo gears or motor. To release a package, the servo arm is swung 90°, allowing the package to drop down internally onto the ramp. The release stage was designed to be performed with the ramp in the fully retracted position, minimizing the distance the package has to drop.

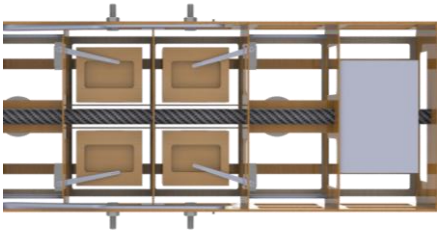

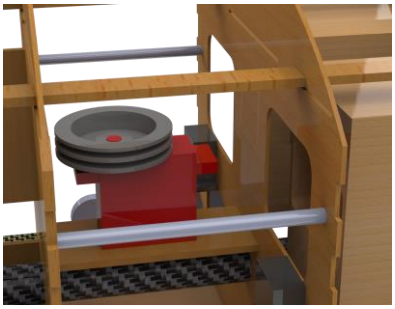

Figure 5.8: Closeups of Release Mechanism from Bottom with Ramp Removed (left) and Lowering Mechanism Pulley Servo (right)

The lowering mechanism consists of a ramp operated by two continuous rotation pulley servos, each connected to two winch lines via dual spools (see Figure 5.8 above). One servo controls the two lines attached to the front of the ramp, and the other controls the two lines attached to the back. This allows the ramp to be lowered straight down parallel to the ground and then tilted slightly at the end so the package can slide gently off the ramp (see Figure 5.8).

Due to concerns about the amount of wind in Wichita, two supporting guide arms were designed to prevent the ramp from twisting or flipping over and acting as a sail. Each guide arm consists of two sections. One section is attached to the side panel of the fuselage and the other to the ramp. During flight, the arms fold up into the fuselage. The two sections were sized such that at maximum extension, the angle between them does not exceed 180°, allowing the arm to fold back up properly into place.

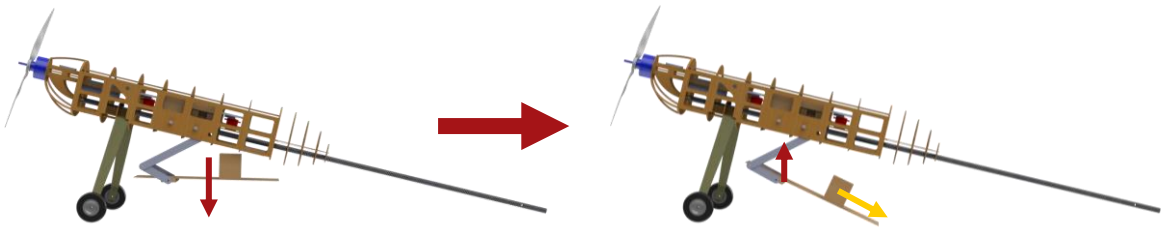

Figure 5.9: Lowering of the Ramp

5.3.7 Propulsion System

The propulsion system consists of a SunnySky X7025-30cc-270 motor spinning an APC 24x12 prop. Two different batteries are used for M2 and M3 in order to optimize performance. For a complete description of the design of the propulsion system, see section 4.5. Static testing in conjunction with flight testing confirmed that the propulsion system met thrust, power, and endurance requirements. The table below shows breakdowns of the propulsion system for each mission.

Table 5.2: Propulsion System Component Breakdown

Component	Mission 1 and 2	Mission 3
Motor	SunnySky X7025-30cc-270 (270 Kv)	
Propeller	APC 24x12	
Propulsion Battery	Turnigy Graphene Panther 3000 mAh 6S 75C	Turnigy Nano-Tech 4500 mAh 6s 45/90C
ESC	AeroStar Advance 150 A HV (6~12S)	
Receiver Battery	Tattu 3S 850 mAh 75C	
Receiver	FrSky X8R 8/16Ch	

5.4 Weight and Balance

The aircraft CAD model in Solidworks was used to determine the CG for each component. The weights were estimated based on component volumes with known densities, measured component weights, and previous WUDBF aircraft. The leading edge of the center of the wing was taken to be the origin, and a mutually orthogonal coordinate system was established with the positive X-axis pointing out the nose of the aircraft, the positive Z-axis extending below the aircraft, and the positive Y-axis directed out of the right wing when viewing the aircraft from behind. The table below shows the estimates for each mission.

Table 5.3: Weight and Balance for Each Mission

Component	Weight [kgf]	CG_x [mm]	CG_y [mm]	CG_z [mm]
Wing	1.82	-299.7	0.00	-56.39
Fuselage	1.37	-321.3	0.00	-42.16
VT	0.03	-1390	0.00	-190.5
HT	0.04	-1458	0.00	-26.42
Main Gear	0.34	19.05	0.00	104.6
Tailwheel	0.01	-1267	-12.45	12.45
7x Control Servos	0.09	-833.4	19.56	-72.90
4x Release Servos	0.05	-201.2	0.00	-46.23
2x Pulley Servos	0.11	-204.7	0.00	-64.77
ESC	0.12	257.3	0.00	-123.4
Control Electronics	0.54	-274.1	0.00	-55.63
Propulsion Battery	0.75	125.0	0.00	-74.93
Motor	0.61	350.0	0.00	-100.08
M1				
Overall	**5.68**	**-157.5**	**0.00**	**-35.81**
M2				
Syringes	0.76	-197.1	0.00	-59.94
Overall	**6.44**	**-162.3**	**0.00**	**-38.35**
M3				
Package 1	0.23	-249.9	-80.01	-50.04
Package 2	0.23	-249.9	-80.01	50.04
Package 3	0.23	-150.1	-80.01	-50.04
Package 4	0.23	-150.1	-80.01	50.04
Overall (4 Packages)	**6.59**	**-163.1**	**0.00**	**-41.91**
Overall (3 Packages)	**6.36**	**-160.0**	**2.03**	**-40.39**
Overall (2 Packages)	**6.13**	**-160.5**	**0.00**	**-38.86**
Overall (1 Package)	**5.91**	**-157.2**	**-2.03**	**-37.34**

The vehicle is designed such that the position of the CG can be adjusted using battery placement and ballast, allowing the aircraft to be stable in all flight configurations. For M3, the packages were located in a way that longitudinal CG shifts are minimized following package deployment. The lateral and longitudinal CG shifts are small enough that they can be counteracted with pre-programmed trim that will be determined during test fights.

5.5 Structural Performance

In order to verify structural performance of the aircraft, WUDBF utilized Solidworks finite element analysis (FEA) to simulate the major structural components of the aircraft under their maximum expected load conditions.

5.5.1 Fuselage FEA

To verify the strength of the fuselage design and confirm its ability to withstand aerodynamic loads from the wing, FEA was performed on the main fuselage structure. A load factor of 2.5 on the wing was simulated at the wing's attachment points on each side panel, the two bolt holes and the hole for the CF spar. The resulting stress plot is shown below.

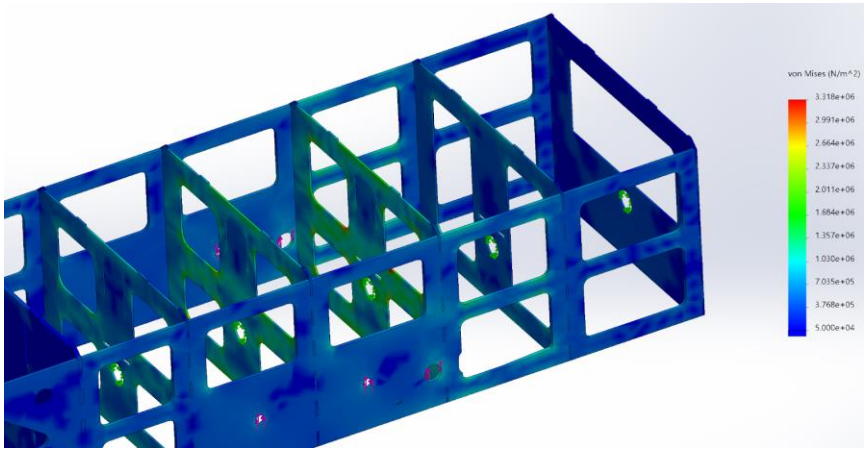

Figure 5.10: von Mises Stress Plot of the Fuselage Experiencing a Load Factor of 2.5

The largest loads ranged from 1-3.3 MPa distributed through the two ribs directly adjacent to the holes. Stress concentrations occurred at the corners of the weight saving cuts, shown in red. Given that the minimum tensile strength of birch plywood, the material selected for the formers, is 27.6 MPa [12], the fuselage structure had an adequate factor of safety of 8.36.

5.5.2 Wing Spar FEA

FEA was performed in Solidworks on the CF spar to ensure the wing could withstand a wingtip loading test (approximate load factor of 2.5). The finite lift distribution was approximated by XFLR5 to be near elliptical. In order to input the distribution into Solidworks, curve fitting was performed in MATLAB to generate a continuous distribution as shown in the figure below. Note that the lift distribution is plotted as a fraction of total lift as a function of unit span.

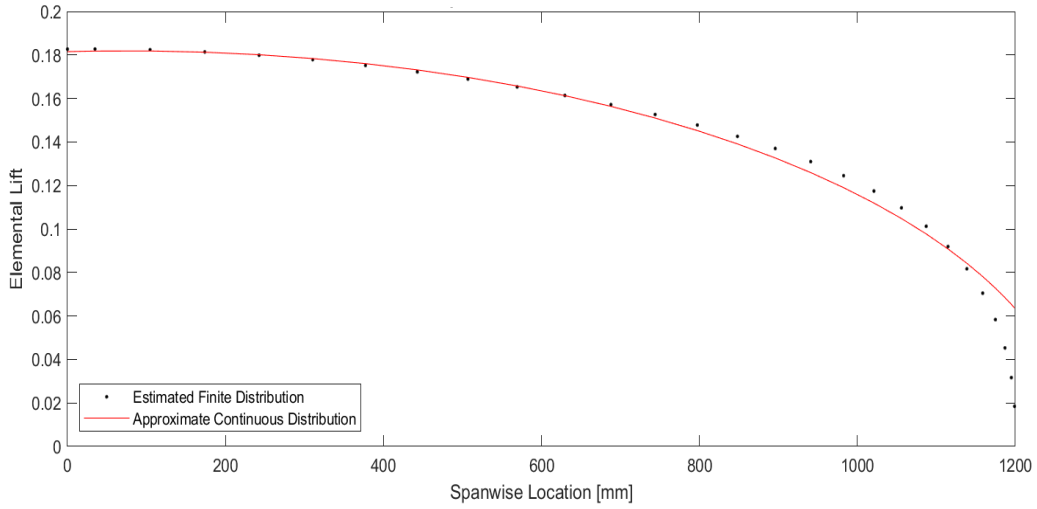

Figure 5.11: Finite and Continuous Spanwise Lift Distribution

Using the continuous lift distribution and applying a load factor of 2.5, the following von Mises stress plot was generated using Solidworks.

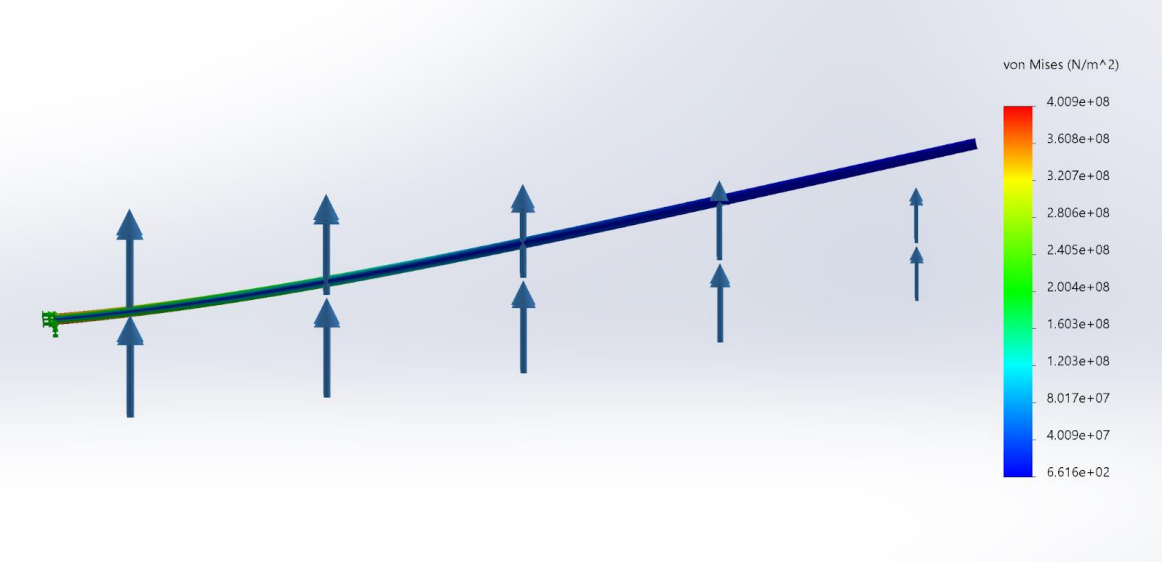

Figure 5.12: Von Mises Stress Plot of Wing CF Spar Experiencing a Load Factor of 2.5

Based on the simulation, the maximum flexural stress experienced by the CF spar is 401 MPa. Given a maximum tensile strength of 1896 MPa from the manufacturer, this results in an adequate factor of safety of 4.7 [13]. Based on the FEA, the 2.5g load case also produced a wingtip displacement of 6.29 in or 8.4°, which was considered reasonable given that the actual displacement of the spar would be lower with the addition of the wooden structure around it.

5.5.3 Main Landing Gear FEA

A FEA was performed on the front landing gear to ensure it had the structural integrity to survive landing. A landing load factor of 3 was applied to the top surface of the gear to model a normal landing, and a von Mises stress plot was generated as shown in the figure below.

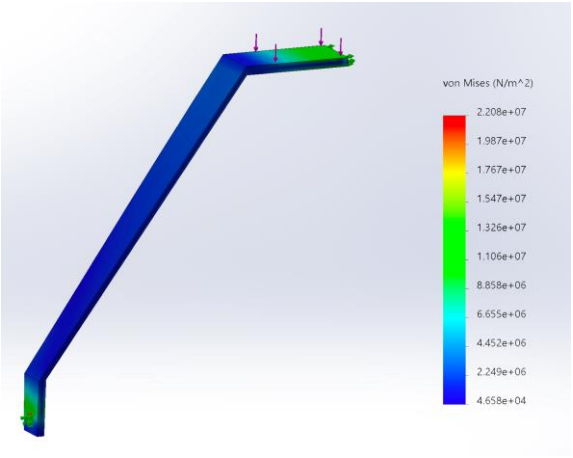

Figure 5.13: von Mises Stress Plot of the Main Landing Gear Experiencing a Load Factor of 3

As shown in Figure 5.13 the max von Mises stress was 22.1 MPa. Given a maximum tensile strength of 1896 MPa for carbon fiber, this gives a more than adequate factor of safety of 85.8 [13]. Additionally, the maximum displacement experienced by the landing gear was 0.005 in, which was acceptable since there was 6.5 in of designed prop clearance.

5.6 Predicted Final Aircraft Performance

Using the updated weights in Table 5.4, Km_sim was used to simulate the expected flight and mission performance of the final aircraft. The extracted performance estimates are shown in the table below. To obtain normalized scores, best scores for M2 and M3 were estimated based on Section 3.3.

Table 5.4: Predicted Final Aircraft Performance

	Mission 1	Mission 2	Mission 3			
Inputs						
All-Up Weight [kgf]	5.68	6.44	6.59	6.36	6.13	5.91
Payload Weight [kgf]	-	0.76	0.92	0.69	0.46	0.23
Wing Loading [kgf/m^2]	5.70	6.47	6.62	6.39	6.15	5.93
$C_{L,max}$	1.44	1.44	1.44			
Static Thrust [kgf]	10.54	10.54	10.54			
Cruise Throttle	1	1	0.7			
Turn Load Factor	2.5	2.5	2.5			
Outputs						
Ground Roll [m]	3.332 (10.93 ft)	3.386 (11.11 ft)	3.427 (11.24 ft)	3.420 (11.22 ft)	3.412 (11.19 ft)	3.405 (11.17 ft)
$C_{L,cruise}$	0.411	0.411	0.411	0.411	0.411	0.411
$C_{D,cruise}$	0.411	0.411	0.411	0.411	0.411	0.411
Cruise Velocity [m/s]	21.83	21.89	20.73	20.69	20.65	20.62
Number of Laps	3	3	4			
Lap Time [s]	47.41	43.84	56.86	56.81	56.73	56.68
Mission Time [min]	2.371	2.192	3.784 (excluding ground phase)			
Scoring						
WUDBF Score	1	18.25	4			
Normalized Score	1	1.616	2.667			

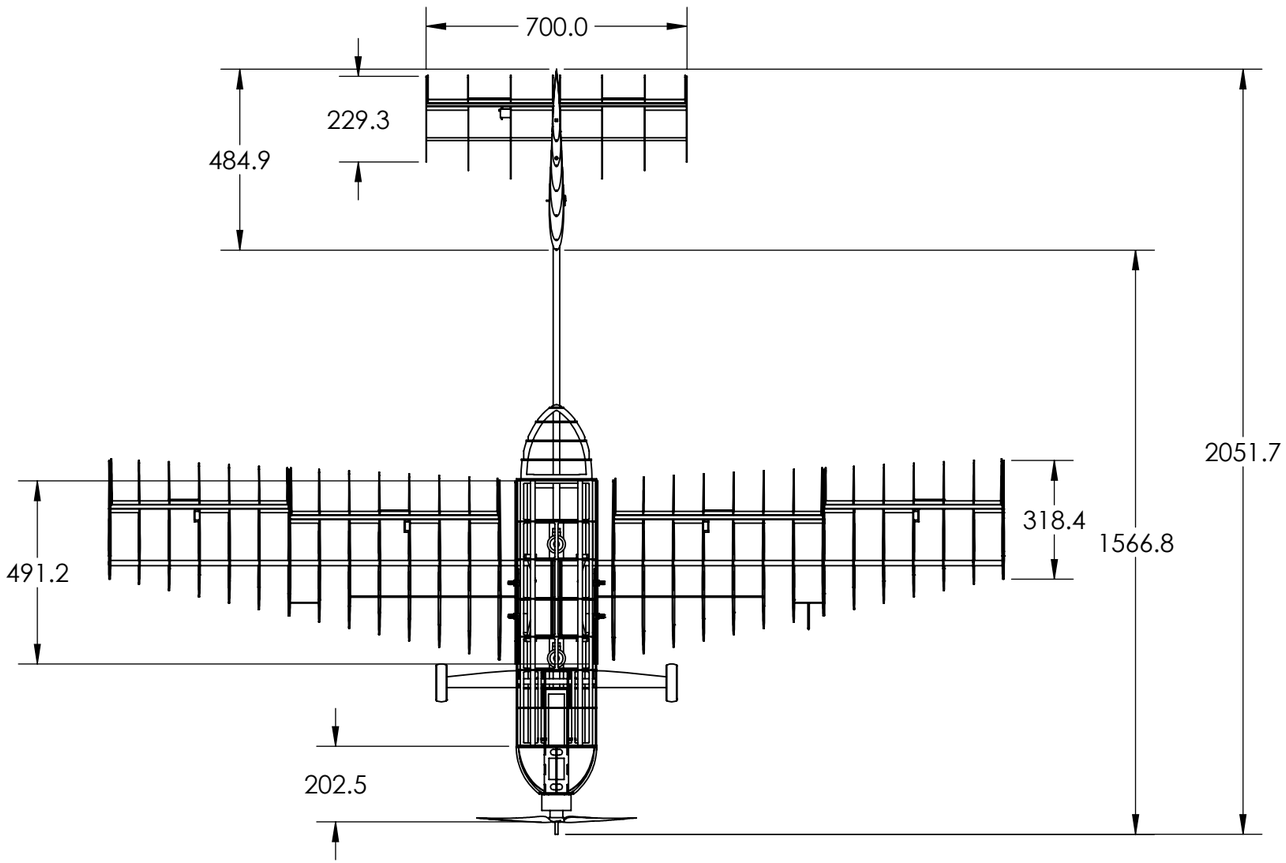

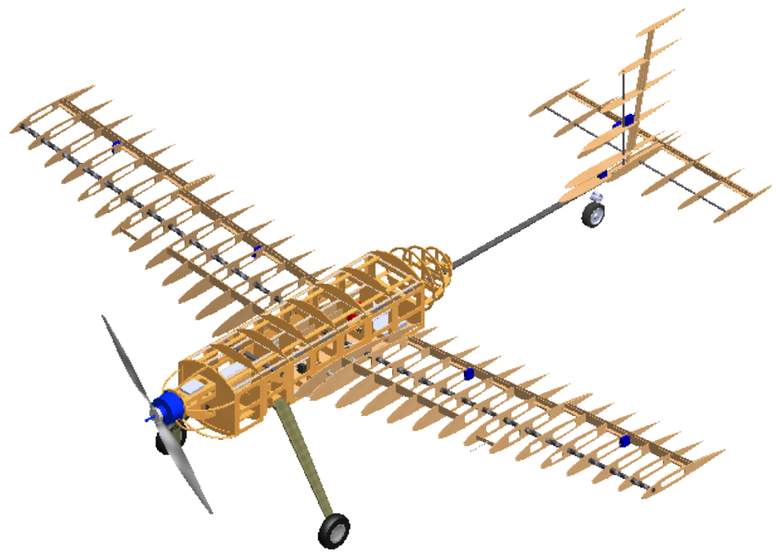

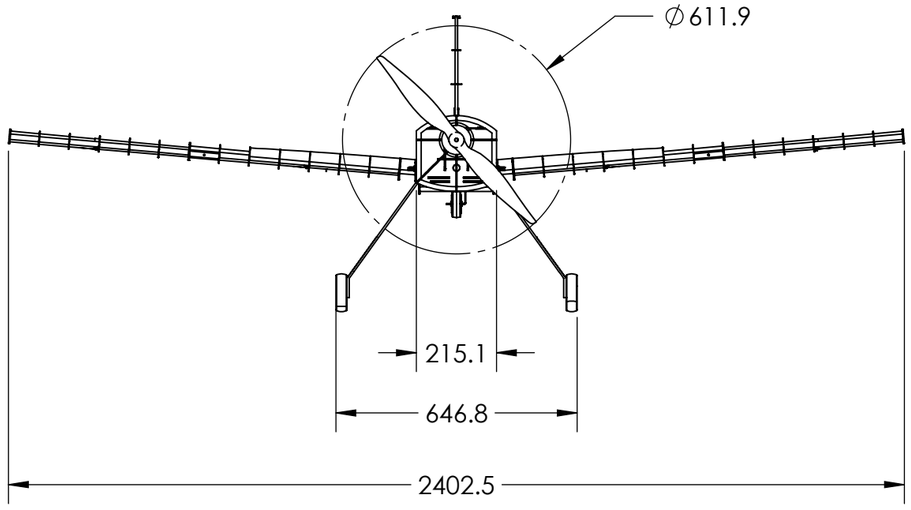

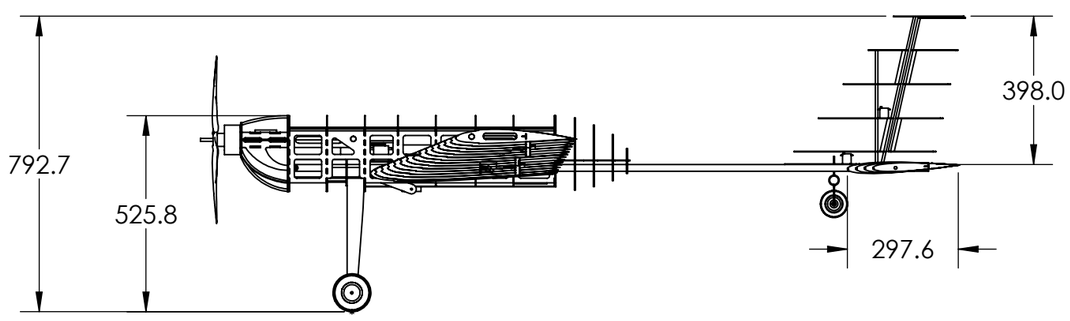

ALL DIMENSIONS ARE IN MILLIMETERS

Washington University in St. Louis AIAA Design Build Fly 2022		
Name: Pflyzer	Aircraft 3-View	
SCALE: 1:16		SHEET 1 OF 4

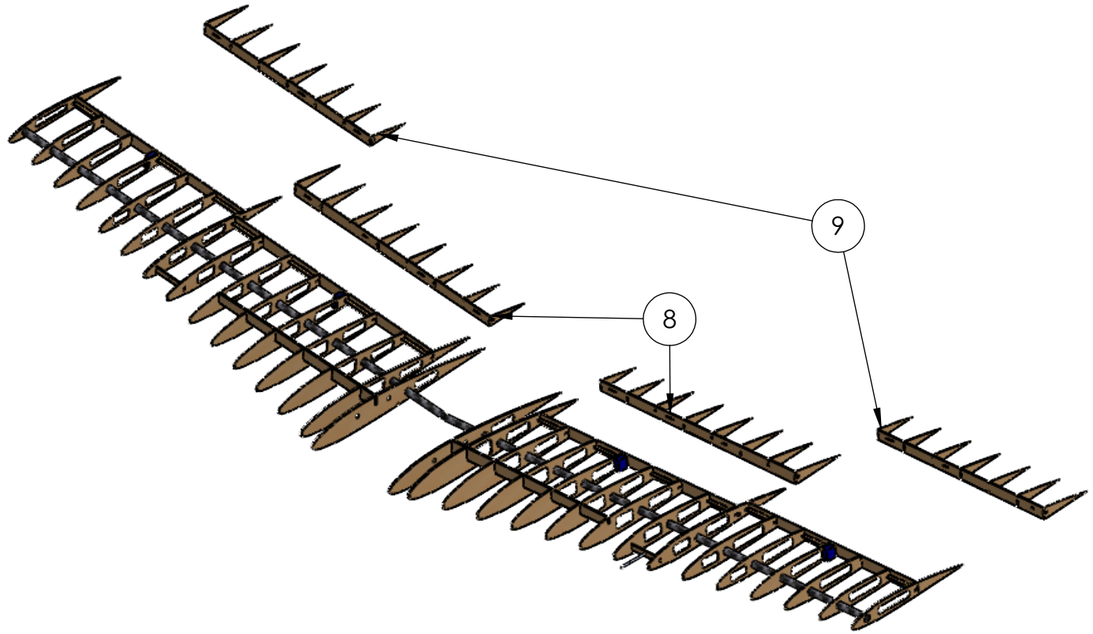

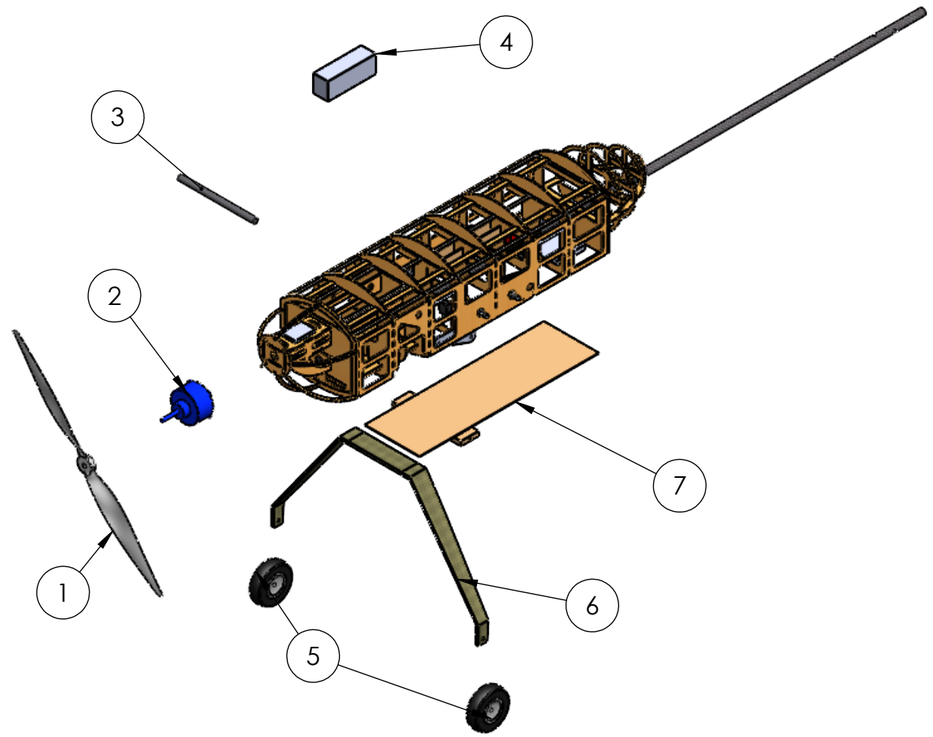

Bill of Materials			
Item No.	Item Name	Qty	Material
1	Propeller	1	Nylon
2	Motor	1	Aluminum
3	Motor Mount Spar	1	CF
4	Battery	1	Lithium Polymer
5	Front Landing Gear Wheels	2	Nylon
6	Front Landing Gear	1	CF
7	Ramp	1	Basswood
8	Flaps	2	Balsa
9	Ailerons	2	Balsa
10	Elevator	1	Balsa
11	Rudder	1	Balsa
12	Rear Landing Gear Spring	1	Aluminum
13	Rear Landing Gear Wheel	1	Foam

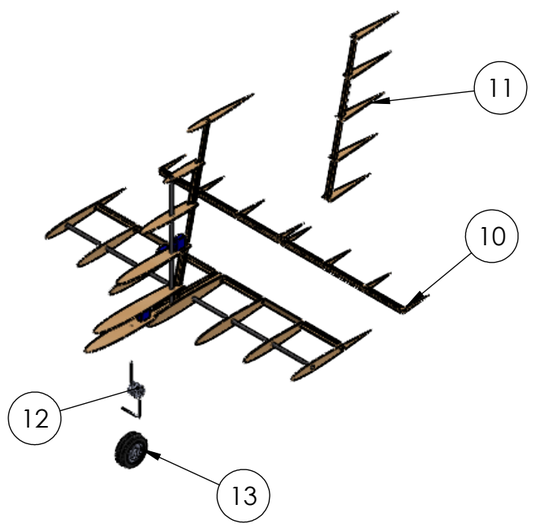

Washington University in St. Louis
AIAA Design Build Fly 2022

Name: Pflyzer

Aircraft Exploded Layout

SCALE: 1:12

SHEET 2 OF 4

MOTOR MOUNT STRUCTURE

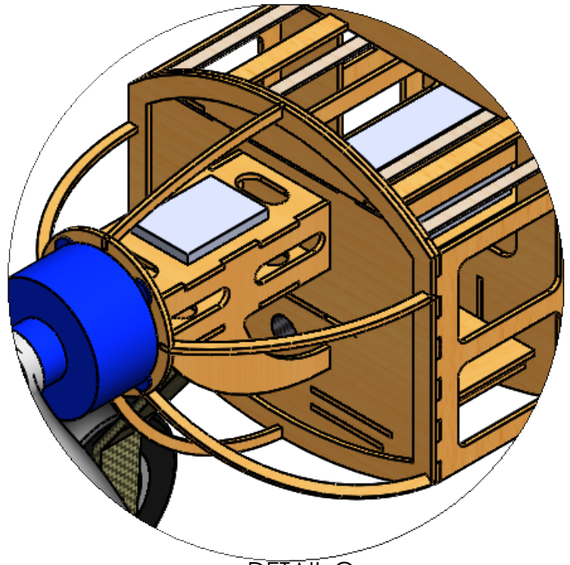

DETAIL C
SCALE 1 : 3

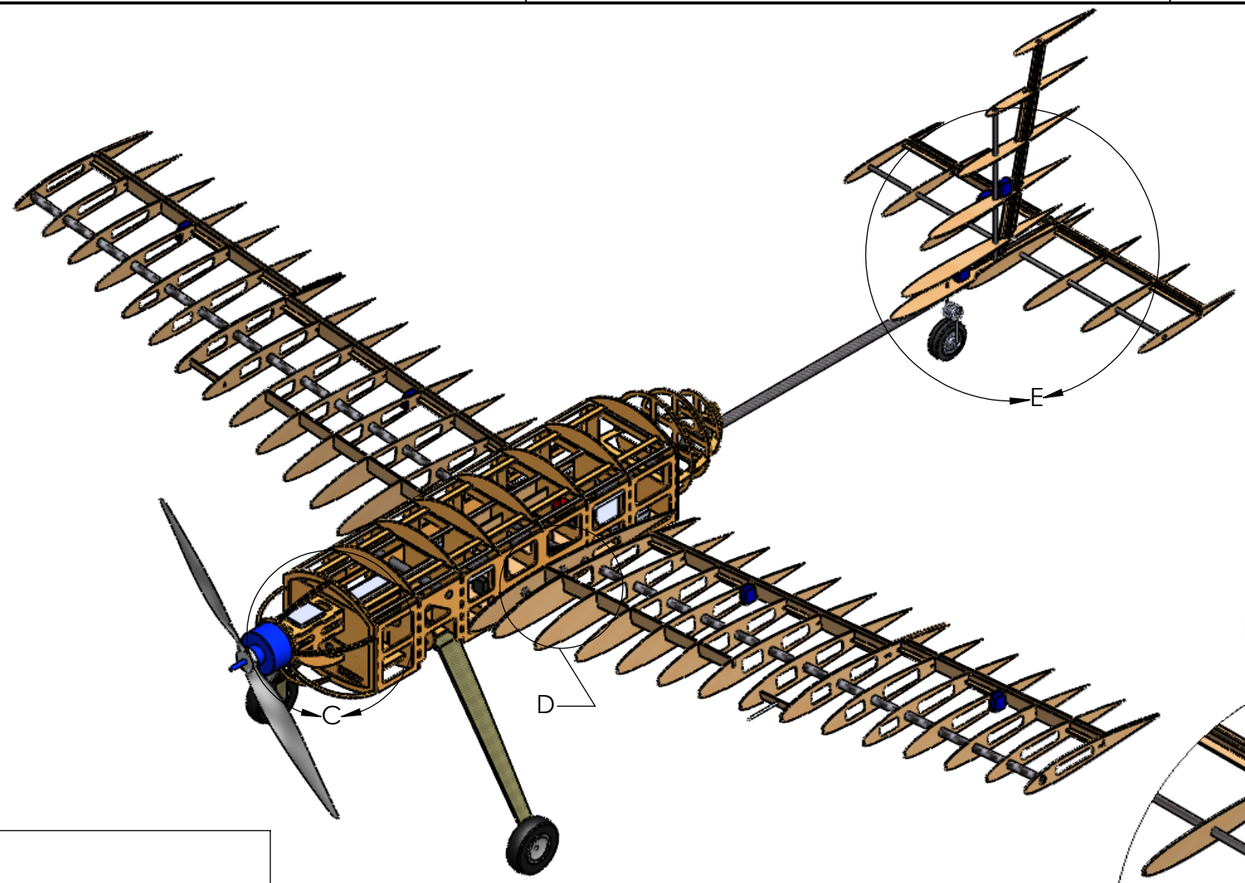

EMPENNAGE CONNECTION

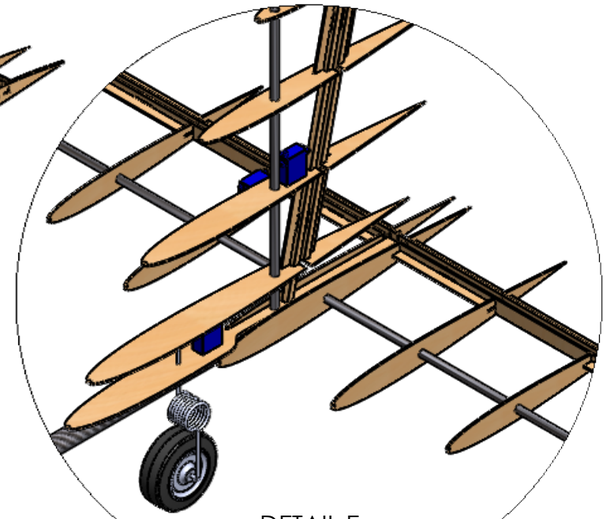

DETAIL E
SCALE 1 : 5

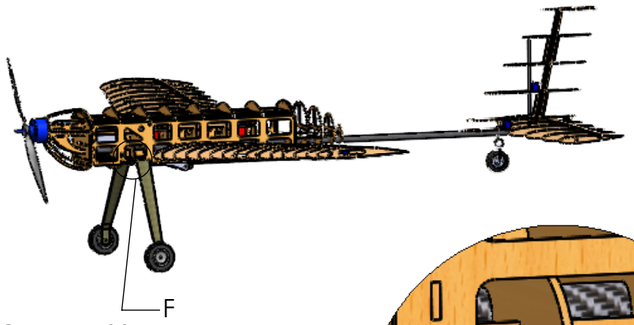

SCALE 1 : 20

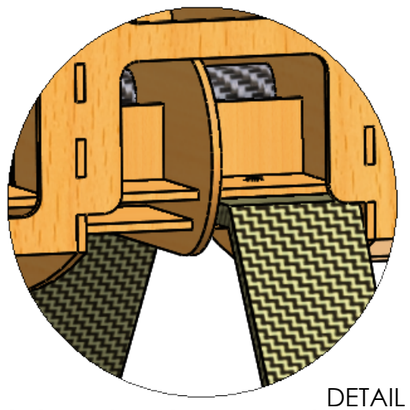

LANDING GEAR STRUCTURE

DETAIL F
SCALE 1 : 2

WING-FUSELAGE CONNECTION

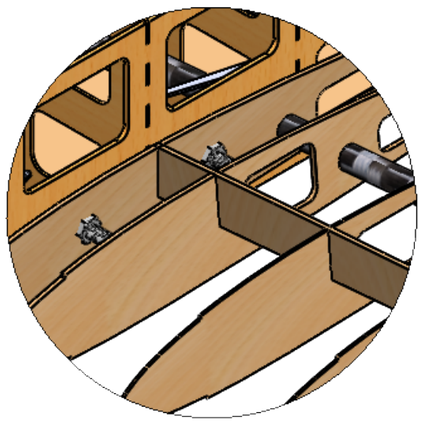

DETAIL D
SCALE 1 : 3

Washington University in St. Louis AIAA Design Build Fly 2022		
Name: Pflyzer	Aircraft Detail	
SCALE: 1:10		SHEET 3 OF 4

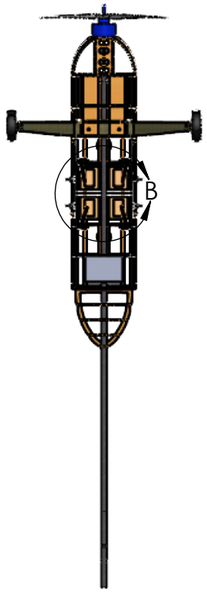

SCALE 1 : 20

PACKAGE RELEASE MECHANISM
(BOTTOM VIEW, RAMP HIDDEN)

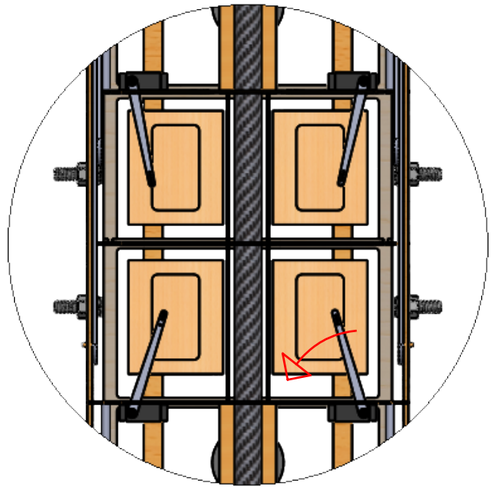

DETAIL B
SCALE 1 : 4

PACKAGE DEPLOYMENT MECHANISM
(ARROWS DESCRIBE MOTION OF THE PACKAGE)

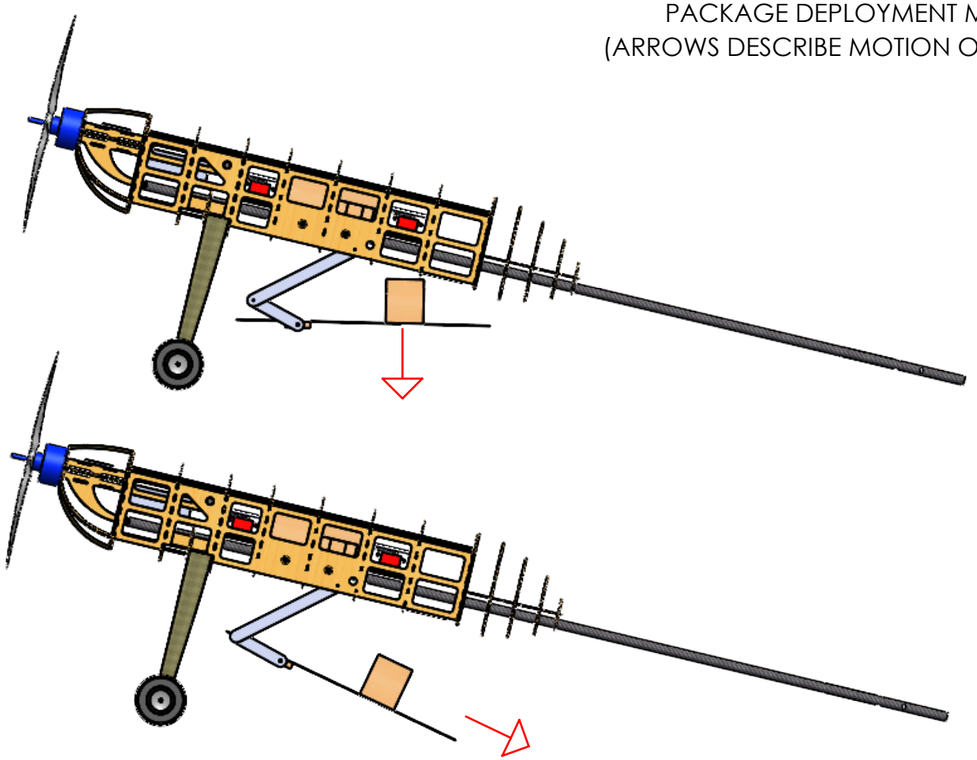

DEPLOYMENT MECHANISM LIST OF MATERIALS
(TOP VIEW, SIDE WALLS HIDDEN)

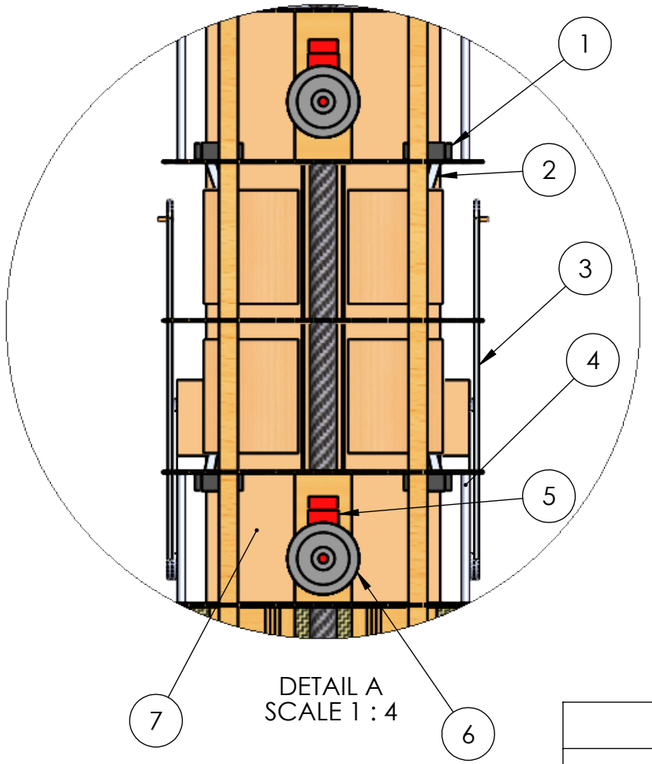

DETAIL A
SCALE 1 : 4

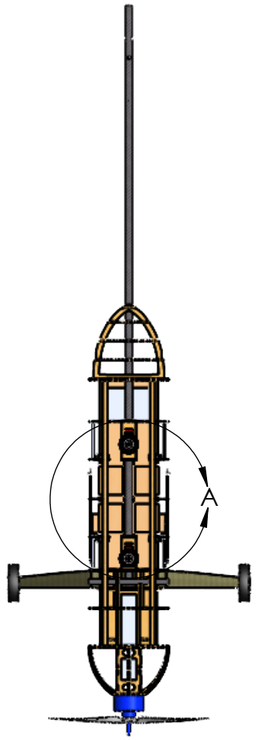

SCALE 1 : 16

Bill of Materials		
Item No.	Item Name	Qty
1	Package Release Servo	4
2	Package Release Servo Arm	4
3	Deployment Guide Arm	2
4	V Groove Pulley Rod	4
5	Winch Pulley Servo	2
6	Winch Pulley	2
7	Ramp	1

Washington University in St. Louis
AIAA Design Build Fly 2022

Name: Pflyzer	Payload Accomodation
SCALE: 1:12	SHEET 4 OF 4

6. Manufacturing Plan

6.1 Selection of Manufacturing Processes

Multiple manufacturing processes were considered to identify the best method for constructing the aircraft and the various subsystems.

6.1.1 Selection Criteria

Key evaluation criteria included ease of construction, effectiveness, feasibility, and weight. Materials which had been used in past aircraft were generally preferred, given manufacturing methods for those materials had already been refined. Finally, cost was also considered due to WUDBF's limited budget.

6.1.2 Solid Foam

Solid foam components could be designed and fabricated quickly since there are no internal bracing structures. However, achieving accurate shapes in foam requires using a hot-wire cutter, something WUDBF has little past experience with. It would be necessary to design and build a hot wire cutter and the necessary jigs, which would increase the time needed to build the aircraft. Although foam is light and has sufficient strength when paired with CF or fiberglass, the time constraints meant it was not chosen.

6.1.3 Additive Manufacturing

3D printing has advantages during construction due to the ease of fabricating structures as single components and the streamlined workflow from CAD to printer. However, 3D printers are slower than other methods for constructing large shapes. 3D printed parts are also heavier and weaker than those made from other materials, especially in shear along the seams between layers. While WUDBF ultimately did not make use of 3D printed parts for the main aircraft structure, more intricate components that don't bear significant loads such as servo mounts were 3D printed due to the flexibility and ease of 3D printing.

6.1.4 Composite Layup

Fiberglass or CF composite layup methods were considered due to their high strength and low weight. These methods however require construction of molds or plugs, which were determined to be too time-consuming and difficult to manufacture with current resources. WUDBF also has limited experience with these methods. That being said, prefabricated CF rods and fiberglass layups were used to reinforce the major load bearing components on the aircraft.

6.1.5 Wood Construction

Wood construction is the manufacturing technique WUDBF is most experienced with. WUDBF has a laser cutter that can be used to rapidly cut out wooden parts. Balsa, basswood, and birch ply are the primary woods used for RC aircraft, and each have different material properties. This offers flexibility when choosing where weight can be saved or where extra strength is needed. Assembly of wooden components can be done using CA glue and epoxy. CA glue dries quickly and forms a strong bond, making it the primary adhesive in wooden construction. Two-part epoxy offers a stronger alternative for components that bear more structural loads. In order to maintain the aerodynamic shape of the aircraft,

the frame can be covered in Monokote, a heat shrinking plastic film that can be tacked onto the frame of the aircraft then heated to pull it tight across the aircraft. Monokote is relatively thin and susceptible to tearing but can be quickly and easily repaired.

6.1.6 Processes Selected for Major Components

Wood construction, with Monokote coating, was chosen as the primary manufacturing method for all major components due to its structural qualities and WUDBF's previous experience. All wooden components including wing ribs and fuselage formers are cut using a laser cutter. These pieces are then assembled using CA and epoxy. CF parts and fiberglass reinforcement are added in key areas for structural support. In particular, the central rod, wing spars, and landing gear are CF parts purchased online, and the wood plates connecting the landing gear to the fuselage are reinforced with fiberglass.

6.2 Detailed Manufacturing Processes

The manufacturing processes used in the construction of the aircraft are detailed below. Note that these descriptions are primarily based on the construction of the prototype aircraft and some adjustments may occur for the final aircraft, which has yet to be built.

6.2.1 Fuselage

The fuselage is constructed primarily from birch ply formers, two side panels also made from birch ply, and a mix of basswood and balsa stringers. It was found that balsa stringers warp under the force of the Monokote, so basswood stringers are used at sharp corners. During construction a jig is used to align the formers. This jig consists of a wooden plate with laser cut holes. Jig posts attached to the formers slot into the holes. With the formers properly aligned in the jig, the side panels are attached and stringers CA glued into place. The central CF rod is then inserted and epoxied to the formers. Two basswood landing gear plates are then installed. These plates are reinforced with fiberglass for additional strength. The CF landing gear is sandwiched by these plates and secured using bolts. The nose containing the motor mount is constructed separately from the main fuselage. The nose slides into the main fuselage body and is secured via a horizontal CF rod epoxied to the side panels and a bolt running through a hole drilled in the central CF rod. Following construction of the frame, the entire structure is then covered in Monokote.

6.2.2 Wing

The wing is composed of ribs, stringers, a main CF spar, and a secondary wooden spar. Each half-wing is constructed separately and is designed to be easily removable. The ribs are aligned using slotted basswood jigs, with each rib fitting into a designated slot. Once the ribs are aligned, the CF and wooden spars were inserted and glued using epoxy. A quarter inch square basswood stringer is then attached to the leading edge of the wing and sanded down to achieve the correct curve. Next, the mounting plates for the control surfaces are installed, the jigs cut off and sanded down, and the wing flipped over. Basswood stringers are then added. The leading edge is then formed by wrapping balsa sheets soaked in warm water around the leading edge stringer. 3D printed servo mounts are then glued to the ribs.

Control surfaces are constructed in the same manner as the wing. Hinges are glued to the control surfaces and then to the mounting plates in the wing to secure them in place. Finally, the wing and control surfaces are covered with Monokote.

6.2.3 Wing Attachment

Each half-wing is attached to the fuselage via the side panels. The innermost rib of each half-wing is offset at 5° from the vertical to give the desired wing dihedral when mounted flush with the side panels. Holes in the innermost ribs line up with holes in the side panels, through which bolts are used to secure the wings in place. In addition, an aluminum tube bent to 10° manually while checking with an angle gauge is integrated into the fuselage. The CF spars in the wings slide around this tube to give added support help align the wings.

6.2.4 Empennage

The prototype tail is constructed using basswood stringers, balsa wood, and thin CF rods. Like in the wing, basswood stringers serve as the leading edges. These stringers are sanded to the shape of the desired airfoils. Each component of the tail is constructed separately in an identical manner to the wings, using similarly designed jigs. The elevator and rudder are also constructed separately and then attached to the HT and VT respectively using hinges and CA glue. To connect the tail to the fuselage, holes oriented perpendicularly to each other are drilled in the central CF rod, which extends out of the fuselage and acts as the tail boom. A custom hole drilling jig is used to ensure that the holes are perpendicular to each other and aligned properly with the wings and the rest of the aircraft. Thinner CF rods are then inserted into the holes. The VT and HT are then slid over these CF rods and epoxied into place. Following installation of servos and servo mounts, the tail is then covered in Monokote.

6.2.5 Deployment Mechanism

Owing to the simplicity of the deployment mechanism, no intricate, custom components are required. The guide arms and ramp are laser cut out of wood. The guide arms are connected to each other, the fuselage, and the ramp using bolts. The release servos are fixed to the sides of the payload compartments using the same 3D printed mounts described previously. Aluminum servo arms purchased online are attached to the release servos to support the package during flight and release the packages during the deployment phase. High torque, continuous rotation servos are used for the ramp pulleys and are mounted in front and behind the payload compartment on wooden plates epoxied to the central CF rod. The dual spools attached to the pulley servos can be purchased online. Two synthetic cables are then connected to each spool, with each cable then running over a guide rod mounted between the formers and down to the ramp where they are tied and CA glued into place.

Figure 6.1: Pulley Servo with Dual Spool

6.3 Manufacturing Milestones

A manufacturing schedule was implemented to ensure that components were constructed on time. The construction of the prototype and final aircraft were divided into important subtasks which were then used to create the schedule shown in Figure 6.2 below.

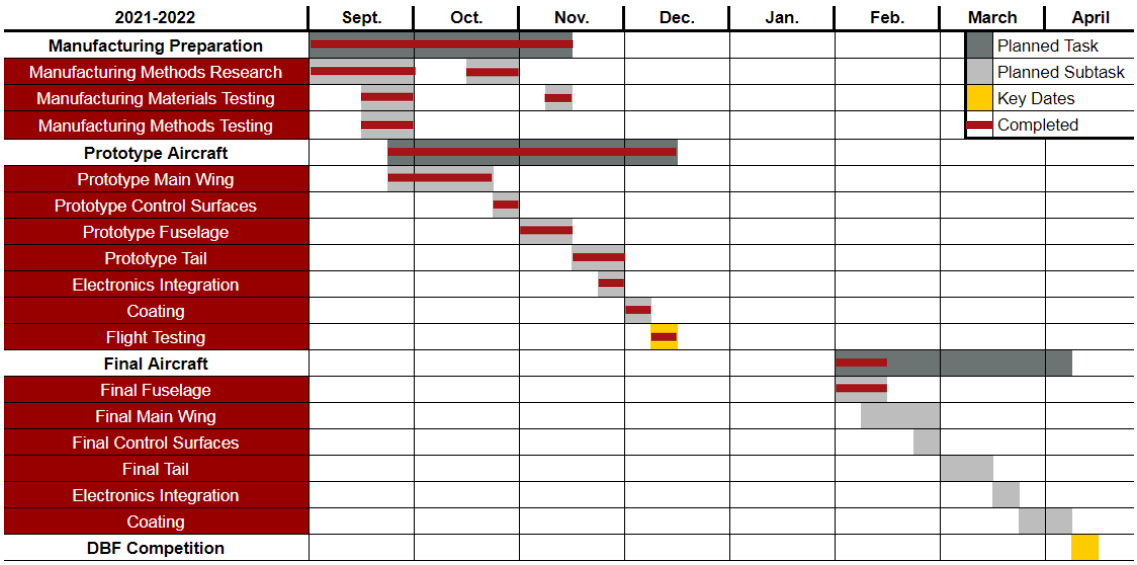

Figure 6.2: Gantt Chart of Manufacturing Schedule for The Prototype and Final Aircraft

7. Testing Plan

Ground and flight testing of the aircraft were performed to validate the design and drive iterations toward the final aircraft design.

7.1 Overall Test Objectives

Primary test objectives are listed in the table below by category. These objectives were achieved through a number of ground and flight tests described in Sections 7.2 and 7.3 respectively.

Table 7.1: Breakdown of Test Objectives

Category	Objective
Propulsion	Collect data from static thrust tests to confirm propulsion performance on the ground. Validate the propulsion system in the air during flight tests to confirm 25 ft takeoff capability, cruise velocity, and endurance.
Manufacturing	Investigate manufacturing processes, in particular the benefits of fiberglassing wood components.
Structures	Conduct wingtip loading tests at maximum AUW to verify structural integrity. Perform torsion and flutter tests to ensure that deflections are not excessive. Confirm integrity of the landing gear via ground tests.
Takeoff	Confirm aircraft can takeoff within 25 ft.
Deployment	Confirm reliability of deployment mechanisms and ensure that shock sensors are not tripped during deployment.
Performance	Record flight data for analysis to confirm performance requirements are met. Obtain feedback from pilot regarding handling qualities.

7.2 Ground Testing

7.2.1 Propulsion Test

Static thrust testing was performed on the chosen propulsion system using an RCbenchmark Series 1585 Dynamometer mounted to a thrust stand. Using RCbenchmark software, thrust, RPM, current draw, and electrical power measurements were collected at incremental throttle levels. The data were then used to validate predicted performance and confirm the propulsion system met the necessary requirements.

7.2.2 Fiberglass Test

WUDBF has had issues in previous years with basswood and/or birch ply landing gear mounting points failing on landing. Thus, it was investigated whether fiberglassing these wooden mounting points could significantly increase strength without excessively increasing weight. Square pieces of balsa, basswood, and birch ply were prepared. Half of the pieces were fiberglassed using 6 oz fiberglass. The test squares were then set up as simply supported beams with force applied to the center of the span, simulating the upwards load resulting from the landing gear hitting the ground. Each square was tested until failure.

7.2.3 Wingtip Test

A wingtip loading test was performed at maximum takeoff weight to validate the structural integrity of the fuselage. This test simulated a 2.5g load case and also verified that the aircraft could survive the wingtip test required at competition. Results from the wingtip test were compared against the FEA performed in Section 5.5.2 to further validate the design.

7.2.4 Structural Motor Thrust and Torque Test

The aircraft structure was tested to verify that it could withstand thrust and torque loads from the motor. Thrust loads were simulated by attaching a spring scale to the motor and pulling at a force of 15 kgf to simulate the expected maximum static thrust of 10.54 kgf times a 1.5 factor of safety. To simulate motor torque, a clamp was fixed to the motor. A spring scale was then attached to the end of the clamp and a 6 N·m torque was applied equivalent to the expected torque of 4 N·m times a 1.5 factor of safety.

7.2.5 Flutter Test

Torsion tests were performed on both the wing and tail to gauge flutter risk, which is an issue WUDBF has had in the past. To conduct the test, a reasonable torque was applied and then quickly released. The resulting vibration was observed for both the magnitude of vibration and the damping characteristics. Since WUBDF did not possess the accelerometers needed to conduct this test quantitatively, qualitative judgments were made to verify that the vibration was broadly acceptable based on prior experience.

7.2.6 Deployment

In order to verify the design of the deployment mechanism, mockups of both the release and lowering mechanisms were built to test their operation. For the release mechanism, the primary objective was to test whether the servo arm could support the weight of the package, and whether the package could be reliably released. For the lowering mechanism, the primary objective was to confirm that the package

could be dropped the short distance required to hit the ramp after internal release and then lowered to the ground without tripping the shock sensors. The maximum height the package can be dropped without tripping the sensor was measured (see Figure below). The maximum ramp angle for which the package could be slid down without tripping the sensor was also measured (see Figure below).

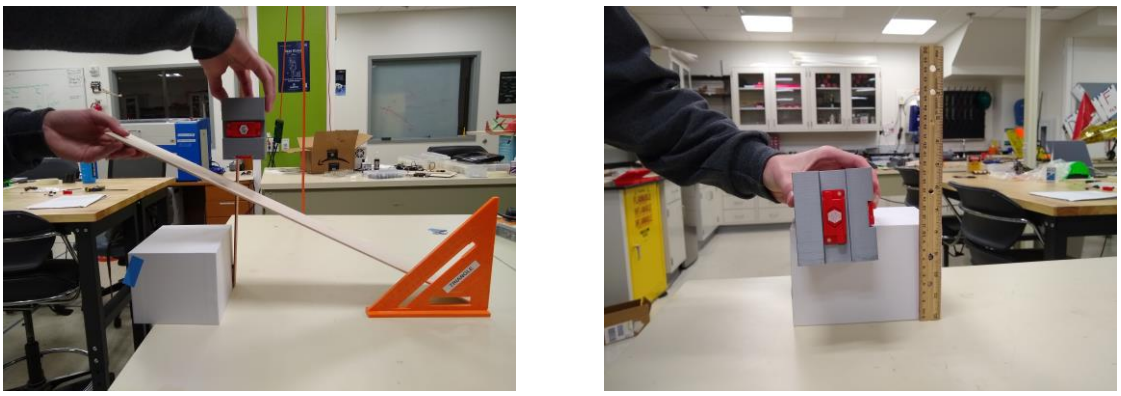

Figure 7.1: Ramp Test Setup (left) and Drop Test Setup (right)

7.3 Flight Testing

Multiple test flights were conducted to verify that the aircraft met design goals. A Pixhawk flight computer was used to capture telemetry during each flight test (see figure below). This data was then analyzed to extract measures of aircraft performance including speed, endurance, and lap times. Feedback from the pilot was also used to evaluate the stability and flight characteristics of the aircraft. Conclusions from flight testing were used to inform changes to the design going from the prototype to the final aircraft. For the full details of each flight test, see the test schedule in Section 7.4.

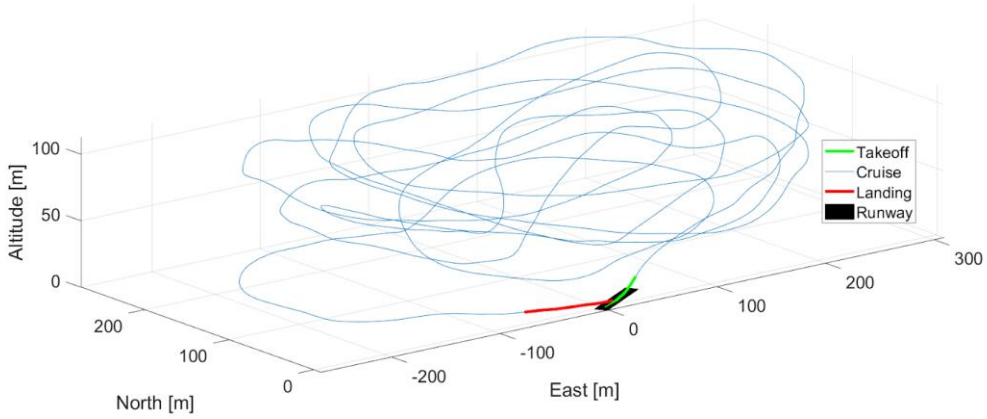

Figure 7.2: Sample Telemetry Data from Test Flight

7.3.1 Ground Inspection and Pre-Flight Checklists

Table 7.2: Ground Inspection Checklist

Component	Tasks
Motor	☐ Motor secured ☐ Propeller free from damage
Fuselage	☐ No cracks or tears ☐ Electronics are connected and secured
Wing	☐ No cracks or tears ☐ Bolted to fuselage ☐ Wingtip test
Payload	☐ Servos connected to receiver ☐ Deployment mechanism moves correctly ☐ Payloads are positioned correctly and secure
Control Surfaces	☐ No cracks or tears ☐ Servos connected to receiver ☐ Control surfaces can deflect fully
Empennage	☐ No cracks or tears ☐ Control surfaces move without interference
Landing Gear	☐ Front wheels secured ☐ Rear wheel alignment check

Table 7.3: Pre- and Post-Flight Checklists

Flight Checklists
Pre-Flight
☐ Payloads secured ☐ Propulsion battery level check ☐ Receiver battery level check ☐ CG position confirmed ☐ Wingtip test ☐ Receiver turned on ☐ Deployment mechanisms armed ☐ Control surfaces test ☐ Landing gear steering test ☐ Range Check ☐ Motor run-up ☐ Fuselage lid is attached and secure
Post-Flight
☐ Throttle down ☐ Arming plug removed ☐ Propulsion battery disconnected ☐ Receiver battery disconnected

7.4 Testing Schedule

Table 7.4: Testing Schedule

Date	Type	Category	Objective
Prototype			
10-16-2021	Ground	Manufacturing	Test fiberglassing of wooden components.
11-20-2021	Ground	Propulsion	Static thrust test to confirm propulsion performance.
11-27-2021	Ground	Structures	Flutter test to check structural stability.
12-12-2021	Ground	Structures	Wingtip test to confirm structure.
12-12-2021	Flight	Performance	Shakedown flight. Test Prototype design. (CRASHED)
Rebuilt Prototype			
1-29-2022	Ground	Deployment	Validation of mock-up deployment design.
2-18-2022	Ground	Structures	Thrust and torque test to ensure verify structure.
2-22-2022	Flight	Performance	Shakedown flight. Test Prototype design.
2-22-2022	Flight	Performance	Full M1 simulated flight. Confirm TOFL.
2-22-2022	Flight	Performance	Full M2 simulated flight. Confirm performance predictions
2-22-2022	Flight	Performance	M3 simulated repeated takeoff-landing with no deployment.
Final Aircraft (Planned)			
3-25-2022	Ground	Performance	Ground mission test.
3-26-2022	Flight	Performance	M1 simulated flight. Evaluate performance.
3-26-2022	Flight	Performance	M2 simulated flight. Evaluate performance.
3-26-2022	Flight	Performance	M3 simulated flight. Test deployment. Evaluate performance.
4-2-2022	Flight	Performance	Practice for competition.
4-9-2022	Flight	Performance	Practice for competition.

8. Performance Results

8.1 Ground Test Results

8.1.1 Propulsion Test Results

Results from the static thrust test confirmed that the propulsion system generally met the desired performance requirements. Test data is compared to eCalc predicted performance in the table below.

Table 8.1: Predicted vs. Actual Performance

Parameter	Prediction	Test Result
RPM	4836	4953
Thrust [Kgf]	10.821	10.05
Max Current [A]	112.94	120.84
Electrical Power [W]	2258.5	2658.48

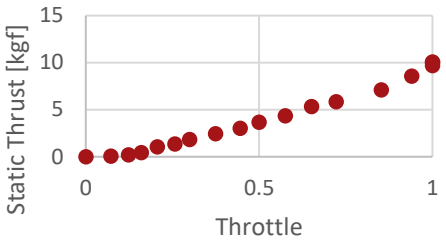

Figure 8.1: Static Thrust Over Increasing Throttle

Based on the static testing, the motor drew slightly more burst current than predicted. This is not an issue, however, since the ESC was sized with significant margin. The efficiency of the actual propulsion system appeared to be slightly lower than predicted, however the static thrust test was conducted indoors, and obstructions and ground effects may have contributed to that decrease in efficiency. Later flight testing confirmed that the propulsion system delivered the desired takeoff capability and cruise performance.

8.1.2 Fiberglass Test Results

Fiberglass testing revealed that fiberglassing basswood increased the strength-to-weight ratio from 101.9 to 225.2 and fiberglassing birch ply increased the strength-to-weight ratio from 164.5 to 311.5. Negligible increases in thickness were observed after fiberglassing. Based on this testing, WUDBF decided to construct the landing gear mounts out of fiberglass reinforced birch ply.

8.1.3 Wingtip Test Results

The plane was supported successfully by just the wingtips. The measured deflection was around 5° in each wing. This agrees with the FEA performed on the CF rod alone in Section 5.5.2 (predicted deflection of 8.4°) since the additional structural elements in the wing provide additional bending support.

8.1.4 Structural Motor Thrust and Torque Test Results

The aircraft structure was able to successfully withstand both the expected thrust and torque loads (times a factor of safety of 1.5).

8.1.5 Flutter Test Results

WUDBF determined that the tail structure was sufficiently strong and would not experience excess fluttering. The torsional rigidity of the fuselage-wing structure, however, was determined to be insufficient and the flutter risk was judged to be beyond acceptable limits. Changes for the final aircraft including changing former material from basswood to birch ply and increasing the size of the side panels were made to improve rigidity.

8.1.6 Deployment Test Results

Testing of the release mechanism determined that an aluminum servo arm could easily support the weight of the package. Since the weight of the package is directed downward, the motor and gears in the servo take minimal load and the majority of the load is taken by the servo body and motor mount. The package drop test determined that the package could be dropped a maximum distance of 3 cm before the sensors are tripped. This is greater than the designed internal distance between the package compartment and the ramp, which validates the design. The ramp test determined that the maximum angle at which the package could be safely slid to the ground without tripping the sensors was 20°. The results of this testing showed that a conventional ramp with one side anchored in the fuselage would not work since the smallest ramp angle that could be achieved was around 30°. This necessitated the twin winch design so that the ramp could be lowered directly downwards allowing for a less steep ramp angle.

8.2 Flight Testing

8.2.1 Dec. 12th, 2021 – Shakedown Flight (Prototype)

The servo wire connecting the elevator servo disconnected just after takeoff. After losing elevator control, the pilot was able to complete one controlled 360° turn before crashing. No flight test data was captured due to the crash. The wing remained largely undamaged, which verified its strength. The fuselage sheared in half longitudinally, with each former snapping in half at the connection (side panels on the prototype extended only halfway up the side of the fuselage). This failure motivated a number of structural redesigns including changing the material of the formers from basswood to birch ply for its stronger, uniform material properties. The side panels for the final aircraft were also increased in height to extend all the way to the top of the fuselage to minimize stress concentrations.

8.2.2 Feb. 22nd, 2022 – Multiple Flights (Rebuilt Prototype)

Table 8.2 summarizes the outcomes of the Feb 22nd test flight.

Table 8.2: Test Flight Outcomes

Flight Description	Result
Shakedown	The aircraft survived the shakedown test. The pilot trimmed the aircraft and was able to achieve stable flight characteristics.
Full Simulated M1	The aircraft was able to takeoff in 10 ft. The mission was completed in 2.6 minutes, which is well within the 5-minute window.
Full Simulated M2	The aircraft was again able to takeoff in about 10 ft. The mission was completed in 2.3 minutes. Max cruise velocity was measured at 21.7 m/s.
M3 Repeated T-L	The aircraft was able to takeoff multiple times within 25 ft while at the fully loaded weight on the same battery. Pilot reported good ground handling characteristics but commented that the landing gear wheels were too hard, leading to bouncing on landing.

During post-flight interviews, the pilot rated the aircraft a 2 on the Cooper-Harper handling qualities rating scale (HQRS). This confirmed that the aircraft's handling characteristics are satisfactory without improvement. Table 8.3 details the actual aircraft performance when compared to predicted performance.

Table 8.3: Predicted Performance versus Actual Performance

Flight Description	Predicted	Actual	Difference
M1 Time [min]	2.371	2.6	-9.2 %
M2 Time [min]	2.192	2.3	-4.8 %
M1 Cruise Velocity [m/s]	21.83	21.7	-0.6 %
M2 Cruise Velocity [m/s]	21.89	21.7	-0.9 %
M3 Cruise Velocity [m/s]	20.67	-	N/A
M3 Battery Endurance [min]	5	6.2	+21.4 %
TOFL (ft)	11	10	-9.5 %

The prototype aircraft generally met or exceeded all performance requirements.

9. Bibliography

[1] "Trainer Design," RC Planes, retrieved 24 February 2021. https://rcplanes.online/design.htm

[2] Gudmundsson, S., *General Aviation Aircraft Design: Applied Methods and Procedures,* 1st ed., Butterworth-Heinemann, Oxford, 2014

[3] "NACA 4 digit airfoil calculator," Airfoil Tools, 25 June 2017. airfoiltools.com

[4] Washington University in St. Louis Design/Build/Fly Team, "Red Bearon," AIAA Design/Build/Fly 2020-2021 Design Report, retrieved 10 February 2022.

[5] Raymer, D. P., *Aircraft Design: A Conceptual Approach*, edited by J. A. Schetz, 6th ed., Astronautics and Aeronautics, AIAA, New York, 2018.

[6] "Horizontal and Vertical Tail Design", AeroToolbox, retrieved 23 October, 2021. https://aerotoolbox.com/design-aircraft-tail/

[7] Foster, T. "Dynamic Stability and Handling Qualities of Small Unmanned-Aerial-Vehicles UNMANNED-AERIAL-VEHICLES." *Theses and Dissertations*, 2004

[8] Hoerner, S. F., *Fluid-Dynamic Drag: Practical Information on Aerodynamic Drag and Hydrodynamic Resistance,* Hoerner Fluid Dynamics, Bakersfield, 1992, p. 6-17

[9] "Reliable Electric Drive Simulations," eCalc, retrieved 8 November 2021. https://www.ecalc.ch/

[10] "Performance Data," APC Propellers, retrieved from 20 January 2022. https://www.apcprop.com/technical-information/performance-data/

[11] Hainline, K., "km_sim," MathWorks File Exchange, retrieved October 30 2021. https://www.mathworks.com/matlabcentral/fileexchange/94968-km_sim

[12] Heath, H., "What Are the Properties of Birch Plywood?," Rampfesthudson, retrieved 22 January 2022 https://www.rampfesthudson.com/what-are-the-properties-of-birch-plywood/

[13] "Carbon Fiber Uni Wrapped Tubing," ACP Composites, retrieved 29 January 2022 https://store.acpcomposites.com/carbon-fiber-uni-roll-wrapped-tubing?quantity=1&dimensions=24&length=46